EDITORIAL: BACTERIAL SURFACE GLYCANS AS THE VIRULENCE AGENT AND THE TARGET FOR PREDATORS, THERAPY, AND THE IMMUNE SYSTEM

EDITED BY: Zuzanna Drulis-Kawa and Felipe Cava
PUBLISHED IN: Frontiers in Microbiology

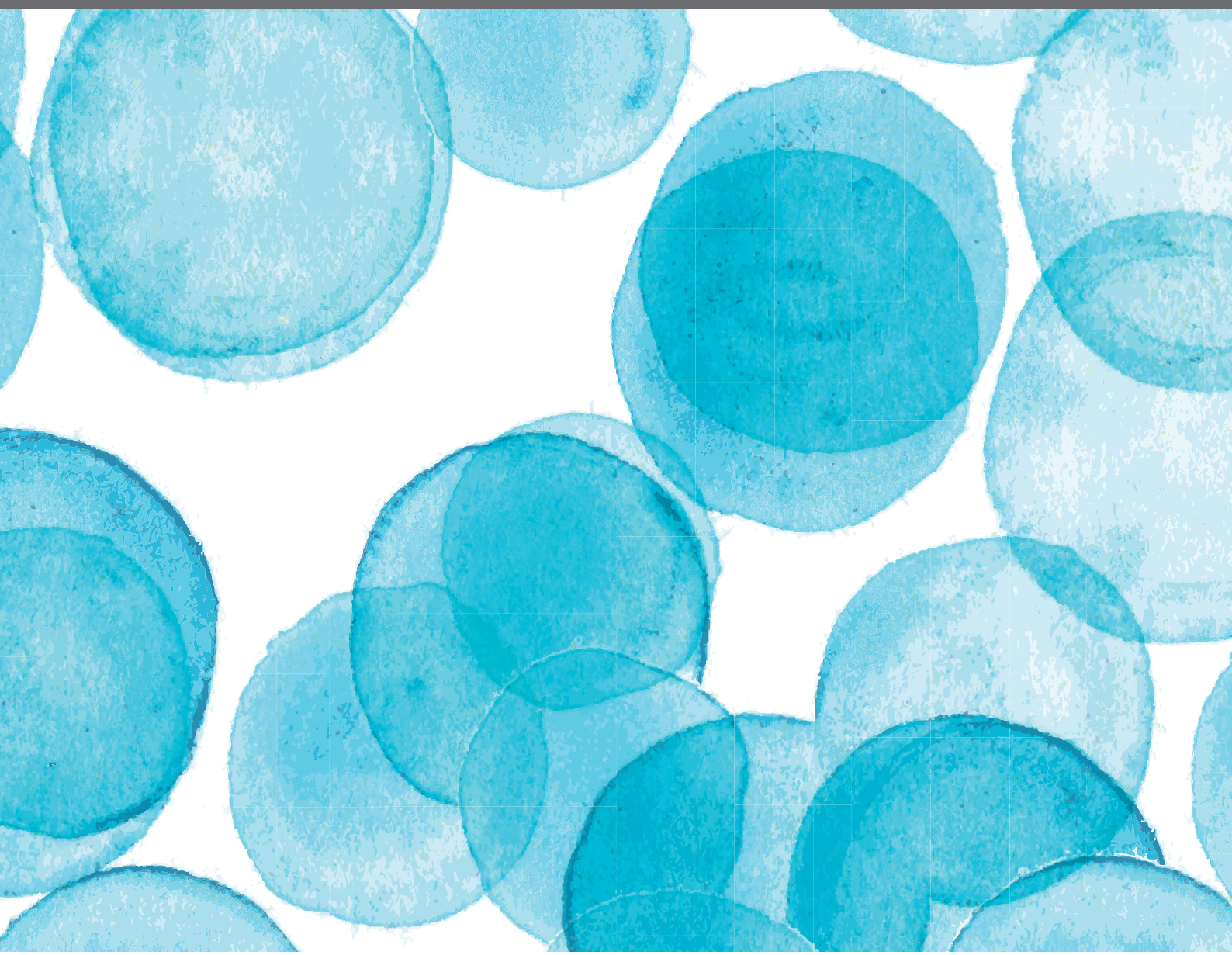

frontiers Research Topics

frontiers

ISSN 1664-8714
ISBN 978-2-88966-449-8
DOI 10.3389/978-2-88966-449-8

About Frontiers

Frontiers is more than just an open-access publisher of scholarly articles: it is a pioneering approach to the world of academia, radically improving the way scholarly research is managed. The grand vision of Frontiers is a world where all people have an equal opportunity to seek, share and generate knowledge. Frontiers provides immediate and permanent online open access to all its publications, but this alone is not enough to realize our grand goals.

Frontiers Journal Series

The Frontiers Journal Series is a multi-tier and interdisciplinary set of open-access, online journals, promising a paradigm shift from the current review, selection and dissemination processes in academic publishing. All Frontiers journals are driven by researchers for researchers; therefore, they constitute a service to the scholarly community. At the same time, the Frontiers Journal Series operates on a revolutionary invention, the tiered publishing system, initially addressing specific communities of scholars, and gradually climbing up to broader public understanding, thus serving the interests of the lay society, too.

Dedication to Quality

Each Frontiers article is a landmark of the highest quality, thanks to genuinely collaborative interactions between authors and review editors, who include some of the world's best academicians. Research must be certified by peers before entering a stream of knowledge that may eventually reach the public - and shape society; therefore, Frontiers only applies the most rigorous and unbiased reviews.
Frontiers revolutionizes research publishing by freely delivering the most outstanding research, evaluated with no bias from both the academic and social point of view. By applying the most advanced information technologies, Frontiers is catapulting scholarly publishing into a new generation.

What are Frontiers Research Topics?

Frontiers Research Topics are very popular trademarks of the Frontiers Journals Series: they are collections of at least ten articles, all centered on a particular subject. With their unique mix of varied contributions from Original Research to Review Articles, Frontiers Research Topics unify the most influential researchers, the latest key findings and historical advances in a hot research area! Find out more on how to host your own Frontiers Research Topic or contribute to one as an author by contacting the Frontiers Editorial Office: frontiersin.org/about/contact

EDITORIAL: BACTERIAL SURFACE GLYCANS AS THE VIRULENCE AGENT AND THE TARGET FOR PREDATORS, THERAPY, AND THE IMMUNE SYSTEM

Topic Editors:
Zuzanna Drulis-Kawa, University of Wrocław, Poland
Felipe Cava, Umeå University, Sweden

Citation: Drulis-Kawa, Z., Cava, F., eds. (2021). Editorial: Bacterial surface glycans as the virulence agent and the target for predators, therapy, and the immune system. Lausanne: Frontiers Media SA. doi: 10.3389/978-2-88966-449-8

Table of Contents

frontiers in Microbiology

EDITORIAL
published: 16 December 2020
doi: 10.3389/fmicb.2020.624964

Editorial: Bacterial Surface Glycans as the Virulence Agent and the Target for Predators, Therapy, and the Immune System

*Zuzanna Drulis-Kawa**

Department of Pathogen Biology and Immunology, Institute of Genetics and Microbiology, University of Wroclaw, Wrocław, Poland

Keywords: bacterial glycans, virulence, phage receptor recognition, enzymes degrading bacterial glycans, phage resistance mechanism

Editorial on the Research Topic

Bacterial Surface Glycans as the Virulence Agent and the Target for Predators, Therapy, and the Immune System

The Research Topic entitled "Bacterial surface glycans as the virulence agent and the target for predators, therapy, and the immune system," was dedicated to reports and reviews on novel discoveries about bacterial glycans biodiversity, and recognition by the immune system, as well as about phage interactions with glycan receptors, and phage-derived enzymes recognizing/degrading bacterial glycans.

Bacterial surface molecules both of protein and carbohydrate nature such as type IV pili (T4P), outer membrane proteins, flagella, or capsule (CPS), exopolysaccharides (EPS), lipopolysaccharide (LPS), and peptidoglycan (PG) are targeted by bacterial predators (phages) as receptors. The successful phage adherence is accompanied by the passage of diverse carbohydrate barriers. For that purpose bacterial viruses are equipped with various virion-associated and soluble enzymes, called polysaccharide depolymerases and lysins, that recognize, bind, and degrade glycan compounds (Latka et al., 2017).

Nowadays, more and more papers describe the phage-encoded enzymes able to degrade CPS, EPS, or LPS of the host bacteria. Those are found not only within podoviruses but also in phages representing *Ackermannviridae*, *Myoviridae*, and *Siphoviridae* families. The minireview of Knecht et al., describes the diversity and function of different tail spike proteins (TSP) of phages propagating on the most common pathogens. It is an interesting work combining the current knowledge of known phages targeting single, dual, and multiple CPS/LPS serotypes of the bacterial host. Therefore, the authors propose possible systems connecting TSPs with the baseplate in different phage genera to enlarge phage specificity to more than one type of targeted glycan.

The above idea has been further continued in detail in the model of *Klebsiella* phages (Latka et al.). This work is dedicated to *in silico* modeling of Receptor Binding Proteins (RBPs) architecture based on the experimental structural results done previously by Leiman group in *E. coli* phages. A detailed bioinformatic analysis shows that RBPs are structured with conservative and divergent domains. The N-terminal domain responsible for RBP assembly to the virion/baseplate may be complemented with a specific T4gp10-like domain providing the attachment site for the secondary RBP in a so-called branching system. The *in silico* modeling shows the possible commitment of the T4gp10-like domain in the RBPs architecture of multi-serotype targeting *Klebsiella* phages. Moreover, this idea has been lately confirmed by this group in the structural and functional study on *Klebsiella* phage capsule-degrading depolymerase KP32gp38.

The second type of phage-borne enzymes as potential antibacterials are lysins, peptidoglycan-degrading proteins. These enzymes are efficiently applied against Gram-positive bacteria whereas

OPEN ACCESS

Edited by:
Dieter Jahn,
Technische Universitat Braunschweig, Germany

Reviewed by:
Bernd Lepenies,
University of Veterinary Medicine Hannover, Germany

***Correspondence:**
Zuzanna Drulis-Kawa
zuzanna.drulis-kawa@uwr.edu.pl

Specialty section:
This article was submitted to Infectious Diseases, a section of the journal Frontiers in Microbiology

Received: *01 November 2020*
Accepted: *24 November 2020*
Published: *16 December 2020*

Citation:
Drulis-Kawa Z (2020) Editorial: Bacterial Surface Glycans as the Virulence Agent and the Target for Predators, Therapy, and the Immune System. Front. Microbiol. 11:624964. doi: 10.3389/fmicb.2020.624964

with some limitations against Gram-negatives because of the protective outer membrane layer blocking the access to targeted peptidoglycan. To overcome this obstacle lysins can be combined with membrane-disrupting agents. The work of Ciepluch et al. describes the pros and cons of dendronized silver nanoparticles utilization as bacterial membrane permeabilizers together with lysins against *P. aeruginosa*. It turned out that cationic nanoparticles were interacting with the O-chain of LPS with no direct access to the OM surface. Only the dendronized AgNPs PEGylation overcame the LPS barrier and efficiently enhanced the antibacterial effect of lysins.

In this Research Topic, we were looking for current findings referring to phage interactions with glycan receptors to see if the naturally occurring heterogenicity in surface polysaccharides impacts the phage predation. On the other hand, the phage introduction might select a phage-resistance in the targeted host leading to the modification of a specific phage receptor. In other words, the variation of the capsule, LPS, or other types of surface glycan, the main molecular patterns for the immune system recognition would entail the diminishing virulence of bacterial pathogens.

Indeed, the work of Cai et al., shows the correlation between the spontaneous mutations in the genes of three capsular polysaccharide synthesis-related glucosyltransferases (GT-1, GT-2, and WcaJ) and both the prevention of phage GH-K3 infection and reduced virulence of *K. pneumoniae* K7. The rough-type phage-resistant mutant induced mitogen-activated protein kinase (MAPK) signaling pathway in macrophages becoming significantly more prone to endocytosis compared to the wild-type strain. The authors also found that phage GH-K3 was able to bound to modified CPS residues of K7(ΔGT-1) and K7(ΔwcaJ) mutants but with lower efficiency.

There is another very interesting mechanism of phage-bacterial glycan interaction in *Campylobacter jejuni* (Sacher et al.). This study was focused on the role of specific phage-encoded FlaGrab protein responsible for the phage attachment to the motile *C. jejuni* flagella. It turned out that FlaGrab recognizes the glycosylated flagella and triggers the bacterial response-signal inhibiting the growth and downregulating energy metabolism. It serves for the prevention of phage propagation. Moreover, it was proposed that the variation in flagella glycosylation provides resistance to phage infection. This study is a good starting point to get insight into unknown mechanisms of generating flagellar glycan diversity also in the context of *C. jejuni* virulence.

Bacteria had developed a panel of strategies to avoid the immune system response and phage attack. Indeed, the outer membrane vesicles (OMVs) bearing LPS molecules in the outer leaflet are used by Gram-negative bacteria as a perfect decoy attracting and sequestrating phages present in bacterial surroundings (Caruana and Walper, 2020). The manuscript of Stephan et al., presents the *in vitro* analysis of O-antigen-specific phage P22 inactivation by *Salmonella* Typhimurium OMVs. It was shown that phages were effectively neutralized by the deposition on the surface of the vesicles. A part of phages actively ejected their DNA into the OMVs interior and it was more intense in the presence of membrane proteins in native OMVs.

Glycoconjugates are the main bacterial virulence factors being at the same time molecular patterns as well as phage targets for efficient adsorption. Moreover, a high structure specificity of bacterial glycans may serve for bacterial identification, diagnostics, and vaccine compounds. The minireview prepared by Campanero-Rhodes et al. provides the view of the current state-of-the-art and prospects for the implementation of microarray strategies for exploring bacterial surface glycans and their interactions with glycan-binding proteins. This sensitive and high-throughput system allows for fast identification and differentiation of glycan-protein interactions further used in bacterial diagnostics, the immune system effectors recognition, glycan-degrading enzymes detection as well as vaccine development. The different microarray platforms may incorporate glycan molecules, cell wall fragments, or entire bacterial cells as a template.

Summarizing the content of this Special Issue focused on bacterial glycans as the key element both for bacterial virulence as well as phage targeted receptors, we may conclude that co-evolutionary interactions between bacteria and its host, bacteria and its predators forced microorganisms to develop sophisticated strategies to avoid the immune response and viral propagation. The deepened knowledge on bacterial glycan variability and glycan-directed phage specificity will allow us to understand the evolutionary linkages and mutual bacteria-phage impact on biodiversity, as well as in the context of future application perspectives in medicine, industry, agriculture, or biotechnology.

AUTHOR CONTRIBUTIONS

ZD-K wrote the editorial note.

FUNDING

This study was supported by National Science Centre, Poland grants 2017/26/M/NZ1/00233 and 2015/18/M/NZ6/00413.

REFERENCES

Caruana, J. C., and Walper, S. A. Bacterial membrane vesicles as mediators of microbe - microbe and microbe - host community interactions. *Front. Microbiol.* (2020) 11:432. doi: 10.3389/fmicb.2020.00432

Latka, A., Maciejewska, B., Majkowska-Skrobek, G., Briers, Y., and Drulis-Kawa, Z. Bacteriophage-encoded virion-associated enzymes to overcome the carbohydrate barriers during the infection process. *Appl. Microbiol. Biotechnol.* (2017) 101, 3103–3119. doi: 10.1007/s00253-017-8224-6

Conflict of Interest: The author declares that the research was conducted in the absence of any commercial or financial relationships that could be construed as a potential conflict of interest.

frontiers in Microbiology

ORIGINAL RESEARCH
published: 28 May 2019
doi: 10.3389/fmicb.2019.01189

Three Capsular Polysaccharide Synthesis-Related Glucosyltransferases, GT-1, GT-2 and WcaJ, Are Associated With Virulence and Phage Sensitivity of *Klebsiella pneumoniae*

Ruopeng Cai[1], Gang Wang[1], Shuai Le[2], Mei Wu[3], Mengjun Cheng[1], Zhimin Guo[4], Yalu Ji[1], Hengyu Xi[1], Caijun Zhao[1], Xinwu Wang[1], Yibing Xue[1], Zijing Wang[1], Hao Zhang[1], Yunhe Fu[1], Changjiang Sun[1], Xin Feng[1], Liancheng Lei[1], Yongjun Yang[1], Sadeeq ur Rahman[5], Xiaoyun Liu[6], Wenyu Han[1,7]* and Jingmin Gu[1]**

[1] Key Laboratory of Zoonosis Research, Ministry of Education, College of Veterinary Medicine, Jilin University, Changchun, China, [2] Department of Microbiology, Army Medical University, Chongqing, China, [3] Institute of Analytical Chemistry and Synthetic and Functional Biomolecules Center, College of Chemistry and Molecular Engineering, Peking University, Beijing, China, [4] Department of Clinical Laboratory, The First Hospital of Jilin University, Changchun, China, [5] College of Veterinary Sciences and Animal Husbandry, Abdul Wali Khan University, Mardan, Pakistan, [6] Department of Microbiology, School of Basic Medical Sciences, Peking University Health Science Center, Beijing, China, [7] Jiangsu Co-Innovation Center for the Prevention and Control of Important Animal Infectious Disease and Zoonose, Yangzhou University, Yangzhou, China

OPEN ACCESS

Edited by:
Zuzanna Drulis-Kawa, University of Wrocław, Poland

Reviewed by:
Grazyna Majkowska-Skrobek, University of Wrocław, Poland
Stefanie Barbirz, Universität Potsdam, Germany

***Correspondence:**
Xiaoyun Liu
xiaoyun.liu@pku.edu.cn
Wenyu Han
hanwy@jlu.edu.cn
Jingmin Gu
jingmin0629@163.com

Specialty section:
This article was submitted to Infectious Diseases, a section of the journal Frontiers in Microbiology

Received: *23 January 2019*
Accepted: *10 May 2019*
Published: *28 May 2019*

Citation:
Cai R, Wang G, Le S, Wu M, Cheng M, Guo Z, Ji Y, Xi H, Zhao C, Wang X, Xue Y, Wang Z, Zhang H, Fu Y, Sun C, Feng X, Lei L, Yang Y, ur Rahman S, Liu X, Han W and Gu J (2019) Three Capsular Polysaccharide Synthesis-Related Glucosyltransferases, GT-1, GT-2 and WcaJ, Are Associated With Virulence and Phage Sensitivity of Klebsiella pneumoniae. Front. Microbiol. 10:1189. doi: 10.3389/fmicb.2019.01189

Klebsiella pneumoniae (*K. pneumoniae*) spp. are important nosocomial and community-acquired opportunistic pathogens, which cause various infections. We observed that *K. pneumoniae* strain K7 abruptly mutates to rough-type phage-resistant phenotype upon treatment with phage GH-K3. In the present study, the rough-type phage-resistant mutant named K7R^R showed much lower virulence than K7. Liquid chromatography-tandem mass spectrometry (LC-MS-MS) analysis indicated that WcaJ and two undefined glycosyltransferases (GTs)- named GT-1, GT-2- were found to be down-regulated drastically in K7R^R as compared to K7 strain. *GT-1*, *GT-2,* and *wcaJ* are all located in the gene cluster of capsular polysaccharide (CPS). Upon deletion, even of single component, of *GT-1*, *GT-2,* and *wcaJ* resulted clearly in significant decline of CPS synthesis with concomitant development of GH-K3 resistance and decline of virulence of *K. pneumoniae*, indicating that all these three GTs are more likely involved in maintenance of phage sensitivity and bacterial virulence. Additionally, K7R^R and GT-deficient strains were found sensitive to endocytosis of macrophages. Mitogen-activated protein kinase (MAPK) signaling pathway of macrophages was significantly activated by K7R^R and GT-deficient strains comparing with that of K7. Interestingly, in the presence of macromolecular CPS residues (>250 KD), K7(Δ*GT-1*) and K7(Δ*wcaJ*) could still be bounded by GH-K3, though with a modest adsorption efficiency, and showed minor virulence, suggesting that the CPS residues accumulated upon deletion

of *GT-1* or *wcaJ* did retain phage binding sites as well maintain mild virulence. In brief, our study defines, for the first time, the potential roles of GT-1, GT-2, and WcaJ in *K. pneumoniae* in bacterial virulence and generation of rough-type mutation under the pressure of bacteriophage.

Keywords: *Klebsiella pneumoniae*, phage resistance, virulence, glucosyltransferase (GT), WcaJ

INTRODUCTION

As important nosocomial and community-acquired opportunistic pathogens, *Klebsiella pneumoniae* (*K. pneumoniae*) spp. cause various infections, such as pneumonia, liver abscess, urinary tract infections, and complicated bacteremia (Podschun and Ullmann, 1998). In recent years, with the prevalence of antibiotic-resistant strains, traditional antibiotic therapies for infections caused by multidrug-resistant (MDR) *K. pneumoniae* has been limited (Munoz-Price et al., 2013; Robilotti and Deresinski, 2014; Humphries and Hemarajata, 2017). Therefore, due to the urgent need for alternative of antibiotic therapies, phage therapies have regained attention (Nobrega et al., 2015). However, *K. pneumoniae* strains are highly inclined to form phage-resistant mutants during phage treatment, which greatly limits the phage therapies (Labrie et al., 2010).

With sophisticated mechanisms, anti-phage mutations of bacteria usually occur at various stages of phage infection (Labrie et al., 2010). Especially, the abortion of adsorption is the most common bacteriophage resistance mechanism (Silva et al., 2016). Similar to other Gram-negative bacteria, the first and second phage adsorption receptors based on polysaccharides and outer membrane proteins of *K. pneumoniae* have been described (Cai et al., 2018). During the interaction of phage and host strain, majority of the anti-phage mutant colonies became small-rough type due to loss of cell-surface polysaccharides. Polysaccharides of various Gram-negative bacteria mainly comprised of lipopolysaccharide (LPS) (O antigen) and capsular polysaccharide (CPS) (K antigen) on the cell surface, which are directly regulated by *lps* and *cps* gene clusters, respectively (Whitfield, 2006). The LPS or CPS have been recognized as adsorption receptors for many phages (Pickard et al., 2010; Kiljunen et al., 2011; Sorensen et al., 2011). With mutation in LPS or CPS synthetic genes, O antigen or K antigen of phage-resistant strains is generally lost resulting phenotype with comparatively smaller colony and much lower phage adsorption efficiency than the parental wild type strains (Le et al., 2014; Li et al., 2018). Both O antigen and K antigen are involved in phage adsorption on *K. pneumoniae* (Thurow et al., 1975; Tomás et al., 1987), but which component serves as primary phage adsorption receptor is still inconclusive.

Because of enhancing bacterial adherence and protecting the strains from complement-mediated killing through opsonophagocytosis, LPS and CPS have also been widely recognized as the virulence factors (Alberti et al., 1996; Mushtaq et al., 2005). In our previous study, the virulence of *K. pneumoniae* K7-derived phage resistant strains were dramatically weaker than the wild-type strain (Gu et al., 2012), indicating that the variation of virulence factor might have occurred. With at least 79 serotypes have been recognized (Hsu et al., 2013; Pan et al., 2015a), virulence factor coding genes of *K. pneumoniae* are highly diverse. In addition to polysaccharides-related gene clusters, bacterial virulence is also regulated by transcriptional factors. It had been reported that the regulator of mucoid phenotype A (RmpA) plays as an important regulatory factor for maintaining mucoidy and pathogenicity of *K. pneumoniae* (Lai et al., 2003; Hsu et al., 2011). Rcs phosphorelay system also serves as modulators for polysaccharide synthesis-associated gene clusters (Su et al., 2018). Besides, the regulation of CPS synthesis by RcsB depends on the auxiliary role of RmpA (Cheng et al., 2010).

In the present work, the mechanisms of anti-phage mutation and virulence reduction of rough-type phage-resistant *K. pneumoniae* were revealed. By quantitative analysis with liquid chromatography-tandem mass spectrometry (LC-MS-MS), the abundance of three glycosyltransferases, GT-1, GT-2, and WcaJ was drastically altered in $K7R^R$ compared with the wild-type K7. Then the potential roles of three glycosyltransferases in bacterial virulence reduction and phage-resistance were studied.

MATERIALS AND METHODS

Ethics Statement

C57BL/6J mice (Female, 18–20 g) were purchased from Liaoning Changsheng Biotechnology Co. LTD (Benxi, Liaoning, China). All animal managements and experiments were strictly abided by the Regulations for the Administration of Affairs Concerning Experimental Animals approved by the State Council of the People's Republic of China (1.11.1988) and approved by the Animal Welfare and Research Ethics Committee at Jilin University.

Bacterial Strains and Phage

Phage GH-K3 and its host strain *K. pneumoniae* K7 were previously isolated and maintained in our laboratory (Gu et al., 2012). A rough-type, phage-resistant *K. pneumoniae* mutant strain was isolated and named as $K7R^R$ in a previous study (Cai et al., 2018).

Phage Adsorption Assay

Klebsiella pneumoniae strains were cultured until late-exponential phase (2×10^9 CFU/ml) and mixed with phages at the quantity ratio of 100:1 (bacteria: phage). The mixtures were incubated for 10 min at 37°C with shaking and then centrifuged at 4°C (13,000 × *g*, 5 min). After the supernatants were filtered with 0.22 μm filters (Millipore, Billerica, MA, United States), the phage particles remaining in supernatants were measured

by double-plate assay in triplicate and the phage adsorption efficiency were calculated as previously described (Le et al., 2013; Cai et al., 2018).

LC-MS-MS Analyses

K7 and K7R^R samples (three biological replicates) used for proteomic analyses were prepared as previously described (Hu et al., 2014; Liu et al., 2015). LC-MS-MS analyses were executed using a linear ion trap mass spectrometer (LTQ Velos Pro, Thermo Scientific, San Jose, CA, United States) equipped with nanoflow reversed-phase liquid chromatography (EASY-nLC 1000; Thermo Scientific, San Jose, CA, United States) at Peking University. Instrument parameter settings, sample loadings and subsequent data analyses were referred to our previous study (Cai et al., 2018). Raw MS files were searched with Mascot (version 2.3.02; Matrix Science Inc.) against annotated protein sequences of *K. pneumoniae* K7 (Genbank accession number: NKQH00000000). In order to classify differentially expressed protein data visually, a heat map analysis was performed by Heml 1.0 (Deng et al., 2014). Nomenclature of the heat map numbering scale and COG analysis were both processed by STRING (Szklarczyk et al., 2017).

Scanning Electron Microscopy

Klebsiella pneumoniae strains were grown to exponential phase (OD_{600} = 0.4–0.6) and then washed three times with sterile phosphate-buffered saline (PBS). After immobilized with 4% glutaraldehyde overnight, the strains were dehydrated by ethanol with different concentrations (20, 50, 70, 90, and 100%) and subsequently freeze-dried on cover glasses. Finally, bacterial surface morphology was observed by scanning electron microscopy (SEM) (Hitachi S-3400N, Hitachi High-Technologies Europe GmbH, Krefeld, Germany).

Construction of Gene Deleted Mutant Strains

K7(Δ*GT-1*), K7(Δ*GT-2*), and K7(Δ*wcaJ*) were constructed as previously described (Guo et al., 2014). Briefly, homologous recombination arms of *GT-1*, *GT-2,* and *wcaJ* obtained by overlap extension PCR were amplified and cloned into pUC19 cloning vector. After digestion with *Sal* I, these sequences used for target gene replacement were individually ligated to pCVD442(Km^r). Followed by electrotransformation into *Escherichia coli* SM10 λpir, the plasmid bearing strains were mixed with the recipient strain- *K. pneumoniae* K7 (1:1 *v*/*v*). The mixed bacteria were then centrifuged at 6,000 × *g* for 10 min and suspended with LB medium on a sterile membrane (Millipore, Billerica, MA, United States) at 30°C overnight. The mixed bacteria attached to the membrane were eluted with sterile saline and plated onto LB plates containing 30 μg/ml kanamycin and 100 μg/ml ampicillin. After 12 h of culture, the putative transconjugants of K7(Δ*GT-1*), K7(Δ*GT-2*), and K7(Δ*wcaJ*) were screened and verified by PCR. All primers used in this study are listed in **Supplementary Table S1**. The strains and plasmids used in this work are listed in **Supplementary Table S2**.

Polysaccharide Extraction and Electrophoresis

For polysaccharide analyses, *K. pneumoniae* strains were inoculated in LB medium and cultured overnight. Exopolysaccharide (EPS), including both CPS and LPS, were isolated from equal amounts of *K. pneumoniae* strains (1.0×10^9 CFU) by hot water-phenol extraction method as previously reported (Chuang et al., 2006). The polysaccharide solution obtained by chloroform extraction was further purified according to the method as previously described (Majkowska-Skrobek et al., 2016). Briefly, the nucleic acids and proteins in supernatant were precipitated by the addition of trichloroacetic acid (TCA; 20% *w*/*v*), and the solution was then centrifuged to discard the precipitate (16,000 × *g*, 1 h, 4°C). Next, the supernatant was passed through 3 volumes of 96% cold ethanol and placed at −20°C for 24 h, then the precipitate was collected by centrifugation (16,000 × *g*, 1 h, 4°C) and resuspended in deionized water. After removal of the LPS component by ultracentrifugation (100,000 × *g*, 20 h, 4°C), the crude CPS was dialyzed against an excess deionized water using a SERVAPOR® dialysis tubing (Serva, Heidelberg, Germany) with a molecular weight cut-off (MWCO) of 12–14 kDa. After removing low molecular weight impurities for 24 h (4°C), the purified CPS was lyophilized and weighed. The purity of CPS was verified as previously described (Cano et al., 2009).

Lipopolysaccharide of these strains was purified with LPS extraction kit (17141, iNtRON Biotechnology, Korea) according to the manufacturer's instructions. After separated by 12%-sodium dodecylsulfate-polyacrylamide gel electrophoresis (SDS-PAGE), CPS and LPS were visualized by alcian blue staining and silver staining, respectively (Fomsgaard et al., 1990; Moller et al., 1993). Additionally, polysaccharide quantification was performed by using BCPS-PURPALD ASSAY KIT as per manufacturer's instruction (GenMed Scientifics, Shanghai, China).

Quantitative Analyses of mRNA Level

The strain cultures were pelleted and washed twice with PBS. Then the total RNA was extracted using the Bacterial RNA Kit (Omega Bio-Tek Inc., Norcross, GA, United States). Less than 1 μg of total RNA was converted to cDNA using the PrimeScript RT reagent Kit with gDNA Eraser (Takara, Dalian, China). Subsequently, qRT-PCR was carried out utilizing SYBR® Premix Ex Taq^{TM} II (Tli RNaseH Plus) (Takara, Dalian, China). The primers were listed in **Supplementary Table S1**. Two-step programs were run on Applied Biosystems® 7500 Real-Time PCR System (Thermo Fisher, Germany) and all reactions were run in triplicate. Reactions were performed as follows: initial denaturation at 95°C for 30 s, followed by 40 cycles of 5 s at 95°C and 30 s at 60°C. Lastly, the temperature was increased from 55 to 95°C at a rate of 0.2°C/s to establish a melting curve. Gene expression levels were calculated by the delta CT method as follows: fold-change = $2^{-\Delta\Delta Ct}$, where ΔCt = Ct (specific transcript)-Ct (housekeeping transcript) and ΔΔCt = ΔCt (treatment) – ΔCt (control).

Determination of Virulence of Wild-Type and Mutant *K. pneumoniae* Strains

The virulence of wild-type and mutant *K. pneumoniae* strains were determined according to a previous study with some modifications (Xia et al., 2016). The mice were anesthetized intraperitoneally with ketamine (100 mg/kg) and xylazine (10 mg/kg), and were inoculated intranasally with different doses of *K. pneumoniae* K7, K7R^R, K7(Δ*GT-1*), K7(Δ*GT-2*), and K7(Δ*wcaJ*) suspensions (5×10^5, 5×10^6, 5×10^7, 5×10^8, 1×10^9, or 5×10^9 CFU/mouse) to determine the minimum dose that triggered 100% mortality over a 7-day follow-up period (minimum lethal dose [MLD]). In addition, in order to detect the survival rate of the same infection level, mice were challenged intranasally with 1×10^7 CFU/mouse [2 × MLD of K7] of *K. pneumoniae* K7, K7R^R, K7(Δ*GT-1*), K7(Δ*GT-2*), and K7(Δ*wcaJ*) (n = 10 in each group). The number of dead mice was recorded on daily basis. Finally, all the surviving mice were euthanized by intravenous injection of Fatal Plus (pentobarbital sodium) (100 mg/kg).

From each treatment group, three mice were randomly selected at 48 h post infection and were euthanized with Fatal Plus (pentobarbital sodium) (100 mg/kg). After carefully removed from thoracic cavity and photographed, the left and right lung tissues were separated and weighed immediately. The left lungs were fixed in 4% formalin and then embedded in paraffin. Then hematoxylin and eosin (H&E) staining was performed (Feldman and Wolfe, 2014). Briefly, paraffin sections were re-hydrated and stained with hematoxylin for 2–4 min. After washing with water, they were subsequently stained with eosin for 0.5–1 min. Followed by dehydration treatment, the sections were mounted with xylene based mounting medium. After that, histopathology analyses were performed by microscopy. To measure the level of cytokines, the right lung lobes were lysed using Tissue Extraction Reagent (Invitrogen, Waltham, MA, United States) according to the manufacturer's instructions followed by homogenition with a probe sonicator (Branson Ultrasonics, Danbury, CT, United States). The supernatants from the homogenates were obtained by centrifugation (5,000 × *g*, 10 min) at 4°C. Concentrations of interleukin-1β (IL-1β), interleukin-6 (IL-6), tumor necrosis factor-alpha (TNF-α), and interferon gamma (IFN-γ) in supernatants were detected using enzyme-linked immunosorbent assay (ELISA) kits (eBioscience, San Diego, CA, United States) according to the manufacturer's instructions.

Macrophage Phagocytosis and Cell Cytotoxicity Assay

The RAW264.7 cell line (ATCC HTB37) was purchased from the American Type Culture Collection (ATCC, Rockville, MD, United States) and maintained in Dulbecco's modified Eagle's medium (DMEM) (10% FBS, 100 U/ml penicillin and 100 mg/ml streptomycin) (all from Gibco BRL, Gaithersburg, MD, United States) at 37°C and 5% CO_2.

Klebsiella pneumoniae K7, K7R^R, K7(Δ*GT-1*), K7(Δ*GT-2*), and K7(Δ*wcaJ*) were stained with SYTO^{TM} 9 Green Fluorescent Nucleic Acid Stain (catalog number: S34854, Invitrogen, Carlsbad, CA, United States) according to the manufacturer's instructions and washed two times with PBS. RAW264.7 cells were seeded on 35 mm glass bottom culture dishes (801001, NEST, Wuxi, China). When adherent cells reached a density of 5×10^5 cells per well, the cell culture medium was changed to fresh DMEM without adding antibiotics and FBS, and the stained *K. pneumoniae* strains were added to the supernatants at a multiplicity of infection (MOI) of 10:1. After co-incubated with strains at 37°C for 2 h, the cells were washed three times and treated with gentamicin (200 μg/ml) for 1 h to kill the extracellular bacteria. The cells were then fixed in 4% paraformaldehyde (Sigma-Aldrich, St. Louis, MO, United States) for 15 min. Followed by permeabilization with 0.5% Triton X-100 (Sigma-Aldrich, St. Louis, MO, United States), cytoskeleton was stained with Phalloidin-iFluor 555 (ab176756; Abcam, Cambridge, MA, United States) (1:200 in 1% BSA) for 30 min. After two washes, nucleus was stained with Hoechst 33342 (Invitrogen, Waltham, MA, United States) (1:200) for 10 min. Endocytosis of cells incubated with *K. pneumoniae* was detected with laser scanning confocal microscopy (LSM710; Carl Zeiss, Germany).

Quantitative detection of intracellular bacterial loads was performed as previously described (Shi et al., 2016). The RAW264.7 cells were cultured in 12-well plates. When adherent cells reached a density of 5×10^5 cells per well, the *K. pneumoniae* strains were added to the supernatants (without antibiotics and FBS) at an MOI of 10:1 and coincubated for 2 h at 37°C. After gentamicin treated and washing three times with sterile PBS, the cells were lysed in 1% Triton X-100 immediately. Finally, the bacterial loads in each cell samples were measured by plating onto LB agar with multiple serial dilutions.

Meanwhile, cytotoxicity of the cells was measured in a 96-well plate by using CellTiter 96® AQ_{ueous} One Solution Reagent (MTS) (Promega, Madison, WI, United States) according to the manufacturer's instructions after incubation with purified CPS from K7 (10 μg) and different *K. pneumoniae* for 2 or 12 h. Cells without any treatment were served as controls. Cell viability was calculated as: ($OD_{490\ sample}$- $OD_{490\ blank}$)/($OD_{490\ control}$-$OD_{490\ blank}$) × 100. In addition, the multiplication efficacy of different bacteria in DMEM was measured by bacterial count.

Western Blot Analyses

To detected the expression levels of GT-1, GT-2, and WcaJ in different *K. pneumoniae* strains, polyclonal antibodies targeting the peptide antigens (**Supplementary Table S3**) of glucosyltransferases were prepared by PolyExpress^{TM} at GenScript Biological Technology Co., Ltd (Nanjing, China). To measure the signaling pathways of RAW264.7 cells, phospho-p38 monoclonal antibody (4511) and phospho-NF-κB p65 monoclonal antibody (4025) were purchased from Cell Signaling Technology (Danvers, MA, United States). Total proteins in RAW264.7 cells were extracted by T-PER^{TM} Tissue Protein Extraction Reagent and quantified by Pierce^{TM} BCA Protein Assay Kit according to the manufacturer's instructions (both from Thermo Scientific, Rockford, IL, United States). Identical amounts of each protein sample were separated by 12% SDS-PAGE prior to transfer to polyvinylidene difluoride (PVDF) membranes (Millipore, Billerica, MA, United States).

Immunoblot membranes were sequentially incubated with primary antibodies [anti-GT-1 (1: 1000), anti-GT-2 (1: 1000), anti-WcaJ (1: 2000), anti-OmpC (1: 1000), anti-DnaK (1: 2000), anti-pp38 (1: 1000), anti-pp65 (1: 1000), or anti-β-actin (1:1000)] and labeled with horseradish peroxidase (HRP)-conjugated goat anti-rabbit antibody (ab205718; Abcam, Cambridge, MA, United States) (1: 5000). Immunoblotting was performed using Immobilon^{TM} Western Chemiluminescent HRP Substrate (Millipore, Billerica, MA, United States) and detected with a chemiluminescence imaging system (Tanon 5200, Shanghai, China).

Statistical Analysis

Survival curve analyses were performed using log-rank (Mantel–Cox) test. While other statistical data presented in this study were processed by One-way or Two-way analysis of variance (ANOVA) or Student's *t*-tests. All charts are generated by GraphPad Prism 6 (GraphPad Software, Inc., San Diego, CA, United States). Standard error of the mean was represented by error bars. The data differences were considered statistically significant at P-values < 0.05.

RESULTS

K7R^R Showed Low Virulence in Mice Model

GH-K3 could not form plaques on *K. pneumoniae* K7R^R like other phage-resistant strains. Compared with *K. pneumoniae* K7, the precipitate of K7R^R was compact after centrifugation (10,000 × *g*, 5 min) (**Figure 1A**). Phage GH-K3 had been confirmed to possess an extremely low adsorption efficiency on *K. pneumoniae* K7R^R (3.9%) (Cai et al., 2018). We found that the adsorption efficiency of this phage showed very little improvement after prolonging the infection time to 1 h (8.9%) (**Figure 1B**). Besides, GH-K3 could not form spots on a lawn of K7R^R (**Figure 1C**). SEM analyses also showed that the boundaries of K7R^R were clearer than those of K7 strains (**Figure 1D**). Additionally, compared with the high- molecular weight CPS in K7, the molecular weight distribution of the polysaccharide residues in K7R^R was very wide, and some oligosaccharides (approximately 50 KD) were also included (**Figure 1E**), suggesting that the capsule synthesis was possibly interrupted on the cell surface of K7R^R. While, with the increased contents, the LPS components in K7R^R were not affected by the loss of CPS (**Supplementary Figure S1A**).

As a hypervirulent *K. pneumoniae* strain with K2 serotype (Cai et al., 2018), the minimum lethal dose (MLD) of intranasal inoculation of K7 was determined as 5.0×10^6 CFU/mouse. However, the rough-type variant strain K7R^R showed much weaker virulence with an MLD of 1.0×10^9 CFU/mouse. K7 infection (1.0×10^7 CFU/mouse, intranasally) significantly induced the up-regulation of pro-inflammatory cytokines in mice. The mice infected with K7 were all died within 96 h and the alveolar structures of their lungs were found almost completely lost. By contrast, mice challenged with K7R^R (same dose as K7) were all survived and showed much reduced damage to lungs.

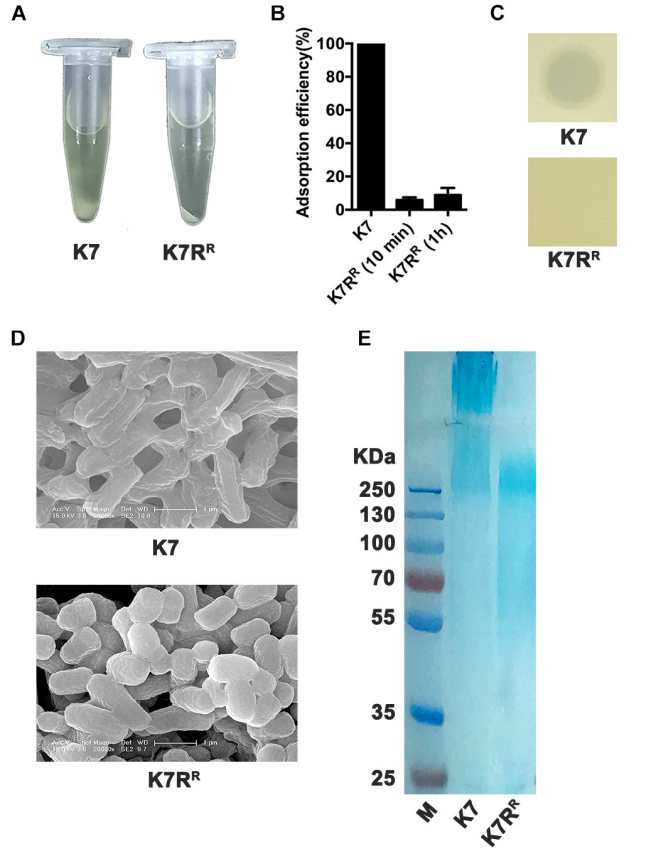

FIGURE 1 | Characteristics of *K. pneumoniae* K7 and K7R^R. **(A)** Centrifugation analysis of *K. pneumoniae* K7 and K7R^R. The cultures were centrifuged at 10,000 × *g* for 5 min at 4°C. **(B)** Adsorption efficiency of GH-K3 binding to *K. pneumoniae* K7 and K7R^R. Data represent the mean ± SEM of triplicate experiments. **(C)** Spot assays for GH-K3 on *K. pneumoniae* K7 and K7R^R. Five μl of phage solutions were spotted onto freshly lawns of *K. pneumoniae* K7 and K7R^R for 6 h at 37°C before observation. **(D)** SEM analyses of the surface morphology of *K. pneumoniae* K7 and K7R^R. Scale bars represent 1 μm. **(E)** CPS samples were extracted from equal amounts of *K. pneumoniae* strains (1.0×10^9 CFU). After separated by 12% SDS-PAGE, CPS phenotypes of K7 and K7R^R were visualized by alcian blue staining.

In addition, no significant difference was detected in the levels of cytokines including IL-1β, IL-6, TNF-α, and IFN-γ comparing with those of healthy mice at 48 h after infection (**Figure 2**).

Differential Protein Expression Between K7 and K7R^R

About 3100 proteins of K7 and K7R^R were compared after analyzed by LC-MS-MS. A total of 46 proteins of K7R^R were identified as differential proteins, including 16 up-regulated proteins and 30 down-regulated proteins (**Figure 3A**). Of these proteins, three glycosyltransferases in K7R^R were drastically repressed in abundance, including GT-1 (∼16.7-fold), GT-2 (∼14.2-fold), and WcaJ (∼8.1-fold) (**Figures 3A,B**), which belonged to Pfam family Glycos_transf_1 (PF00534), Pfam Family: Glyco_trans_1_4 (PF13692) and Pfam Family: Bac_transf (PF02397), respectively. Western blot and qPCR analyses further

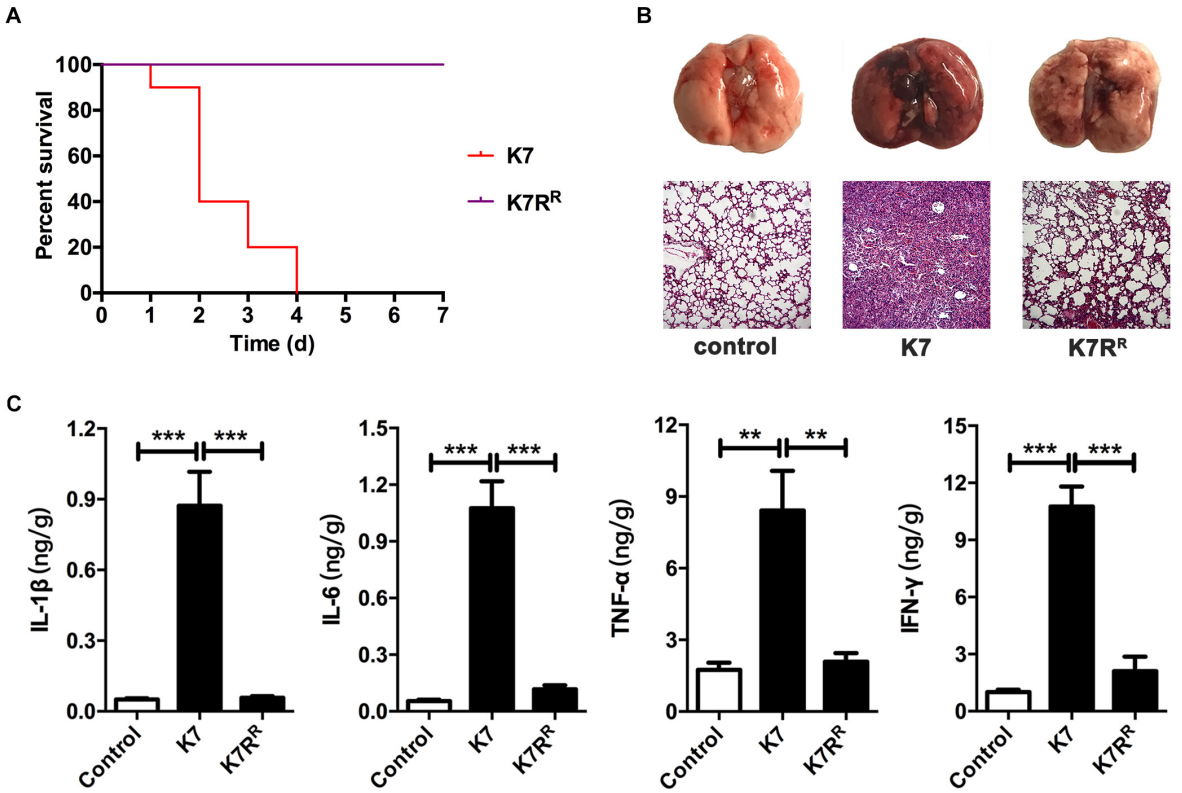

FIGURE 2 | Virulence evaluation of *K. pneumoniae* K7 and K7R^R *in vivo*. All the mice were challenged intranasally with 1 × 10^7 CFU/mouse of *K. pneumoniae* K7 and K7R^R. **(A)** Survival rates of mice challenged with *K. pneumoniae* K7 and K7R^R. Each group contained ten mice. Statistical analysis was performed using the Kaplan–Meier method [$P < 0.0001$, log-rank (Mantel–Cox) test]. **(B)** Pathological observation. At 48 h after infection, the lungs from mice challenged with *K. pneumoniae* K7 and K7R^R were carefully removed and photographed after euthanasia. Lung tissue sections were stained with hematoxylin and eosin (H&E) and then observed in a microscope at a magnification 100×. Lung tissues of healthy mice were served as controls. **(C)** The levels of cytokines. The levels of IL-1β, IL-6, TNF-α, and IFN-γ in lung tissue homogenates of mice infected by *K. pneumoniae* K7 and K7R^R were determined. Lung tissue homogenates of healthy mice were served as controls. ** and *** represent significant differences at $P < 0.01$ and $P < 0.001$, respectively. Data represent the mean ± SEM of triplicate experiments.

confirmed the down-regulation of these three proteins at the protein and mRNA levels, respectively (**Figure 3C** and **Supplementary Figure S2A**). As a colanic acid biosynthesis UDP-glucose lipid carrier transferase, WcaJ is mainly found in the strains with K1, K2, K5, K14, or K64 serotype CPS, serving as an important basis for the capsule classification of *K. pneumoniae* (Shu et al., 2009; Pan et al., 2015b). Besides *WcaJ*, *GT-1,* and *GT-2* are also located in a *cps* gene cluster consisting of 18 ORFs (between *galF* and *ugd*) (**Figure 3D**). So far, the actual roles of GT-1 and GT-2 in *K. pneumoniae* have not been reported. Surprisingly, besides *GT-1*, *GT-2,* and *wcaJ*, *K. pneumoniae* K7R^R has no genetic mutation at the genome level compared to K7.

Except for GT-1, GT-2, and WcaJ, the expression levels of other encoded proteins in the *cps* cluster showed no obviously change in K7R^R (**Figure 3B**). In addition, the expression levels of LPS synthesis-related proteins in K7R^R have also been changed. WabH, a lipopolysaccharide core biosynthesis glycosyl transferase, was upregulated ∼2.5-fold in abundance. ATP-binding-cassette (ABC) transporters typically drive uptake or secretion of substrates at the expense of ATP hydrolysis to ensure energy supply during sugar chain polymerization (Whitfield, 2006). Some of them were also moderately altered for ∼2.0-fold to 3.0-fold in expression levels, including three down-regulated proteins (KPN_00622, YrbF and KPN_02289) and two up-regulated proteins (MsbA and KPN_01617) (**Figure 3A**).

Deletions of GT-1, GT-2, or WcaJ Created Resistant Phenotype to Phage GH-K3

To identify the effects of GT-1, GT-2, and WcaJ in K7 on phage sensitivity, single gene deletion of *GT-1*, *GT-2,* and *wcaJ*, respectively, was performed in K7. As shown in **Figure 4A**, all the three GT-deficient strains K7(Δ*GT-1*), K7(Δ*GT-2*), and K7(Δ*wcaJ*) appeared small and rough type in colony morphology. Besides, compared with K7, the three mutant strains tend to form compact precipitation as K7R^R during centrifugation and mucoid polysaccharide capsules on the cell surface were almost disappeared (**Figures 4B,C**). Interestingly, K7(Δ*wcaJ*) resembled cocci unlike rod shape of K7, indicating that WcaJ may play a critical role in maintenance of bacterial morphology.

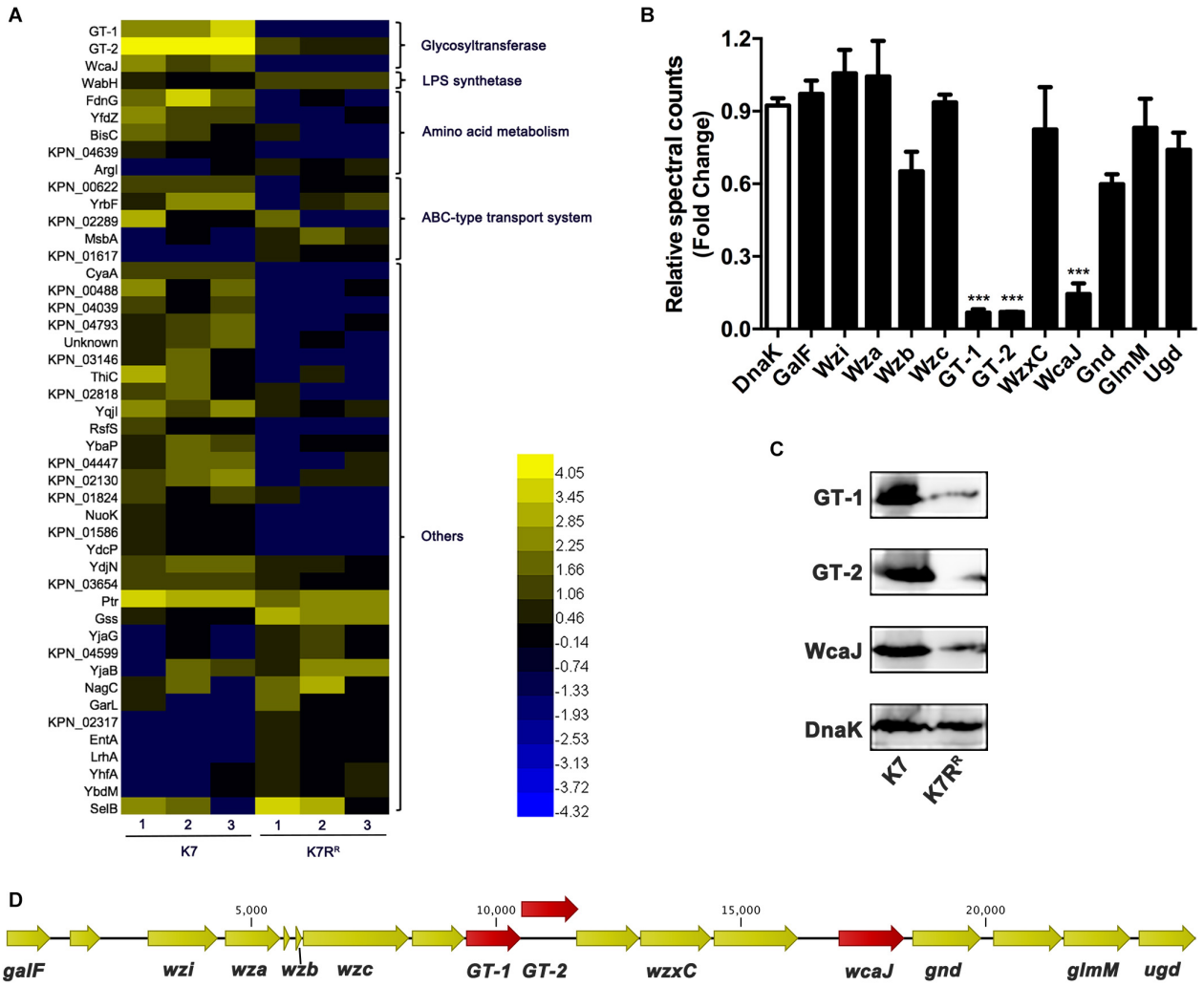

FIGURE 3 | The differentially expressed proteins between *K. pneumoniae* K7 and K7R^R. **(A)** Heat-map analysis of differentially expressed proteins between *K. pneumoniae* K7 and K7R^R. The heat-map was generated by Heml 1.0. Lanes 1–3 represent three biological replicates at each sampling time. Protein functional classification was performed by STRING, version 10.5. **(B)** Spectral count fold changes. The relative spectral counts of proteins encoded by *cps* gene cluster between *K. pneumoniae* K7 and K7R^R were analyzed. DnaK served as a loading control. Relative spectral count fold changes = (spectral counts of K7R^R)/(spectral counts of K7). ***represents significant differences at $P < 0.001$. Data represent the mean ± SEM of triplicate biological experiments at each sampling time. **(C)** Western blot analyses of GT-1, GT-2, and WcaJ. Expression levels of GT-1, GT-2, and WcaJ in *K. pneumoniae* K7 and K7R^R were detected. Expression of DnaK was detected as a control. **(D)** Schematic of *cps* gene cluster of *K. pneumoniae* K7 indicated by arrows with different colors. The arrow represents the direction of transcription.

By alcian blue staining, the molecular weights of polysaccharides in K7(Δ*GT-1*) and K7(Δ*wcaJ*) were found above 250 KD, but much lower than the CPS polymer of K7. While, like K7R^R, molecular weight of polysaccharide residues in K7(Δ*GT-2*) was widely distributed and some oligosaccharides (approximately 50 kD) were also detected. (**Figure 4D**), indicating that sugar chain polymerization in K7(Δ*GT-2*) might be further hindered compared with K7(Δ*GT-1*) and K7(Δ*wcaJ*). In addition, the composition of LPS in three GT-deficient strains was not changed and the production was obviously higher than that of K7 (**Supplementary Figure S1B**).

By western blot and qPCR analyses, the regulatory relationships among GT-1, GT-2, and WcaJ has been revealed. In both mRNA and protein levels, WcaJ was also down-regulated when the *GT-1* was deleted. The expression level of GT-2 was severely affected when *wcaJ* was deleted. However, the deletion of *GT-2* did not have a significant effect on the expression of GT-1 and WcaJ (**Supplementary Figures S2B, S3**), indicating that this glucosyltransferase may play an independent role in the assembly of sugar chains.

The sensitivity of K7(Δ*GT-1*), K7(Δ*GT-2*), and K7(Δ*wcaJ*) to phage GH-K3 was further measured. GH-K3 was unable to form plaques on any of the deficient strains K7(Δ*GT-1*), K7(Δ*GT-2*), and K7(Δ*wcaJ*). However, the phage could form spots on lawns of both K7(Δ*GT-1*) and K7(Δ*wcaJ*) (**Figure 5A**), suggesting that some phage-encoded proteins (such as lysin or depolymerase) of GH-K3 may recognize the macromolecular CPS residues of these two mutant strains. In spite of the

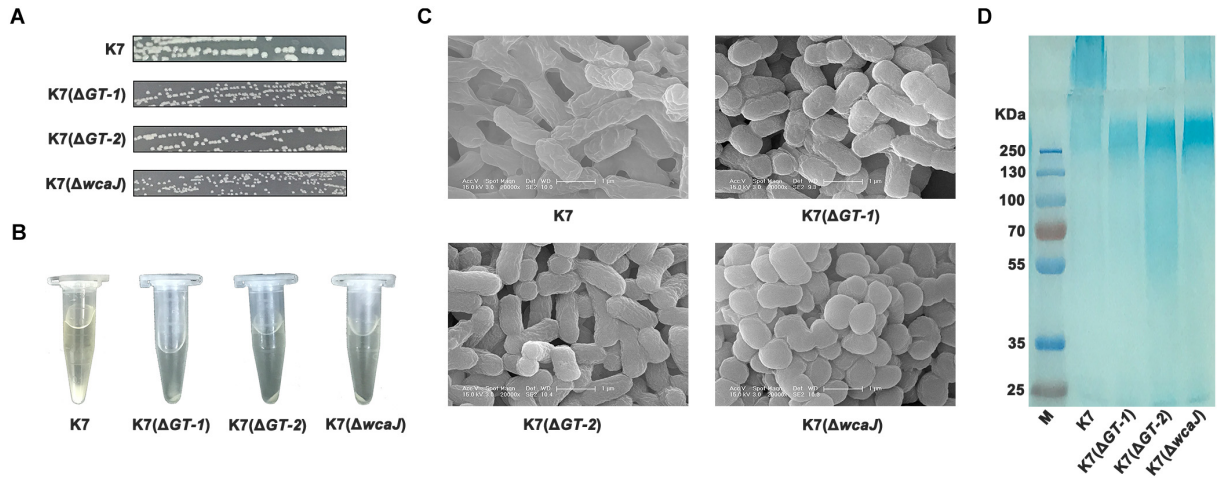

FIGURE 4 | Characteristics of *K. pneumoniae* K7(Δ*GT-1*), K7(Δ*GT-2*), and K7(Δ*wcaJ*). **(A)** Colony morphologies of *K. pneumoniae* K7(Δ*GT-1*), K7(Δ*GT-2*), and K7(Δ*wcaJ*). Colonies of K7(Δ*GT-1*), K7(Δ*GT-2*), and K7(Δ*wcaJ*) were cultured on LB plates at 37°C for 12 h after streak plating. The three mutant strains all form rough-type colonies. K7 was used as a control. **(B)** Centrifugation analysis of *K. pneumoniae* K7(Δ*GT-1*), K7(Δ*GT-2*), and K7(Δ*wcaJ*). The cultures were centrifuged at 10,000 × *g* for 5 min. K7 was used as a control. **(C)** SEM analyses of the surface morphology of *K. pneumoniae* K7(Δ*GT-1*), K7(Δ*GT-2*), and K7(Δ*wcaJ*). Scale bars represent 1 μm. K7 was used as a control. **(D)** CPS samples were extracted from equal amounts of *K. pneumoniae* strains (1.0×10^9 CFU). After separated by 12% SDS-PAGE, CPS phenotypes of K7(Δ*GT-1*), K7(Δ*GT-2*), and K7(Δ*wcaJ*) were visualized by alcian blue staining. CPS of K7 was used as a control.

adsorption efficiencies of GH-K3 on K7(Δ*GT-1*), K7(Δ*GT-2*), and K7(Δ*wcaJ*) were all markedly reduced (down to 21.1, 5.5, and 48.9%, respectively), the adsorption efficiencies of phage GH-K3 on both K7(Δ*GT-1*) and K7(Δ*wcaJ*) have a significant improvement after prolonging the adsorption time (1 h), with the adsorption efficiencies of 47.8 and 84.2%, respectively. However, the adsorption efficiency of GH-K3 on K7(Δ*GT-2*) did not change significantly with the extension of time, only reached 8.0% finally (**Figure 5B**).

Deletions of GT-1, GT-2, or WcaJ Resulted in the Decline of Virulence

For C57BL/6J mice, the MLDs for intranasal inoculation of K7(Δ*GT-1*), K7(Δ*GT-2*), and K7(Δ*wcaJ*) are 5.0×10^8 CFU/mouse, 1.0×10^9 CFU/mouse, and 5.0×10^8 CFU/mouse, respectively. According to the results of our 7-day monitoring, mice in all three groups survived after undergoing transient respiratory symptoms after administration with different mutant strains at a dose of 1.0×10^7 CFU/mouse (**Figure 6A**). Like $K7R^R$-infected mice, the lungs of K7(Δ*GT-1*), K7(Δ*GT-2*), and K7(Δ*wcaJ*)-challenged mice showed mild hyperemia, but the texture was still tough. The histopathological changes of lung tissues in K7(Δ*GT-1*) and K7(Δ*wcaJ*) infection groups were very similar. Although the alveolar walls had partial telangiectasia with a small amount of collapse, most of the alveolar structures maintained their normal morphology. While the lung tissues of mice infected with K7(Δ*GT-2*) had a better condition, similar to that of healthy mice (**Figure 6B**). In addition, cytokine levels in the K7(Δ*GT-2*) group was close to the level of healthy mice at 48 h post infection, while K7(Δ*GT-1*) and K7(Δ*wcaJ*) group were slightly higher than that of K7(Δ*GT-2*) group (**Figure 6C**).

GTs-Deficient *K. pneumoniae* Strains Promote Endocytosis and Activation Effects of Macrophages and Show Weaker Cytotoxicity

Both immunofluorescence analysis and plating assay showed that almost no intracellular *K. pneumoniae* K7 in RAW264.7 cells was detected, but $K7R^R$ had a high probability of being endocytosed. Like $K7R^R$, a large number of K7(Δ*GT-1*), K7(Δ*GT-2*), and K7(Δ*wcaJ*) strains could be recognized and endocytosed by macrophages. However, among the three strains, K7(Δ*GT-2*) seemed to have the highest macrophage endocytosis efficiency (**Figures 7A,B**), indicating that K7(Δ*GT-2*) is most easily cleared by the immune cells.

NF-κB and MAPKs signaling pathways of macrophages were detected when treated with *K. pneumoniae* strains. The expression levels of pp38 in RAW264.7 cells were substantially increased after co-incubation with $K7R^R$, K7(Δ*GT-1*), K7(Δ*GT-2*), or K7(Δ*wcaJ*). However, whether co-incubated with K7 or GT-deficient strains, pp65 expression levels remained unchanged in macrophages (**Figure 7C**). These suggest that induction of p38 phosphorylation is an important step to activate macrophages by *K. pneumoniae* after CPS loss.

The viability of the cells was measured by the amount of formazan produced by the cells (Cano et al., 2009). In spite of pure CPS from K7 (10 μg) has no obvious cytotoxic effect, capsular *K. pneumoniae* K7 has a significant killing effect on cells. After 2 h incubation with *K. pneumoniae* K7, the viability of the cells was reduced to 89.6%. Once the incubation time was increased to 12 h, the viability K7-incubated cells was only 26.2%. However, although, other non-capsulated bacteria did not show significant cytotoxicity within 2 h, the viability of the cells in these treatment groups was also decreased after 12 h.

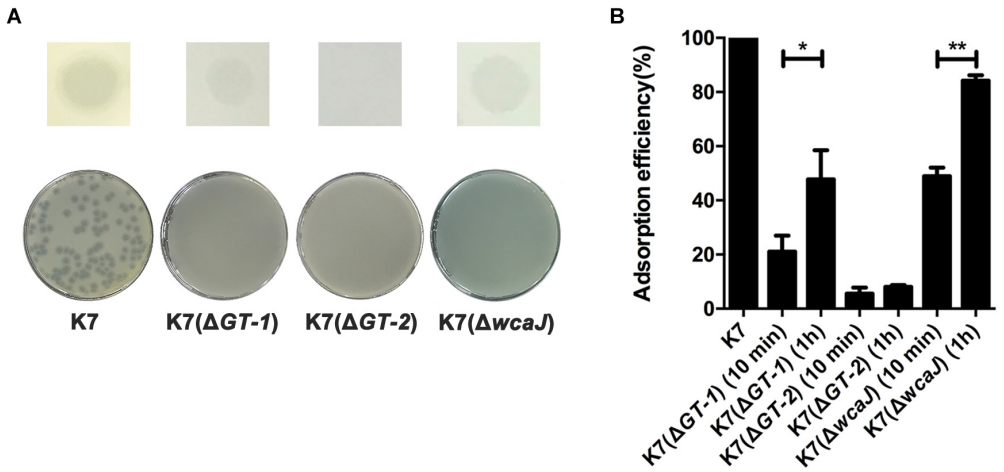

FIGURE 5 | Sensitivity of *K. pneumoniae* K7(Δ*GT-1*), K7(Δ*GT-2*), and K7(Δ*wcaJ*) to GH-K3. **(A)** Spot and plaque forming assays. Five μl of GH-K3 solutions were spotted onto freshly seeded lawns of *K. pneumoniae* K7(Δ*GT-1*), K7(Δ*GT-2*), and K7(Δ*wcaJ*) for 6 h at 37°C before observation (top). Meanwhile, the sensitivity of *K. pneumoniae* K7(Δ*GT-1*), K7(Δ*GT-2*), and K7(Δ*wcaJ*) to GH-K3 were determined by plaque assays (bottom). K7 was used as a control. **(B)** Adsorption efficiency. The adsorption efficiency of GH-K3 binding to *K. pneumoniae* K7(Δ*GT-1*), K7(Δ*GT-2*), and K7(Δ*wcaJ*) were determined. * and ** significant differences at $P < 0.05$ and $P < 0.01$, respectively. Data represent the mean ± SEM of triplicate experiments.

After K7(Δ*GT-1*) and K7(Δ*wcaJ*) incubation, the cell viability was 70.1 and 70.2%, respectively, which was lower than the 76.1% cell viability of K7(Δ*GT-2*)-incubated cells, suggesting that K7(Δ*GT-1*) and K7(Δ*wcaJ*) with macromolecular CPS residues could cause more severe cell damage than K7(Δ*GT-2*) (**Figure 7D**). However, *K. pneumoniae* K7, K7R^R, K7(Δ*GT-1*), K7(Δ*GT-2*), and K7(Δ*wcaJ*) grew almost synchronously within 12 h in DMEM (**Supplementary Figure S4**), indicating that the cytotoxicity comparison of K7 and other non-capsulated *K. pneumoniae* might be able to rule out the factor of multiplication efficacy. Thus, these data further demonstrate that the cytotoxicity of *K. pneumoniae* should be attributed to other bacterial components other than CPS. However, the capsular strain relies on the capsule to resist phagocytosis of macrophages, thereby accumulating cytotoxicity by stabilizing proliferation and causing significant cell-killing effects.

DISCUSSION

Rough-type phage-resistant *K. pneumoniae* strains caused by the mutations of primary phage receptors (cell surface polysaccharides) are much more common than the smooth-type after co-incubation of phage and host strain (Cai et al., 2018). In the present study, with intact LPS, CPS loss was found in a rough-type phage-resistant *K. pneumoniae* strain, K7R^R. At the same time, K7R^R showed virulence decline comparing with K7, which are consistent with the previous views of CPS to serve as primary phage receptor and as well as main virulence factor of *K. pneumoniae* K7 (Thurow et al., 1975; Paczosa and Mecsas, 2016). Previous studies have shown that rough-type phage-resistant mutant strains are generally accompanied by the loss of polysaccharide synthesis-associated proteins (Le et al., 2014; Li et al., 2018). However, the CPS synthesis-associated proteins that involved in K7R^R-like anti-phage mutation are still uncertain. Therefore, differential protein profile of K7 and K7R^R was detected by mass spectrometry and this was further verified by immunoblot analysis. In K7R^R, three glucosyltransferases (GT-1, GT-2, and WcaJ) encoded in the *cps* gene cluster were radically down-regulated in abundance with the reduction of CPS, suggesting that they might be associated with synthesis of cell surface polysaccharides, thereby maintaining phage sensitivity and bacterial virulence.

To further reveal the roles of GT-1, GT-2, and WcaJ in *K. pneumoniae*, the encoding genes were individually deleted. K7(Δ*GT-1*), K7(Δ*GT-2*), and K7(Δ*wcaJ*) all showed the loss of thick surface layers of CPS. Besides, all the GT-deficient strains presented no sensitivity to GH-K3. In our previous study, we identified that outer membrane protein C (OmpC) serves as secondary phage receptor for GH-K3 invasion, but its expression level was not repressed in K7R^R (Cai et al., 2018). Besides, deletion of *GT-1*, *GT-2,* or *wcaJ* in K7 did not cause down-regulation of OmpC (**Supplementary Figure S5**), suggesting that phage resistance mutation in this rough bacteria may be independent of the secondary phage receptor.

GH-K3 adsorption efficiency of periodate-treated K7 was substantially increased after prolonged incubation time (1 h) (Cai et al., 2018). However, the adsorption efficiency of K7R^R was almost unchanged within the same time period. Besides, unlike IO_4^- treated-K7, K7R^R had a stable non-mucoid colony morphology and cannot restore the capsule morphology after subculture (**Supplementary Figures S6A,B**). Additionally, compared with K7R^R, the expression levels of GT-1, GT-2, and WcaJ in IO_4^- treated-K7 were not obviously changed (**Supplementary Figure S7A**), suggesting that the three glucosyltransferases may be associated with the stable inheritance of capsular traits in *K. pneumoniae* K7. However, genetic

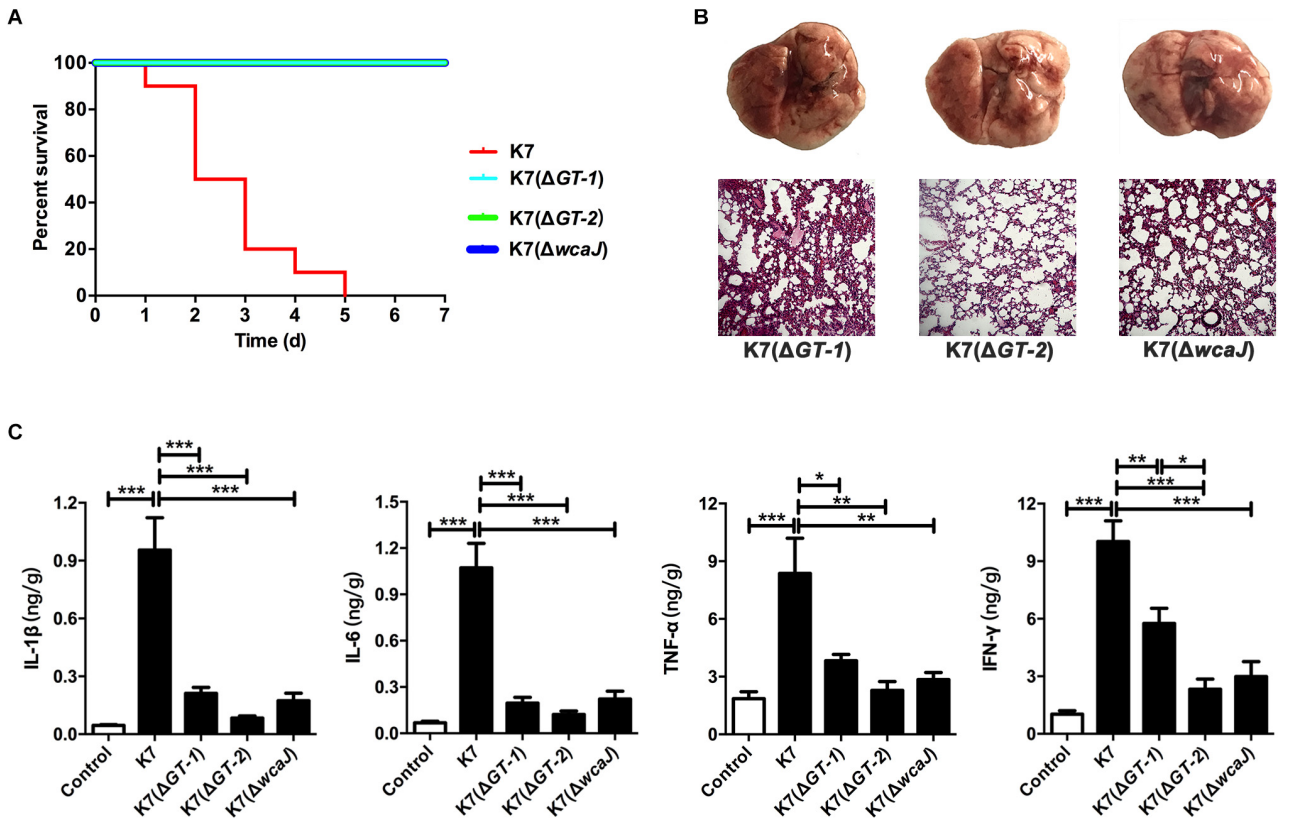

FIGURE 6 | Virulence evaluation of *K. pneumoniae* K7(Δ*GT-1*), K7(Δ*GT-2*), and K7(Δ*wcaJ*). All the mice were challenged intranasally with 1×10^7 CFU/mouse of *K. pneumoniae* K7, K7(Δ*GT-1*), K7(Δ*GT-2*), and K7(Δ*wcaJ*). **(A)** Survival rates. Survival rates of mice challenged with *K. pneumoniae* K7(Δ*GT-1*), K7(Δ*GT-2*), and K7(Δ*wcaJ*) were determined. Each group contained ten mice. Statistical analysis was performed using the Kaplan–Meier method by [$P < 0.0001$, log-rank (Mantel-Cox) test]. **(B)** Pathological observation. At 48 h after infection, the lungs of mice challenged with *K. pneumoniae* K7(Δ*GT-1*), K7(Δ*GT-2*), and K7(Δ*wcaJ*) were carefully removed and photographed after euthanasia. Lung tissue sections were stained with H&E and then observed in a microscope at a magnification 100×. Lung tissues of healthy mice were served as controls. **(C)** The levels of four cytokines. The levels of IL-1β, IL-6, TNF-α, and IFN-γ in lung tissue homogenates of mice infected by *K. pneumoniae* K7(Δ*GT-1*), K7(Δ*GT-2*), and K7(Δ*wcaJ*) were determined. Lung tissue homogenates of healthy mice were served as controls. *, **, and *** represent significant differences at $P < 0.05$, $P < 0.01$, and $P < 0.001$, respectively. Data represent the mean ± SEM of triplicate experiments.

mutations have not been detected in the whole genome of K7R^R including *GT-1*, *GT-2*, and *wcaJ* compared to wild-type strain. Thus, in this phage-resistant strain, we hypothesized that the down-regulation of transcription and expression levels of three glucosyltransferases may result from epigenetic modifications, such as DNA methylation (Goldfarb et al., 2015).

Compared with K7, both K7R^R and IO_4^- treated-K7 have undergone the processes of CPS loss. However, different from K7R^R, the molecular weight of polysaccharide residues of IO_4^- treated-K7 was similar to that of K7(Δ*GT-1*) and K7(Δ*wcaJ*) (**Supplementary Figure S7B**). Both K7(Δ*GT-1*) and K7(Δ*wcaJ*) also increased their GH-K3 adsorption efficiencies significantly by prolonging the incubation time. Besides, the phage can form blurred spots on the two strains. While, with K7R^R-like polysaccharide residues, K7(Δ*GT-2*) also cannot improve its low GH-K3 adsorption efficiency after prolonging the incubation time. These data may indicate that GH-K3 still has certain recognition and adsorption capacity for macromolecular CPS residues caused by IO_4^- treatment or *GT-1*, *wcaJ* deletion, but not for polysaccharide residues in K7R^R or K7(Δ*GT-2*).

In K7R^R and three GT-deficient strains, the sharp decline in the yield of CPS was accompanied by the production of a large amount of LPS. Additionally, the down-regulated glucosyltransferases in K7R^R caused moderate up-regulated of some LPS synthetases, such as WabH. In addition to the loss phage receptors, the blocking of receptors is also an important strategy of preventing phage adsorption (Labrie et al., 2010). Thus, despite GH-K3 seems to be able to adsorb to macromolecular CPS residues, its binding to the host outer membrane protein may be blocked by a new physical barrier that could be formed by the increased LPS. Previously, relationships of interdependence and transformation between CPS and LPS have been identified (Izquierdo et al., 2003; Ren et al., 2016). In the present work, the total bacterial polysaccharide contents of equal amounts (1.0×10^9 CFU) of K7 and K7R^R were almost the same (166 vs. 168 μg), indicating the synthesis of CPS and LPS seemed to have a dynamic equilibrium relationship. Moreover, the alteration in abundance of ABC-type transport system may imply the readjusting of the energy supply in mutant cells during CPS loss and LPS production.

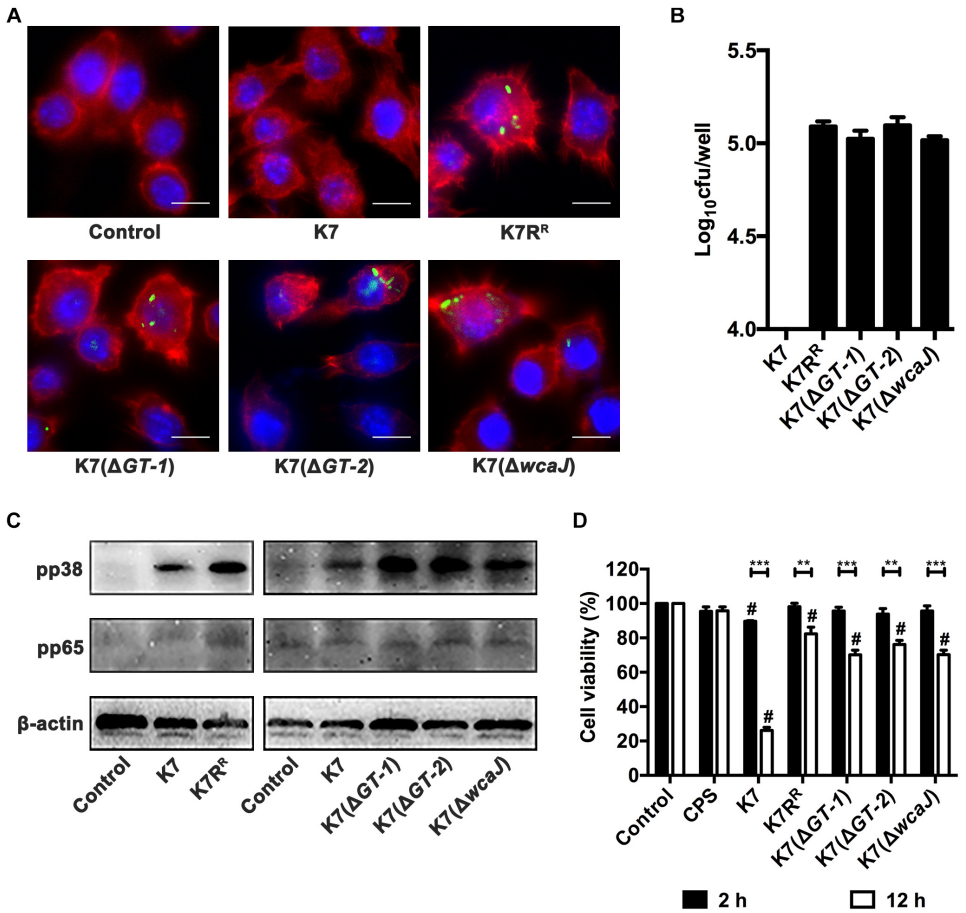

FIGURE 7 | Endocytosis, activation and cytotoxicity of RAW264.7 cells after incubation with different *K. pneumoniae* strains. **(A)** Immunofluorescence analysis of endocytosis effects of RAW264.7 cells after incubation with different *K. pneumoniae* strains. *K. pneumoniae* K7, K7R^R, K7(Δ*GT-1*), K7(Δ*GT-2*), and K7(Δ*wcaJ*) were stained with SYTO^{TM} 9 Green Fluorescent Nucleic Acid Stain. The *K. pneumoniae* strains were then co-incubated with RAW264.7 cells in antibiotic-free supernatants. Cytoskeleton and nuclei were stained with Phalloidin-iFluor 555 and Hoechst 33342, respectively. The endocytosis of these *K. pneumoniae* strains in RAW264.7 cells was determined with a laser scanning confocal microscope and then observed at a magnification 1000× (scale bar, 10 μm. Images shown are representative of three independent experiments). **(B)** The bacterial loads of intracellular *K. pneumoniae* in RAW264.7 cells. Cells (5×10^5) were incubated with K7, K7R^R, K7(Δ*GT-1*), K7(Δ*GT-2*), and K7(Δ*wcaJ*) at 37°C for 2 h. After gentamicin treatment and cell lysis, bacterial loads in each cell samples were determined by plating. Data represent the mean ± SEM of triplicate experiments. **(C)** Expression levels of pp38 and pp65 in RAW264.7 cells after incubation with *K. pneumoniae* K7, K7R^R, K7(Δ*GT-1*), K7(Δ*GT-2*), and K7(Δ*wcaJ*). Untreated cells were used as controls. β-actin served as a loading control. **(D)** Cytotoxicity analysis of RAW264.7 cells after incubation with purified CPS from K7 (10 μg) or different *K. pneumoniae* for 2 or 12 h. Cells without any treatment were served as controls and their viability was set as 100%. The statistical differences between different treatment groups and control group were labled with # ($P < 0.05$); the statistical differences of the same treatment groups at different time periods (2 or 12 h) were labled with ** ($P < 0.01$), and *** ($P < 0.001$). Data represent the mean ± SEM of triplicate experiments.

With extremely obvious lesions at 48 h after infection, the level of pro-inflammatory cytokines in K7-infected mice was significantly higher than in other groups of mice infected with non-capsulated bacteria. This observation at first sight, seems to be contradictory as non-capsular *K. pneumoniae* strains are expected to elicit potent inflammatory responses than the capsular strains (Yoshida et al., 2000, 2001). However, these previous results were generally based on data obtained during early stage of infection (approximately 6–24 h), whereby, the unencapsulated *K. pneumoniae* strains tend to be bound by complement C3, which greatly increases their probability of being phagocytosed by macrophages and then eliminated by cell-killing effects, such as those mediated by neutrophils or complements (Alvarez et al., 2000; Cortes et al., 2002). Similarly, *K. pneumoniae* K7R^R, K7(Δ*GT-1*), K7(Δ*GT-2*), and K7(Δ*wcaJ*) are more susceptible to be endocytosed by RAW 264.7 cells. Due to the rapid recognition by the immune cells, capsule-deficient bacteria also can quickly induce the up-regulation of pro-inflammatory cytokines in the body. However, these bacteria are cleared by the immune responses in a short period of time, which is likely to cause the cytokine levels to rise and fall (Renois et al., 2011). Surprisingly, histopathological examination and ELISA test demonstrated that the mice in the K7(Δ*GT-1*) and K7(Δ*wcaJ*)-infected groups showed an insignificant inflammatory response after 48 h of infection. Moreover, macrophages had lower endocytosis efficiencies on K7(Δ*GT-1*)

and K7(Δ*wcaJ*) than K7(Δ*GT-2*). The macromolecular CPS residues of K7(Δ*GT-1*) and K7(Δ*wcaJ*) may cause certain obstacles for macrophage phagocytosis and complement binding. Therefore, these factors may together cause the invasiveness of K7(Δ*GT-1*) and K7(Δ*wcaJ*) to be slightly lower than that of K7(Δ*GT-2*).

With the prolongation of time, the level of pro-inflammatory cytokines produced by the capsular *K. pneumoniae*-infected organism is generally in an increasing trend (Yoshida et al., 2000; 2001). In addition to impeding the complement binding, *K. pneumoniae* with K2 serotype lacks the specific mannose residue repeats are recognized by macrophages, thereby avoiding phagocytosis (Corsaro et al., 2005; March et al., 2013). We also found that *K. pneumoniae* K7 can hardly be endocytosed by RAW264.7 cells. In spite of capsular bacteria cannot induce the rapid production of pro-inflammatory cytokines in the early stage of infection, they can stably proliferate in the infected host (Lee et al., 2017). Further, the accumulated capsular strains induce the secretion of pro-inflammatory cytokines through various signaling pathways, such as TLR4 (Yang et al., 2011) or NLRP3 (Hua et al., 2015), ultimately leading to irreversible organic damage, just like the lung tissues of K7-challenged mice at 48 h after infection.

In summary, our study confirmed that the phage resistance and virulence decline of *K. pneumoniae* strains are mainly linked with the decline of CPS. By mass spectrometry and gene deletion assays, the CPS reduction is most likely associated with the downregulation of the abundance of three glycosyltransferases encoded by the *cps* gene cluster including GT-1, GT-2, and WcaJ. To further determining the specific functions of the three glycosyltransferases, wild-type genes *GT-1*, *GT-2,* and *wcaJ* were also individually reintroduced into mutant strains-K7(Δ*GT-1*), K7(Δ*GT-2*), and K7(Δ*wcaJ*) by pUC18K plasmid. However, these complement plasmids could not be stably maintained in these mutant strains. Therefore, in our follow-up studies, we will continue to seek other suitable complement plasmids to break through this technical bottleneck. Moreover, as a potential new mechanism for inducing phage resistance and virulence decline in *K. pneumoniae*, the mechanism of the decrease in the expression of three glucosyltransferases is also worthy of further exploration.

ETHICS STATEMENT

C57BL/6J mice (Female, 18–20 g) were purchased from Liaoning Changsheng Biotechnology Co. Ltd (Benxi, Liaoning, China). All animal managements and experiments were strictly abided by the Regulations for the Administration of Affairs Concerning Experimental Animals approved by the State Council of the People's Republic of China (1.11.1988) and approved by the Animal Welfare and Research Ethics Committee at Jilin University.

AUTHOR CONTRIBUTIONS

JG and WH conceived and designed the study. RC, SL, MC, ZG, YJ, HX, CZ, XW, YX, ZW, HZ, YF, CS, XF, LL, and YY performed the laboratory testing. RC, MW, and XL contributed to the LC-MS-MS analyses. RC, GW, and SR were responsible for the writing and revision of the manuscript. All authors read and approved the final manuscript.

FUNDING

This work was financially supported through grants from the National Natural Science Foundation of China (Nos. 31872505 and 31572553), the National Key Research and Development Program of China (No. 2018YFD0500504), the Achievement Transformation Project of the First Hospital of Jilin University (No. JDYYZH-1902025), and the Jilin Province Science Foundation for Youths (Changchun, China; Grant No. 20190103106JH).

SUPPLEMENTARY MATERIAL

The Supplementary Material for this article can be found online at: https://www.frontiersin.org/articles/10.3389/fmicb.2019.01189/full#supplementary-material

REFERENCES

Alberti, S., Alvarez, D., Merino, S., Casado, M. T., Vivanco, F., Tomas, J. M., et al. (1996). Analysis of complement C3 deposition and degradation on *Klebsiella pneumoniae*. *Infect. Immun.* 64, 4726–4732.

Alvarez, D., Merino, S., Tomas, J. M., Benedi, V. J., and Alberti, S. (2000). Capsular polysaccharide is a major complement resistance factor in lipopolysaccharide O side chain-deficient *Klebsiella pneumoniae* clinical isolates. *Infect. Immun.* 68, 953–955. doi: 10.1128/iai.68.2.953-955.2000

Cai, R., Wu, M., Zhang, H., Zhang, Y., Cheng, M., Guo, Z., et al. (2018). A smooth-type, phage-resistant *Klebsiella pneumoniae* mutant strain reveals OmpC is indispensable for GH-K3 infection. *Appl. Environ. Microbiol.* 84:e1585-18. doi: 10.1128/AEM.01585-18

Cano, V., Moranta, D., Llobet-Brossa, E., Bengoechea, J. A., and Garmendia, J. (2009). *Klebsiella pneumoniae* triggers a cytotoxic effect on airway epithelial cells. *BMC Microbiol.* 9:156. doi: 10.1186/1471-2180-9-156

Cheng, H. Y., Chen, Y. S., Wu, C. Y., Chang, H. Y., Lai, Y. C., and Peng, H. L. (2010). RmpA regulation of capsular polysaccharide biosynthesis in *Klebsiella pneumoniae* CG43. *J. Bacteriol.* 192, 3144–3158. doi: 10.1128/JB.00031-10

Chuang, Y. P., Fang, C. T., Lai, S. Y., Chang, S. C., and Wang, J. T. (2006). Genetic determinants of capsular serotype K1 of *Klebsiella pneumoniae* causing primary pyogenic liver abscess. *J. Infect. Dis.* 193, 645–654. doi: 10.1086/499968

Corsaro, M. M., De Castro, C., Naldi, T., Parrilli, M., Tomas, J. M., and Regue, M. (2005). 1H and 13C NMR characterization and secondary structure of the K2 polysaccharide of *Klebsiella pneumoniae* strain 52145. *Carbohydr. Res.* 340, 2212–2217. doi: 10.1016/j.carres.2005.07.006

Cortes, G., Borrell, N., de Astorza, B., Gomez, C., Sauleda, J., and Alberti, S. (2002). Molecular analysis of the contribution of the capsular polysaccharide and the lipopolysaccharide O side chain to the virulence of *Klebsiella pneumoniae* in a murine model of pneumonia. *Infect. Immun.* 70, 2583–2590. doi: 10.1128/iai.70.5.2583-2590.2002

Deng, W., Wang, Y., Liu, Z., Cheng, H., and Xue, Y. (2014). HemI: a toolkit for illustrating heatmaps. *PLoS One* 9:e111988. doi: 10.1371/journal.pone.0111988

Feldman, A. T., and Wolfe, D. (2014). Tissue processing and hematoxylin and eosin staining. *Methods Mol. Biol.* 1180, 31–43. doi: 10.1007/978-1-4939-1050-2_3

Fomsgaard, A., Freudenberg, M. A., and Galanos, C. (1990). Modification of the silver staining technique to detect lipopolysaccharide in polyacrylamide gels. *J. Clin. Microbiol.* 28, 2627–2631.

Goldfarb, T., Sberro, H., Weinstock, E., Cohen, O., Doron, S., Charpak-Amikam, Y., et al. (2015). BREX is a novel phage resistance system widespread in microbial genomes. *EMBO J.* 34, 169–183. doi: 10.15252/embj.201489455

Gu, J., Liu, X., Li, Y., Han, W., Lei, L., Yang, Y., et al. (2012). A method for generation phage cocktail with great therapeutic potential. *PLoS One* 7:e31698. doi: 10.1371/journal.pone.0031698

Guo, X., Cao, C., Wang, Y., Li, C., Wu, M., Chen, Y., et al. (2014). Effect of the inactivation of lactate dehydrogenase, ethanol dehydrogenase, and phosphotransacetylase on 2,3-butanediol production in *Klebsiella pneumoniae* strain. *Biotechnol. Biofuels* 7:44. doi: 10.1186/1754-6834-7-44

Hsu, C. R., Lin, T. L., Chen, Y. C., Chou, H. C., and Wang, J. T. (2011). The role of *Klebsiella pneumoniae* rmpA in capsular polysaccharide synthesis and virulence revisited. *Microbiology* 157(Pt 12), 3446–3457. doi: 10.1099/mic.0.050336-0

Hsu, C. R., Lin, T. L., Pan, Y. J., Hsieh, P. F., and Wang, J. T. (2013). Isolation of a bacteriophage specific for a new capsular type of *Klebsiella pneumoniae* and characterization of its polysaccharide depolymerase. *PLoS One* 8:e70092. doi: 10.1371/journal.pone.0070092

Hu, M., Liu, Y., Yu, K., and Liu, X. (2014). Decreasing the amount of trypsin in in-gel digestion leads to diminished chemical noise and improved protein identifications. *J. Proteom.* 109, 16–25. doi: 10.1016/j.jprot.2014.06.017

Hua, K. F., Yang, F. L., Chiu, H. W., Chou, J. C., Dong, W. C., Lin, C. N., et al. (2015). Capsular polysaccharide is involved in nlrp3 inflammasome activation by *Klebsiella pneumoniae* serotype K1. *Infect. Immun.* 83, 3396–3409. doi: 10.1128/IAI.00125-15

Humphries, R. M., and Hemarajata, P. (2017). Resistance to ceftazidime-avibactam in *Klebsiella pneumoniae* due to porin mutations and the increased expression of KPC-3. *Antimicrob. Agents Chemother.* 61:e537-17.

Izquierdo, L., Coderch, N., Pique, N., Bedini, E., Corsaro, M. M., Merino, S., et al. (2003). The *Klebsiella pneumoniae* wabG gene: role in biosynthesis of the core lipopolysaccharide and virulence. *J. Bacteriol.* 185, 7213–7221. doi: 10.1128/jb.185.24.7213-7221.2003

Kiljunen, S., Datta, N., Dentovskaya, S. V., Anisimov, A. P., Knirel, Y. A., Bengoechea, J. A., et al. (2011). Identification of the lipopolysaccharide core of *Yersinia pestis* and *Yersinia pseudotuberculosis* as the receptor for bacteriophage phiA1122. *J. Bacteriol.* 193, 4963–4972. doi: 10.1128/JB.00339-11

Labrie, S. J., Samson, J. E., and Moineau, S. (2010). Bacteriophage resistance mechanisms. *Nat. Rev. Microbiol.* 8, 317–327. doi: 10.1038/nrmicro2315

Lai, Y. C., Peng, H. L., and Chang, H. Y. (2003). RmpA2, an activator of capsule biosynthesis in *Klebsiella pneumoniae* CG43, regulates K2 cps gene expression at the transcriptional level. *J. Bacteriol.* 185, 788–800. doi: 10.1128/jb.185.3.788-800.2003

Le, S., He, X., Tan, Y., Huang, G., Zhang, L., Lux, R., et al. (2013). Mapping the tail fiber as the receptor binding protein responsible for differential host specificity of *Pseudomonas aeruginosa* bacteriophages PaP1 and JG004. *PLoS One* 8:e68562. doi: 10.1371/journal.pone.0068562

Le, S., Yao, X., Lu, S., Tan, Y., Rao, X., Li, M., et al. (2014). Chromosomal DNA deletion confers phage resistance to *Pseudomonas aeruginosa*. *Sci. Rep.* 4:4738. doi: 10.1038/srep04738

Lee, C. H., Chuah, S. K., Tai, W. C., Chang, C. C., and Chen, F. J. (2017). Delay in human neutrophil constitutive apoptosis after infection with *Klebsiella pneumoniae* Serotype K1. *Front. Cell. Infect. Microbiol.* 7:87. doi: 10.3389/fcimb.2017.00087

Li, G., Shen, M., Yang, Y., Le, S., Li, M., Wang, J., et al. (2018). Adaptation of *Pseudomonas aeruginosa* to phage PaP1 predation via O-antigen polymerase mutation. *Front. microbiol.* 9:1170. doi: 10.3389/fmicb.2018.01170

Liu, Y., Zhang, Q., Hu, M., Yu, K., Fu, J., Zhou, F., et al. (2015). Proteomic analyses of intracellular *Salmonella enterica* serovar typhimurium reveal extensive bacterial adaptations to infected host epithelial cells. *Infect. Immun.* 83, 2897–2906. doi: 10.1128/IAI.02882-14

Majkowska-Skrobek, G., Latka, A., Berisio, R., Maciejewska, B., Squeglia, F., Romano, M., et al. (2016). Capsule-targeting depolymerase, derived from *Klebsiella* KP36 phage, as a tool for the development of anti-virulent strategy. *Viruses* 8:E324. doi: 10.3390/v8120324

March, C., Cano, V., Moranta, D., Llobet, E., Perez-Gutierrez, C., Tomas, J. M., et al. (2013). Role of bacterial surface structures on the interaction of *Klebsiella pneumoniae* with phagocytes. *PLoS One* 8:e56847. doi: 10.1371/journal.pone.0056847

Moller, H. J., Heinegard, D., and Poulsen, J. H. (1993). Combined alcian blue and silver staining of subnanogram quantities of proteoglycans and glycosaminoglycans in sodium dodecyl sulfate-polyacrylamide gels. *Anal. Biochem.* 209, 169–175. doi: 10.1006/abio.1993.1098

Munoz-Price, L. S., Poirel, L., Bonomo, R. A., Schwaber, M. J., Daikos, G. L., Cormican, M., et al. (2013). Clinical epidemiology of the global expansion of *Klebsiella pneumoniae* carbapenemases. *Lancet Infect. Dis.* 13, 785–796. doi: 10.1016/S1473-3099(13)70190-7

Mushtaq, N., Redpath, M. B., Luzio, J. P., and Taylor, P. W. (2005). Treatment of experimental *Escherichia coli* infection with recombinant bacteriophage-derived capsule depolymerase. *J. Antimicrob. Chemother.* 56, 160–165. doi: 10.1093/jac/dki177

Nobrega, F. L., Costa, A. R., Kluskens, L. D., and Azeredo, J. (2015). Revisiting phage therapy: new applications for old resources. *Trends Microbiol.* 23, 185–191. doi: 10.1016/j.tim.2015.01.006

Paczosa, M. K., and Mecsas, J. (2016). *Klebsiella pneumoniae*: going on the offense with a strong defense. *Microbiol. Mol. Biol. Rev.* 80, 629–661. doi: 10.1128/MMBR.00078-15

Pan, Y. J., Lin, T. L., Chen, C. T., Chen, Y. Y., Hsieh, P. F., Hsu, C. R., et al. (2015a). Genetic analysis of capsular polysaccharide synthesis gene clusters in 79 capsular types of *Klebsiella* spp. *Sci. Rep.* 5:15573. doi: 10.1038/srep15573

Pan, Y. J., Lin, T. L., Lin, Y. T., Su, P. A., Chen, C. T., Hsieh, P. F., et al. (2015b). Identification of capsular types in carbapenem-resistant *Klebsiella pneumoniae* strains by wzc sequencing and implications for capsule depolymerase treatment. *Antimicrob. Agents Chemother.* 59, 1038–1047. doi: 10.1128/AAC.03560-14

Pickard, D., Toribio, A. L., Petty, N. K., van Tonder, A., Yu, L., Goulding, D., et al. (2010). A conserved acetyl esterase domain targets diverse bacteriophages to the Vi capsular receptor of *Salmonella enterica* serovar typhi. *J. Bacteriol.* 192, 5746–5754. doi: 10.1128/JB.00659-10

Podschun, R., and Ullmann, U. (1998). *Klebsiella* spp. as nosocomial pathogens: epidemiology, taxonomy, typing methods, and pathogenicity factors. *Clin. Microbiol. Rev.* 11, 589–603. doi: 10.1128/cmr.11.4.589

Ren, G., Wang, Z., Li, Y., Hu, X., and Wang, X. (2016). Effects of lipopolysaccharide core sugar deficiency on colanic acid biosynthesis in *Escherichia coli*. *J. Bacteriol.* 198, 1576–1584. doi: 10.1128/JB.00094-16

Renois, F., Jacques, J., Guillard, T., Moret, H., Pluot, M., Andreoletti, L., et al. (2011). Preliminary investigation of a mice model of *Klebsiella pneumoniae* subsp. ozaenae induced pneumonia. *Microbes Infect.* 13, 1045–1051. doi: 10.1016/j.micinf.2011.05.013

Robilotti, E., and Deresinski, S. (2014). Carbapenemase-producing *Klebsiella pneumoniae*. *F1000Prime Rep.* 6:80. doi: 10.12703/P6-80

Shi, S. H., Yang, W. T., Huang, K. Y., Jiang, Y. L., Yang, G. L., Wang, C. F., et al. (2016). beta-glucans from *Coriolus versicolor* protect mice against *S. typhimurium* challenge by activation of macrophages. *Int. J. Biol. Macromol.* 86, 352–361. doi: 10.1016/j.ijbiomac.2016.01.058

Shu, H. Y., Fung, C. P., Liu, Y. M., Wu, K. M., Chen, Y. T., Li, L. H., et al. (2009). Genetic diversity of capsular polysaccharide biosynthesis in *Klebsiella pneumoniae* clinical isolates. *Microbiology* 155(Pt 12), 4170–4183. doi: 10.1099/mic.0.029017-0

Silva, J. B., Storms, Z., and Sauvageau, D. (2016). Host receptors for bacteriophage adsorption. *FEMS Microbiol. Lett.* 363:fnw002. doi: 10.1093/femsle/fnw002

Sorensen, M. C., van Alphen, L. B., Harboe, A., Li, J., Christensen, B. B., Szymanski, C. M., et al. (2011). Bacteriophage F336 recognizes the capsular phosphoramidate modification of *Campylobacter jejuni* NCTC11168. *J. Bacteriol.* 193, 6742–6749. doi: 10.1128/JB.05276-11

Su, K., Zhou, X., Luo, M., Xu, X., Liu, P., Li, X., et al. (2018). Genome-wide identification of genes regulated by RcsA, RcsB, and RcsAB phosphorelay regulators in *Klebsiella pneumoniae* NTUH-K2044. *Microb. Pathog.* 123, 36–41. doi: 10.1016/j.micpath.2018.06.036

Szklarczyk, D., Morris, J. H., Cook, H., Kuhn, M., Wyder, S., Simonovic, M., et al. (2017). The STRING database in 2017: quality-controlled protein-protein association networks, made broadly accessible. *Nucleic Acids Res.* 45, D362–D368. doi: 10.1093/nar/gkw937

Thurow, H., Niemann, H., and Stirm, S. (1975). Bacteriophage-borne enzymes in carbohydrate chemistry. Part I. On the glycanase activity associated with particles of *Klebsiella bacteriophage* no. 11. *Carbohydr. Res.* 41, 257–271. doi: 10.1016/s0008-6215(00)87024-x

Tomás, J. M., Benedí, V. J., and Jofre, J. T. (1987). Identification of the cell surface receptor for FC3-2, FC3-3 and FC3-6 bacteriophages from *Klebsiella pneumoniae*. *FEMS Microbiol. Lett.* 41, 223–228. doi: 10.1016/0378-1097(87)90243-6

Whitfield, C. (2006). Biosynthesis and assembly of capsular polysaccharides in *Escherichia coli*. *Annu. Rev. Biochem.* 75, 39–68. doi: 10.1146/annurev.biochem.75.103004.142545

Xia, F., Li, X., Wang, B., Gong, P., Xiao, F., Yang, M., et al. (2016). Combination therapy of LysGH15 and apigenin as a new strategy for treating pneumonia caused by *Staphylococcus aureus*. *Appl. Environ. Microbiol.* 82, 87–94. doi: 10.1128/AEM.02581-15

Yang, F. L., Yang, Y. L., Liao, P. C., Chou, J. C., Tsai, K. C., Yang, A. S., et al. (2011). Structure and immunological characterization of the capsular polysaccharide of a pyrogenic liver abscess caused by *Klebsiella pneumoniae*: activation of macrophages through toll-like receptor 4. *J. Biol. Chem.* 286, 21041–21051. doi: 10.1074/jbc.M111.222091

Yoshida, K., Matsumoto, T., Tateda, K., Uchida, K., Tsujimoto, S., and Yamaguchi, K. (2000). Role of bacterial capsule in local and systemic inflammatory responses of mice during pulmonary infection with *Klebsiella pneumoniae*. *J. Med. Microbiol.* 49, 1003–1010. doi: 10.1099/0022-1317-49-11-1003

Yoshida, K., Matsumoto, T., Tateda, K., Uchida, K., Tsujimoto, S., and Yamaguchi, K. (2001). Induction of interleukin-10 and down-regulation of cytokine production by *Klebsiella pneumoniae* capsule in mice with pulmonary infection. *J. Med. Microbiol.* 50, 456–461. doi: 10.1099/0022-1317-50-5-456

Conflict of Interest Statement: The authors declare that the research was conducted in the absence of any commercial or financial relationships that could be construed as a potential conflict of interest.

frontiers in Microbiology

ORIGINAL RESEARCH
published: 15 November 2019
doi: 10.3389/fmicb.2019.02649

Modeling the Architecture of Depolymerase-Containing Receptor Binding Proteins in *Klebsiella* Phages

Agnieszka Latka[1,2], Petr G. Leiman[3], Zuzanna Drulis-Kawa[2] and Yves Briers[1]**

[1] *Laboratory of Applied Biotechnology, Department of Biotechnology, Ghent University, Ghent, Belgium,* [2] *Department of Pathogen Biology and Immunology, Institute of Genetics and Microbiology, University of Wrocław, Wrocław, Poland,* [3] *Sealy Center for Structural Biology and Molecular Biophysics, Department of Biochemistry and Molecular Biology, The University of Texas Medical Branch, Galveston, TX, United States*

Klebsiella pneumoniae carries a thick polysaccharide capsule. This highly variable chemical structure plays an important role in its virulence. Many *Klebsiella* bacteriophages recognize this capsule with a receptor binding protein (RBP) that contains a depolymerase domain. This domain degrades the capsule to initiate phage infection. RBPs are highly specific and thus largely determine the host spectrum of the phage. A majority of known *Klebsiella* phages have only one or two RBPs, but phages with up to 11 RBPs with depolymerase activity and a broad host spectrum have been identified. A detailed bioinformatic analysis shows that similar RBP domains repeatedly occur in *K. pneumoniae* phages with structural RBP domains for attachment of an RBP to the phage tail (anchor domain) or for branching of RBPs (T4gp10-like domain). Structural domains determining the RBP architecture are located at the N-terminus, while the depolymerase is located in the center of protein. Occasionally, the RBP is complemented with an autocleavable chaperone domain at the distal end serving for folding and multimerization. The enzymatic domain is subjected to an intense horizontal transfer to rapidly shift the phage host spectrum without affecting the RBP architecture. These analyses allowed to model a set of conserved RBP architectures, indicating evolutionary linkages.

Keywords: horizontal transfer, tail fiber genes, receptor binding protein, phage evolution, depolymerase

OPEN ACCESS

Edited by:
Caroline Westwater, Medical University of South Carolina, United States

Reviewed by:
Stefanie Barbirz, University of Potsdam, Germany
Carmela Garcia Doval, University of Zurich, Switzerland

****Correspondence:***
Zuzanna Drulis-Kawa
zuzanna.drulis-kawa@uwr.edu.pl
Yves Briers
yves.briers@ugent.be

Specialty section:
This article was submitted to Infectious Diseases, a section of the journal Frontiers in Microbiology

Received: *11 July 2019*
Accepted: *30 October 2019*
Published: *15 November 2019*

Citation:
Latka A, Leiman PG, Drulis-Kawa Z and Briers Y (2019) Modeling the Architecture of Depolymerase-Containing Receptor Binding Proteins in Klebsiella Phages. Front. Microbiol. 10:2649. doi: 10.3389/fmicb.2019.02649

INTRODUCTION

Klebsiella pneumoniae is a Gram-negative bacillus. In spite of being part of the natural human and animal flora, *K. pneumoniae* is also the widespread cause of both nosocomial and community acquired infections. Since 2013 *K. pneumoniae* has been marked as a prominent member of the carbapenem-resistant *Enterobacteriaceae* (CRE), featured by a multidrug-resistant phenotype and labeled as a class of antibiotic-resistant bacteria for which novel ways of therapy are most urgent (Weiner et al., 2016; Calfee, 2017). As natural bacterial predators, bacteriophages have since long been proposed as promising alternatives to antibiotic therapy. The large majority of phages is highly specific with a host spectrum defined at the species/strain level. This high specificity necessitates the selection of a phage sur-mesure for a personalized treatment or the use of a phage cocktail that covers a broader host range. Major determinants of host specificity are the phage receptor

binding proteins (RBPs) that mediate the initial contact with the receptor on the host cell envelope (Williams et al., 2008). This initial contact can be based on a direct binding of long tail fibers or shorter tailspikes to the cell surface receptor. Some RBPs possess a depolymerase activity to degrade bacterial exopolysaccharides comprising the capsule (CPS), lipopolysaccharides (LPS) or biofilm matrix (Majkowska-Skrobek et al., 2016, 2018; Olszak et al., 2017). Interaction of RBPs with their cell wall receptors are essential to initiate the infection process (Andres et al., 2010; Broeker et al., 2018).

The primary receptor targeted by RBPs of many *Klebsiella* specific phages is the thick polysaccharide capsule, which is a hallmark feature of *K. pneumoniae*. The capsule is a crucial virulence factor as it forms a physical barrier to some antibiotics and host immune mechanisms, enabling bacteria to avoid phagocytosis or complement-mediated killing (Cortés et al., 2002; Lee et al., 2017; Majkowska-Skrobek et al., 2018). Differences in sugar composition, the specific ratio of various sugar components as well as variation in the locus organization are the base to distinguish at least 79 capsular serotypes called K antigens and 134 capsular loci (KL) among *Klebsiella* species (Pan et al., 2015; Wyres et al., 2016; Wick et al., 2018). This capsular diversity correlates to a correspondingly high variation of *Klebsiella* phage RBPs that contain a specific polysaccharide-depolymerizing domain (Schmid et al., 2015; Latka et al., 2017). Such domains cleave the O-glycosidic bond of capsular polysaccharides following either a hydrolase or a lyase mechanism. Hydrolases (e.g., sialidases, rhamnosidases, levanases, dextranases, and xylanases) involve a water molecule for cleavage, whereas lyases [e.g., hyaluronate lyases (hyaluronidases), pectin/pectate lyases, alginate lyases, K5 lyases] cleave by β-elimination with introduction of new double bond (Davies and Henrissat, 1995; Sutherland, 1995; Pires et al., 2016). In spite of a high diversity in enzyme specificity and primary amino acid sequence, many known depolymerases contain an elongated, highly interwoven β-helical domain that forms the specific catalytic pocket. In addition, this β-helical domain contributes to a high protein stability in harsh environments (Yan et al., 2014; Majkowska-Skrobek et al., 2016). An overview of (experimentally confirmed) RBPs with depolymerase activity has been recently reported (Latka et al., 2017).

Receptor binding protein with depolymerase activity have a modular structure with the enzymatic domain located in the central part (**Figure 1C**). The C-terminus of the RBP may comprise a chaperone that assists in a proper folding and trimerization followed by autoproteolytic removal or an additional domain involved in host cell recognition (Weigele et al., 2003; Cornelissen et al., 2011; Schwarzer et al., 2012; Seul et al., 2014; Yan et al., 2014). Autocleavage of the C-terminal chaperone was also reported as a common feature among endosialidases and other tail spikes and tail fibers, necessary to increase the unfolding barrier and to trap the mature trimer in a more kinetically stable conformation (Schwarzer et al., 2007). The N-terminal dome-like domain attaches the RBP to the phage particle by a flexible connector. A modular architecture of RBPs allows for rapid evolution via horizontal gene transfer leading to host range modification. Whereas structural domains responsible for attachment to the tail apparatus are repeatedly present in many phylogenetically related phages, the domains for host cell receptor recognition/degradation are subjected to intense exchanges across phylogenetic borders. In addition, the latter RBP domains undergo further constant modification through vertical transfer and accumulation of mutations (Stummeyer et al., 2006; Barbirz et al., 2008; Leiman and Molineux, 2008; Schwarzer et al., 2012; Latka et al., 2017). The tail fibers of *E. coli* phage T7 and its relative K1F are type examples of a horizontal transfer of the C-terminal RBP domain. These tail fibers share a conserved N-terminal domain of ∼140 resides that anchors the tail fiber to the phage particle (**Figure 1**). However, T7 has a C-terminal domain that recognizes and binds lipopolysaccharide, whereas K1F produces an endosialidase specific for recognition and cleavage of *E. coli* K1 capsular polysaccharide (Steven et al., 1988; Stummeyer et al., 2005).

Phages with a single RBP such as T7 and K1F are most frequently described in the literature. However, several phages belonging to *Podoviridae* have also acquired two different RBPs corresponding to a dual receptor-specificity. E.g., *K. pneumoniae* podoviruses K5-2, K5-4, and KP32 possess two RBPs with a depolymerase domain with different enzymatic specificity (Hsieh et al., 2017; Majkowska-Skrobek et al., 2018). In the last decade, an increasing body of knowledge about the genetic and structural organization of RBPs of such bispecific phages has been acquired, particularly for different T7-like phages such as K1-5 and SP6 (Stummeyer et al., 2006; Leiman et al., 2007; Gebhart et al., 2017; Tu et al., 2017). These phages use a small trimeric adapter protein of approximately 300 amino acids, sharing a high N-terminal sequence identity to T7 and K1F tail fibers (**Figure 1**). In addition, phage K1-5 encodes a K5 lyase (gp46) and an endosialidase (gp47), which are specific for *E. coli* K5 and K1 capsule, respectively. CryoEM studies and bioinformatics suggest that K5 lyase binds through a heptapeptide (MAKLTKP) to a specific site in the middle of the K1-5 adapter protein, whereas the second tailspike (endosialidase) binds to a different specific site in its C-terminal part through an undecapeptide (MIQRLGSSLVK) (Leiman et al., 2007). The heptapeptide, undecapeptide, and adapter sequences are conserved among other T7-like phages that infect different bacterial species and that carry two different RBPs on the phage particle (e.g., SP6), demonstrating a conserved mechanism for attachment of two RBPs (**Figure 1**). Notably, domains recognizing the same host receptor can have highly similar amino acid sequence but can be incorporated into a different RBP architecture. For example, the K1F and K1-5 endosialidase domains specific to K1 capsule show 72% identity with a coverage of 86%, but in phage K1F the endosialidase domain is present in a single RBP with anchor domain, whereas in phage K1-5 the endosialidase is connected to the phage particle via an intermediate adapter protein. A homolog of the endosialidase domain of podovirus K1F is also present in the multivalent *E. coli* myovirus phi92 (EndoN92; 53% identity with a coverage of 83%), demonstrating exchange of the domain across members of the *Podoviridae* and *Myoviridae* families with highly different tail structures (Schwarzer et al., 2012, 2015).

More recently, a different organization of two types of RBPs in a single phage particle has been reported based on structural,

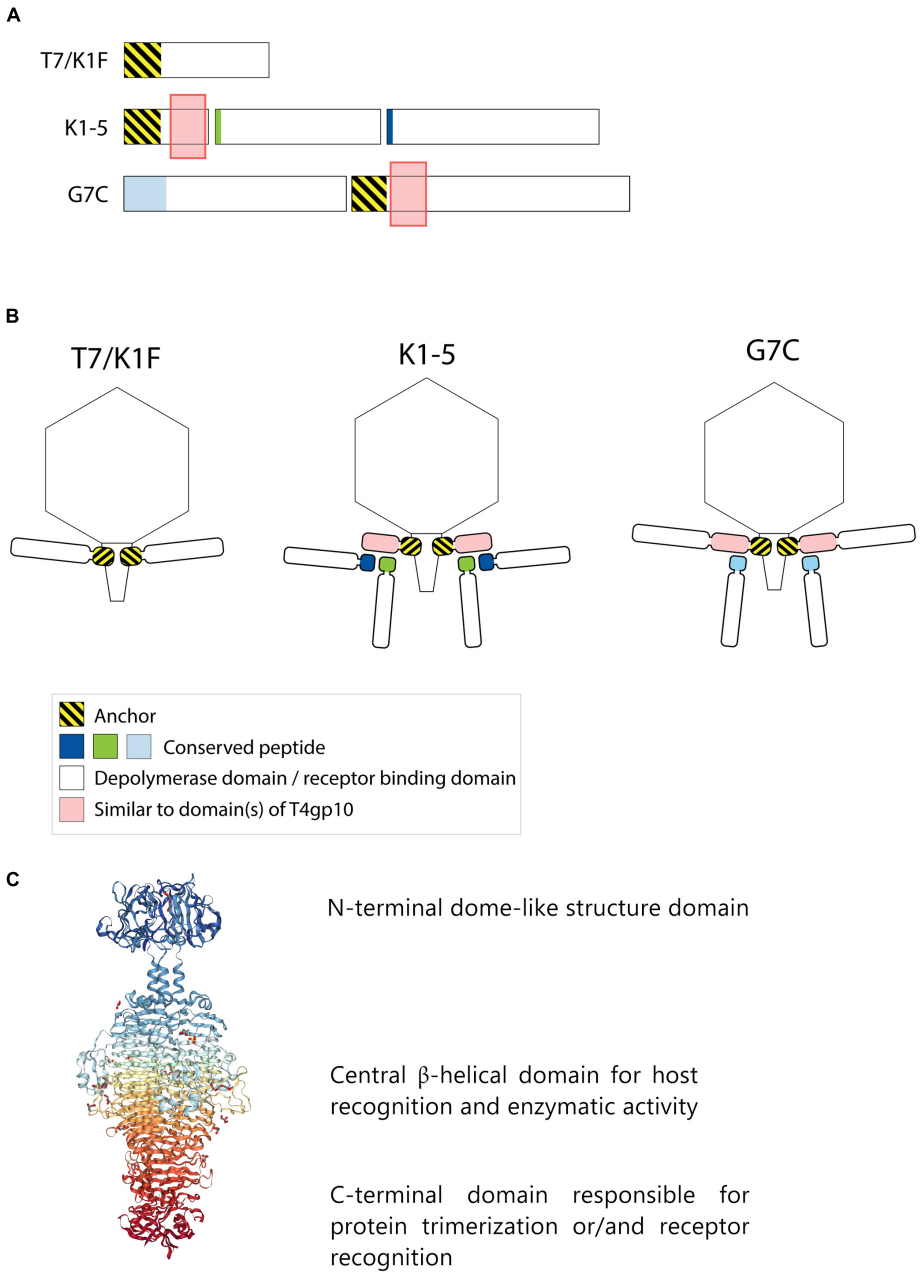

FIGURE 1 | Anchor and anchor-branched receptor binding protein (RBP) complexes confirmed by structural experiments. **(A)** The modular genetic organization of RBPs in single (T7 and K1F) and double RBP systems (K1-5 and G7C phages). **(B)** Schematic modeling of four different RBP systems in the virion structure. The T7 tail fiber (gene 17, T7p52) and K1F tail fiber (gene 17, CKV1F_gp36) have only an N-terminal anchor domain; K1-5 uses an adapter protein (gp37 with T4gp10-like domain) interacting with K5 lyase (gp46) and K1 endosialidase (gp47) *via* a conserved hepta- and undecapeptide, respectively; Phage G7C produces an anchor-branched complex with one anchored RBP (gp66) having a T4gp10-like domain and the second RBP connected *via* a conserved peptide to theT4gp10-like domain. **(C)** Modular structure of the model tail spike of *Salmonella* phage P22 (PDB ID 2XC1), illustrating a typical modular structure of RBPs. A N-terminal dome-like structure domain, a central β-helical domain for host recognition and enzymatic activity and a C-terminal domain responsible for protein trimerization or/and receptor recognition are shown (Berman et al., 2000; Seul et al., 2014; Rose et al., 2018).

genetic and biochemical studies of the RBPs of *E. coli* N4-like podovirus G7C (Prokhorov et al., 2017). G7C carries two RBPs – a longer G7Cgp66 and a shorter G7Cgp63.1 protein. The specificity of the longer G7cgp66 protein is unknown, but the shorter G7Cgp63.1 RBP was shown to deacetylate the O-antigen of *E. coli* 4S while leaving the backbone of the sugar intact. G7Cgp63.1 does not interact with the phage particle directly. Instead, it binds to G7Cgp66, which is attached to the phage particle with its N-terminal anchor domain (**Figure 1B**). The gp63.1 binding region of G7Cgp66 (residues 138–294) is

homologous to subdomains D2 and D3 of phage T4 gp10. In phage T4, these subdomains of gp10 serve as an attachment site for two proteins – gp11, which interacts with the long tail fiber RBP or short tail fiber RBP, depending on the state of the phage particle, and gp12, the short tail fiber RBP (Taylor et al., 2016). This protein complex represents a *bona fide* branched structure involved in the transmission of the signal of reversible host binding, culminating in irreversible binding, sheath contraction and DNA ejection. The T4gp10-like domains are prevalent in RBPs of unrelated phages across *Podoviridae* and *Myoviridae*, which may reflect its ancient evolutionary role in the transduction from reversible to irreversible binding during phage adsorption (Prokhorov et al., 2017).

Interestingly, the T4gp10-like region of G7Cgp66 covers both subdomain D2 and D3 of T4gp10 to which T4gp11 and T4gp12 are attached. Though, G7Cgp66 and G7Cgp63.1 form a 1:1 complex, suggesting that G7Cgp63.1 occupies only one of the two RBP binding sites on G7Cgp66. Notably, orthologs of G7Cgp66 in some G7C-like viruses do not contain a putative enzymatic domain but nevertheless retain the N-terminal particle-binding domain and the T4gp10-like domains. As such their attachment apparatus becomes similar to the adapter system of phage K1-5. The N-terminal part of G7Cgp63.1 that interacts with the T4gp10-like domain of G7Cgp66 is also found at the N-terminus of other tail spikes that have a branched structure, such as CBA120 phage tail spike 1 (Chen et al., 2014) and other putative tail spikes of Vil-like phages (Adriaenssens et al., 2012). CBA120 encodes four tail spikes (TSP1-4) from which two (TSP2 and TSP4) are equipped with T4gp10-like domains D2 and D3. These domains provide side or off-axis attachment sites for TSP1 and TSP3. The conserved N-terminal part of TSP4 attaches the whole branched structure composed of four TSPs to the baseplate of the virion (Plattner et al., 2019).

Klebsiella jumbo viruses may also have a multitude of RBPs resulting accordingly in a broader host spectrum. The highest variation of depolymerases has been described for the jumbo ΦK64-1 phage, which is able to infect *K. pneumoniae* of 10 different capsular serotypes and for which 11 different polysaccharide depolymerases have been identified (Pan et al., 2017). Also, the jumbo vB_KleM-RaK2 phage encodes a multitude of putative depolymerases (Simoliūnas et al., 2013). Electron microscopy images of such jumbo phages typically show an elaborated tail fiber apparatus with a high structural complexity, but for which structural insights are currently lacking.

In this study we present an extensive bioinformatic analysis of the structural and genetic organization of depolymerase-containing RBPs in *Klebsiella* phages. Next-generation sequencing technologies have recently led to a large number of sequenced phage genomes in public databases including *Klebsiella* viruses (n = 97). In a large proportion of these phages (59/97; 61%) we could predict an RBP with depolymerase activity. The observed large diversity of depolymerase domains accommodates the high diversity of capsular serotypes among *Klebsiella* strains. Based on an integrated analysis, we propose diverse RBP architectures in *Klebsiella* phages.

MATERIALS AND METHODS

At first, *Klebsiella* phages were collected from the GenBank database (retrieved at 15.08.2018). A number of 59 phages were finally analyzed (**Supplementary Table S1**). From these phages proteins annotated as tail fibers or tail spikes were analyzed with BlastP[1] (Altschul et al., 1990), Phyre2[2] (Kelley et al., 2015), SWISS-MODEL[3] (Bordoli et al., 2009; Bordoli and Schwede, 2012), HMMER[4] (Finn et al., 2011) and HHPred[5] (Zimmermann et al., 2018) to identify phages that encode RBPs with putative depolymerase activity (**Supplementary Table S2**). If neither a tail fiber nor a tail spike gene was found in the genome, we analyzed all genes located in the vicinity of annotated structural genes. BlastP (protein–protein Blast) was performed against the non-redundant protein sequences (nr) database using standard parameters (expect threshold: 10, word size: 6, MATRIX: BLOSUM62, Gap cost: existence 11, extension 1, conditional compositional score matrix adjustment). HMMER was used in the quick search mode against: Reference Proteomes, UniProtKB, SwissProt, and Pfam with significance E-values: 0.01 (sequence) and 0.03 (hit). For Phyre2 the normal modeling mode was used. HHPred homology detection structure prediction was run using the PDB_mmCIF70 database and the following parameters [MSA generation method: HHblits uniclust30_2018_08; Maximal no. of MSA generation steps: 3; E-value incl. threshold for MSA generation: 1e-3; minimal sequence identity of MSA hits with query (%): 0; minimal coverage of MSA hits (%) 20; Secondary structure scoring: during alignment; Alignment Mode: Realign with MAC: local:norealign; MAC realignment threshold: 0.3; No. of target sequences: 250; Min. probability in hit list (>10%): 20].

Criteria for the prediction of putative depolymerase activity were (**Supplementary Table S2**): (1) the protein must be longer than 200 residues; (2) the protein must be annotated as tail fiber/tail spike/hypothetical protein in the NCBI database; (3) the protein must show homology to domains annotated as lyase [hyaluronate lyases (hyaluronidases), pectin/pectate lyases, alginate lyases, K5 lyases] or hydrolase (sialidases, rhamnosidases, levanases, dextranases, and xylanases) with a confidence of at least 40% in Phyre2 or the enzymatic domain should also be recognized by at least SWISS-MODEL, HMMER, or BlastP; (4) the length of homology with one of these enzymatic domains should span at least 100 residues; (5) a typical β-helical structure should be predicted by Phyre2. These RBP depolymerases are indicated without additional labeling in the tables. Proteins possessing experimentally confirmed depolymerizing activity were marked in the tables with (a). When the RBP was only partially fulfilling the above-mentioned criteria, it was indicated with label (b). These putative depolymerases that could only be predicted with a lower probability were fulfilling criteria 1 and 2, but the confidence of the Phyre2 prediction was below 40% or only SWISS-MODEL, HMMER or BLASTP gave

[1] blast.ncbi.nlm.nih.gov
[2] sbg.bio.ic.ac.uk
[3] swissmodel.expasy.org
[4] hmmer.org
[5] toolkit.tuebingen.mpg.de

TABLE 1 | Overview of RBPs of KP32viruses with (predicted) depolymerase activity grouped according to the different observed RBP systems.

Phage	First RBP (protein 2, Figure 2)						Second RBP (protein 3, Figure 2)					
	Accession number	Number of aa	Alignment with first RBP from KP32				Accession number	Number of aa	Alignment with second RBP from KP32			
			Cover	E-value	Identity	Identity range			Cover	E-value	Identity	Identity range
Group A (two RBPs: anchor-branch attachment mode)												
KP32	YP_003347555.1[a]	869	100%	0.0	100%	869/869	YP_003347556.1[a]	576	100%	0.0	100%	576/576
K11	YP_002003830.1	875	40%	5E-144	68%	241/355	YP_002003831.1	596	88%	5E-41	27%	149/543
KP32 194	AWN07125.1	777	39%	2E-139	67%	233/347	AWN07126.1	555	8%	0.0001	51%	30/59
KpV763	AOT28172.1	777	39%	2E-139	67%	232/347	AOT28173.1	524	8%	0.0001	51%	30/59
KP32 192	AWN07083.1	777	39%	5E-139	67%	232/347	AWN07084.1	555	8%	0.00006	53%	31/59
K5-2	APZ82804.1[a]	792	35%	6E-139	71%	219/307	APZ82805.1[a]	685	5%	0.00009	87%	26/30
KP32 196	AWN07213.1	903	40%	6E-134	64%	227/354	AWN07214.1	613	23%	0.00001	34%	48/143
KpV766	AOZ65569.1	903	40%	6E-133	64%	226/354	AOZ65570.1[b]	511	30%	7E-12	38%	42/111
KpV289	YP_009215498.1	903	40%	7E-133	63%	224/354	YP_009215499.1[b]	511	18%	0.0008	38%	42/111
IME 205	ALT58497.1	793	37%	7E-132	64%	209/329	ALT58498.1	641	5%	0.001	83%	24/29
K5	YP_009198668.1	817	43%	2E-131	59%	225/381	YP_009198669.1	575	99%	0.0	87%	498/575
K5-4	APZ82847.1[a]	744	44%	2E-120	55%	218/396	APZ82848.1[a]	684	5%	0.000008	88%	28/32
Group B (one RBP: anchor attachment mode)												
KP32 195	AWN07172.1	1017	33%	1E-51	46%	136/293	No second RBP present					
SH-Kp 152410	AUV61507.1	1017	33%	4E-50	46%	134/293						
IL33	ARB12452.1[b]	1242	33%	3E-59	72%	119/166						
PRA33	ARB12406.1[b]	1242	33%	4E-58	71%	119/168						
BIS33	ARB12500.1[b]	1242	33%	1E-57	70%	117/166						
IME321	AXE28435.1[c]	820	22%	1E-53	59%	114/194						
Kp1	YP_009190948.1[d]	1017	62%	2E-59	39%	166/422						
Group C (two RBPs: anchor-branch attachment mode, second RBP truncated)												
KpV767	AOZ65519.1	843 aa	39%	2E-127	61%	212/347	AOZ65520.1[c]	69 aa	9%	0.000003	51%	28/55
Group D (two RBPs: anchor-branch attachment mode, first RBP truncated)												
2044-307w	ASZ78307.1[c]	347 aa	33%	4E-122	65%	192/295	ASZ78308.1[b]	556 aa	8%	0.002	55%	28/51

*The different RBP systems of KP32viruses are visualized in **Figure 2**. [a]RBP for which the depolymerase activity has been experimentally verified (Hsieh et al., 2017; Majkowska-Skrobek et al., 2018). [b]RBP with a lower probability on depolymerizing activity. [c]RBP without enzymatic activity. [d]The N-terminal part of this protein is lacking under the corresponding accession code, yet the full protein is encoded by nucleotide positions 38449–40114 and 1–1388 of the full genome (NC_028688.1). BLASTp was used as computational alignment algorithm and pairwise alignments were performed against the corresponding first and second RBP from phage KP32, respectively. The accession number of each RBP is given, along with its length and alignment characteristics (cover-coverage, E-value,% identity, identity range-number of identical amino acids/length) of the region over which identical amino acids are found by Blastp, starting from the N-terminus (amino acid 1). HHPred analysis revealed homology in the first RBPs to T4gp10-like domains: Group A – 197–256 aa compared to 170–246 aa of T4gp10 (Probability 86.48) and 206–254 aa compared to 299–383 aa of T4gp10 (Probability 82.04); Group C – 188–256 aa compared to 163–246 aa of T4gp10 (Probability 85.35) and 209–254 aa compared to 303–383 aa of T4gp10 (Probability 84.24); Group D – 196–257 aa compared to 169–246 aa of T4gp10 (Probability 60.26) and 204–255 aa compared to 298–383 aa of T4gp10 (Probability 71.57). Values are shown for KP32 (group A), KpV767 (group C) and 2044-307w (group D). In group B no homology to T4gp10-like domain was detected.*

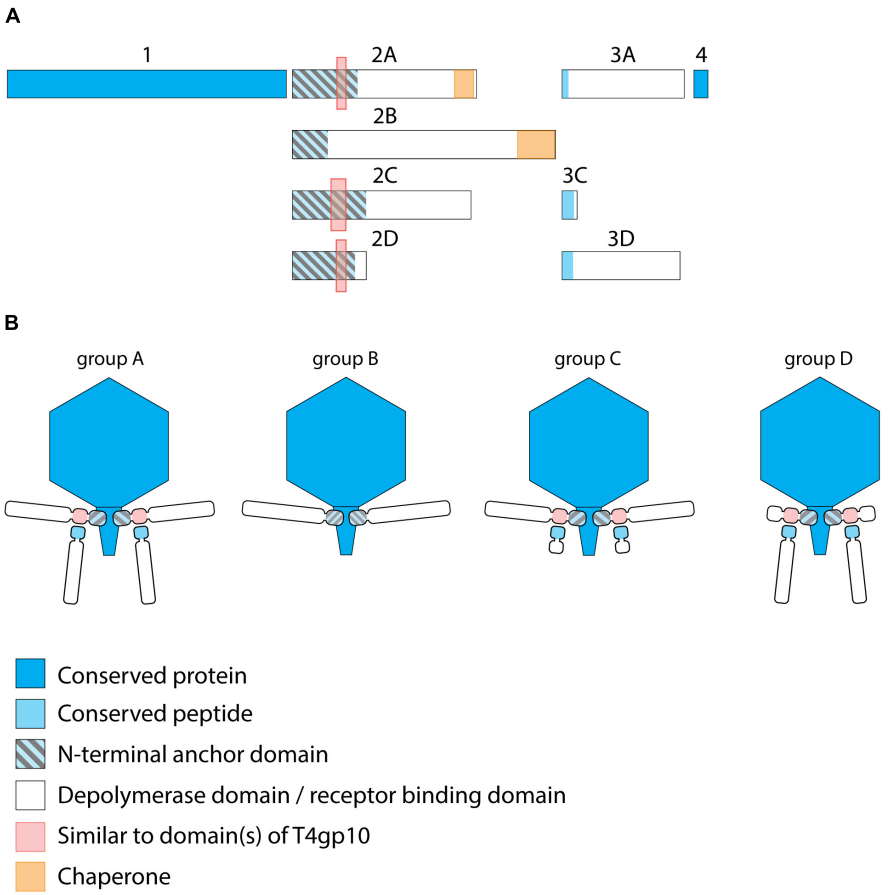

FIGURE 2 | Receptor binding protein systems of KP32viruses. Phages and their RBPs that are proposed to follow these systems, including their grouping into groups A, B, C and D, are summarized in **Table 1**. **(A)** The modular composition of RBP genes of phages belonging to four different groups (A, B, C, and D) is shown relative to the broken gene synteny of phage KP32. For simplicity, only one flanking gene conserved across all groups is shown at each side. Annotations are given according to GenBank or according to their modeled function in this study (between brackets): Protein (1) – internal virion protein D; (2) – tail fiber protein (2A,B,C – anchor with depolymerase; 2D – anchor with truncated protein); (3) – hypothetical protein (3A,D – depolymerase with conserved peptide, 3C – truncated protein with conserved peptide); (4) – lysis protein. **(B)** Schematic models of RBP systems in phage particles of KP32viruses. Group A – two RBPs: anchor-branch attachment mode; Group B – one RBP: anchor attachment mode; Group C – two RBPs: anchor-branch attachment mode, second RBP truncated; Group D – two RBPs: anchor-branch attachment mode, first RBP truncated.

a positive prediction. In addition, the homologous domain only spans between 50 and100 amino acids and no β-helical structure could be predicted with Phyre2 (for details see **Supplementary Table S2**).

All selected *Klebsiella* phages were then grouped based on gene homology and a conserved gene synteny into KP32viruses, KP34viruses, and KP36viruses and into groups containing only *Klebsiella*-specific phages similar to phage JD001 (belonging to Jedunavirus), similar to phage Menlow (belonging to Ackermannviridae), similar to phage ΦK64-1 (belonging to Alcyoneusvirus). Within each group, further subdivisions were proposed for the purpose of this study, based on the organization of the RBP gene cluster (number of RBPs, length of different genes, presence of anchor, or branching domains).

When there was one RBP, a domain in the N-terminus of a RBP was annotated as 'anchor' when there was at least an identity of 39% (BLASTP) over at least 166 residues starting from the N-terminus of the corresponding protein among phages belonging to the same group. These parameters were set empirically based on the shortest identity region found among all RBPs, specifically in the first RBP of phage IL33, belonging to KP32viruses group B (166 amino acids) and the identity% of the first RBP of phage Kp1. When more than one RBP was present, the anchor domain was annotated in the RBP in which also a T4gp10-like domain was detected. In the other RBP(s) the N-terminal conserved sequence was called 'conserved peptide,' which was also generally shorter than the anchor domains. To define consensus sequences of the anchor domains and conserved peptides, multiple sequence or pairwise alignment were used, since these structures are highly conserved among phages from the same group. To identify domains involved in the branching of RBPs, the sequences were analyzed by HHPred performing protein structure prediction[5] (Zimmermann et al., 2018) in search for domains homologous to T4gp10 domain 2 and 3

as experimentally confirmed attachment sites (Prokhorov et al., 2017). WebLogos of the anchor domains and conserved peptides were created with the online available tool[6] (Crooks et al., 2004).

RESULTS

Taxonomically closely related phages are characterized by a synteny of conserved structural genes interrupted by divergent RBP genes, which are subject to intensive horizontal transfer. We therefore inspected the region of structural genes across different *Klebsiella* phages within specific phage genera to identify potential RBPs based on a broken synteny. Subsequently, we analyzed the presence of putative enzymatic domains within the identified RBPs. Based on homology, protein size and structure, we looked for conserved domains (anchor domain, T4gp10-like domain) that may explain the RBP architecture of the particular phage. To further refine this architecture, we analyzed the sequence for the presence of conserved peptides that may mediate attachment to putative T4gp10-like domains. We integrated all these data to model the RBP apparatus of an extensive and diverse set of *Klebsiella* phages with (predicted) depolymerase activity.

RBPs From Selected *Klebsiella* Podoviruses

KP32viruses

KP32viruses belong to *Podoviridae* and have tail fibers attached to a short, non-contractile tail. A similar synteny of highly conserved structural genes is observed across twenty-one KP32viruses (**Supplementary Table S1A**). Yet, one or two non-conserved genes of different lengths interrupt this synteny after the gene encoding the internal virion protein D. They were identified as putative RBPs and in a few cases also experimentally verified (Hsieh et al., 2017; Majkowska-Skrobek et al., 2018; Solovieva et al., 2018) (**Table 1**). We found four different RBP organizations (groups A, B, C, and D; **Figure 2**). The N-termini of the first RBPs are shared with high sequence identity (46–72%) across all KP32viruses. Specifically, residues 1–154 of the first RBPs are highly similar to the N-terminal domain of the phage T7 tail fiber (pfam03906). In group A of KP32viruses, this conserved N-terminal domain (**Supplementary Figure S1A**) also contains a region that is similar to a fragment of a T4gp10 branching domain, offering a potential attachment point for a secondary tail fiber. The other domain(s) of these 744–903 aa long first RBPs do not share identity with the corresponding domain of the group A model phage KP32. All central domains are predicted to possess enzymatic activity (hydrolase, lyase) but with different specificity. In addition, they all are predicted to possess a characteristic β-helical structure (**Supplementary Table S2**). In phage KP32, there is an additional C-terminal domain with predicted chaperone activity, which is absent in all other RBPs of the group A KP32viruses.

The second RBP that interrupts the gene synteny in group A KP32viruses is recently demonstrated to have depolymerase activity against capsular serotype K21, whereas the first RBP has depolymerase activity against capsular serotype K3 (Majkowska-Skrobek et al., 2018). These specificities correspond to the host spectrum of phage KP32. Other phages of group A KP32viruses also possess this second putative RBP. The second RBP has no conserved N-terminal anchor domain but has a peptide sequence that is conserved across group A KP32viruses with a consensus sequence over the first 29 amino acids (**Supplementary Figure S1B**). Similarly to the phage G7C RBP system this conserved peptide may be responsible for attachment to the T4gp10-like domain present in the first RBP. Also for the second RBPs, there is a high diversity in the central sequence with a few exceptions. E.g., in phage K5 and KP32, a highly similar sequence is observed, which hints that the second RBP of phage K5 also targets capsular serotype K21. No chaperone is predicted in any second RBP. Integrating these elements, we model the structural organization of group A KP32viruses as depicted in **Figure 2B** with a conserved anchor-branched attachment mode but with swapped enzymatic domains for specific capsule/host recognition.

Group B KP32viruses (**Table 1**) have a simpler RBP organization with a single anchor-based RBP. Six out of seven analyzed phages have an RBP with a putative enzymatic domain, while the seventh phage (IME321) apparently lacks enzymatic activity and might rather encode a tail fiber. The N-terminal conserved anchor domain is shorter (166 amino acids) compared to the corresponding domain in group A KP32viruses (307 amino acids). The RBP also lacks a T4gp10-like domain, which is consistent with the absence of a second RBP in group B KP32viruses (**Figure 2**).

Phage KpV767 (**Table 1**) represents another variant of KP32viruses (coined group C). The phage has a first anchor-based RBP, including a fragment of a T4gp10-like domain, but the second RBP is largely truncated to only 69 amino acids, including the conserved N-terminal 29 amino acids for attachment to the T4gp10-like domain (**Supplementary Figure S1B**). KpV767 appears to result from a retrograde evolution, having lost the potential to infect hosts belonging to two different serotypes.

Finally, phage 2044-307w (group D) is as an opposite example of truncation. The first RBP lacks an enzymatic or receptor binding domain but contains an N-terminal anchor including a fragment of a T4gp10-like domain, while the second tail fiber is a full-featured RBP that contains a conserved N-terminal peptide and a depolymerase domain (**Supplementary Figure S1B**).

KP34viruses

Seventeen phages from the genus of KP34viruses were analyzed (**Table 2**). Potential proteins involved in host cell recognition could be clearly identified as two genes interrupting the synteny of highly conserved structural genes and genes required for phage particle maturation. Interestingly, both genes are not clustered as in KP32viruses, but are separated by five to eight intervening genes encoding DNA maturases, hypothetical proteins and endolysins, depending on the specific phage. Three different groups (A, B, and C) can be categorized based on differences in length of both genes. Ten group A phages have a short first protein of approximately 300 amino acids annotated as tail fiber. This protein does not encode a putative enzymatic

[6] weblogo.berkeley.edu

TABLE 2 | Overview of RBPs of KP34viruses with (predicted) depolymerase activity grouped according to the different observed RBP systems.

Phage	First RBP (protein 2, Figure 3)						Second RBP (protein 10, Figure 3)		
	Accession number	Number of aa	Alignment with KP34 first RBP				Accession number	Number of aa	Alignment with KP34 second RBP
			Cover	E-value	Identity	Identity range			
Group A (two RBPs: anchor-branch attachment mode, first RBP truncated)									
KP34	YP_003347643.1[c]	307 aa	100%	0.0	100%	307/307	YP_003347651.1	630 aa	
SU503	YP_009199929.1[c]	307 aa	100%	0.0	94%	288/307	YP_009199937.1	500 aa	
F19	YP_009006065.2[c]	307 aa	100%	0.0	93%	284/307	YP_009006074.1	577 aa	
KpV475	YP_009280712.1[c]	318 aa	100%	0.0	88%	279/318	YP_009280720.1[b]	651 aa	
KpV71	YP_009302749.1[c]	318 aa	100%	0.0	91%	288/318	YP_009302756.1[a]	651 aa	
NTUH-K2044-K1-1	YP_009098379.1[c]	318 aa	100%	0.0	90%	287/318	YP_009098385.1[a]	651 aa	No similarity except for the short conserved heptapeptide
KPV811	APD20665.1[c]	318 aa	100%	0.0	87%	278/318	APD20657.1	563 aa	
KpV48	AOZ65257.1[c]	318 aa	100%	0.0	86%	275/318	AOZ65265.1	669 aa	
phiBO1E	AIT13620.1[c]	318 aa	100%	0.0	86%	275/318	AIT13628.1	494 aa	
AltoGao	ASV44938.1[c]	307 aa	99%	2E-162	74%	227/305	ASV44946.1	563 aa	
myPSH1235	30838–31279[c,d]	314 aa	99%	2E-172	76%	239/316	35768–37564[d]	598 aa	
Group B (two RBPs: anchor-branch attachment mode)									
Kp2	YP_009188359.1[c]	530 aa	83%	6E-137	81%	207/256	YP_009188367.1	660 aa	
SU552A	YP_009204835.1	793 aa	81%	3E-111	65%	170/261	YP_009204843.1	548 aa	
KpV41	YP_009188788.1[b]	858 aa	94%	2E-110	57%	187/327	YP_009188797.1[b]	651 aa	
phiKpS2	AWK24039.1	946 aa	85%	1E-107	63%	174/275	AWK24047.1	581 aa	
KpV74	APZ82760.1[c]	602 aa	84%	1E-129	72%	186/260	APZ82768.1[a]	577 aa	
Group C (two RBPs: anchor-branch attachment mode, second RBP truncated)									
KP-Rio/2015	36399–38783 [d]	794 aa	90%	9E-116	60%	175/290	42918–43105[c,d]	61 aa	

The different RBP systems of KP34viruses are visualized in ***Figure 3****. [a]RBP for which the depolymerase activity has been experimentally verified (Lin et al., 2014; Solovieva et al., 2018). [b]RBP with a lower probability on depolymerizing activity. [c]RBP without enzymatic activity. [d]Protein is not annotated in the genome, but the nucleotide positions of the open reading frame are indicated instead. BLASTp was used as computational alignment algorithm and pairwise alignments were performed against the corresponding first RBP from phage KP34. The accession number of each RBP is given, along with its length and alignment characteristics (cover-coverage, E-value,% identity, identity range-number of identical amino acids/length) of the region over which identical amino acids are found by Blastp, starting from the N-terminus (amino acid 1). HHPred analysis revealed homology in first RBPs to T4gp10-like domains: Group A – 186–242 aa compared to 165–244 aa of T4gp10 (Probability 82.81) and 200–243 aa compared to 303–384 aa of T4gp10 (Probability 94.36); Group B – 187–242 aa compared to 167–244 aa of T4gp10 (Probability 83.96) and 200–243 aa compared to 303–384 aa of T4gp10 (Probability 94.63); Group C – 196–253 aa compared to 165–245 aa of T4gp10 (Probability 79) and 210–253 aa compared to 303–384 aa of T4gp10 (Probability 91.72). Values are shown for KP34 (group A), Kp2 (group B), and KP-Rio/2015 (group C).*

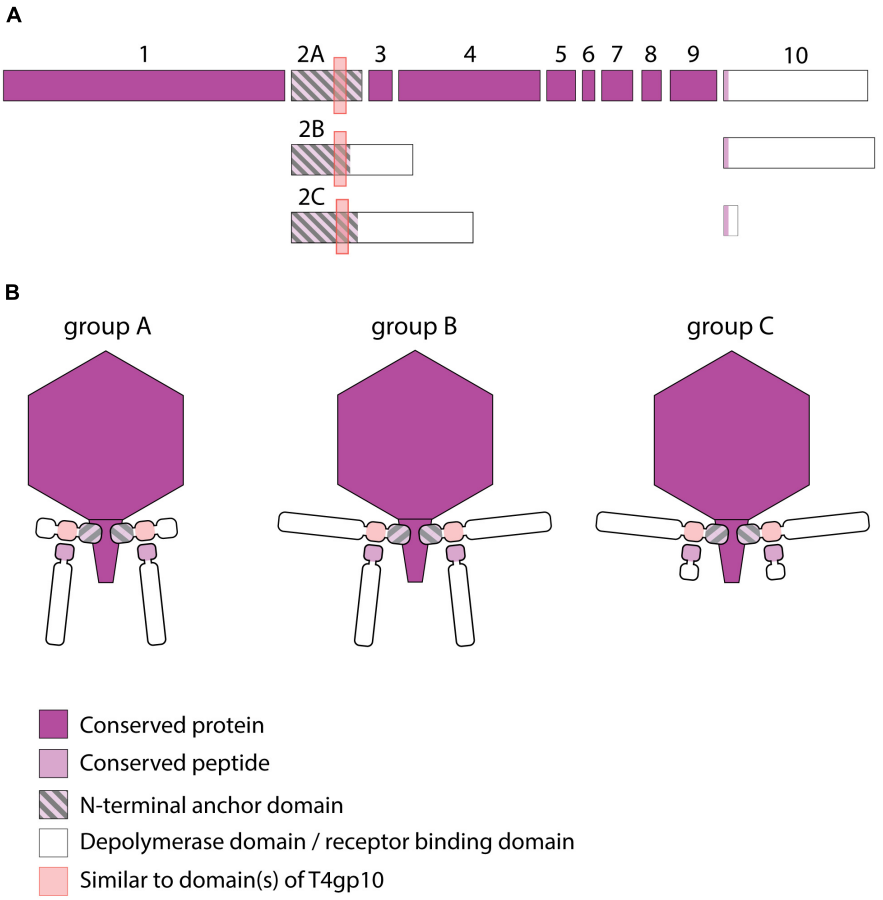

FIGURE 3 | Receptor binding protein systems of KP34viruses. Phages and their RBPs that are proposed to follow these systems, including their grouping into groups A, B and C, are summarized in **Table 2**. **(A)** The modular composition of RBP genes of phages belonging to three different groups (A, B, and C) is shown relative to the broken gene synteny of phage KP34. For simplicity, only one conserved gene preceding the first RBP and the conserved, intervening genes of phage KP34 are shown. Annotations are given according to GenBank or according to their modeled function in this study (between brackets): (1) – putative internal core protein; (2) – putative tail fiber protein (2A – anchor; 2B,C – anchor with depolymerase); (3) – putative DNA maturase A; (4) – putative DNA maturase B; (5) – hypothetical protein; (6) – hypothetical protein; (7) – hypothetical protein; (8) – hypothetical protein; (9) – endolysin; (10) – hypothetical protein (depolymerase with conserved peptide). **(B)** Schematic models of RBP systems in phage particles of KP34viruses. Group A – two RBPs: anchor-branch attachment mode, first RBP truncated; Group B – two RBPs: anchor-branch attachment mode; Group C – two RBPs: anchor-branch attachment mode, second RBP truncated.

TABLE 3 | Overview of RBPs of phages belonging to the JD001 group and with (predicted) depolymerase activity.

			Alignment with JD001 protein			
Phage	**Accession number**	**Number of aa**	**Coverage**	**E-value**	**Identity**	**Identity range**
First RBP with anchor truncated (protein 2, Figure 4)						
JD001	YP_007392884.1[c]	285 aa	100%	0.0	100%	285/285
KpV52	AOZ65389.1[c]	297 aa	38%	5E-53	83%	91/109
KpV79	ATI16499.1[c]	199 aa	29%	3E-46	77%	64/83
Second RBP with conserved peptide (protein 5, Figure 4)						
JD001	YP_007392887.1	757 aa	100%	0.0	100%	757/757
KpV52	AOZ65386.1	668 aa	25%	1E-16	51%	85/166
KpV79	ATI16495.1	721 aa	100%	2E-115	37%	289/780

*The RBP system of phages belonging to the JD001 group is visualized in **Figure 4**. [c]RBP without enzymatic activity. BLASTp was used as computational alignment algorithm and pairwise alignments were performed against the corresponding first and second RBP from phage JD001, respectively. The accession number of each RBP is given, along with its length and alignment characteristics (cover-coverage, E-value,% identity, identity range-number of identical amino acids/length) of the region over which identical amino acids are found by Blastp, starting from the N-terminus (amino acid 1).*

domain, but its N-terminal domain shows high homology to the N-terminus of the phage T7 tail fiber (pfam03906, aa 14–142), similar to the first RBPs of KP32viruses. In addition, the protein contains a fragment of a T4gp10-like domain located at its C-terminus (aa 186–242), which may serve as the attachment point for the second RBP. This protein is highly conserved among all phages of group A KP34viruses (at least 74% identity) (**Supplementary Figure S1C**). The second RBP sequence encodes a putative enzymatic domain with most such domains forming a β-helical structure. The N-terminal heptapeptide of these proteins contains universally conserved hydrophobic residues (MALxxLV) (**Supplementary Figure S1D**). These observations suggest that the organization of the RBP apparatus of group A KP34viruses is similar to the system of phage 2044-307w (group D KP32viruses), albeit with a much shorter conserved peptide (**Figure 3**). Similar short conserved peptides (heptapeptide and undecapeptide) for interaction with the anchor protein have been observed for *E. coli* phages K1E and K1-5 and *Salmonella* phage SP6 (Leiman et al., 2007).

Group B KP34viruses contain large first RBPs with a size between 530 and 948 aa. Four out of five RBPs encode an enzymatic domain in the C-terminal or central part of the protein. The corresponding gene in the fifth virus (phage KpV74) contains no predicted enzymatic domain. Group B KP34viruses also encode a second RBP with a predicted enzymatic activity and the same conserved heptapeptide motif as in the second RBP of group A KP34viruses (MALxxLV). The organization of the RBPs in group B KP34viruses is thus similar to that of group A KP32viruses. We found two incongruences in this genus, specifically viruses KP-Rio/2015 and myPSH1235. They both share the gene synteny of KP34viruses but no RBPs were annotated in their genomes. Further genome analysis revealed two open reading frames that presumably fulfill the role of RBPs. We found that phage myPSH1235 follows the RBP organization of group A KP34viruses, while phage KP-Rio/2015 encodes a large first RBP with a predicted enzymatic activity (and a fragment of a T4gp10-like domain) and a second protein that is only 61 aa long, which likely represents a truncated, non-functional RBP. Therefore, phage KP-Rio/2015 forms a different group C with an RBP organization analogous to KP32viruses group C.

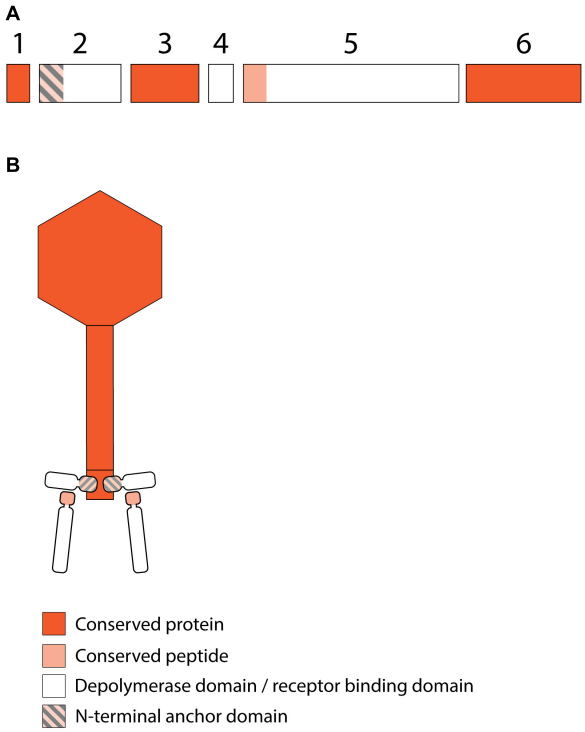

FIGURE 4 | Receptor binding protein systems of viruses of the JD001 group. Phages and their RBPs that are proposed to follow this system are summarized in **Table 3**. **(A)** The modular composition of RBP genes is shown relative to the broken gene synteny of JD001. Two flanking conserved hypothetical genes are shown. Annotations are given according to GenBank or according to their modeled function in this study (between brackets): (1) – hypothetical protein; (2) – putative tail fiber protein (anchor); (3) – hypothetical protein; (4) – hypothetical protein; (5) – gluconolaconase (depolymerase with conserved peptide); (6) – hypothetical protein. **(B)** Schematic model of the RBP system in JD001 group with an anchor-branch attachment mode and the first RBP truncated.

RBPs From Selected *Klebsiella* Myoviruses

Myoviruses have a contractile tail with a baseplate at the head-distal end of the tail. The tail fibers are directly connected to this baseplate. In addition, there is often a central spike (sometimes annotated as 'fiber') protruding from the baseplate. Nine *Klebsiella* phages analyzed in this study belong to three different myovirus groups (JD001 group, Menlow group, and ΦK64-1 group) with the latter two groups having a potentially broad host spectrum since they encode between five and nine (Menlow group; phage RaK2) (Hsu et al., 2013; Simoliūnas et al., 2013) or even 11 different depolymerases (phage ΦK64-1) (Pan et al., 2017) (**Supplementary Tables S1C–E**), necessitating elaborated structural organizations for RBP attachment. We should note that the JD001, Menlow, and ΦK64-1 phages are no taxonomic groups but were grouped in this study for their genetic similarities in the RBP genes. In addition, viruses belonging to the Menlow group have been recently reclassified from *Myoviridae* to *Ackermannviridae* (Adriaenssens et al., 2018). *Ackermannviridae* are characterized by a conserved genome organization and have typical morphology of myoviruses (long contracting tail) but with a different distal end of the tail, which ends with "stars" or "prongs," being identified as tailspikes (Day et al., 2018).

Viruses Belonging to the JD001 Group

The putative RBP genes of the viruses of the JD001 group (**Table 3**) were identified in a region of hypothetical proteins, preceding the DNA polymerase gene. Both genes are located at separate sites with two (JD001, KpV52) or three (KpV79) intervening genes. They all encode a single putative depolymerase, annotated as gluconolaconase, putative tail fiber family protein or tail fiber protein/pectate lyase superfamily protein, respectively. This RBP with depolymerase activity is most likely attached to the anchor protein via a conserved

N-terminal domain of about 70 aa, which is distinct from the conserved peptides/domains found in both KP32- and KP34viruses. The anchor protein has no T4gp10-like domain, indicating a different mechanism of interaction (**Figures 4A,B**).

Viruses Belonging to the Menlow Group

The viruses of the Menlow group encode, amid a conserved synteny of structural genes, four non-conserved putative RBPs and one conserved RBP, all with putative depolymerase activity (**Figure 5A**). Phages KpS110 and 0507-KN2-1 encode an additional sixth RBP with a predicted depolymerase domain (**Table 4**). The first two non-conserved RBPs (protein 2 and 3 in **Figure 5**) have N-terminal domains of 412 and 195 aa long, respectively, which is conserved among the four members of the Menlow group. The following two non-conserved RBPs have a shorter domain/peptide of 38 and 67 aa, respectively, conserved among all members of the Menlow group (**Supplementary Figures S1E–H**).

To explore how this high number of putative RBPs might be structurally organized, we searched for homology to T4gp10-like domains 2/3 and N-terminally conserved domains/peptides as they suggest branching points. Two domains homologous to T4gp10 were located in the N-terminal part of RBP 2 (RBP with anchor domain) and RBP 3, whereas RBPs 3, 5, 7 (**Figure 5A**) contain conserved peptides in their N-terminus. A fifth RBP (protein 8 is present and highly identical) in all members of the Menlow group, while a sixth RBP with putative depolymerase activity is only present in phage KpS110 and phage 0507-KN2-1. Integrating the presence/absence of these structural elements (**Figure 5B**) a possible model implies that the first RBP (protein 2, **Figure 5A**) is directly attached to the tail *via* a conserved N-terminal anchor and that its T4gp10-like domain probably provides an attachment site for at least two RBPs (3 and 5 or 7 or 8, **Figure 5B**). Subsequently, the second RBP (protein 3) provides attachment sites *via* its T4gp10-like domains for two more RBPs (proteins 5 or 7 or 8). Together they constitute a unit of branched tail fibers. The highly conserved fifth RBP (protein 8) may be the central tail fiber that protrudes from below the plane of the baseplate (Nobrega et al., 2018). More structural and genetic studies will be needed for an improved understanding of the elaborated RBP system in viruses from the Menlow group.

Viruses Belonging to the ΦK64-1 Group

Klebsiella phages belonging to ΦK64-1 group (ΦK61-1 and RaK2; **Supplementary Table S1E**) have likely evolved the most elaborate RBP apparatus (**Table 5**). ΦK64-1 encodes 11 proteins recognized as putative depolymerases, while in the genome of RaK2 10 putative depolymerases are predicted. The middle and C-terminal regions of five RBPs are different between the corresponding genes of ΦK61-1 and RaK2, reflecting the diversity of capsular serotypes that can be recognized by putative depolymerases of these two phages, whereas the middle and C-terminal parts of other RBPs show more than 75% identity between both phages, suggesting an overlap in the host spectrum (Pan et al., 2017). We found in this study that these proteins also contain a slew of structural elements found in other complex tail fiber machineries such as one N-terminal anchor domain, four short conserved peptides at the N-terminus and five T4gp10-like domains (**Supplementary Figures S1I–M**), indicating that phages of the ΦK64-1 group also re-use standardized units to build up a highly complex RBP apparatus (**Figure 6**).

RBPs From *Klebsiella* Siphoviruses

KP36viruses

All 12 identified *Klebsiella* siphoviruses belong to the KP36viruses. They are also featured by a synteny of genes encoding structural proteins such as the tail length tape-measure protein, minor tail proteins and a putative tail assembly protein. This synteny is disrupted by one or two genes, depending on the phage. Three groups can be categorized with the majority of phages belonging to group A, while phage PKP126 (group B) and phage 1513 (group C) represent exceptions from the general structure of group A (**Figure 7A** and **Table 6**). Members of group A KP36viruses (including the reference phage KP36) have a single predicted RBP with putative depolymerase activity. It has been demonstrated that the RBP of KP36 is enzymatically active against capsular serotype K63 (Majkowska-Skrobek et al., 2016). The modular structure of this RBP is similar to that of the RBP of group B KP32viruses, having an N-terminal anchor domain, a highly variable central domain with enzymatic activity, and a C-terminal chaperone. KP36viruses belonging to group B and group C also have an RBP with a similar N-terminal anchor domain (**Supplementary Figure S1N**). Phage PKP126 RBP (group B) has a predicted enzymatic activity in the central domain in contrast to the truncated RBP of phage 1513 (group C). The chaperone domain is missing in the RBP of both groups B and C.

No T4gp10-like domain was found in the N-terminal region of KP36gp50 (RBP). Instead, a small domain (residues 4–63) homologous to domain B (92–155 aa) of the distal tail protein (Dit or T5pb9) of siphovirus T5 has been detected. Dit is located in the T5 tail tip at the junction between the tail tube and the ultimate conical structure and is composed of two domains. Domain A forms a hexameric structure and connects to the end of the tail tube, whereas domain B constitutes the attachment site for three L-shaped tail fibers (Flayhan et al., 2014). These L-shaped tail fibers initially bind reversibly to polymannose containing O-antigens (Heller and Braun, 1982). Remarkably, domain A of T5pb9 has not been found in KP36gp50 but is instead present in the KP36 minor tail protein (residues 22–77 corresponding to amino acids 27–85 of T5pb9) that is encoded four genes upstream of KP36gp50. This horizontal transfer event indicates that in KP36viruses the conserved minor tail protein only comprises domain A, which is located at the junction of the tail tube and the conical tip of the tail. Domain A of the minor tail protein is proposed to interact with the RBP *via* its N-terminal domain B. This RBP may thus represent the side tail fibers similar to the L-shaped tail fibers in phage T5. In other words, the distal tail protein has been split into two separate elements in KP36viruses.

Phage PKP126 and 1513 (groups B and C, respectively) have an additional RBP with putative depolymerase activity. Its exact role is difficult to predict and typical elements

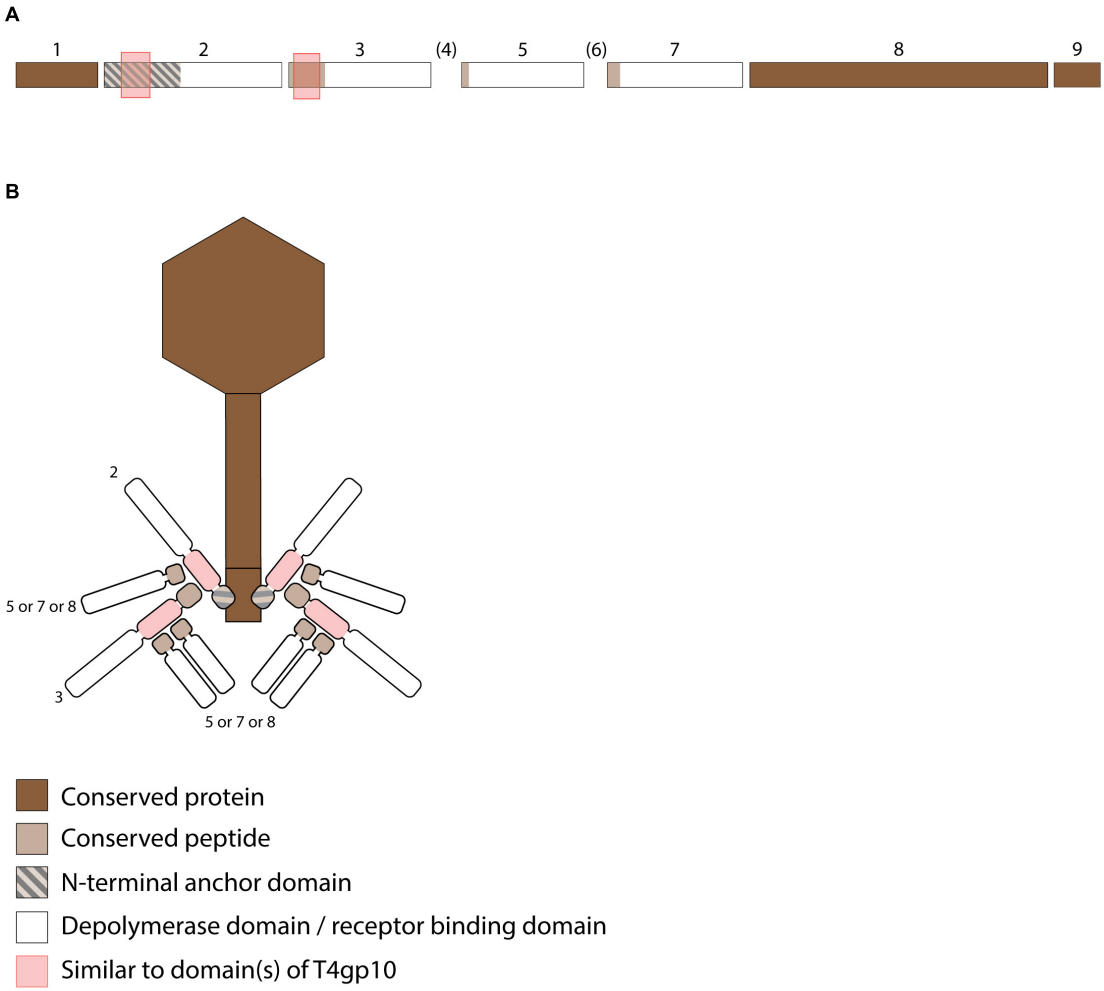

FIGURE 5 | Receptor binding protein systems of the Menlow group. Phages and their RBPs that are proposed to follow this system are summarized in **Table 4**. **(A)** The modular composition of the RBP genes is shown relative to the broken gene synteny of Menlow. Annotations are given according to GenBank or according to their modeled function as annotated in this study (between brackets): (1) – putative tail protein; (2) – tail spike protein (anchor with depolymerase); (3) – tail spike protein (depolymerase with conserved peptide); (4) – hypothetical protein; this protein is not present in all Menlow group phages; (5) – tail spike protein (depolymerase with conserved peptide); (6) – hypothetical protein; this protein is not present in all Menlow group phages; (7) – tail spike protein (depolymerase with conserved peptide); (8) – hypothetical protein (depolymerase); (9) – neck protein. **(B)** Schematic model of the RBP system in Menlow with an anchor-mulibranched attachment mode.

hinting at a specific structural organization such as a conserved peptide or anchor domain are missing. We hypothesize that those enzymes are not incorporated in the phage particle, but rather are produced as soluble proteins. Upon cell lysis the neighboring cells are sensitized for infection through enzymatic removal of the capsule by the soluble, diffusible depolymerase. This mechanism would be especially beneficial for phages lacking depolymerase activity in the their first RBP (e.g., group C phage 1513).

An additional preceding RBP (**Figure 7A**; protein 2) is highly conserved across all analyzed KP36viruses, except in phage 1513. The role of this RBP is unclear. One possibility is that it is a second side RBP as observed in some T5viruses (DT57C and DT571) (Golomidova et al., 2016; Nobrega et al., 2018). An alternative possibility is that this protein represents the central tail fiber. Given its ambiguous role and location, this RBP was not included in the model depicted in **Figure 7B**.

DISCUSSION

In this work we have performed an extensive *in silico* analysis of the RBPs of *Klebsiella* phages genomes with a focus on RBPs with depolymerase activity. The tripartite relationship between depolymerase specificity, capsular serotype and phage host spectrum has now extensively been demonstrated for *Klebsiella* phages (Hsu et al., 2013; Lin et al., 2014; Majkowska-Skrobek et al., 2016; Hsieh et al., 2017; Pan et al., 2017; Solovieva et al., 2018). Podovirus KP32 possesses two experimentally confirmed depolymerases, which are

enzymatically active against capsule serotype K3 and K21, respectively. Correspondingly, all strains infected by phage KP32 have either a K3 or K21 serotype (Majkowska-Skrobek et al., 2018). Podovirus KpV71 infects strains with serotype K1, which perfectly matches the specificity of its experimentally verified depolymerase. However, podovirus KpV74, which has also a single RBP, infects strains with serotype K2 and K13. These observations were explained by the structural similarity of capsule types K2 and K13, which were also found to cross-react with specific antibodies (Pieroni et al., 1994; Pan et al., 2015; Volozhantsev et al., 2016; Solovieva et al., 2018). The more diverse capsular specificity of podoviruses KpV763, KpV766, and KpV289 (Volozhantsev et al., 2016; Solovieva et al., 2018) is now explained in this study by the observed presence of two RBPs (**Table 1**). Some large jumbo phages such as phage ΦK64-1 produce an elaborated, broad-spectrum RBP apparatus. Phage ΦK64-1 encodes 11 putative RBPs from which nine are confirmed to possess enzymatic activity against 10 serotypes in total (K1, K11, K21, K25, K30/K69, K35, K64, KN4, and KN5). Whereas eight RBPs are active against a single but different serotype, the ninth RBP is active against two capsular serotypes (protein 10, **Figure 6**; active against K30 and K69) (Pan et al., 2017).

Based on the structural knowledge of RBPs of mainly *E. coli* phages such as T7, K1F, K1-5, G7C and T5, we have identified structurally conserved building blocks to model the RBP apparatus of *Klebsiella* phages. The modularity of RBPs in combination with intensive horizontal transfer of genes

TABLE 4 | Overview of RBPs of phages belonging to the Menlow group and with (predicted) depolymerase activity.

			Alignment with Menlow RBP			
Phage	**Accession number**	**Number of aa**	**Coverage**	**E-value**	**Identity**	**Identity range**
First RBP with anchor (protein 2, Figure 5)						
Menlow	AUG87748.1	960 aa	100%	0.0	100%	960/960
KpS110	AUV59228.1[c]	960 aa	42%	0.0	95%	383/424
May	AUG87958.1	1180 aa	44%	0.0	90%	392/412
0507-KN2-1	YP_008532046.1[c]	1072 aa	43%	0.0	90%	385/427
Second RBP with conserved peptide (protein 3, Figure 5)						
Menlow	AUG87749.1	768 aa	100%	0.0	100%	768/768
KpS110	AUV59230.1	857 aa	25%	4E-120	96%	189/196
May	AUG87959.1[b]	1288 aa	27%	1E-105	84%	178/212
0507-KN2-1	YP_008532047.1[a]	1245 aa	25%	5E-112	92%	180/195
Third RBP with conserved peptide (protein 5, Figure 5)						
Menlow	AUG87751.1[b]	660 aa	100%	0.0	100%	660/660
KpS110	AUV59232.1	674 aa	13%	6E-22	60%	55/91
May	AUG87960.1[b]	660 aa	100%	0.0	99%	657/660
0507-KN2-1	YP_008532048.1[b]	657 aa	27%	8E-37	48%	91/190
Fourth RBP with conserved peptide (protein 7, Figure 5)						
Menlow	AUG87753.1	730 aa	100%	0.0	100%	730/730
KpS110	AUV59234.1	685 aa	19%	1E-40	61%	86/141
May	AUG87962.1	692 aa	16%	2E-40	71%	86/121
0507-KN2-1	YP_008532049.1[b]	607 aa	14%	1E-35	72%	79/109
Fifth RBP (protein 8, Figure 5)						
Menlow	AUG87754.1[b]	1612 aa	100%	0.0	100%	1612/1612
KpS110	AUV59236.1[b]	1612 aa	100%	0.0	99%	1602/1612
May	AUG87963.1[b]	1612 aa	100%	0.0	99%	1591/1612
0507-KN2-1	YP_008532051.1[b]	1616 aa	100%	0.0	99%	1604/1612
Additional RBP (not present in genome of Menlow)						
Menlow	No protein					
KpS110	AUV59229.1	554 aa		Not applicable		
May	No protein					
0507-KN2-1	YP_008532050.1	542 aa				

The RBP system of phages belonging to the Menlow group is visualized in ***Figure 5****.* [a]*RBP for which the depolymerase activity has been experimentally verified (Hsu et al., 2013).* [b]*RBP with a lower probability on depolymerizing activity.* [c]*RBP without enzymatic activity. BLASTp was used as computational alignment algorithm and pairwise alignments were performed against the respective RBP from phage Menlow. The accession number of each RBP is given, along with its length and alignment characteristics (cover-coverage, E-value,% identity, identity range-number of identical amino acids/length) of the region over which identical amino acids are found by Blastp, starting from the N-terminus (amino acid 1). HHPred analysis revealed homology in RBPs to T4gp10-like domains: First RBP (protein 2) – 94–252 aa compared to 61–248 aa of T4gp10 (Probability 99.88) and 92–251 aa compared to 214–386 aa of T4gp10 (Probability 44.31); Second RBP (protein 3) – 26–204 aa compared to 68–296 aa of T4gp10 (Probability 94.08) and 26–162 aa compared to 165–384 aa of T4gp10 (Probability 95.39) and 41–83 aa compared to 303–383 aa of T4gp10 (Probability 73.93). Values are shown for template phage Menlow.*

or gene domains (Casjens and Molineux, 2012) allows for a maximum re-use of conserved, evolutionary optimized elements. Simultaneously, the possibility to rapidly shift the host spectrum based on an exchange of the depolymerase domain is retained. Indeed, specific RBP domains, sometimes in pair with their cognate chaperone, are present in each RBP system. This is well-illustrated by the high similarity of the experimentally verified depolymerase domains of KP36gp50 and KP34gp57. Both proteins target capsular serotype K63, but have either an N-terminal anchor or conserved peptide, respectively.

The high adaptability of *Klebsiella* phage RBPs is essential since *K. pneumoniae* is featured by a high capsular diversity.

TABLE 5 | Overview of RBPs of phages belonging to the ΦK64-1 group and with (predicted) depolymerase activity.

	RBP					
			Alignment with ΦK64-1 RBP			
Phage	**Accession number**	**Number of aa**	**Coverage**	**E-value**	**Identity**	**Identity range**
First RBP (protein 1, Figure 6)						
ΦK64-1	YP_009153165.1[b]	595 aa	100%	0.0	100%	595/595
RaK2	YP_007007253[b]	595 aa	100%	0.0	100%	595/595
Second RBP with conserved peptide (protein 2, Figure 6)						
ΦK64-1	YP_009153195.1[a]	736 aa	100%	0.0	100%	736/736
RaK2	YP_007007681.1[b]	580 aa	15%	3E-30	61%	75/122
Third RBP (protein 3, Figure 6)						
ΦK64-1	YP_009153196.1[a]	651 aa	100%	0.0	100%	651/651
RaK2	no protein					
Fourth RBP with conserved peptide (protein 4, Figure 6)						
ΦK64-1	YP_009153197.1[a]	702 aa	100%	0.0	100%	702/702
RaK2	YP_007007682.1	715 aa	96%	2E-39	26%	187/718
Fifth RBP with anchor (protein 5, Figure 6)						
ΦK64-1	YP_009153198.1[a]	1193 aa	100%	0.0	100%	1193/1193
RaK2	YP_007007683.1	1113 aa	52%	0.0	82%	518/633
Sixth RBP (protein 6, Figure 6)						
ΦK64-1	YP_009153199.1[a]	584 aa	100%	0.0	100%	584/584
RaK2	YP_007007684.1	584 aa	100%	0.0	99%	581/584
Seventh RBP (protein 7, Figure 6)						
ΦK64-1	YP_009153200.1[a]	779 aa	100%	0.0	100%	779/779
RaK2	YP_007007685.1	779 aa	100%	0.0	97%	754/779
Eighth RBP with conserved peptide (protein 8, Figure 6)						
ΦK64-1	YP_009153201.1[a]	888 aa	100%	0.0	100%	888/888
RaK2	YP_007007686.1	895 aa	29%	1E-147	89%	231/259
Ninth RBP with conserved peptide (protein 9, Figure 6)						
ΦK64-1	YP_009153202.1[a]	996 aa	100%	0.0	100%	996/996
RaK2	YP_007007687.1	806 aa	28%	2E-129	76%	225/298
Tenth RBP (protein 10, Figure 6)						
ΦK64-1	YP_009153203.1[a]	767 aa	100%	0.0	100%	767/767
RaK2	YP_007007688.1	767 aa	100%	0.0	90%	690/767
Eleventh RBP (protein 11, Figure 6)						
ΦK64-1	YP_009153204.1[b]	719 aa	100%	0.0	100%	605/605
RaK2	YP_007007689.1[b]	688 aa	100%	0.0	75%	454/605

The gene syntheny of phages belonging to the ΦK64-1 group is visualized in ***Figure 6****.* [a]*RBP for which the depolymerase activity has been experimentally verified (Pan et al., 2017).* [b]*RBP without enzymatic activity. BLASTp was used as computational alignment algorithm and pairwise alignments were performed against the respective RBP from phage ΦK64-1, respectively. The accession number of each RBP is given, along with its length and alignment characteristics (cover-coverage, E-value,% identity, identity range-number of identical amino acids/length) of the region over which identical amino acids are found by Blastp, starting from the N-terminus (amino acid 1). HHPred analysis revealed homology in RBPs to T4gp10-like domains: Fifth RBP (protein 5) – 113–305 aa compared to 68–384 aa of T4gp10 (Probability 93.67) and 108–241 aa compared to 160–385 aa of T4gp10 (Probability 90.92) and 130–171 aa compared to 305–384 aa of T4gp10 (Probability 48.74); Eighth RBP (protein 8) – 67–221 aa compared to 151–393 aa of T4gp10 (Probability 96.28) and 95–138 aa compared to 303–384 aa of T4gp10 (Probability 74.61) and 79–214 aa compared to 66–247 aa of T4gp10 (Probability 71.93); Ninth RBP (protein 9) – 175–225 aa compared to 303–390 aa of T4gp10 (Probability 92.73) and 160–219 aa compared to 164–245 aa of T4gp10 (Probability 90.38); Tenth RBP (protein 10) – 165–217 aa compared to 303–392 aa of T4gp10 (Probability 89.93) and 123–209 aa compared to 136–254 aa of T4gp10 (Probability 89.87). Values are shown for template phage ΦK64-1.*

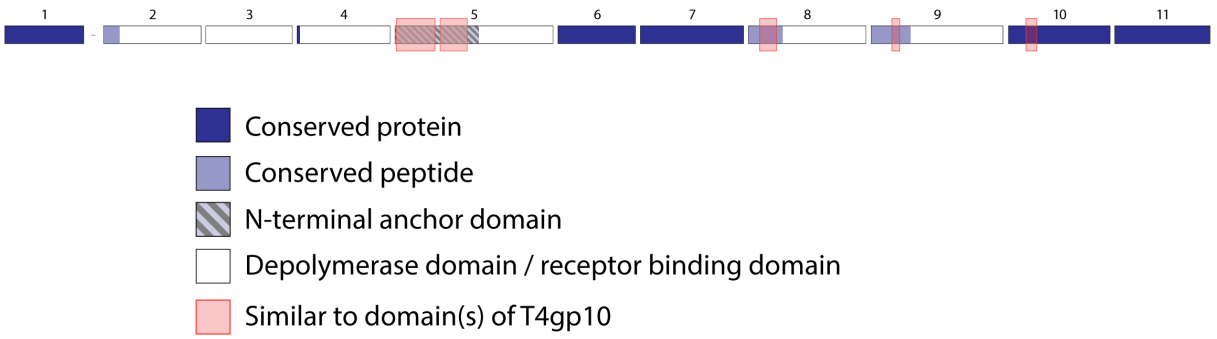

FIGURE 6 | Receptor binding protein systems of phage ΦK64-1 and RaK2. Phages and their RBPs that are proposed to follow this system are summarized in **Table 5**. The modular composition of RBP genes is shown relative to the broken gene synteny. Annotations are given according to GenBank or according to their modeled function in this study (between brackets): (1) – putative tail fiber protein (depolymerase); (2) – tail spike protein (depolymerase with conserved peptide); (3) – tail spike protein (depolymerase); (4)– putative tail fiber protein (depolymerase with conserved peptide); (5) – putative tail fiber protein (anchor with depolymerase); (6) – putative tail fiber protein (depolymerase); (7) – putative structural protein (depolymerase); (8) – putative tail fiber protein (depolymerase with conserved peptide); (9) – putative tail fiber protein (depolymerase with conserved peptide); (10) – putative structural protein (depolymerase); (11) – putative tail fiber protein (depolymerase).

Consequently, *Klebsiella* phages have often a very narrow spectrum limited to strains from one or two capsular serotypes. Colonization of new niches occupied by *K. pneumoniae* isolates with a different capsular serotype thus necessitates a flexible system for rapid adaptation. In addition, the same flexibility is needed to respond to phenotypic serotype switches of *K. pneumoniae* strains (Pan et al., 2015; Wyres et al., 2015).

In this study, we propose that RBPs of *Klebsiella* phages are organized according to several distinct systems (**Figure 8**). The simplest mechanism is similar to the anchor-based system

TABLE 6 | Overview of RBPs of phages belonging to the KP36viruses and with (predicted) depolymerase activity.

Phage	RBP (protein 3, Figure 7)					
			Alignment with KP36 RBP			
	Accession number	Number of aa	Coverage	E-value	Identity	Identity range
Group A (RBP with anchor)						
KP36	YP_009226011.1[a]	883 aa	100%	0.0	100%	883/883
KLPN1	YP_009195383.1	756 aa	30%	3E-99	67%	187/280
KOX1	ARM70347.1	765 aa	21%	1E-89	90%	170/189
JY917	AVI03134.1[c]	812 aa	21%	2E-88	86%	173/201
Sushi	YP_009196676.1[b]	832 aa	18%	2E-75	82%	144/176
MezzoGao	ASV44964.1[b]	973 aa	20%	1E-72	78%	152/194
NJS1	AXF39389.1[b]	992 aa	18%	4E-72	81%	142/176
GML-KpCol1	AUE22051.1[b]	972 aa	18%	8E-71	80%	140/176
KpV522	AOZ65310.1[b]	1141 aa	20%	1E-68	72%	139/193
KPN N141	ASW27458.1[b]	879 aa	18%	1E-59	80%	140/174
Group B (RBP with anchor plus second depolymerase)						
PKP126	YP_009284923.1[b]	833 aa	18%	1E-70	76%	137/180
	YP_009284924	251 aa	hypothetical protein, no similarity			
Group C (RBP with anchor plus second RBP)						
1513	YP_009197878.1[c]	659 aa	21%	4E-86	88%	171/194
	YP_009197879.1	541 aa	Hypothetical protein, no similarity			

*The RBP system of KP36viruses is visualized in **Figure 7**. [a]RBP for which the depolymerase activity has been experimentally verified (Majkowska-Skrobek et al., 2016). [b]RBP with a lower probability on depolymerizing activity. [c]RBP without enzymatic activity. BLASTp was used as computational alignment algorithm and pairwise alignments were performed against the respective RBP from phage KP36. The accession number of each RBP is given, along with its length and alignment characteristics (cover-coverage, E-value,% identity, identity range-number of identical amino acids/length) of the region over which identical amino acids are found by Blastp, starting from the N-terminus (amino acid 1).*

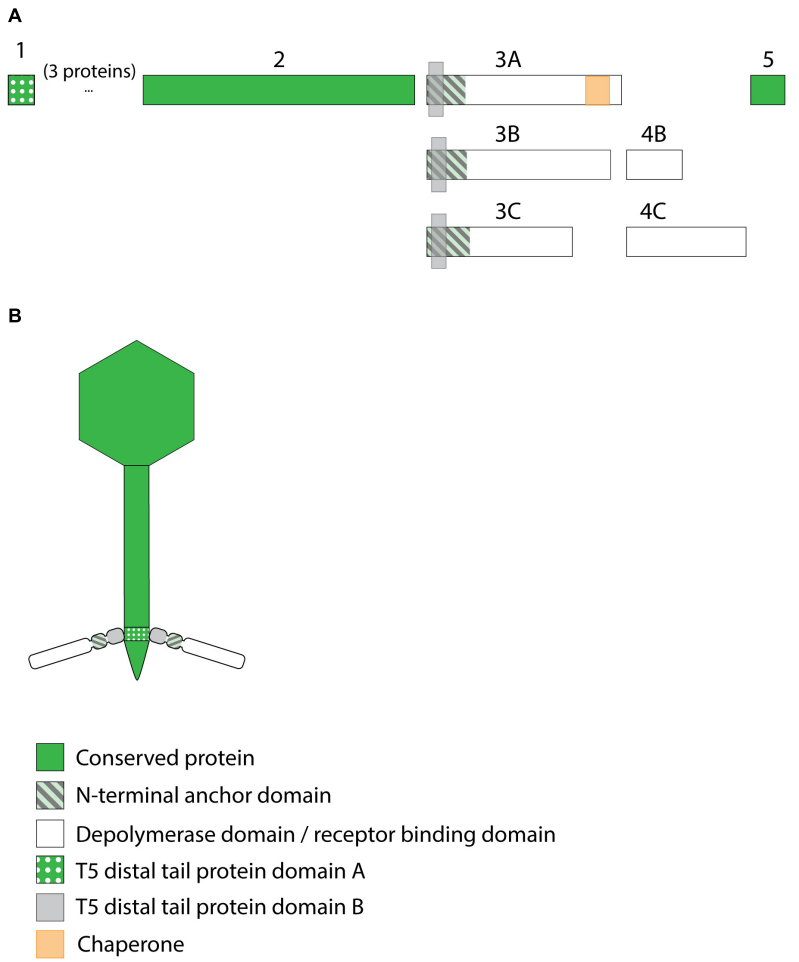

FIGURE 7 | Receptor binding protein systems of the KP36viruses. Phages and their RBPs that are proposed to follow this system, including their grouping into groups A, B and C, are summarized in **Table 6**. **(A)** The modular composition of the RBP genes is shown relative to the broken gene synteny of the reference phage KP36. Annotations are given according to GenBank or according to their modeled function in this study (between brackets): (1) – minor tail protein; (2) – tail fiber protein; (3) – putative tail fiber protein (3A,B – anchor with depolymerase; 3C – anchor); (4) – hypothetical protein (4B,C – depolymerase); (5) – putative single-stranded DNA binding protein. Proteins 1, 2, and 5 are present in all KP36viruses. **(B)** Schematic model of the RBP system in phage particles of KP36viruses group A with a split T5 distal tail protein. Domain A is encoded by short minor tail protein forming a ring at the end of the phage tail tube and offers an attachment point for domain B, which is incorporated in the anchoring part of the RBP that represents the putative side tail fiber.

described for phage T7 and K1F. In phages from KP32viruses group B and KP36viruses, the single RBP is directly connected with the phage particle *via* its conserved N-terminal anchor domain. Other phages (KP32viruses group A; KP34 viruses group B) that produce two RBPs encode the structural elements for an anchor-branched mechanism as reported for phage G7C. Here, the first RBP contains a conserved N-terminal anchor serving for attachment to the virion, followed by a specific fragment of a T4gp10-like domain providing the docking site for a second RBP. Notably, the fragment encoding the T4gp10-like docking site in those *Klebsiella* phages is shorter compared to the corresponding domain in T4 and may therefore correspond to a single attachment site. The second RBP is presumably attached *via* a conserved peptide (KP32viruses, KP34viruses, JD001 group, Menlow group, ΦK64-1 group). This conserved peptide is different for each group of phages, varies in length and can be as short as seven amino acids. Such attachment *via* a short peptide is in line with the RBP complex of K1E/K1-5/SP6-like phages where both RBPs carry either a 7- or 11-residue conserved peptide at their respective N-terminus. In the case of *E. coli* phage G7C the shorter G7Cgp63.1 RBP carries a positively charged surface that binds to the T4gp10-like domain of G7Cgp66, yet, the conserved peptides in *Klebsiella* phages lack this positive charge, inferring that different interacting forces take place between the first and second RBP. Similar to the RBPs of phage K1-5, the two experimentally verified depolymerases of phage KP32 target two different capsular serotypes. In both cases the double RBP system thus expands the host spectrum.

The presence of either an anchor- or an anchor-branched system is not directly linked to the taxonomic organization. In addition, there is no sequence homology between functionally similar, structural building blocks across those phage groups.

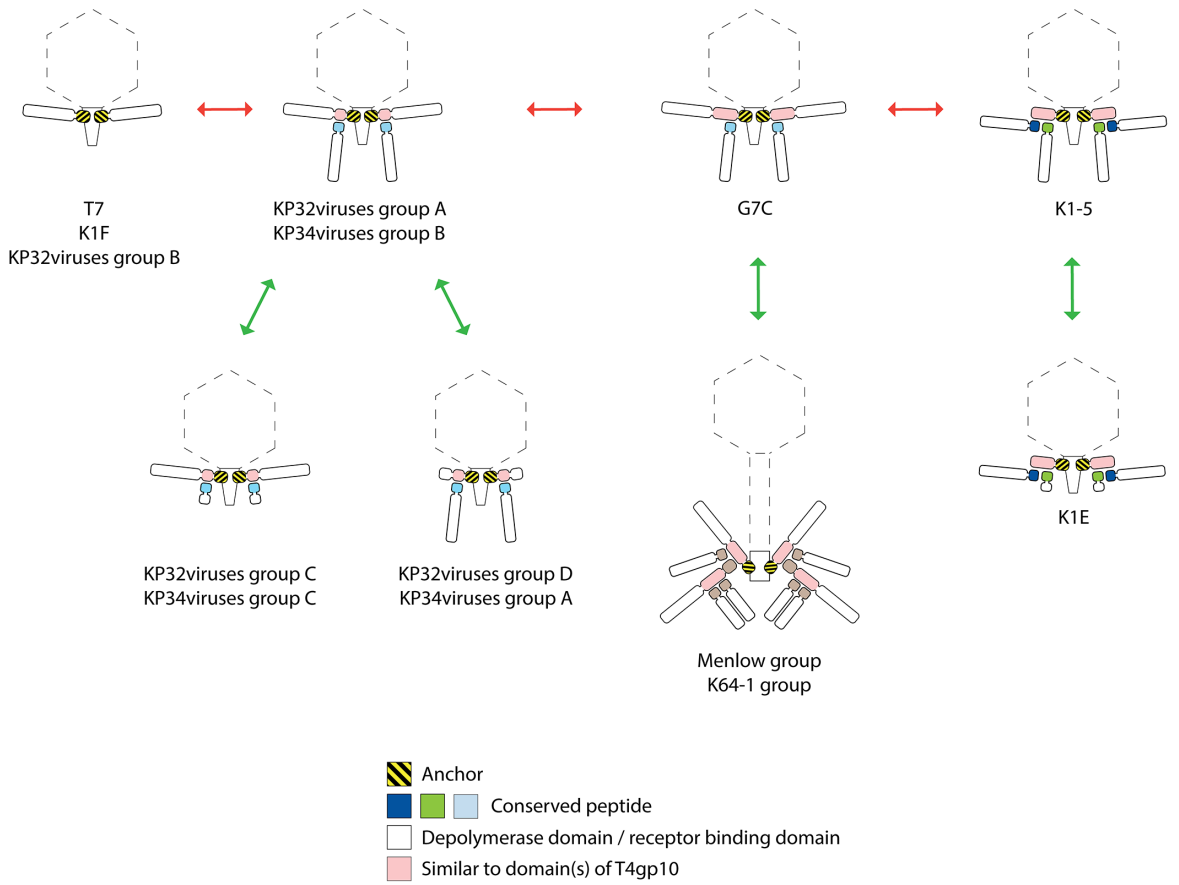

FIGURE 8 | Possible evolutionary linkages between diverse RBP systems, driven by the acquisition and loss of domains. The model RBP systems of phage T7, K1F, G7C, K1-5, and K1-E have been reported before. The RBP systems of KP32viruses groups A, B, C, D (**Figure 2** and **Table 1**), KP34viruses groups A, B, C (**Figure 3** and **Table 2**), phages belonging to the Menlow group (**Figure 5** and **Table 4**) and phage belonging to the ΦK64-1 group (**Figure 6** and **Table 5**) have been studied in this work.

E.g., the first 140 amino acids of the N-terminal anchor domains of RBPs encoded by *Klebsiella* phages belonging to *Podoviridae* show similarity with the well-characterized N-terminal domain of T7 tail fiber and their first 300 amino acids are conserved across different podoviruses analyzed in this study. The T7 tail fiber attaches with its N-terminal anchor domain to the region where the adaptor (gp11) interacts with nozzle (gp12) of the short tail complex (Cuervo et al., 2013). The corresponding proteins of phage KP32 share 62 and 61% sequence identity with the adaptor and nozzle protein of phage T7, respectively, while in the case of KP34 the identity is lower (29% identity with a coverage of 67% for the adaptor protein and 23% identity with a coverage of 98% for the nozzle protein). There is no amino acid similarity between the conserved N-terminal anchor domains in RBPs from different taxonomic groups of *Klebsiella* phages indicating that also the interacting partner in the tail structure has also evolved accordingly. In the case of KP36viruses (*Siphoviridae*), a remarkable horizontal transfer event has taken place between the distal tail protein and the tail fiber of KP36viruses when comparing to the siphovirus T5 model. Domain B of the distal tail protein has been transferred to the N-terminus of the tail fiber protein in KP36viruses. Whereas in phage T5 protein–protein interaction occurs between the N-terminus of the RBP and domain B of the distal tail protein, novel interactions between domain A of the minor tail protein and domain B embedded in the tail fiber must have been evolved to compensate for the loss of interaction by a direct covalent bond as in phage T5.

Interestingly, several phages with a single enzymatic RBP do not follow the anchor system as described for phage T7, but use the anchor-branched system of G7C with either the first (KP32virus group D; KP34virus group A; JD001 group) or second RBP (KP32virus group C; KP34virus group C) being truncated. In the case of KP34viruses it is even the predominant RBP system. The occurrence of these intermediate RBP systems suggests evolutionary linkages between the different RBP architectures. Starting from the simplest organization with a single RBP (T7, K1F, and KP32viruses group B), the acquisition of a fragment of a T4gp10-like domain allowed for the attachment of a second RBP (KP32viruses group A and KP34viruses group B). The first RBP from *E. coli* phage G7C has acquired a full T4gp10-like domain (similarity to both subdomain D2 and D3 of T4gp10), offering a potential second

attachment site for a different RBP. This second site is not occupied in phage G7C, whereas the *E. coli* model phages K1-5, SP6, and K1E have effectively two RBPs attached to the same intermediate protein that also comprises both subdomain D2 and D3. In K1-5, SP6 and K1E, this intermediate protein with the full T4gp10-like domain has lost its C-terminal receptor-binding domain, resulting in an 'adapter' system – a short protein with two sites for binding two different RBPs and no domain beyond these two domains (**Figure 8**). It should be noted that a simple adapter protein that provides attachment sites for two RBPs as described for *E. coli* phage K1-5 and *Salmonella* phage SP6 is not observed in the case of *Klebsiella* podoviruses. Obviously, an opposite evolutionary trajectory of RBP systems (from adapter to anchor) cannot be excluded as well. The success of the modular build-up of the RBP apparatus and the extensive number of horizontal transfer events have obscured possible insight in the direction of this evolution. The assumption that evolution generally takes place from simple to more complex systems, hints at the first direction (from anchor to adapter). KP32viruses group C and D, and KP34viruses groups A and C may have lost a second intact RBP by retrograde evolution when thriving in a new environment that is dominated by a single serotype *Klebsiella* strain. Having a truncated second RBP may provide a fitness advantage in such a situation. The truncated RBP may remain as a temporal docking site to acquire a new RBP for host range expansion by horizontal transfer when moving to a niche with different *Klebsiella* serotypes. Phages belonging to the Menlow group and ΦK64-1 group carry multiple RBPs that obviously recycle established structural elements such as a conserved N-terminal domain, short conserved peptides and a T4gp10-like domain (or fragments thereof). Yet, more experimental (structural, genetic, biochemical) studies are required to make a plausible prediction on the structural organization of these elaborated RBP systems.

In summary, we have modeled the organization of diverse RBP systems in *Klebsiella* phages. The modular composition and re-use of established structural domains for anchoring and branching provide the phages the full potential to rapidly shift capsular serotype specificity or to expand the spectrum. We expect that the increasing amount of (meta)genome sequencing data will reveal further evolutionary relationships between some of the groups we describe in this analysis, but the main groups will remain in place. The data available to us today clearly show that the architecture of RBP systems is dominated by horizontal transfer events of modules that can be as small as short peptides to as large as multiple domains. Although our analysis was based on experimentally confirmed interactions of *E. coli* phage RBPs (Leiman et al., 2007; Prokhorov et al., 2017), further experimental validation of the presented models is needed and has already been initiated by our team. To analyze the interactions between the T4gp10-like domains and conserved peptides, protein–protein interactions can be studied by various techniques such as isothermal calorimetry (ITC), two-hybrid systems, surface plasmon resonance (SPR), cryoEM, or an enzyme-linked immunosorbent assay (ELISA). This work also adds improved functional annotations to genes to which previously no specific function has been assigned, but which are putative tail fibers/spikes with depolymerizing activity. The high number of newly predicted depolymerases in this study can be verified by their recombinant production followed by activity tests against strains with particular capsular serotypes.

DATA AVAILABILITY STATEMENT

The datasets analyzed for this study can be found in the GenBank. All genome and protein accession numbers are listed in the tables and **Supplementary Material**.

AUTHOR CONTRIBUTIONS

AL, ZD-K, and YB designed the *in silico* search approach of RBPs domains and modeled the RBP assembly systems. PL introduced the concept of branching RBPs. AL performed *in silico* analysis and collected the data. AL, PL, ZD-K, and YB analyzed the data and worked on the manuscript. All authors read and accepted the final version of the manuscript.

FUNDING

This study was supported by National Science Centre, Poland (Grant Numbers UMO-2015/19/N/NZ1/00014 to AL, ZD-K, UMO-2017/26/M/NZ1/00233 to ZD-K, AL) and by a doctoral scholarship of "Bijzonder Onderzoeksfonds" of Ghent University (Grant Number BOF16/FJD/007 to AL).

SUPPLEMENTARY MATERIAL

The Supplementary Material for this article can be found online at: https://www.frontiersin.org/articles/10.3389/fmicb.2019.02649/full#supplementary-material

REFERENCES

Adriaenssens, E. M., Ackermann, H. W., Anany, H., Blasdel, B., Connerton, I. F., Goulding, D., et al. (2012). A suggested new bacteriophage genus: "Viunalikevirus". *Arch. Virol.* 157, 2035–2046. doi: 10.1007/s00705-012-1360-1365

Adriaenssens, E. M., Wittmann, J., Kuhn, J. H., Turner, D., Sullivan, M. B., Dutilh, B. E., et al. (2018). Taxonomy of prokaryotic viruses: 2017 update from the ICTV bacterial and archaeal viruses subcommittee. *Arch. Virol.* 163, 1125–1129. doi: 10.1007/s00705-018-3723-z

Altschul, S. F., Gish, W., Miller, W., Myers, E. W., and Lipman, D. J. (1990). Basic local alignment search tool. *J. Mol. Biol.* 215, 403–410. doi: 10.1016/S0022-2836(05)80360-80362

Andres, D., Baxa, U., Hanke, C., Seckler, R., and Barbirz, S. (2010). Carbohydrate binding of *Salmonella* phage P22 tailspike protein and its role during host cell infection. *Biochem. Soc. Trans.* 38, 1386–1389. doi: 10.1042/BST0381386

Barbirz, S., Muller, J. J., Uetrecht, C., Clark, A. J., Heinemann, U., and Seckler, R. (2008). Crystal structure of *Escherichia coli* phage HK620 tailspike: podoviral tailspike endoglycosidase modules are evolutionarily related. *Mol. Microbiol.* 69, 303–316. doi: 10.1111/j.1365-2958.2008.06311.x

Berman, H. M., Westbrook, J., Feng, Z., Gilliland, G., Bhat, T. N., Weissig, H., et al. (2000). The protein data bank. *Nucleic Acids Res.* 28, 235–242. doi: 10.1093/nar/28.1.235

Bordoli, L., Kiefer, F., Arnold, K., Benkert, P., Battey, J., and Schwede, T. (2009). Protein structure homology modeling using SWISS-MODEL workspace. *Nat. Protoc.* 4, 1–13. doi: 10.1038/nprot.2008.197

Bordoli, L., and Schwede, T. (2012). Automated protein structure modeling with SWISS-MODEL workspace and the protein model portal. *Methods Mol. Biol.* 857, 107–136. doi: 10.1007/978-1-61779-588-6-5

Broeker, N. K., Kiele, F., Casjens, S. R., Gilcrease, E. B., Thalhammer, A., Koetz, J., et al. (2018). *In Vitro* studies of lipopolysaccharide-mediated DNA release of podovirus HK620. *Viruses* 10:E289. doi: 10.3390/v10060289

Calfee, D. P. (2017). Recent advances in the understanding and management of *Klebsiella pneumoniae*. *F1000Res* 6:1760. doi: 10.12688/f1000research.11532.1

Casjens, S. R., and Molineux, I. J. (2012). Short noncontractile tail machines: adsorption and DNA delivery by podoviruses. *Adv. Exp. Med. Biol.* 726, 143–179. doi: 10.1007/978-1-4614-0980-9-7

Chen, Z., Liu, M., Cui, Y., Wang, L., Zhang, Y., Qiu, J., et al. (2014). A novel PCR-based genotyping scheme for clinical *Klebsiella pneumoniae*. *Future Microbiol.* 9, 21–32. doi: 10.2217/fmb.13.137

Cornelissen, A., Ceyssens, P. J., T'Syen, J., Van Praet, H., Noben, J. P., Shaburova, O. V., et al. (2011). The T7-related *Pseudomonas putida* phage phi 15 displays virion-associated biofilm degradation properties. *PLoS One* 6:e18597. doi: 10.1371/journal.pone.0018597

Cortés, G., Borrell, N., de Astorza, B., Gómez, C., Sauleda, J., and Albertí, S. (2002). Molecular analysis of the contribution of the capsular polysaccharide and the lipopolysaccharide O side chain to the virulence of *Klebsiella pneumoniae* in a murine model of pneumonia. *Infect. Immun.* 70, 2583–2590. doi: 10.1128/iai.70.5.2583-2590.2002

Crooks, G. E., Hon, G., Chandonia, J. M., and Brenner, S. E. (2004). WebLogo: a sequence logo generator. *Genome Res.* 14, 1188–1190. doi: 10.1101/gr.849004

Cuervo, A., Pulido-Cid, M., Chagoyen, M., Arranz, R., González-García, V. A., Garcia-Doval, C., et al. (2013). Structural characterization of the bacteriophage T7 tail machinery. *J. Biol. Chem.* 288, 26290–26299. doi: 10.1074/jbc.M113.491209

Davies, G., and Henrissat, B. (1995). Structures and mechanisms of glycosyl hydrolases. *Structure* 3, 853–859. doi: 10.1016/S0969-2126(01)00220-229

Day, A., Ahn, J., and Salmond, G. P. C. (2018). Jumbo bacteriophages are represented within an increasing diversity of environmental viruses infecting the emerging phytopathogen, dickeya solani. *Front. Microbiol.* 9:2169. doi: 10.3389/fmicb.2018.02169

Finn, R. D., Clements, J., and Eddy, S. R. (2011). HMMER web server: interactive sequence similarity searching. *Nucleic Acids Res.* 39, W29–W37. doi: 10.1093/nar/gkr367

Flayhan, A., Vellieux, F. M., Lurz, R., Maury, O., Contreras-Martel, C., and Girard, E. (2014). Crystal structure of pb9, the distal tail protein of bacteriophage T5: a conserved structural motif among all siphophages. *J. Virol.* 88, 820–828. doi: 10.1128/JVI.02135-2113

Gebhart, D., Williams, S. R., and Scholl, D. (2017). Bacteriophage SP6 encodes a second tailspike protein that recognizes *Salmonella enterica* serogroups C2 and C3. *Virology* 507, 263–266. doi: 10.1016/j.virol.2017.02.025

Golomidova, A. K., Kulikov, E. E., Prokhorov, N. S., Guerrero-Ferreira, R., Knirel, Y. A., Kostryukova, E. S., et al. (2016). Branched lateral tail fiber organization in T5-like bacteriophages DT57C and DT571/2 is revealed by genetic and functional analysis. *Viruses* 8:26. doi: 10.3390/v8010026

Heller, K., and Braun, V. (1982). Polymannose O-antigens of *Escherichia coli*, the binding sites for the reversible adsorption of bacteriophage T5+ via the L-shaped tail fibers. *J. Virol.* 41, 222–227.

Hsieh, P. F., Lin, H. H., Lin, T. L., Chen, Y. Y., and Wang, J. T. (2017). Two T7-like bacteriophages, K5-2 and K5-4, each encodes two capsule depolymerases: isolation and functional characterization. *Sci. Rep.* 7:4624. doi: 10.1038/s41598-017-04644-4642

Hsu, C. R., Lin, T. L., Pan, Y. J., Hsieh, P. F., and Wang, J. T. (2013). Isolation of a bacteriophage specific for a new capsular type of *Klebsiella pneumoniae* and characterization of its polysaccharide depolymerase. *PLoS One* 8:e70092. doi: 10.1371/journal.pone.0070092

Kelley, L. A., Mezulis, S., Yates, C. M., Wass, M. N., and Sternberg, M. J. (2015). The Phyre2 web portal for protein modeling, prediction and analysis. *Nat. Protoc.* 10, 845–858. doi: 10.1038/nprot.2015.053

Latka, A., Maciejewska, B., Majkowska-Skrobek, G., Briers, Y., and Drulis-Kawa, Z. (2017). Bacteriophage-encoded virion-associated enzymes to overcome the carbohydrate barriers during the infection process. *Appl. Microbiol. Biotechnol.* 101, 3103–3119. doi: 10.1007/s00253-017-8224-8226

Lee, C. R., Lee, J. H., Park, K. S., Jeon, J. H., Kim, Y. B., Cha, C. J., et al. (2017). Antimicrobial resistance of hypervirulent *Klebsiella pneumoniae*: epidemiology, hypervirulence-associated dete rminants, and resistance mechanisms. *Front. Cell Infect. Microbiol.* 7:483. doi: 10.3389/fcimb.2017.00483

Leiman, P. G., Battisti, A. J., Bowman, V. D., Stummeyer, K., Mühlenhoff, M., Gerardy-Schahn, R., et al. (2007). The structures of bacteriophages K1E and K1-5 explain processive degradation of polysaccharide capsules and evolution of new host specificities. *J. Mol. Biol.* 371, 836–849. doi: 10.1016/j.jmb.2007.05.083

Leiman, P. G., and Molineux, I. J. (2008). Evolution of a new enzyme activity from the same motif fold. *Mol. Microbiol.* 69, 287–290. doi: 10.1111/j.1365-2958.2008.06241.x

Lin, T. L., Hsieh, P. F., Huang, Y. T., Lee, W. C., Tsai, Y. T., Su, P. A., et al. (2014). Isolation of a bacteriophage and its depolymerase specific for K1 capsule of *Klebsiella pneumoniae*: implication in typing and treatment. *J. Infect. Dis.* 210, 1734–1744. doi: 10.1093/infdis/jiu332

Majkowska-Skrobek, G., Łątka, A., Berisio, R., Maciejewska, B., Squeglia, F., Romano, M., et al. (2016). Capsule-targeting depolymerase, derived from *Klebsiella* KP36 phage, as a tool for the development of anti-virulent strategy. *Viruses* 8:324. doi: 10.3390/v8120324

Majkowska-Skrobek, G., Latka, A., Berisio, R., Squeglia, F., Maciejewska, B., Briers, Y., et al. (2018). Phage-borne depolymerases decrease *Klebsiella pneumoniae* resistance to innate defense mechanisms. *Front. Microbiol.* 9:2517. doi: 10.3389/fmicb.2018.02517

Nobrega, F. L., Vlot, M., de Jonge, P. A., Dreesens, L. L., Beaumont, H. J. E., Lavigne, R., et al. (2018). Targeting mechanisms of tailed bacteriophages. *Nat. Rev. Microbiol.* 16, 760–773. doi: 10.1038/s41579-018-0070-78

Olszak, T., Shneider, M. M., Latka, A., Maciejewska, B., Browning, C., Sycheva, L. V., et al. (2017). The O-specific polysaccharide lyase from the phage LKA1 tailspike reduces *Pseudomonas* virulence. *Sci. Rep.* 7:16302. doi: 10.1038/s41598-017-16411-4.

Pan, Y. J., Lin, T. L., Chen, C. C., Tsai, Y. T., Cheng, Y. H., Chen, Y. Y., et al. (2017). *Klebsiella* phage ΦK64-1 encodes multiple depolymerases for multiple host capsular types. *J. Virol.* 91:e2457-16. doi: 10.1128/JVI.02457-2416

Pan, Y. J., Lin, T. L., Chen, C. T., Chen, Y. Y., Hsieh, P. F., Hsu, C. R., et al. (2015). Genetic analysis of capsular polysaccharide synthesis gene clusters in 79 capsular types of *Klebsiella* spp. *Sci. Rep.* 5:15573. doi: 10.1038/srep15573

Pieroni, P., Rennie, R. P., Ziola, B., and Deneer, H. G. (1994). The use of bacteriophages to differentiate serologically cross-reactive isolates of *Klebsiella pneumoniae*. *J. Med. Microbiol.* 41, 423–429. doi: 10.1099/00222615-41-6-423

Pires, D. P., Oliveira, H., Melo, L. D., Sillankorva, S., and Azeredo, J. (2016). Bacteriophage-encoded depolymerases: their diversity and biotechnological applications. *Appl. Microbiol. Biotechnol.* 100, 2141–2151. doi: 10.1007/s00253-015-7247-7240

Plattner, M., Shneider, M. M., Arbatsky, N. P., Shashkov, A. S., Chizhov, A. O., Nazarov, S., et al. (2019). Structure and function of the branched receptor-binding complex of bacteriophage CBA120. *J. Mol. Biol.* 431, 3718–3739. doi: 10.1016/j.jmb.2019.07.022

Prokhorov, N. S., Riccio, C., Zdorovenko, E. L., Shneider, M. M., Browning, C., Knirel, Y. A., et al. (2017). Function of bacteriophage G7C esterase tailspike in host cell adsorption. *Mol. Microbiol.* 105, 385–398. doi: 10.1111/mmi.13710

Rose, A. S., Bradley, A. R., Valasatava, Y., Duarte, J. M., Prlic, A., and Rose, P. W. (2018). NGL viewer: web-based molecular graphics for large complexes. *Bioinformatics* 34, 3755–3758. doi: 10.1093/bioinformatics/bty419

Schmid, J., Sieber, V., and Rehm, B. (2015). Bacterial exopolysaccharides: biosynthesis pathways and engineering strategies. *Front. Microbiol.* 6:496. doi: 10.3389/fmicb.2015.00496

Schwarzer, D., Browning, C., Stummeyer, K., Oberbeck, A., Mühlenhoff, M., Gerardy-Schahn, R., et al. (2015). Structure and biochemical characterization of

bacteriophage phi92 endosialidase. *Virology* 477, 133–143. doi: 10.1016/j.virol.2014.11.002

Schwarzer, D., Buettner, F. F., Browning, C., Nazarov, S., Rabsch, W., Bethe, A., et al. (2012). A multivalent adsorption apparatus explains the broad host range of phage phi92: a comprehensive genomic and structural analysis. *J. Virol.* 86, 10384–10398. doi: 10.1128/JVI.00801-812

Schwarzer, D., Stummeyer, K., Gerardy-Schahn, R., and Mühlenhoff, M. (2007). Characterization of a novel intramolecular chaperone domain conserved in endosialidases and other bacteriophage tail spike and fiber proteins. *J. Biol. Chem.* 282, 2821–2831. doi: 10.1074/jbc.M609543200

Seul, A., Müller, J. J., Andres, D., Stettner, E., Heinemann, U., and Seckler, R. (2014). Bacteriophage P22 tailspike: structure of the complete protein and function of the interdomain linker. *Acta Crystallogr. D Biol. Crystallogr.* 70(Pt 5), 1336–1345. doi: 10.1107/S1399004714002685

Simoliūnas, E., Kaliniene, L., Truncaitė, L., Zajančkauskaitė, A., Staniulis, J., Kaupinis, A., et al. (2013). Klebsiella phage vB_KleM-RaK2 - a giant singleton virus of the family *Myoviridae*. *PLoS One* 8:e60717. doi: 10.1371/journal.pone.0060717

Solovieva, E. V., Myakinina, V. P., Kislichkina, A. A., Krasilnikova, V. M., Verevkin, V. V., Mochalov, V. V., et al. (2018). Comparative genome analysis of novel *Podoviruses* lytic for hypermucoviscous *Klebsiella pneumoniae* of K1, K2, and K57 capsular types. *Virus Res.* 243, 10–18. doi: 10.1016/j.virusres.2017.09.026

Steven, A. C., Trus, B. L., Maizel, J. V., Unser, M., Parry, D. A., Wall, J. S., et al. (1988). Molecular substructure of a viral receptor-recognition protein. The gp17 tail-fiber of bacteriophage T7. *J. Mol. Biol.* 200, 351–365. doi: 10.1016/0022-2836(88)90246-X

Stummeyer, K., Dickmanns, A., Mühlenhoff, M., Gerardy-Schahn, R., and Ficner, R. (2005). Crystal structure of the polysialic acid-degrading endosialidase of bacteriophage K1F. *Nat. Struct. Mol. Biol.* 12, 90–96. doi: 10.1038/nsmb874

Stummeyer, K., Schwarzer, D., Claus, H., Vogel, U., Gerardy-Schahn, R., and Mühlenhoff, M. (2006). Evolution of bacteriophages infecting encapsulated bacteria: lessons from *Escherichia coli* K1-specific phages. *Mol. Microbiol.* 60, 1123–1135. doi: 10.1111/j.1365-2958.2006.05173.x

Sutherland, I. W. (1995). Polysaccharide lyases. *FEMS Microbiol. Rev.* 16, 323–347. doi: 10.1111/j.1574-6976.1995.tb00179.x

Taylor, N. M., Prokhorov, N. S., Guerrero-Ferreira, R. C., Shneider, M. M., Browning, C., Goldie, K. N., et al. (2016). Structure of the T4 baseplate and its function in triggering sheath contraction. *Nature* 533, 346–352. doi: 10.1038/nature17971

Tu, J., Park, T., Morado, D. R., Hughes, K. T., Molineux, I. J., and Liu, J. (2017). Dual host specificity of phage SP6 is facilitated by tailspike rotation. *Virology* 507, 206–215. doi: 10.1016/j.virol.2017.04.017

Volozhantsev, N. V., Myakinina, V. P., Popova, A. V., Kislichkina, A. A., Komisarova, E. V., Knyazeva, A. I., et al. (2016). Complete genome sequence of novel T7-like virus vB_KpnP_KpV289 with lytic activity against *Klebsiella pneumoniae*. *Arch. Virol.* 161, 499–501. doi: 10.1007/s00705-015-2680-z

Weigele, P. R., Scanlon, E., and King, J. (2003). Homotrimeric, beta-stranded viral adhesins and tail proteins. *J. Bacteriol.* 185, 4022–4030. doi: 10.1128/jb.185.14.4022-4030.2003

Weiner, L. M., Webb, A. K., Limbago, B., Dudeck, M. A., Patel, J., Kallen, A. J., et al. (2016). Antimicrobial-resistant pathogens associated with healthcare-associated infections: summary of data reported to the national healthcare safety network at the centers for disease control and prevention, 2011-2014. *Infect. Control Hosp. Epidemiol.* 37, 1288–1301. doi: 10.1017/ice.2016.174

Wick, R. R., Heinz, E., Holt, K. E., and Wyres, K. L. (2018). Kaptive web: user-friendly capsule and lipopolysaccharide serotype prediction for *Klebsiella* Genomes. *J. Clin. Microbiol.* 56:e197-18. doi: 10.1128/JCM.00197-118

Williams, S. R., Gebhart, D., Martin, D. W., and Scholl, D. (2008). Retargeting R-type pyocins to generate novel bactericidal protein complexes. *Appl. Environ. Microbiol.* 74, 3868–3876. doi: 10.1128/AEM.00141-148

Wyres, K. L., Gorrie, C., Edwards, D. J., Wertheim, H. F., Hsu, L. Y., Van Kinh, N., et al. (2015). Extensive capsule locus variation and large-scale genomic recombination within the *Klebsiella pneumoniae* clonal group 258. *Genom. Biol. Evol.* 7, 1267–1279. doi: 10.1093/gbe/evv062

Wyres, K. L., Wick, R. R., Gorrie, C., Jenney, A., Follador, R., Thomson, N. R., et al. (2016). Identification of *Klebsiella* capsule synthesis loci from whole genome data. *Microb. Genom.* 2:e000102. doi: 10.1099/mgen.0.000102

Yan, J., Mao, J., and Xie, J. (2014). Bacteriophage polysaccharide depolymerases and biomedical applications. *Biodrugs* 28, 265–274. doi: 10.1007/s40259-013-0081-y

Zimmermann, L., Stephens, A., Nam, S. Z., Rau, D., Kübler, J., Lozajic, M., et al. (2018). A completely reimplemented MPI bioinformatics toolkit with a new HHpred server at its core. *J. Mol. Biol.* 430, 2237–2243. doi: 10.1016/j.jmb.2017.12.007

Conflict of Interest: The authors declare that the research was conducted in the absence of any commercial or financial relationships that could be construed as a potential conflict of interest.

frontiers in Microbiology

ORIGINAL RESEARCH
published: 06 December 2019
doi: 10.3389/fmicb.2019.02771

Dendronized Silver Nanoparticles as Bacterial Membrane Permeabilizers and Their Interactions With *P. aeruginosa* Lipopolysaccharides, Lysozymes, and Phage-Derived Endolysins

Karol Ciepluch[1], Kinga Skrzyniarz[1], Andrea Barrios-Gumiel[2,3,4], Sara Quintana[2,3], Javier Sánchez-Nieves[2,3,4], F. Javier de la Mata[2,3,4], Barbara Maciejewska[5], Zuzanna Drulis-Kawa[5] and Michał Arabski[1]*

[1] Department of Biochemistry and Genetics, Jan Kochanowski University, Kielce, Poland, [2] Department of Organic and Inorganic Chemistry, Chemistry Research Institute "Andrés M. del Río" (IQAR), University of Alcalá, Madrid, Spain, [3] Networking Research Center on Bioengineering, Biomaterials and Nanomedicine (CIBER-BBN), Madrid, Spain, [4] Institute Ramón y Cajal for Health Research (IRYCIS), Madrid, Spain, [5] Department of Pathogen Biology and Immunology, Institute of Genetics and Microbiology, University of Wrocław, Wrocław, Poland

OPEN ACCESS

Edited by:
Dieter Jahn, Technische Universitat Braunschweig, Germany

Reviewed by:
Kenneth K. Y. Wong, The University of Hong Kong, Hong Kong
Paola Sperandeo, University of Milan, Italy

***Correspondence:**
Karol Ciepluch
karol.ciepluch@ujk.edu.pl

Specialty section:
This article was submitted to Infectious Diseases, a section of the journal Frontiers in Microbiology

Received: *26 September 2019*
Accepted: *13 November 2019*
Published: *06 December 2019*

Citation:
Ciepluch K, Skrzyniarz K, Barrios-Gumiel A, Quintana S, Sánchez-Nieves J, de la Mata FJ, Maciejewska B, Drulis-Kawa Z and Arabski M (2019) Dendronized Silver Nanoparticles as Bacterial Membrane Permeabilizers and Their Interactions With P. aeruginosa Lipopolysaccharides, Lysozymes, and Phage-Derived Endolysins. Front. Microbiol. 10:2771. doi: 10.3389/fmicb.2019.02771

Antimicrobial proteins, like lysozymes produced by animals or bacteriophage lysins, enable the degradation of bacterial peptidoglycan (PG) and, consequently, lead to bacterial cell lysis. However, the activity of those enzymes is not satisfactory against gram-negative bacteria because of the presence of an outer membrane (OM) barrier. Lytic enzymes can therefore be combined with membrane-disrupting agents, such as dendritic silver nanoparticles. Nevertheless, a lipopolysaccharide (LPS), especially the smooth type, could be the main hindrance for highly charged nanoparticles to get direct access to the bacterial OM and to help lytic enzymes to reach their target PG. Herein, we have investigated the interactions of PEGylated carbosilane dendritic nanoparticles with *P. aeruginosa* 010 LPS in the presence of lysozymes and KP27 endolysin to find out the main aspects of the OM destabilization process. Our results showed that PEGylated dendronized AgNPs overcame the LPS barrier and enhanced the antibacterial effect of endolysin more efficiently than unPEGylated nanoparticles.

Keywords: silver nanoparticles, endolysin, PEGylation, lipopolysaccharide, peptidoglycan

INTRODUCTION

Multidrug-resistant (MDR) pathogens are an established and growing worldwide public health problem. Among others, the ESKAPE group (*Enterococcus, Staphylococcus, Klebsiella, Acinetobacter, Pseudomonas,* and *Enterobacter*) seems to be the most crucial and particularly dangerous. These are MDR gram-positive and gram-negative bacteria with a broad spectrum of virulence factors causing serious damage to host tissues and efficiently evading the immune system response (Pendleton et al., 2013). Since the variety of MDR bacteria has expanded, therapeutic and prevention options have become limited.

Nowadays, there are several possible strategies to overcome MDR mechanisms, including the application of bacterial viruses (phages). Currently, the interest in lytic phages is constantly

growing (Maciejewska et al., 2018). The latest studies showed that phage-derived proteins, especially peptidoglycan (PG)-degrading enzymes (lysins), act as efficient antimicrobials and exhibit an economical potential (Latka et al., 2017; Maciejewska et al., 2018). The PG-degrading effect provided by lysins can be seen in seconds as the osmotic lysis of targeted cell, making these enzymes a desired and efficient antibacterial agent (Nelson et al., 2012; Latka et al., 2017).

It is known that phage lysins, as well as. lysozyme, present a high effectiveness against gram-positive pathogens but have limited activity on gram-negative bacteria due to impeded penetration through the outer membrane (OM) layer. There are several options to improve the antibacterial activity of lysins toward gram-negative bacteria, e.g., using OM destabilizing agents in a mixture or genetically modifying enzymes such as Artilysins (Briers et al., 2014; Peng et al., 2017). Cationic nanoparticles, e.g., dendrimers, are one type of compound that is able to destabilize OM and, in combination with phage endolysin, have improved the antibacterial activity of the mixture (Ciepluch et al., 2019). Additionally, cationic dendrimers are antimicrobial agents itself (Fuentes-Paniagua et al., 2016). The synthesis and further modification of polycationic dendrimers allow for an effective internalization with gram-negative cells (Vankoten et al., 2016). Another class of systems with antibacterial properties are silver nanoparticles (Kim et al., 2007). Silver nanoparticles demonstrated an efficient antibacterial effect; however, the mode of action is still unclear. It is known that AgNPs may kill drug-resistant bacteria and prevent biofilm formation. AgNPs may interact with gram-negative OM, produce reactive oxygen species ROS in bacteria, and the released Ag^+ ions interact with biomolecules affecting different metabolic pathways, leading to cell death (Qing et al., 2018). AgNPs administered to an animal body can cross the blood–brain barrier as well as accumulate in the liver, spleen, kidney, and brain (Liao et al., 2019).

Both dendrimers and silver nanoparticles (AgNPs) can also be cytotoxic to eukaryotic cells, and they are therefore usually modified with polyethylenoglycol (PEG) to reduce an unfavorable toxic effect and to improve bioavailability and stability (Turecek et al., 2016). Recently, it was shown that dendronization of AgNPs with cationic carbosilane dendrons increases the antibacterial properties of nanoparticles (Peña-González et al., 2017). The activity/toxicity balance was further improved by PEGylation of these dendronized AgNPs. The AgNPs did not induce the resistance in bacteria, and the PEGylated one also prevent biofilm formation at concentrations far below the minimum bactericidal concentration (MBC).

The antibacterial mode of action of these nanoparticles is still unknown. Moreover, the effect of PEGylation of dendronized AgNPs on their interactions with the bacterial OM and lipopolysaccharides (LPSs) have not been tested yet. In our study, we have therefore focused on the PEGylation effect on the interaction between dendronized AgNPs and LPS as well as on the antimicrobial activity of PG-degrading enzymes (lysozyme and KP27 endolysin). An LPS, as a virulence factor, is also a hindrance for many of cationic nanoparticles to reach and destabilize the bacterial OM. Knowledge about the behavior of tested nanoparticles can lead to an assessment of whether PEGylation can improve the antibacterial effect of dendritic AgNPs and enhance antibacterial efficacy of endolysin against gram-negative bacteria. We tested two AgNPs, one dendronized with cationic carbosilane dendrons of the first generation (Dend-AgNP) and the modified version containing PEG ligands on the surface (PEG-Dend-AgNP).

MATERIALS AND METHODS

Dendronized AgNPs Preparation

The dendronized AgNPs, Dend-AgNPs (Peña-González et al., 2017), and PEG-Dend-AgNPs (Barrios-Gumiel et al., 2019; **Figure 1**) used here were prepared following the methodology previously described in **Supplementary Material**.

Recombinant Endolysin Preparation

The recombinant phage-borne endolysin was prepared according to the method described previously by Maciejewska et al. (2017). Briefly, the coding sequence of *Klebsiella* phage KP27 endopeptidase was amplified using Pfu polymerase (Thermo Fisher Scientific, Waltham, MA, United States) and cloned into the commercially available pEXP-5-CT/TOPO® TA expression vector (Invitrogen, Thermo Fisher Scientific, Waltham, MA, United States) according to the manufacturer recommendations. The expression was conducted for 18 h at 20°C using *E. coli* BL21 (DE3) pLysS (Agilent Technologies, Santa Clara, CA, United States) and isopropyl-β-D-1-thiogalactopyranoside (IPTG; the final concentration of 0.5 mmol/L) as an inductor of the expression. The recombinant protein was purified from the filtered supernatant by affinity chromatography using NGC medium pressure chromatography systems (Bio-Rad, Hercules, CA, United States) combined with 5-ml nickel columns using Bio-Scale Mini Profinity IMAC Cartridges (Bio-Rad, Hercules, CA, United States) and dialyzed against a PBS buffer. The concentration of purified recombinant enzyme was then determined fluorimetrically (Qubit® Protein Assay Kit, Molecular Probes, Thermo Fisher Scientific, Waltham, MA, United States).

Dynamic Light Scattering

The dendronized AgNPs particles and the LPS micelles size and size distribution (z-average mean) were measured using the dynamic light scattering (DLS) in a photon correlation spectrometer (Anton Paar Light sizer 500, Austria). The refraction factor was assumed at 1.33 while the detection angles were 15°, 90°, and 175°, and the wavelength was 658 nm. Samples in 10 mmol/L Na-phosphate buffer, pH 7.4, were placed in the plastic cells and measured. The data were analyzed using the Anton Paar software. Three measurements were collected for each experiment and the average was calculated.

PG Degradation Assay

The enzymatic activity of lysozymes (Sigma-Aldrich, United States) and KP27 endolysin were tested by measuring

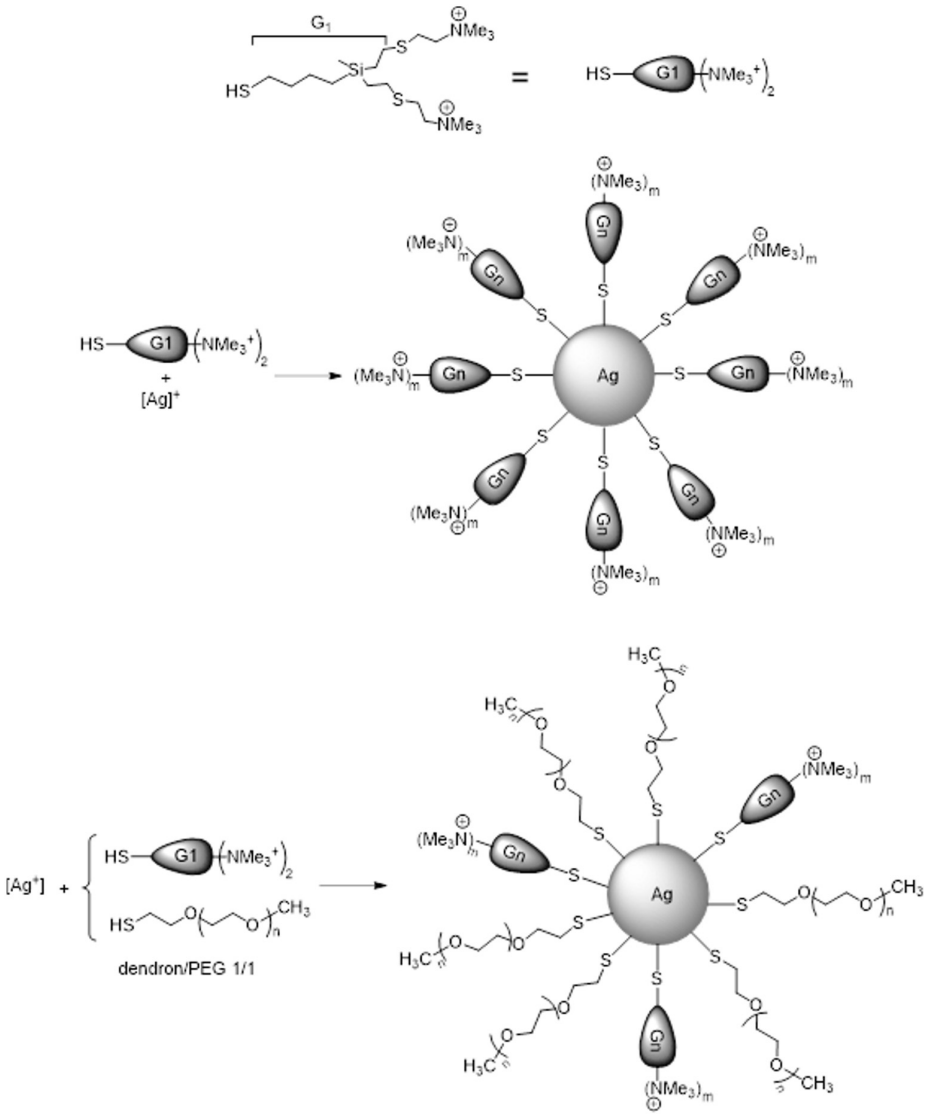

FIGURE 1 | Drawing of first generation cationic carbosilane dendron (top) and reaction schemes of AgNP synthesis (middle, Dend-AgNP; bottom, PEG-Dend-AgNP).

PG degradation. PG was isolated from *E. coli* ATCC 8739 cells. Briefly, *E. coli* was cultivated under aerobic conditions in a fermenter (BioStat A, Sartorius Stedim Biotech) in nutrient broth (BTL, Poland) under controlled conditions (37°C, pH 7.2–7.4, pO2 70–86%). Cells were harvested at the end of the logarithmic growth phase, centrifuged (5,000 *g*, 30 min), washed with distilled water, and lyophilized. PG was isolated in accordance with the method described by Bera et al. (2005). The rate of degradation was evaluated spectrophotometrically in the presence of dendronized AgNPs. The enzyme (5 μmol/L) was tested alone or preincubated with both types of dendronized AgNPs (PEGylated and unPEGylated one) at the concentration of 30 μg/mL in PBS solution. The 0.25 mg/ml of PG was added to the sample and the kinetics of its degradation was measured at 560 nm using Microplate Reader TECAN Infinite 200 PRO (Tecan Group Ltd., Switzerland) for 80 min. The measurements were done at 37°C. Experiments were repeated twice.

Protein Secondary Structure Analysis

The potential influence of nanoparticles on enzymes' secondary structure was measured by Circular Dichroism (CD) at the far-UV region using J-815 CD spectrometer (Jasco, Japan). The experiments were done in 10 mmol/L sodium phosphate buffer (pH 7.4). The concentration of proteins (lysozyme and KP27 endolysin) was 0.5 μmol/L. CD spectra of protein alone and in the presence of nanoparticles were obtained in the range between 260 and 195 nm. Quartz 0.5 cm path length cells (Hellma, Germany) were used for all CD experiments. The CD spectra were taken for protein alone and after adding of nanoparticles at concentration of 14 μg/mL.

Intrinsic Protein Fluorescence Analysis – Fluorescence Quenching Method

The potential influence of nanoparticles on protein folding and dynamics was studied by the intrinsic protein fluorescence as the fluorescence quenching of tryptophan residues (Stern and Volmer, 1919). Lysozyme and KP27 endolysin were dissolved in PBS at a concentration of 2 μmol/L. An excitation wavelength of 290 nm was used, and the emission was recorded at 350 nm. Next, increasing concentrations of dendronized AgNPs (quencher,Q) were added and fluorescence spectra were recorded. The same experiment was repeated with the addition of LPS at a concentration of 0.01 mg/mL. The experiments were repeated twice.

Nanoparticle Morphology Analysis by Transmission Electron Microscopy

The potential influence of proteins and LPS on nanoparticle organization (morphology) was verified by transmission electron microscopy (TEM) (Tecnai G2 Spirit, FEI Company). The dendronized AgNPs morphology alone and in the presence of a lysozyme and LPS was visualized. A lysozyme was added to nanoparticles dissolved in 10 mmol/L sodium phosphate buffer (pH 7.4), where the molar ratio of protein:nanoparticles was 10:1. The concentration of nanoparticles and LPS was the same as was described in DLS method. The resulting mixture was placed on a carbon-coated 200-mesh copper grid (Ted Pella, Inc), incubated for 10 min and drained. Samples were negatively stained for 2 min with 2% (w/v) uranyl acetate. Magnification of 60,000× was used to examine dendronized AgNPs morphology.

Antimicrobial Activity Assay

The antibacterial activity of PG-degrading enzymes combined with dendrimers was tested using *P. aeruginosa* PAO1 wild-type and its knock-out Δ*wbpL* mutant deficient in the biosynthesis of A-band and B-band O-antigens provided by Andrew M. Kropinski from the Laboratory of Foodborne Zoonoses, Guelph, ON, Canada. The antibacterial activity of dendronized AgNPs and KP27 endolysin was measured on an exponentially growing *P. aeruginosa* culture (OD_{600}) by spectrometric method at 600 nm. The dendronized AgNPs alone (concentration from 5 μg/mL to 50 μg/mL) and dendronized AgNPs combined with endolysin (5 μmol/L) were added and the effect was expressed as the percentage of *P. aeruginosa* culture growth (optical density OD_{600}) compared to the non-treated bacterial culture (control) using Microplate Reader TECAN Infinite 200 PRO (Tecan Group Ltd., Switzerland). Experiments were repeated twice.

RESULTS

Interactions of Dendronized AgNPs With LPS

To observe the influence of dendronized AgNPs and PEGylated dendronized AgNPs on tested enzymes in the mimicking OM environment, it was necessary to first characterize the properties (aggregation and size) of these nanoparticles and LPS alone as well as of the nanoparticles/LPS mixture in phosphate buffer solution. The size of tested nanoparticles (measured by Dynamic Light Scattering method) can be presented as a hydrodynamic radius (R*h*), whereas the autocorrelation function informs us about the homogeneity of samples. The experimentally recorded intensity autocorrelation function $g^1(q,t)$ is directly linked to the theoretically amenable first-order electric field autocorrelation function $g^1(q,t)$ through the Siegert (1943) relationship:

$$g^2(q,t) = 1 + Bg^1(q,t)^2 \quad (1)$$

where $B(\leq 1)$ is an instrumental parameter, and the magnitude of the wave vector, q, is $q = (4\pi n/\lambda)\sin(\theta/2)$, where λ is wavelength of light, n is a reflective index, and θ is the scattering angle.

At 25°C, the correlation functions were found to exhibit two relaxation modes (polydisperse dynamic relaxation):

$$g^1(t) = \int_0^\infty G(\Gamma)\exp(-\Gamma\tau)d\Gamma \quad (2)$$

where τ is a relaxation time and Γ = q2D. From the formula we were able to calculate the hydrodynamic radii (R_h) via the Stokes–Einstein relationship $R_h = k_BT/6\pi\eta_0 D$, where k_B is the Boltzmann constant, T is temperature, η_0 is the solvent viscosity, and D is the mutual diffusion coefficient.

The characteristics of the hydrodynamic radius of dendronized AgNPs (dendronized AgNPs) and PEG-dendronized AgNPs are presented in **Figure 2A**. In the case of PEG-dendronized AgNPs, two populations of size distribution with a radius of 13 nm and 98 nm could be observed. However, including the volume intensity given by the software, the particles with radius of 13 nm dealt 93% and 98 nm dealt 4% of a total number of particles in solution. The shape correlation function of PEG-dendronized AgNPs presented in **Figure 2B** was very near to one relaxation mode (homogeneous samples) in contrast to the results obtained for unpegylated dendronized AgNPs. The radius of unpegylated nanoparticles was 176 nm (**Figure 2A**), and the correlation function was definitely in a two relaxation mode, which suggested heterogeneity of the sample (**Figure 2B**).

Figure 3 shows the size distribution of the LPS in a buffer solution. Here, two populations were found, one with a radius of 71 nm and the second with a small population around 1,000 nm, suggestive of a small amount of aggregates or dust (**Figure 2C**). The shape of correlation function means a one relaxation mode (**Figure 2D**). DLS results for dendronized AgNPs in the presence of LPS micelles are displayed in **Figure 4**. In **Figure 2E**, we can see the size distribution of PEG-dendronized AgNPs in the presence of LPS (concentration 0.1 mg/ml or 0.2 mg/ml). The peak with the highest intensity (around 115 nm) indicates the complexation of PEG-dendronized AgNPs with LPS micelles and the lower peak (around 15 nm) is associated with free nanoparticles. At a higher concentration of LPS, the lower peak starts to disappear whereas the higher one increases up to 145 nm. It means that fewer free nanoparticles are present in the solution and more complexes are visible. In **Figure 2F**, the size distribution of dendronized AgNPs with LPS micelles (0.1 mg/ml or 0.2 mg/ml) is presented. The distribution of peaks is very similar to results obtained for PEGylated nanoparticles. However, the size of the LPS

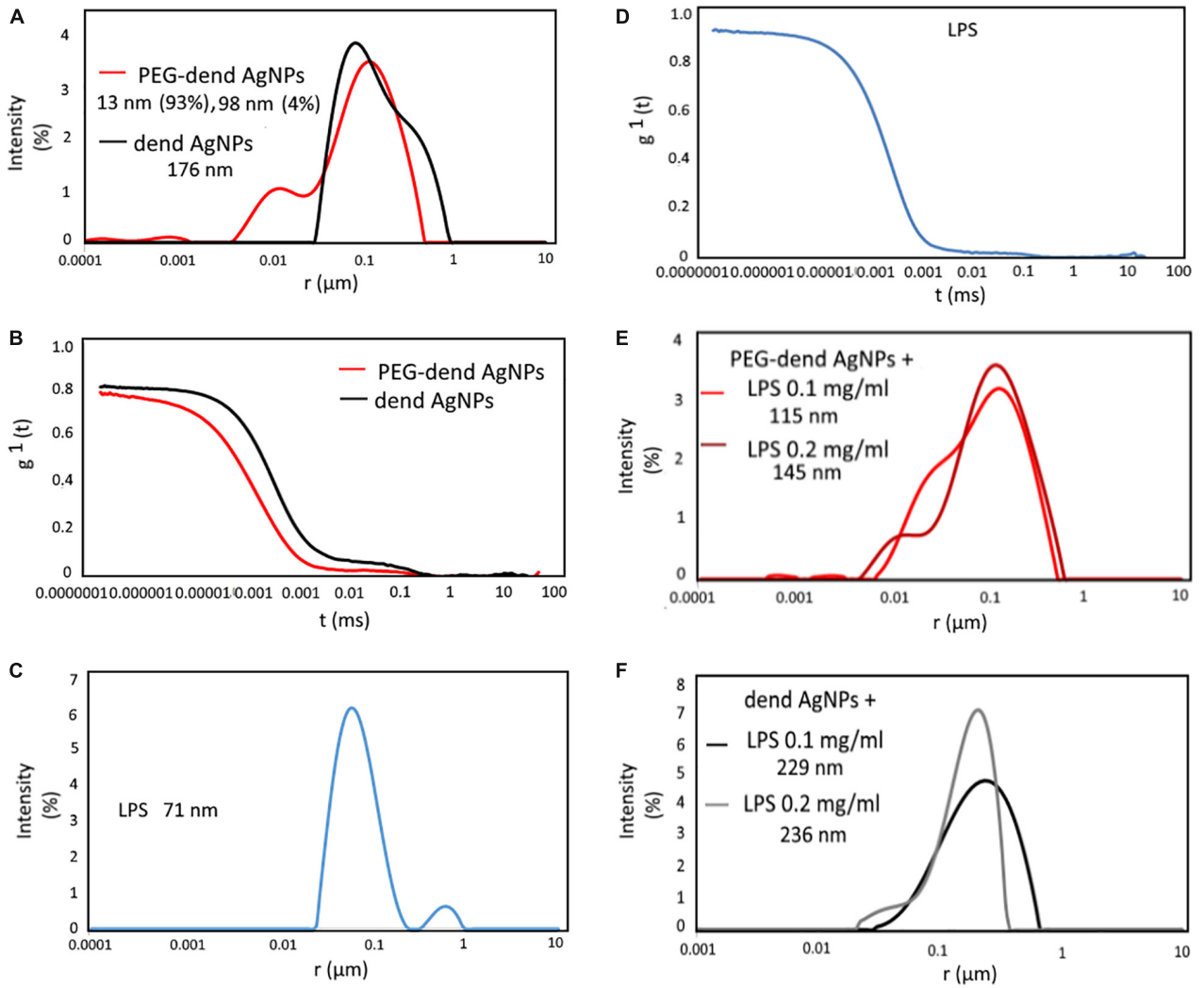

FIGURE 2 | (A) Size distribution of dendronized AgNPs and PEG-dendronized AgNPs in PBS buffer (0.01 mol/L) at 25°C. **(B)** Plots of first-order electric autocorrelation function $g^1(t)$ versus time for dendronized AgNPs and PEG-dendronized AgNPs. For dendronized AgNPs, two relaxation mode (polydisperse dynamic relaxation) was observed. **(C)** Size distribution of LPS in PBS buffer (0.01 mol/L) at 25°C. **(D)** Plots of first-order electric autocorrelation function $g^1(t)$ versus time for LPS micelles (concentration is 0.1 mg/ml). **(E)** The size distribution of PEG-dendronized AgNPs and **(F)** dendronized AgNPs with LPS (0.1 mg/ml and 0.2 mg/ml) in PBS buffer (0.01 mol/L) at 25°C.

dendronized-AgNPs complex is much bigger (around 229 nm), increasing along the concentration of the LPS (up to 236 nm).

Interactions of Dendronized AgNPs With Antimicrobial Proteins in the Presence of LPS

The properties of dendritic silver nanoparticles in the presence of LPS are crucial. However, to consider the synergistic effect of NPs together with an antimicrobial protein, the most important issue is to check these interactions also in the presence of an LPS in order to mimic the natural environment of gram-negatives surface macromolecules.

To analyze the influence of dendronized nanoparticles on biological properties of antimicrobial proteins (lysozyme and KP27 endolysin) and their properties in the presence of an LPS as a major component of gram-negative OM, four techniques were applied: PG degradation assay, CD, TEM, and the fluorescence quenching method.

The enzymatic activity of lysozyme and KP27 endolysin in the presence of nanoparticles was measured by PG degradation in a function of time (**Figure 3**). Since PG is not soluble in water, the absorbance increases over time as an effect of murein aggregates degradation (A/A0), where A0 is the initial absorbance (time t = 0 min) and A is the absorbance at a particular time. The addition of PEG-Dend-AgNPs to PG caused a small inhibitory effect on enzyme activity. In the presence of unmodified AgNPs (Dend-AgNPs), the slope of the curve is less steep (higher inhibitory effect) compared to the slopes of a free lysozyme and a lysozyme with PEG-Dend-AgNPs. The enzymatic activity

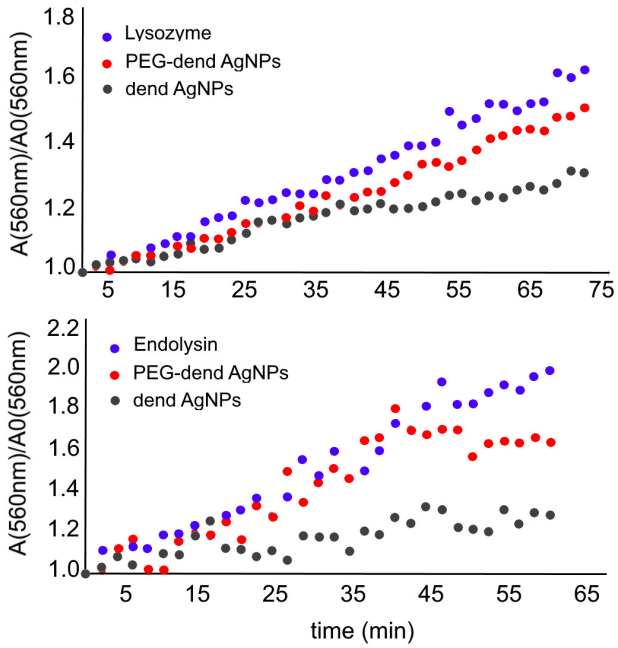

FIGURE 3 | Enzymatic activity of lysozyme and KP27 endolysin in the presence of dendronized AgNPs at 25°C. The activity is described as the ratio of absorbance in time at 560 nm to the absorbance at time $t = 0$. The increase of absorbance means PG degradation by the enzyme in time.

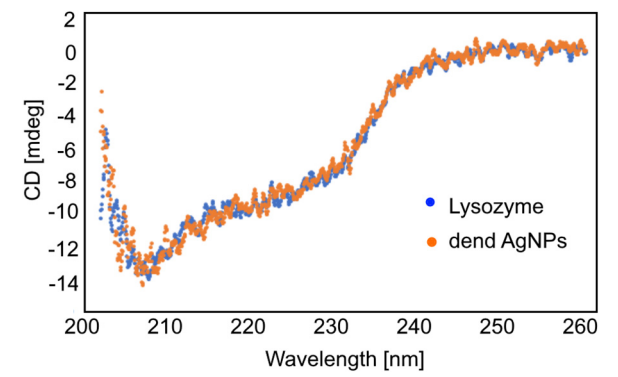

FIGURE 4 | The CD spectra of the lysozyme alone and the lysozyme in the presence of unmodified dendronized AgNPs.

of KP27 endolysin alone and in the presence of AgNPs was measured the same way as for lysozyme. The curve of absorbance dependence in time is steeper compared to that of the lysozyme alone (after 65 min the A/A0 reach 2.0 for endolysin and 1.5 for lysozyme). The addition of PEG-Dend-AgNPs to KP27 endolysin stopped the PG degradation after 40 min of incubation, whereas Dend-AgNPs after 20–25 min.

To check whether the inhibitory effect of dendronized AgNPs (unmodified and modified with PEG) on the activity of enzymes is connected with the structural conformation changes, the measurement of the secondary structure composition of both proteins was carried out. The CD spectra of both enzymes are characteristic for protein with dominant of α-helix structure with two minima at 208 nm and 220 nm. After the addition of excess AgNPs to both protein solutions, no changes in the shape of spectra were observed. An example of the CD spectra of the lysozyme after the addition of dendronized AgNPs is presented in **Figure 4**. The spectra of KP27 endolysin alone and after the addition of dendronized AgNPs were the same as observed for the lysozyme.

The fluorescence quenching of tryptophan residues in proteins was measured to check whether any of the interactions existed between dendronized AgNPs and tested enzymes (**Figure 5**). A lysozyme contains six tryptophan residues (at positions 28, 62, 63, 108, 111, and 123), while in KP27 endolysin only three tryptophan residues can be found (at positions 79, 86, and 110). The intensity of tryptophan fluorescence in KP27 endolysin decreased with the successive addition of each type of AgNPs (an increase of F0/F, where F0 is fluorescence intensity without nanoparticle and F is intensity after nanoparticles addition). The data was presented as Stern-Volmer plots. The concentration of nanoparticles was from 1 to 14 μg/mL and the concentration of KP27 endolysin was 2 μmol/L. The decrease of fluorescence intensity of KP27 endolysin after PEGylated dendronized AgNPs addition in the presence of an LPS was somewhat smaller compared to the condition without an LPS. This effect was not observed for unmodified dendronized AgNPs in the presence of an LPS. Surprisingly, in this case a decrease of fluorescence intensity was even higher compared to the condition without an LPS. The quenching of tryptophan residues in lysozymes after nanoparticle addition was also measured. No visible differences between the quenching of the fluorescence of lysozymes after the addition of PEG-Dend-AgNPs in the presence of or without an LPS. The difference was observed for unmodified Dend-AgNPs, where a decrease of fluorescence quenching is visible in the presence of LPS. The shape of Stern–Volmer plots for both proteins after nanoparticles addition suggests the typical dynamic (collisional) mechanism, where the contact can be due to diffusive encounters. It is worth mentioning that, for KP27 endolysin, the stronger quenching is visible with the PEGylated nanoparticles combination. However, there is no difference in quenching between PEGylated and unPEGylated nanoparticles incubated with lysozyme.

The morphology of dendronized AgNPs in the presence of a lysozyme and an LPS was examined by TEM. Due to the same size and type of interactions of lysozyme and KP27 endolysin, only the lysozyme was tested by TEM. PEGylated AgNPs (**Figure 6A**) have no tendency to aggregate and they were visible on the TEM grid as a mixture of single particles with a size close to that obtained from DLS (around 15 nm). There are no differences in the morphology of PEG-dendronized-AgNPs in the presence of lysozyme (**Figure 6B**). The addition of LPS to a protein-nanoparticles mixture changes the morphology of tested nanoparticles (**Figure 6C**). PEG-dendronized-AgNPs start to aggregate in the presence of LPS and create a "worm-like" structures. UnPEGylated dendronized-AgNPs, due to the high number of cationic groups, have a higher tendency to

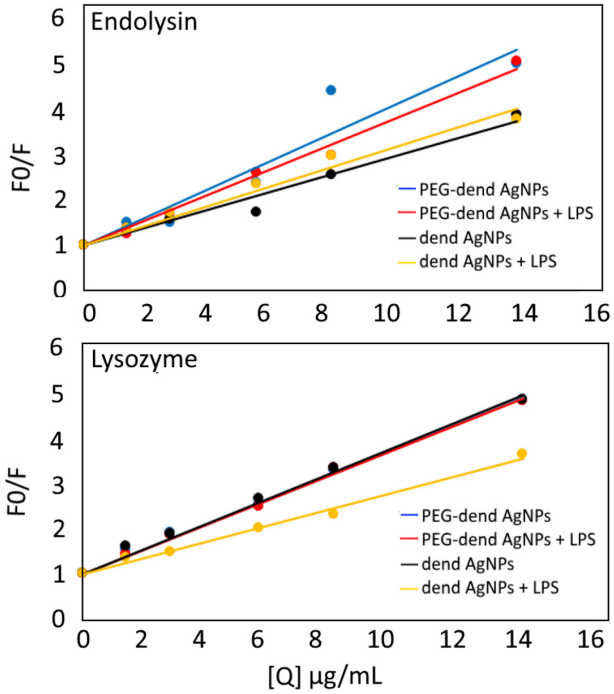

FIGURE 5 | Stern–Volmer plots for protein fluorescence quenching by dendronized AgNPs. λ_{ex} = 290 nm and λ_{em} = 350 nm. Q (quencher) means the concentrations of dendronized AgNPs.

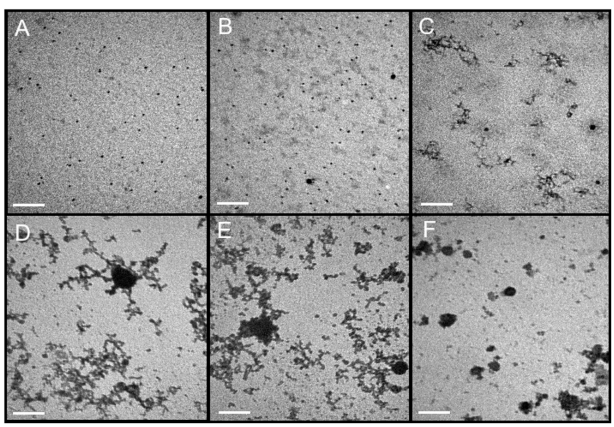

FIGURE 6 | Electron microphotographs of PEGylated dendronized AgNPs **(A)** with lysozyme **(B)** and lysozyme in presence of LPS **(C)**. The morphology of unPEGylated dendronized AgNPs alone **(D)** with lysozyme **(E)** and lysozyme in the presence of LPS **(F)**. The protein/nanoparticles molar ratio was 10:1. Dendrimers and proteins were dissolved in Na-phosphate buffer 10 mmol/L, pH 7.4. The magnification was 60,000×. The bar indicate was 200 nm.

create aggregates (**Figure 6D**). In the presence of a lysozyme (**Figure 6E**), the aggregation effect is even stronger. However, the addition of an LPS caused the formation of smaller aggregates (**Figure 6F**).

The above measurements clearly showed that PEGylated NPs have less influence on the activity of both antimicrobial proteins. Moreover, both tested nanoparticles did not affect the secondary structure of endolysin and lysozyme. The interactions between dendritic AgNPs and both enzymes are characterized by collisional interactions, without creating bonds between them. It is worth mentioning that these interactions may also depend on the physical properties of nanoparticles, e.g., the tendency to aggregation at a high concentration and in presence of an LPS, as was observed in TEM experiments.

Dual Antimicrobial Effect of Dendronized AgNPs and KP27 Endolysin on *P. aeruginosa* Cells

In the end we checked whether dendronized AgNPs combined with antimicrobial proteins against *P.aeruginosa* showed the synergistic effect. To verify if the LPS presence affected dendronized AgNPs/protein interactions, two different bacterial strains were used in experiments: a wild type and a mutant lacking an LPS. This experiment let us explain the role of LPS in the synergistic properties of NPs and protein.

Due to the stronger hydrolytic activity of KP27 endolysin in comparison to the lysozyme (**Figure 3**), we decided to use only the endolysin in this experiment. The dual antimicrobial effect of PEGylated and unmodified dendronized AgNPs combined with KP27 endolysin was evaluated spectrometrically, by measuring the optical density changes of the bacterial culture at 600 nm. Bacterial strains differed in the length and type of LPS O-chain, and the influence of nanoparticles with or without endolysin on wild-type *P. aeruginosa* PAO1 and its LPS knock-out mutant (Δ*wbpL*) was therefore analyzed (**Figure 7**). For the experiment, different concentrations of nanoparticles (5–50 µg/mL) and a constant concentration of KP27 endolysin (5 µmol/L) were used. No significant decrease in OD was observed for both tested strains treated with PEGylated nanoparticles at a concentration of 10 µg/mL. The addition of endolysin in this condition leads to a decrease of OD by several percent compared to untreated bacteria and bacteria treated with 10 µg/mL of nanoparticles only. A higher reduction of OD (by 25% and 82% for PAO1 and Δ*wbpL,* respectively) was observed in the presence of PEGylated nanoparticles at the concentration of 20 µg/mL. The antibacterial effect after addition of unmodified dendronized AgNPs was also reached at a concentration of 50 µg/mL. The addition of endolysin led to a further decrease of OD of PAO1 and Δ*wbpL* mutant (from 70% to 30% and from 80% to 40%, respectively). Obtained results clearly showed a synergic effect of PEgylated dendronized AgNPs and endolysin against gram-negative bacteria.

DISCUSSION

There are numerous research works about the antibacterial effect of dendronized nanoparticles, e.g., dendrimers and AgNPs (Gholami et al., 2017; Peña-González et al., 2017). The mixture of metal nanoparticles with dendrimers may be very promising for the development of new antimicrobial

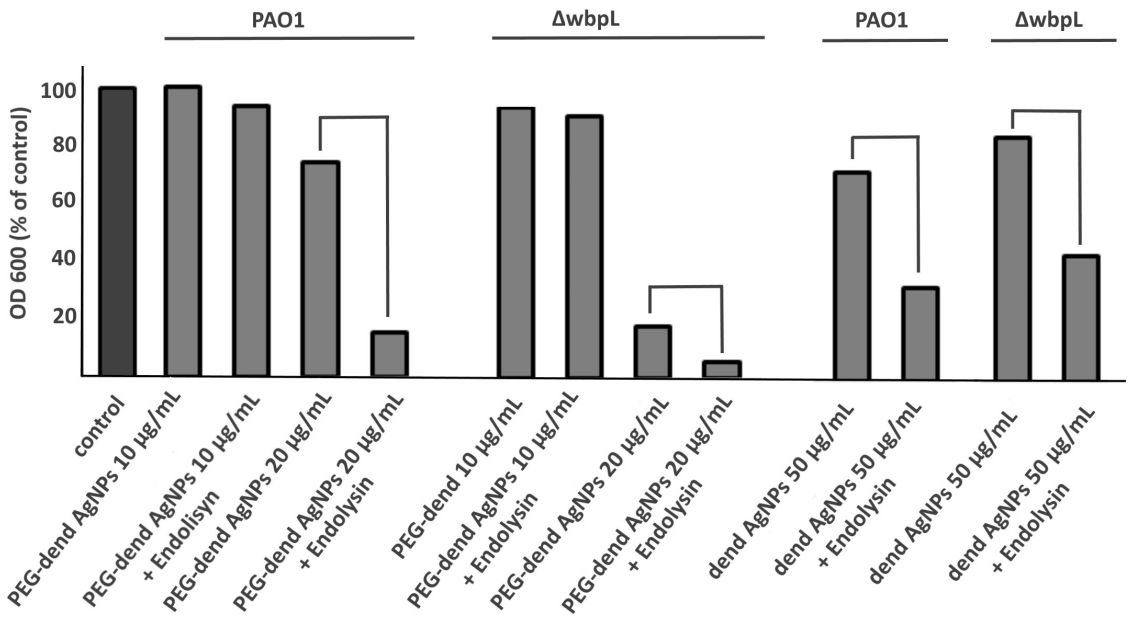

FIGURE 7 | The optical density of PAO1 wild-type and its mutant (ΔwbpL) measured at 600 nm without and in the presence of dendronized AgNPs (at concentrations of 10 μg/mL, 20 μg/mL, and 50 μg/mL) and nanoparticles (the same concentrations) combined with KP27 endolysin (at concentration of 5 μM). The results are expressed as the percentage, where 100% is a non-treated bacterial culture (control). Dend AgNPs means unmodified nanoparticles with PEG. The pair lines indicate the additional effect of endolysin addition. Culture growth for 24 h at 37°C.

systems (Mignani et al., 2017; Peña-González et al., 2017). It is known that antibacterial properties of nanoparticles (both dendrimers and silver NPs) strongly depend on their structure, charge, size, and adsorption ability at the bacterial surface (Felczak et al., 2012; Le Ouay and Stellacci, 2015; Tang and Zheng, 2018). As potential membrane permeabilizers, the dendronized nanoparticles may also enhance the antibacterial effect of antibiotics or antimicrobial proteins, especially against gram-negative bacteria (Winnicka et al., 2013; Serri et al., 2019). Our recent work showed that poly(propylene) imine glycodendrimers improved the antimicrobial properties of phage KP27 endolysin against *P. aeruginosa* cells (Ciepluch et al., 2019). Our studies suggested that cationic charged nanoparticles interacted strongly with bacterial surface glycans like LPS, and those interactions should be taken into account in the design of new antibacterial tools.

Negatively charged LPS is a major element affecting the antibacterial effect of cationic nanoparticles. Therefore, one of the aims of this study was to test the influence of dendronized AgNPs pegylation on their interactions with *P. aeruginosa* LPS. Understanding the nature of these interactions in solution may give very important information in the context of developing new antibacterial tools. DLS technique provides information about the aggregation of nanoparticles alone and the size of an eventual complex between nanoparticles and LPS micelles. The obtained results indicated that unPEGylated Dend-AgNPs have more of a tendency to aggregation compare to PEGylated PEG-Dend-AgNPs. Perhaps this is connected with the hydrophobic/hydrophilic balance of DendAgNPs. The PEGylation decreased the cationic charge of not only the nanoparticles surface but also the number of dendrons, to which the inner structure is highly hydrophobic; these ligands are being substituted by polar PEG moieties, consequently leading to the decrease of aggregation.

The increasing size of dendronized silver NPs (PEGylated and unPEGylated ones) in the presence of LPS, suggested that "LPS: dendronized Ag-NPs corona" may occur during the complexation event. The pegylated NPs do not aggregate, and thus this peak comes from the complex of PEG-dendronized AgNPs and LPS. It is very hard to distinguish separate peaks in a mixture of unPEGylated NPs and LPS micelles; therefore, we may say that both complexes of NPs and LPSs and aggregates of free NPs were formed. We can speculate that the mechanism of unPEGylated NPs binding to LPS seems to be different compared to PEGylated nanoparticles. It is worth mentioning that PEGylated dendronized AgNPs can create a complex with LPS (visible on one broad peak), but the effect of creation the LPS-unPEGylated NPs corona is not favored due to the aggregation tendency of unPEGylated dendronized AgNPs.

The influence of dendronized AgNPs on biological properties of antimicrobial proteins (lysozyme and KP27 endolysin) and their properties in the presence of LPS seems to be crucial as well, especially in the context of the dual antimicrobial effect. First, the effect of dendronized AgNPs on the structure and activity of lysozymes and KP27 endolysin was checked. Circular dichroism data clearly show that tested nanoparticles do not change the secondary structure composition of proteins. However, the enzyme activity assay suggests that dendronized AgNPs inhibit the activity of lysozymes and endolysin. In both cases, unPEGylated nanoparticles have a stronger influence on

enzymes activity. Interestingly, both nanoparticles finally inhibit completely the activity of KP27 endolysin but not of lysozymes. This could be due to the differences in shape, the charge of the active site and the isoelectric point of the lysozyme and KP27 endolysin. Although the charge of the tested lysozyme at pH 7.4 is slightly more positive (isoelectric point is more than 10) compared to endolysin, it is unlikely to expect a "stiff" complex between the protein and NPs. In this case, we should expect rather collisional interaction (where the contact between the protein and nanoparticles can be due to diffusive encounters), which is very common for AgNPs (Wang et al., 2017; Ashrafpour and Tohidi Moghadam, 2018). Our fluorescence data also showed the collisional dynamic interaction between dendronized AgNPs and proteins. However, PEGylated NPs affect KP27 endolysin more (not for lysozyme) compared to unPEGylated ones. The presence of LPS decreased the strength of interaction between NPs and proteins, but the effect depended on the type of protein. The changes in the Stern–Volmer plots were small, but in the case of lysozymes and unPEGylated NPs they were much bigger, suggesting that the LPS has to disturb in collisional interaction between NPs and protein. Due to the negative charge, the LPS molecules would probably compete with the protein to interact with the nanoparticles surface. It may indicate that the LPS could capture the nanoparticles from the solution, leaving more protein particles free and not affected by nanoparticles.

It is known that PEGyaltion of nanoparticles may stabilize the structure and prevent the aggregation (Shkilnyy et al., 2009) due to steric repulsion (Chang et al., 2016). Therefore, we should expect no aggregation of PEGylated dendronized AgNPs in the presence of lysozymes and the LPS. However, there were no differences in PEG-dendronized-AgNPs morphology in the presence of lysozymes, in contrast to the LPS/protein mixture. This may suggest that PEGylated nanoparticles did not easily bind the protein (lysozyme) to the dendronized surface, but they can bind to the LPS. This corresponds to data obtained from the DLS and fluorescence quenching method, where the interactions between LPS and PEGylated AgNPs occurred. What is very interesting is that, in the case of unPEGylated AgNPs, bigger aggregates were visible in the presence of the lysozyme. This is not surprising because AgNPs can bind lysozymes on their surface (Wang et al., 2017). The data obtained from fluorescence quenching and enzyme activity definitively prove that the lysozyme dendronized-AgNPs complexation. At the same time, smaller aggregates were visible in the presence of LPS. This is somehow an unexpected behavior. The addition of negatively charged LPS leads to the increase of aggregate, as was visible in the DLS. It seems that unPEGylated AgNPs may bind the LPS, but this complex may change the charge of the dendronized AgNPs surface so that more neutral and, thus, smaller aggregates are visible when evaporating a buffer while the TEM grid is prepared. Unfortunately, it does not explain whether the lysozyme is still bound to the nanoparticles surface or not. The fluorescence quenching results suggested that the LPS reduces the influence of dendronized AgNPs on lysozymes, making the quenching smaller. Despite forming smaller aggregates of lysozyme-dendronized AgNPs in presence of LPS, the lysozyme seems to be still present on NPs surface.

The biophysical studies of AgNPs interactions with proteins and/or LPS, suggest that the PEGylation may completely change nanoparticle properties. The interaction process with LPSs or proteins depends on the cationic charge of the macromolecules. The tendency toward aggregation is strong but can change in the presence of an LPS or in the presence of an antimicrobial protein. The PEG chain connected to the surface may turn properties of nanoparticles or other compounds in a different way (Chang et al., 2016; Shen et al., 2018). This was observed in an antimicrobial assay done on two *P. aeruginosa* strains (with an LPS and without). The higher antimicrobial effect as membrane permeabilizers was obtained for PEGylated dendronized AgNPs alone versus with unmodified nanoparticles. The enhanced antimicrobial effect was also achieved in combination with KP27 endolysin. The synergic effect was seen in the presence of PEGylated and unPEGylated dend-AgNPs at the concentration of 20 μg/mL and 50 μg/mL, respectively. Unexpectedly, a lower cationic charge of PEGylated particles allowed for OM permeabilization at a lower concentration compared to unPEGylated molecules. We hypothesized that cationic unmodified dendronized AgNPs aggregated at the bacterial membrane (or in the solution), blocking the PG-degrading enzyme from gaining access to the target PG. The PEGylation prevented this undesirable effect. The pegylated nanoparticles showed a stronger synergic antibacterial effect in combination with KP27 endolysin against the LPS-deficient *P. aeruginosa* mutants compared to the wild-type bacteria. In contrast, unPEGylated NPs were equally effective on both *P. aeruginosa* strain. The similar effect of unPEGylated NPs on WT and mutant strains could be due to properties of nanoparticles. The aggregation of unPEGylated NPs may also occur not only in the presence of LPS but also at a high concentration of unPEGylated NPs alone. At a high local concentration of NPs, the attractive interactions between NPs are very common, and thus the aggregation is still possible, even in the absence of an LPS.

CONCLUSION

In conclusion, both PEGyled and unPEGylated dendronized AgNPs are efficient and permeabilize gram-negative bacteria OM to allow the phage endolysin to reach the target PG. Nevertheless, the PEGylation modification increases the OM permeabilizing effect, overcoming the LPS barrier at a lower concentration. This study may bring a new light to the designing of the new tools composed of PG-degrading enzymes like phage lysins and OM permeabilizers, such as dendronized AgNPs, and toward the future development of a satisfactory antibacterial agent against gram-negative bacteria.

DATA AVAILABILITY STATEMENT

All datasets generated for this study are included in the article/**Supplementary Material**.

AUTHOR CONTRIBUTIONS

KC, KS, MA, and ZD-K contributed to the conception and design of the study. AB-G, SQ, JS-N, and FM synthesized the nanoparticles. BM and ZD-K obtained the recombinant endolysin. All authors contributed to the manuscript revision, and read and approved the submitted version.

FUNDING

This study was supported by the Polish National Science Centre research grant number 2017/27/B/NZ6/00199.

ACKNOWLEDGMENTS

We thank Dr. Wojciech Trybus from the Department of Cell Biology at the Jan Kochanowski University, Kielce, Poland, for his help in obtaining the TEM microscopy picture.

SUPPLEMENTARY MATERIAL

The Supplementary Material for this article can be found online at: https://www.frontiersin.org/articles/10.3389/fmicb.2019.02771/full#supplementary-material

REFERENCES

Ashrafpour, S., and Tohidi Moghadam, T. (2018). Interaction of silver nanoparticles with Lysozyme: functional and structural investigations. *Surf. Interfaces* 10, 216–221. doi: 10.1016/j.surfin.2017.09.010

Barrios-Gumiel, A., Sanchez-Nieves, J., Pérez-Serrano, J., Gómez, R., and Javier de la Mata, F. (2019). PEGylated AgNP covered with cationic carbosilane dendrons to enhance antibacterial and inhibition of biofilm properties. *Int. J. Pharm.* 569:118591. doi: 10.1016/j.ijpharm.2019.118591

Bera, A., Herbert, S., Jakob, A., Vollmer, W., and Götz, F. (2005). Why are pathogenic staphylococci so lysozyme resistant? The peptidoglycan O-acetyltransferase OatA is the major determinant for lysozyme resistance of Staphylococcus aureus. *Mol. Microbiol.* 55, 778–787. doi: 10.1111/j.1365-2958.2004.04446.x

Briers, Y., Walmagh, M., Van Puyenbroeck, V., Cornelissen, A., Cenens, W., Aertsen, A., et al. (2014). Engineered endolysin-based "Artilysins" to combat multidrug-resistant gram-negative pathogens. *mBio* 5:e01379–14. doi: 10.1128/mBio.01379-14

Chang, W. C., Tai, J. T., Wang, H. F., Ho, R. M., Hsiao, T. C., and Tsai, D. H. (2016). Surface PEGylation of silver nanoparticles: kinetics of simultaneous surface dissolution and molecular desorption. *Langmuir* 32, 9807–9815. doi: 10.1021/acs.langmuir.6b02338

Ciepluch, K., Maciejewska, B., Gałczyńska, K., Kuc-Ciepluch, D., Bryszewska, M., Appelhans, D., et al. (2019). The influence of cationic dendrimers on antibacterial activity of phage endolysin against P. *aeruginosa cells*. *Bioorg. Chem.* 91:103121. doi: 10.1016/j.bioorg.2019.103121

Felczak, A., Wrońska, N., Janaszewska, A., Klajnert, B., Bryszewska, M., Appelhans, D., et al. (2012). Antimicrobial activity of poly(propylene imine) dendrimers. *New J. Chem.* 36, 2215–2222. doi: 10.1039/c2nj40421d

Fuentes-Paniagua, E., Sánchez-Nieves, J., Hernández-Ros, J. M., Fernández-Ezequiel, A., Soliveri, J., Copa-Patiño, J. L., et al. (2016). Structure-activity relationship study of cationic carbosilane dendritic systems as antibacterial agents. *RSC Adv.* 6, 7022–7033. doi: 10.1039/c5ra25901k

Gholami, M., Mohammadi, R., Arzanlou, M., Akbari Dourbash, F., Kouhsari, E., Majidi, G., et al. (2017). In vitro antibacterial activity of poly (amidoamine)-G7 dendrimer. *BMC Infect. Dis.* 17:395. doi: 10.1186/s12879-017-2513-7

Kim, J. S., Kuk, E., Yu, K. N., Kim, J. H., Park, S. J., Lee, H. J., et al. (2007). Antimicrobial effects of silver nanoparticles. *Nanomedicine* 3, 95–101. doi: 10.1016/j.nano.2006.12.001

Latka, A., Maciejewska, B., Majkowska-Skrobek, G., Briers, Y., and Drulis-Kawa, Z. (2017). Bacteriophage-encoded virion-associated enzymes to overcome the carbohydrate barriers during the infection process. *Appl. Microbiol. Biotechnol.* 101, 3103–3119. doi: 10.1007/s00253-017-8224-8226

Le Ouay, B., and Stellacci, F. (2015). Antibacterial activity of silver nanoparticles: a surface science insight. *Nano Today* 10, 339–354. doi: 10.1016/j.nantod.2015.04.002

Liao, C., Li, Y., and Tjong, S. C. (2019). Bactericidal and cytotoxic properties of silver nanoparticles. *Int. J. Mol Sci.* 20:449. doi: 10.3390/ijms20020449

Maciejewska, B., Olszak, T., and Drulis-Kawa, Z. (2018). Applications of bacteriophages versus phage enzymes to combat and cure bacterial infections: an ambitious and also a realistic application? *Appl. Microbiol. Biotechnol.* 102, 2563–2581. doi: 10.1007/s00253-018-8811-11

Maciejewska, B., Roszniowski, B., Espaillat, A., Kęsik-Szeloch, A., Majkowska-Skrobek, G., Kropinski, A. M., et al. (2017). Klebsiella phages representing a novel clade of viruses with an unknown DNA modification and biotechnologically interesting enzymes. *Appl. Microbiol. Biotechnol.* 101, 673–684. doi: 10.1007/s00253-016-7928-7923

Mignani, S. M., Brahmi, N., El Kazzouli, S., El, Laurent, R., Ladeira, S., et al. (2017). Original Multivalent Gold (III) and Dual Gold (III) -Copper (II) Conjugated Phosphorus Dendrimers as Potent Antitumoral and Antimicrobial. *Mol. Pharm.* 14, 4087–4097. doi: 10.1021/acs.molpharmaceut.7b00771

Nelson, D. C., Schmelcher, M., Rodriguez-Rubio, L., Klumpp, J., Pritchard, D. G., Dong, S., et al. (2012). Endolysins as antimicrobials. *Adv. Virus Res.* 83, 299–365. doi: 10.1016/B978-0-12-394438-2.00007-4

Peña-González, C. E., Pedziwiatr-Werbicka, E., Martín-Pérez, T., Szewczyk, E. M., Copa-Patiño, J. L., Soliveri, J., et al. (2017). Antibacterial and antifungal properties of dendronized silver and gold nanoparticles with cationic carbosilane dendrons. *Int. J. Pharm.* 528, 55–61. doi: 10.1016/j.ijpharm.2017.05.067

Pendleton, J., Gorman, S., and Gilmore, B. (2013). Clinical relevance of the ESKAPE pathogens. *Expert Rev. Anti Infect. Ther.* 11, 297–308. doi: 10.1586/eri.13.12

Peng, S. Y., You, R. I., Lai, M. J., Lin, N. T., Chen, L. K., and Chang, K. C. (2017). Highly potent antimicrobial modified peptides derived from the *Acinetobacter baumannii* phage endolysin LysAB2. *Sci. Rep.* 7, 1–12. doi: 10.1038/s41598-017-11832-11837

Qing, Y., Cheng, L., Li, R., Liu, G., Zhang, Y., Tang, X., et al. (2018). Potential antibacterial mechanism of silver nanoparticles and the optimization of orthopedic implants by advanced modification technologies. *Int. J. Nanomed.* 13, 3311–3327. doi: 10.2147/IJN.S165125

Siegert, A. J. F. (1943). *On the Fluctuations in Signals Returned by many Independently Moving Scatterers*. Cambridge: Massachusetts Institute of Technology.

Serri, A., Mahboubi, A., Zarghi, A., and Moghimi, H. R. (2019). Pamam-dendrimer enhanced antibacterial effect of vancomycin hydrochloride against gram-negative bacteria. *J. Pharm. Pharm. Sci.* 22, 10–21. doi: 10.18433/jpps29659

Shen, Z., Fisher, A., Liu, W. K., and Li, Y. (2018). *PEGylated "Stealth" Nanoparticles and Liposomes*. Amsterdam: Elsevier Ltd, doi: 10.1016/B978-0-08-101750-0.00001-5

Shkilnyy, A., Soucé, M., Dubois, P., Warmont, F., Saboungi, M. L., and Chourpa, I. (2009). Poly(ethylene glycol)-stabilized silver nanoparticles for bioanalytical applications of SERS spectroscopy. *Analyst* 134, 1868–1872. doi: 10.1039/b905694g

Stern, O., and Volmer, M. (1919). über die Abklingzeit der Fluoreszenz. *Zeitschrift für Phys.* 20, 183–188.

Tang, S., and Zheng, J. (2018). Antibacterial activity of silver nanoparticles: structural effects. *Adv. Healthc. Mater.* 7:1701503. doi: 10.1002/adhm.201701503

Turecek, P. L., Bossard, M. J., Schoetens, F., and Ivens, I. A. (2016). PEGylation of biopharmaceuticals: a review of chemistry and nonclinical safety information of approved drugs. *J. Pharm. Sci.* 105, 460–475. doi: 10.1016/j.xphs.2015.11.015

Vankoten, H. W., Dlakic, W. M., Engel, R., and Cloninger, M. J. (2016). Synthesis and biological activity of highly cationic dendrimer antibiotics. *Mol. Pharm.* 13, 3827–3834. doi: 10.1021/acs.molpharmaceut.6b00628

Wang, G., Hou, H., Wang, S., Yan, C., and Liu, Y. (2017). Exploring the interaction of silver nanoparticles with lysozyme: binding behaviors and kinetics. *Colloids Surf. B Biointerfaces* 157, 138–145. doi: 10.1016/j.colsurfb.2017.05.071

Winnicka, K., Wroblewska, M., Wieczorek, P., Sacha, P. T., and Tryniszewska, E. A. (2013). The effect of PAMAM dendrimers on the antibacterial activity of antibiotics with different water solubility. *Molecules* 18, 8607–8617. doi: 10.3390/molecules18078607

Conflict of Interest: The authors declare that the research was conducted in the absence of any commercial or financial relationships that could be construed as a potential conflict of interest.

frontiers in Microbiology

REVIEW
published: 10 January 2020
doi: 10.3389/fmicb.2019.02949

Diversity and Function of Phage Encoded Depolymerases

*Leandra E. Knecht, Marjan Veljkovic and Lars Fieseler**

Institute of Food and Beverage Innovation, Zurich University of Applied Sciences, Wädenswil, Switzerland

Bacteriophages of the *Podoviridae* family often exhibit so-called depolymerases as structural components of the virion. These enzymes appear as tail spike proteins (TSPs). After specific binding to capsular polysaccharides (CPS), exopolysaccharides (EPS) or lipopolysaccharide (LPS) of the host bacteria, polysaccharide-repeating units are specifically cleaved. Finally, the phage reaches the last barrier, the cell wall, injects its DNA, and infects the cell. Recently, similar enzymes from bacteriophages of the *Ackermannviridae*, *Myoviridae*, and *Siphoviridae* families were also described. In this mini-review the diversity and function of phage encoded CPS-, EPS-, and LPS-degrading depolymerases is summarized. The function of the enzymes is described in terms of substrate specificity and applications in biotechnology.

Keywords: bacteriophage, depolymerase, polysaccharide, capsule, lipopolysaccharide

OPEN ACCESS

Edited by:
Zuzanna Drulis-Kawa,
University of Wrocław, Poland

Reviewed by:
Hugo Oliveira,
University of Minho, Portugal
Thomas Klose,
Purdue University, United States

***Correspondence:**
Lars Fieseler
lars.fieseler@zhaw.ch

Specialty section:
This article was submitted to Infectious Diseases, a section of the journal Frontiers in Microbiology

Received: *01 October 2019*
Accepted: *09 December 2019*
Published: *10 January 2020*

Citation:
Knecht LE, Veljkovic M and Fieseler L (2020) Diversity and Function of Phage Encoded Depolymerases. Front. Microbiol. 10:2949. doi: 10.3389/fmicb.2019.02949

PHAGE ENCODED DEPOLYMERASES CLEAVE SURFACE DECORATING POLYSACCHARIDES OF BACTERIA

Bacteriophages (phages) are viruses, which infect bacteria. The infection begins with the adsorption, the recognition of specific ligands at the host surface by tail fiber or tail spike proteins (TSPs). This adsorption process mostly determines host specificity. In many cases, a bacteriophage infects a particular serotype of the target bacterium only. Due to the high host specificity, the accompanying microflora of a target bacterium remains unharmed during phage attack. This is why bacteriophages and phage-derived enzymes became a promising alternative for detection and control of bacterial pathogens in agriculture, food, and medical applications.

Bacterial cell surface decorating polysaccharides, e.g., capsular polysaccharides (CPS), exopolysaccharides (EPS) or lipopolysaccharide (LPS), exhibit important functions in biofilm production, virulence, and in the interaction with bacteriophages. LPS very often serves as a ligand for phage tail fiber proteins during adsorption to the host cell membrane. CPS and EPS layers can reduce the efficacy of plating of some bacteriophages. In these cases, the capsule sterically inhibits the adsorption of the phages to the primary phage receptor. In mutant strains lacking the protective capsule, adsorption of these phages is significantly increased. Other phages, however, adapted to this challenge. These phages bind and digest CPS and EPS antigens, thereby drilling a tunnel through the capsules. After contact with the next physical barrier, the cell wall, the DNA is injected and the bacterium is successfully infected. Bacteria lacking the capsular antigens cannot be infected by these phages. This indicates that these phages do not only overcome the capsule barrier – they highly depend on it for host recognition and infection. Capsules should therefore be regarded as the primary receptor of such phages. However, the steps between capsule binding and cleaving and finally phage DNA injection into the host cell still remain unclear.

The majority of bacteriophages, which rely on bacterial polysaccharides for infection, belong to the *Podoviridae* family. In addition, an interaction with the bacterial capsule is also evident for some

phages belonging to other phage families. Since comparative genomics of bacteriophage genomes enables sophisticated analyses of phylogenetic relationships and revealed a better understanding of bacteriophage evolution, phage taxonomy is currently changing and new phage genera are established. **Table 1** provides an overview of the currently used taxonomy in bacteriophages, which interact with bacterial polysaccharides via so-called depolymerases.

A depolymerase is a structural component of the adsorption apparatus, which facilitates binding and digestion of capsules. The name indicates that the repeating unit of a polysaccharide is cleaved and disintegrated. Biochemically, depolymerases are divided into two groups, lyases and hydrolases. Lyases, in contrast to hydrolases, cleave their substrates non-hydrolytically, meaning that no water molecule is released after substrate cleaving. Most of the well-characterized phage encoded depolymerases, which target EPS or LPS O-polysaccharides, are lyases (Tomlinson and Taylor, 1985; Linnerborg et al., 2001; Olszak et al., 2017). They generally feature a great diversity in substrate specificity. However, it could well be that a particular cleavage site is present in different polysaccharide types, thereby allowing the enzyme to act on two different substrates. LPS-targeting enzymes are mostly referred to as TSP, while capsule-targeting enzymes are often termed depolymerases (Dpo). The term depolymerase can refer to any generic protein that is able to degrade polymers. From this perspective, phage encoded endolysins are also depolymerases, since they cleave the peptidoglycan, a bacterial polysaccharide in general in an hydrolase manner (Schmelcher and Loessner, 2016). However, this review will mainly focus on CPS, EPS, and LPS degrading depolymerases.

As these enzymes protrude from the virion and form spike-like structures we would therefore, instead of referring to them as depolymerase, use the term TSP in this review. On a structural level these enzymes are highly conserved (Latka et al., 2017). In general, they are homotrimers. A monomer exhibits parallel right-handed β-helices. Due their tertiary structure, TSPs are very stable enzymes. They remain functional at elevated temperatures of up to 80°C and acidic conditions (pH 5.0) and are also protease- and SDS-resistant. From this perspective, TSPs seem to be suitable for several biotechnological applications (Majkowska-Skrobek et al., 2016; Latka et al., 2017; Oliveira et al., 2019a; Wang et al., 2019). A phylogenetic analysis of TSPs partly revealed a substrate-specific clustering, instead of a phage genus-related clustering. This suggests, that TSPs of phages infecting a particular host are more closely related to each other than to other TSPs (**Figure 1**).

When a phage with an active TSP forms a plaque in soft agar overlays on a capsulated host bacterium, the clear center of the plaque is often surrounded by a turbid zone. This halo formation is regarded a hallmark of TSP activity and can be used to rapidly identify capsule targeting phages. In some cases, the halo even increases during prolonged incubation. Although the TSP strips the bacteria and removes the capsule, it does not necessarily affect bacterial growth *in vitro*. As a hypothesis, halo formation could be due to the TSP activity in diffusing offspring virions, which do not infect the remaining bacteria. Likely bacteria surrounding a plaque exhibit an altered physiological state, rendering them insensitive to infection. As a second hypothesis, a halo could be formed due to soluble, free TSPs. A TSP could be released as a free enzyme, if an alternative start codon is used for translation. As the free TSP will strip the bacteria of their protective capsule, the bacteria will thereby become insensitive toward infection by lyase bearing virions. Hence, the free TSP would inhibit phage adsorption and proliferation. In biofilms, where the bacteria produce large amounts of EPS, high levels of free TSPs could protect the bacteria from phage attack, which would be contra productive for the bacteriophage. On the contrary, free TSPs could be useful in terms of spreading progeny viruses after infection from the host cell and the biofilm, respectively. Future studies should therefore address the ecological function of free TSPs on the spread of phages under natural conditions, e.g., in a multi-species biofilm.

The most extensively studied TSPs are podovirus derived. Hypothetically, podoviruses may rely more on such lyases than phages of the other phage families, because they have short tails and more difficulties in reaching the internal host receptor. In recent years, however, research on similar non-podoviral enzymes is coming to the fore. Apparently, bacteriophages of the *Ackermannviridae*, *Myoviridae,* and *Siphoviridae* family exhibit multiple putative lyases, which await further characterization.

TSPs TARGETING CAPSULAR POLYSACCHARIDES (CPS)

A capsule is the outer layer that surrounds a bacterium (Limoli et al., 2015; Wen and Zhang, 2015). It consists of CPS, also termed K-antigens in *Escherichia coli*, *Klebsiella pneumonia*, and *Acinetobacter* spp. or Vi-antigens in *Salmonella* and *Citrobacter freundii*, respectively, which are connected to the outer membrane of Gram-negative bacteria via a lipid anchor (Follador et al., 2016; Hu et al., 2017; Sachdeva et al., 2017; Arbatsky et al., 2018). The alginate of *Pseudomonas aeruginosa* is also referred to as a capsule although it rather represents an EPS (Wen and Zhang, 2015). CPS usually exhibits a size of 100 kDa. Hence, they are much larger than other cell wall associated polysaccharides such as the LPS (Wen and Zhang, 2015). However, some long-chain LPS molecules, like the O111-antigen in *E. coli* or the O19- and O57-antigen in *Proteus vulgaris*, are also considered as capsules. CPS are chemically extremely diverse. They are composed of repeating oligosaccharide units, which can be either linear or branched. Not only monosaccharide constituents, but also glycosidic linkages, and substitutions with non-carbohydrates vary. While *P. aeruginosa* exhibits only one serotype, up to 80 different K-antigens have been described in *E. coli* and *K. pneumoniae* so far (Sachdeva et al., 2017). In *Acinetobacter baumannii* more than 125 capsule synthesis loci were identified (Arbatsky et al., 2018), but information on CPS structures is rather limited and typing schemes are not available yet (Limoli et al., 2015). As CPS can be highly immunogenic, many vaccination strategies rely on CPS-based vaccines. CPS mutants and non-capsulated bacteria are often highly attenuated in virulence. This is why CPS is often

TABLE 1 | Tail spike proteins (TSP) in bacteriophages of different phylogenetic affiliation.

Phage	Bacterial host	Family (Subfamily)	Genus	TSP	Accession no.	Specificity	Remarks	References
Phage genera encoding one TSP								
K1F	*E. coli*	*Podoviridae Autographivirinae*	Teseptimavirus (T7virus)	1 TSP EndoNF	Q04830	CPS K1	conserved gp17$_{T7}$-like N-terminal domain in EndoNF	Stummeyer et al., 2006
L1	*E. amylovora*	*Podoviridae Autographivirinae*	Teseptimavirus (T7virus)	1 TSP DpoL1	YP_007005466	EPS	conserved gp17$_{T7}$-like N-terminal domain; diversity of amylovoran has not been studied yet	Born et al., 2014
PHB01	*P. multocida*	*Podoviridae Autographivirinae*	Teseptimavirus (T7virus)	1 TSP	ASD51051	D		Chen et al., 2019b
PHB02	*P. multocida*	*Podoviridae Autographivirinae*	Teseptimavirus (T7virus)	1 TSP Dep-ORF8	ARV77571	A		Chen et al., 2018
Petty	*A. baumannii*	*Podoviridae Autographivirinae*	Phikmvvirus	1 TSP Dpo1	YP_009006536	nd		Hernandez-Morales et al., 2018
NTUH-K2044-K1-1	*K. pneumoniae*	*Podoviridae Autographivirinae*	Phikmvvirus	1 TSP ORF34	YP_009098385	CPS K1		Lin et al., 2014
LKA1	*P. aeruginosa*	*Podoviridae Autographivirinae*	Phikmvvirus	1 TSP Gp49	YP_001522890	LPS	Cleaves the LPS B-band	Olszak et al., 2017
P22	*S. enterica*	*Podoviridae*	Lederbergvirus	1 TSP TSP	NP_059644	LPS Typhimurium Enteritidis		Steinbacher et al., 1996
Sf6	*S. flexneri*	*Podoviridae*	Lederbergvirus	1 TSP TSP	NP_958190	LPS Y-serotype		Chua et al., 1999
HK620	*E. coli*	*Podoviridae*	Lederbergvirus	1 TSP TSP	NP_112090	LPS O18A1		Barbirz et al., 2008
Fri1	*A. baumannii*	*Podoviridae Autographivirinae*	Friunasvirus (Fri1virus)	1 TSP	YP_009203055	nd		
AS11	*A. baumannii*	*Podoviridae Autographivirinae*	Friunasvirus (Fri1virus)	1 TSP				Popova et al., 2017
AS12	*A. baumannii*	*Podoviridae Autographivirinae*	Friunasvirus (Fri1virus)	1 TSP				Popova et al., 2017
AB6	*A. baumannii*	*Podoviridae Autographivirinae*	Friunasvirus (Fri1virus)	1 TSP				Lai et al., 2016
IME200	*A. baumannii*	*Podoviridae Autographivirinae*	Friunasvirus (Fri1virus)	1 TSP Dpo48	ALJ97635	nd		Liu et al., 2019
B3	*A. baumannii*	*Podoviridae Autographivirinae*	Friunasvirus (Fri1virus)	1 TSP Gp42	ASN73401	CPS K2	conserved gp17$_{T7}$-like N-terminal domain	Oliveira et al., 2019b
P1	*A. baumannii*	*Podoviridae Autographivirinae*	Friunasvirus (Fri1virus)	1 TSP Gp43	ASN73504	nd	less specific	Oliveira et al., 2017
P2	*A. baumannii*	*Podoviridae Autographivirinae*	Friunasvirus (Fri1virus)	1 TSP Gp48	ASN73558			Oliveira et al., 2017
P3	*A. baumannii*	*Podoviridae Autographivirinae*	Friunasvirus (Fri1virus)	1 TSP		nd	less specific	Oliveira et al., 2017
N1	*A. baumannii*	*Podoviridae Autographivirinae*	Friunasvirus (Fri1virus)	1 TSP		CPS K2		Oliveira et al., 2017
B1	*A. baumannii*	*Podoviridae Autographivirinae*	Friunasvirus (Fri1virus)	1 TSP Gp45	ASN73353	CPS K9		Oliveira et al., 2017
B2	*A. baumannii*	*Podoviridae Autographivirinae*	Friunasvirus (Fri1virus)	1 TSP				Oliveira et al., 2017
B4	*A. baumannii*	*Podoviridae Autographivirinae*	Friunasvirus (Fri1virus)	1 TSP		nd	less specific	Oliveira et al., 2017
B5	*A. baumannii*	*Podoviridae Autographivirinae*	Friunasvirus (Fri1virus)	1 TSP Gp47	ASN73455	CPS K9		Oliveira et al., 2017
B6	*A. baumannii*	*Podoviridae Autographivirinae*	Friunasvirus (Fri1virus)	1 TSP		nd	less specific	Oliveira et al., 2017

(Continued)

TABLE 1 | Continued

Phage	Bacterial host	Family (Subfamily)	Genus	TSP	Accession no.	Specificity	Remarks	References
B7	*A. baumannii*	*Podoviridae* *Autographivirinae*	Friunasvirus (Fri1virus)	1 TSP		nd	less specific	Oliveira et al., 2017
B8	*A. baumannii*	*Podoviridae* *Autographivirinae*	Friunasvirus (Fri1virus)	1 TSP		CPS K9		Oliveira et al., 2017
IME180	*P. aeruginosa*	*Podoviridae*	nd	1 TSP Gene2	ATG86239	CPS		Mi et al., 2019
KN1-1	*K. pneumoniae*	*Podoviridae*	nd	1 TSP KN1dep	BBF66844	CPS KN1		Pan et al., 2019
KN4-1	*K. pneumoniae*	*Podoviridae*	nd	1 TSP KN4dep		CPS KN4		Pan et al., 2019
JA1	*V. cholera*	*Podoviridae*	nd	1 TSP		LPS O139		Linnerborg et al., 2001
E15	*S. enterica*	*Podoviridae*	nd	1 TSP TSP (gp20)		nd		Guichard et al., 2013
EcoO78	*E. coli*	*Myoviridae*	nd	1 TSP Dpo42		unknown	only distantly related to other depolymerases	Guo et al., 2017
B9	*A. baumannii*	*Myoviridae*	nd	1 TSP Gp69	AWD93192	CPS K45/K30	α-helical protein	Oliveira et al., 2019a
0507-KN2-1	*K. pneumoniae*	*Myoviridae*	Viunavirus (Vilvirus)	1 TSP ORF96	YP_008532047	CPS KN2		Hsu et al., 2013
RAY	*E. amylovora*	*Myoviridae*	nd	1 TSP Gp76	ANH51857	EPS nd	giant jumbophage; Dpo is active on *Pantoea* sp.	Sharma et al., 2019
Phage genera encoding two TSPs								
SP6	*S. enterica*	*Podoviridae* *Autographivirinae*	Zindervirus (SP6virus)	2 TSPs Gp46 Gp47	NP_853609 NP_853610	LPS Typhimurium/ Enteritidis Newport /Kentucky		Gebhart et al., 2017
K1-5	*E. coli*	*Podoviridae* *Autographivirinae*	Zindervirus (SP6virus)	2 TSPs EndoNE (ORF47) K5 lyase (ORF46)	YP_654148 YP_654147	CPS K1 K5	Gp37 serves as an adapter protein that interconnects the 2 Dpo with the capsid	Scholl et al., 2002; Leiman et al., 2007
K1E	*E. coli*	*Podoviridae* *Autographivirinae*	Zindervirus (SP6virus)	1 TSP EndoNE (ORF47)	YP_425013	CPS K1	The EndoNE neighboring ORF46 is truncated;	Stummeyer et al., 2006; Leiman et al., 2007
K5	*E. coli*	*Podoviridae* *Autographivirinae*	Zindervirus (SP6virus)	1 TSP KflA		CPS K5		Thompson et al., 2010
K5-2	*K. pneumoniae*	*Podoviridae* *Autographivirinae*	Przondovirus (KP32virus)	2 TSPs ORF37 ORF38	APZ82804 APZ82805	CPS K5 K30, K69	conserved $gp17_{T7}$-like N-terminal domain in ORF37, but not in ORF38	Hsieh et al., 2017
K5-4	*K. pneumoniae*	*Podoviridae* *Autographivirinae*	Przondovirus (KP32virus)	2 TSPs ORF37 ORF38	APZ82847 APZ82848	CPS K5 K8	conserved $gp17_{T7}$-like N-terminal domain in ORF37, but not in ORF38	Hsieh et al., 2017
KP32	*K. pneumoniae*	*Podoviridae* *Autographivirinae*	Przondovirus (KP32virus)	2 TSPs KP32gp37 Kp32gp38	YP_003347555 YP_003347556	CPS K3 K21	conserved $gp17_{T7}$-like N-terminal domain in KP32gp37, but not in KP32gp38	Majkowska-Skrobek et al., 2018
IME321	*K. pneumoniae*	*Podoviridae* *Autographivirinae*	Przondovirus (KP32virus)	1 TSP Dp42	AXE28435	CPS KN1		Wang et al., 2019
KN3-1	*K. pneumoniae*	*Podoviridae* *Autographivirinae*	nd	2 TSPs KN3dep KN56dep		CPS KN3 KN56	closely related to phage K5-2	Pan et al., 2019
KpV41	*K. pneumoniae*	*Podoviridae* *Autographivirinae*	Drulisvirus (KP34virus)	2 TSPs ORF46 ORF55	ALO80736 KT964103	CPS K1 unknown	conserved $gp17_{T7}$-like N-terminal domain in ORF46, but not in ORF55; no experimental evidence	Solovieva et al., 2018

(Continued)

TABLE 1 | Continued

Phage	Bacterial host	Family (Subfamily)	Genus	TSP	Accession no.	Specificity	Remarks	References
KpV71	*K. pneumoniae*	*Podoviridae* *Autographivirinae*	Drulisvirus (KP34virus)	1 TSP Dep_kvp71	AMQ66478	CPS K1		Solovieva et al., 2018
KpV74	*K. pneumoniae*	*Podoviridae* *Autographivirinae*	Drulisvirus (KP34virus)	1 TSP Dep_kvp74	APZ82768	CPS K2		Solovieva et al., 2018
KLPN1	*K. pneumoniae*	*Siphoviridae* *Tunaviridae*	Webervirus (T1virus)	2 TSPs ORF34 ORF35	YP_009195374 YP_009195375	CPS K1		Hoyles et al., 2015
KP36	*K. pneumoniae*	*Siphoviridae* *Tunaviridae*	Webervirus (T1virus)	1 TSP Gp50	YP_009226011	CPS K63		Majkowska-Skrobek et al., 2016
Phage genera encoding multiple TSPs								
CBA120	*E. coli* *S. enterica*	*Ackermannviridae* *Cvivirinae*	Kuttervirus	4 TSPs TSP1 TSP2 TSP3 TSP4	AEM91896 AEM91897 AEM91898 AEM91899	LPS *S.* Minnesota *E. coli* O157 *E. coli* O77 *E. coli* O78	$Gp10_{T4}$-like protein interconnects the four TSPs	Plattner et al., 2019
K64-1	*K. pneumoniae*	*Myoviridae*	Alcyoneusvirus	11 TSPs S1-1 S1-2 S1-3 S2-1 S2-2 S2-3 S2-4 S2-5 S2-6 S2-7 S2-8	BAW85694 BAW85692 BAW85693 BAW85695 BAW85696 BAW85697 BAW85698 BAQ02780 BAW85699 BAW85700 BAW85701	CPS K11 KN4 K21 KN5 K25 K35 K1 K64 K30, K69 nd nd	9 Dpo were functionally characterized	Pan et al., 2017

Family, Subfamily, and Genus names are provided according to the international committee on the taxonomy of viruses (ICTV). Genus names in brackets refer to previously recommended genus names for ease of understanding. Phage genera are grouped according to the number of TSPs encoded in the phage genomes. The substrate specificity of a single enzyme is provided, if known. nd, not determined.

regarded as a major virulence factor in pathogenic bacteria (Sachdeva et al., 2017).

THE K1 CAPSULE OF NEUROPATHOGENIC *E. coli* IS EFFICIENTLY REMOVED BY PHAGE ENCODED TSPs

Particular strains of *Escherichia coli* predominately cause bacterial meningitis and septicemia in newborn infants. The majority of these neuropathogenic *E. coli* express the capsular K1-antigen, which features an α-2,8-linked poly-N-acetylneuraminic acid (polysialic acid). As this carbohydrate is also part of the glycocalyx, covering cell membranes in human epithelial cells, the *E. coli* K1-antigen is not recognized by the immune system. This renders infections with *E. coli* K1 very severe. Tomlinson and Taylor identified a hydrolytic TSP with N-acetylneuraminidase (endosialidase) activity in bacteriophage K1E, a podovirus of the *Autographivirinae* subfamily, Zindervirus genus, already in 1985 (Tomlinson and Taylor, 1985). In the following years, a similar gene was described in phage K1F (*Autographivirinae* subfamily, Teseptimavirus genus) (Hallenbeck et al., 1987). Other strains of pathogenic *E. coli* exhibit the capsular K5-antigen. The K5-capsule is composed of 4-linked α-N-acetylglucosamine and β-glucuronic acid (N-acetyl heparosin). Bacteriophage K5 (*Autographivirinae* subfamily, Zindervirus genus), a relative of phage K1E, encodes a TSP, which specifically binds and cleaves the K5-capsule (Thompson et al., 2010). For a better overview, every TSP reviewed in this article is listed in **Table 1**.

With respect to the tail spike architecture, Teseptima- and Zinderviruses differ remarkably from each other. In phage T7, the "type phage" of the Teseptimavirus genus, Gp17 is the tail fiber protein (Cuervo et al., 2013). The N-terminal domain of this tail fiber, which connects the protein to the baseplate, is highly conserved in different species of Teseptimaviruses. Compared to $Gp17_{T7}$, TSPs in other Teseptimaviruses exhibit high amino acid identities in this N-terminal domain. The structure of the C-terminal part of $Gp17_{T7}$ has been studied in detail, and it seems that phage T7 uses Gp17 to adsorb to *E. coli* LPS (Garcia-Doval and van Raaij, 2012; Cuervo et al., 2013). The C-terminus of TSPs features the enzymatically active domain, which cleaves the substrate. Due to the high diversity of different polysaccharide substrates and the high diversity in the primary structure of the C-terminal domain, TSPs exhibit a high substrate specificity. All Teseptimaviruses seem to encode a single type of TSP, which is present in six copies per virion.

Zinderviruses can encode two TSPs. These enzymes lack the $Gp17_{T7}$-like N-terminal domain, and are linked to the virion via the small adapter protein Gp37 (Leiman et al., 2007). **Figure 2**

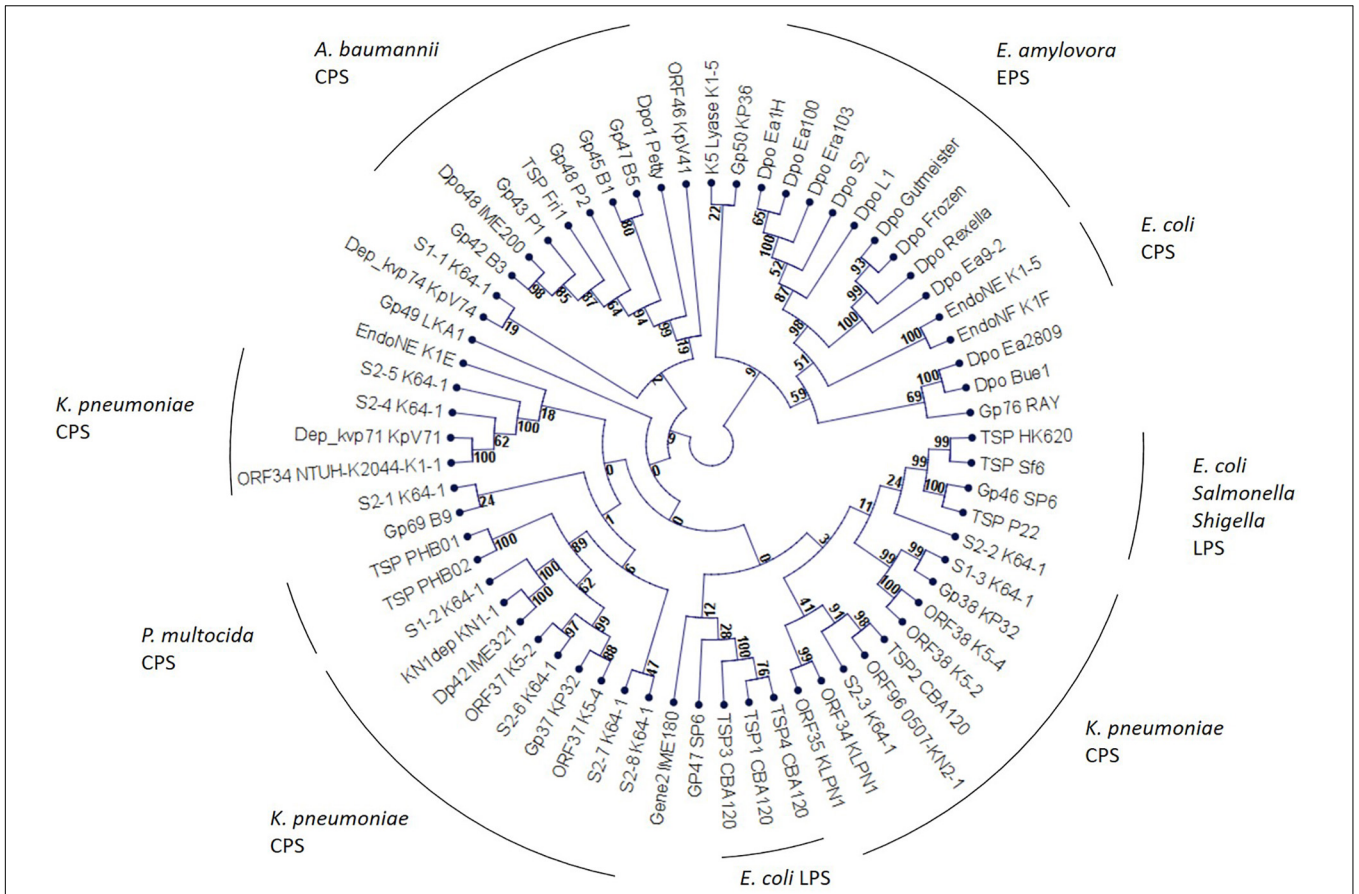

FIGURE 1 | Phylogenetic analysis of phage encoded tail spike proteins. The unrooted cladogram was calculated using neighbor joining and jukes-cantor correction. Bootstrap values are indicated at the nodes. A bootstrap value of 90 is considered significant.

illustrates the differences in TSP architecture. The adapter can link two different TSPs with different substrate specificities to the virion simultaneously. This enables some members of the Zindervirus genus to infect two different capsular K-antigen types as long as both proteins are active. A prominent example for such a phage is bacteriophage K1-5 (Leiman et al., 2007). This phage encodes both, a K1-specific N-acetylneuraminidase, Gp47, and a K5-specific lyase, Gp46 and can therefore infect K1 and K5 strains of *E. coli*. Each protein is present in six copies per baseplate. Phage K1E also belongs to the Zinderviruses. In contrast to phage K1-5, however, it can only infect K1 strains. CryoEM analyses of K1E revealed that Gp37 serves as an adapter protein, connecting Gp46 and Gp47 to the virion. In agreement with its host range, only the K1-specific N-acetylneuraminidase, Gp47, is enzymatically active, while Gp46 is very small and truncated and does not seem to have an enzymatic activity (Leiman et al., 2007). In phylogenetic analyses, however, the architectural differences in TSPs from Teseptimaviruses, Zinderviruses or other phage genera cannot be reflected (**Figure 1**).

With respect to phage evolution Stummeyer et al. (2006) argued that K1-specific phages of *E. coli* are not derived from a common ancestor (Stummeyer et al., 2006). It rather seems that each phage is related to a different progenitor type and that the phage gained host specificity through the acquisition of the endosialidase by horizontal gene transfer. New tail spikes could emerge by combining endosialidase domains with the capsid module (gp37) of the respective ancestor.

The K-antigen specific TSPs of coliphages K1E, K1F, K1H, K5, and K30 were therapeutically applied in animal models. Mushtaq et al. (2004) reported that intraperitoneal administration of a recombinant K1-specific endosialidase (20 μg) prevented bacteremia and death from systemic infection in 3-day-old rats. The enzyme did not affect the viability of the K1 *E. coli* strain, but removed the K1 capsule. Thereby, the K1 strain was identified and eliminated by the rat's complement system (Mushtaq et al., 2004). Lin et al. (2017) found that K1F, K1H, K5, and K30 TSPs could rescue infected mice, but that the K1E enzyme failed to form the expected trimers *in vivo*, which lead to reduced activity (Lin et al., 2017). One year later the same authors tested the robustness of the enzyme across a wider range of conditions. Treatment success rates were reduced by treatment delay. K1- and K5 specific enzymes retained partial efficacy on delay, while K30 lyase did not. Furthermore, the route of administration also affected treatment efficacy (Lin et al., 2018).

In addition to the enzymes derived from podoviruses, Guo et al. (2017) described a novel similar enzyme, Dpo42, derived

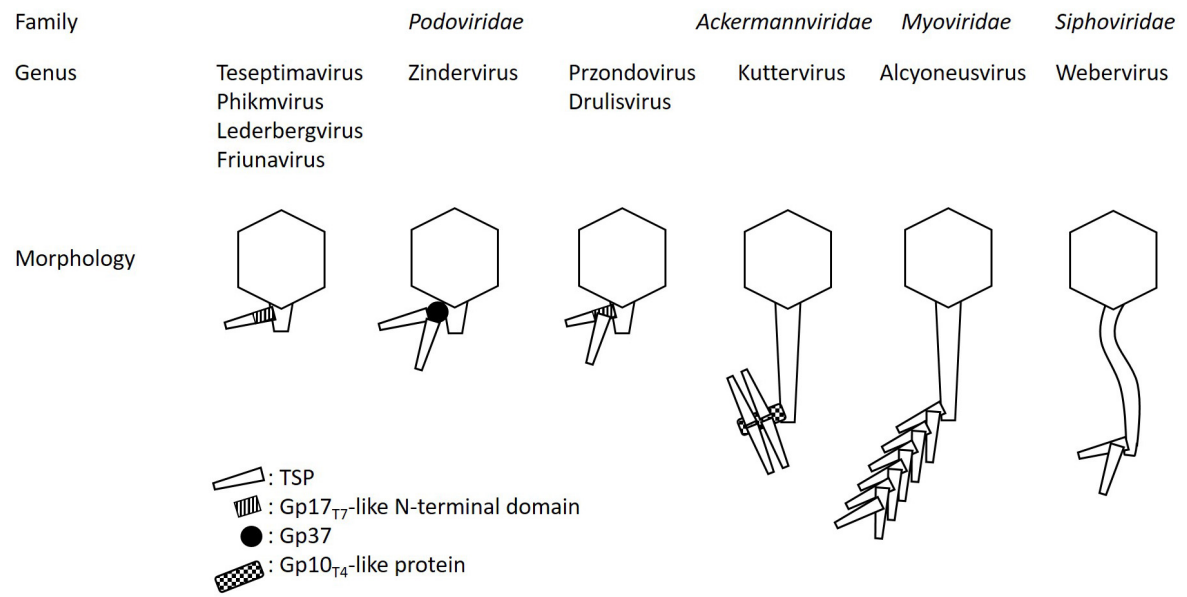

FIGURE 2 | TSP architecture and connection to the virion or baseplate in different phage genera. The schematic is not drawn to scale. For a better overview only one TSP ore branch of TSPs, respectively, is illustrated.

from the myovirus EcoO78, which infected *E. coli* (Guo et al., 2017). Plaques of this phage exhibit a turbid halo surrounding the clear center. Dpo42 seems to effectively prevent biofilm formation of the tested *E. coli* strains, but could not entirely remove an established biofilm. The structure of the CPS in this particular strain of *E. coli* was not mentioned (Guo et al., 2017). Any structural detail of tail fiber proteins in this phage are also unknown so far. It seems that Dpo42 is only distantly related to other depolymerases.

HYPERMUCOVISCOUS STRAINS OF *Klebsiella pneumoniae* ARE SENSITIVE TO SERUM KILLING AFTER TSP TREATMENT

Klebsiella pneumoniae, another member of the *Enterobacteriaceae*, causes nosocomial infections, including pneumonia, urinary tract infections, and to an increasing extent pyogenic liver abscess in humans. The most relevant strains exhibit the K1-, K2-, K5-, K20-, K54-, or K57-antigen (Yu et al., 2008; Hsu et al., 2016). Some experimental data indicate that N-acetylneuraminic acid (polysialic acid) is present in the K1 capsule of *K. pneumoniae*. However, the biochemical composition of many other *K. pneumoniae* capsule antigens, is incomplete and direct links between structural, biochemical, and genetic data for some capsular types are still lacking. In addition, novel K-types, such as capsular antigen types KN1, KN2, amongst others, have just recently been discovered (Yu et al., 2008; Pan et al., 2019). In many strains of *K. pneumoniae* capsule biosynthesis genes have been sequenced. The genomic diversity seems to reflect biochemical diversity of capsular antigens. Notably, genotyping seems to replace traditional biochemical capsule analyses in *Klebsiella* research today.

Bacteriophages targeting various K-antigens of *K. pneumoniae* have been described. Lin et al. (2014) isolated bacteriophage NTUH-K2044-K1-1 which specifically infects capsular type K1. This phage belongs to the *Autographivirinae* subfamily, genus Phikmvvirus, and encodes a single putative lyase (Lin et al., 2014). Solovieva et al. (2018) isolated and characterized eight bacteriophages specific for capsular types K1, K2 or K57, respectively. Two of the eight phages were analyzed in detail and the corresponding TSPs were cloned and functionally characterized. Phage KpV71 and phage KpV74 belong to the *Autographivirinae* subfamily, genus Drulisvirus (Kp34virus). KpV71 infects capsular type K1 and KpV74 capsular type K2. Both phages encoded a single functional enzyme. However, in the KpV71 encoded protein the authors identified two iterative lyase motifs (Solovieva et al., 2018). Any further information on the functionality of the single motifs is not available yet.

Another bacteriophage, IME321, again a member of the *Autographivirinae* subfamily, but from the Przondovirus genus (KP32virus), encodes a functionally active lyase (Dp42) that is specific for capsular type KN1. This enzyme is stable and fully active at a pH range from 5.0 to 12.0. Below pH 5.0 the enzymatic activity decreases significantly. It is also moderately thermostable, but if temperature exceeds 55°C the enzyme is inactivated (Wang et al., 2019). Pan et al. (2019) reported on the discovery of KN1-, and KN4-specific phages. Phage KN1-1 and KN4-1 have been allocated to the *Podoviridae* family (Pan et al., 2019). A more detailed phylogenetic analysis of the two viruses has not been performed. Both exhibit a single enzyme.

Hsieh et al. (2017) isolated two bacteriophages, K5-2 and K5-4 of the Przondovirus genus (KP32virus), which encode two capsule-specific TSPs. Shortly thereafter, similar Przondoviruses, phages KP32 and KN3-1 were described to also encode two different TSPs (Majkowska-Skrobek et al., 2018; Pan et al., 2019). K5-4 infects K5 and K8 capsular types, while KP32 adsorbs to K3 and K21 (Hsieh et al., 2017; Majkowska-Skrobek et al., 2018). Phage KN3-1, a podovirus that was not yet allocated to a phage genus, exhibits specificity to capsular types KN3 and KN56, respectively (Pan et al., 2019). Phage K5-2, however, infects three capsular types, e.g., K5, K30, and K69 although it encodes only two TSPs. Hsieh et al. point out that the K30 and K69 antigens differ only in the location of a pyruvic acetal, which seems to be unimportant for adsorption of K5-2 (Hsieh et al., 2017). In all of these phages, the open reading frames ORF37 and ORF38 encode the enzymes (Hsieh et al., 2017; Majkowska-Skrobek et al., 2018).

Solovieva et al. (2018) identified bacteriophage KpV41, a capsular type K1-specific Drulisvirus, which also encoded two different putative lyases (ORF46 and ORF56). Unfortunately, the proteins were not functionally characterized.

Interestingly, Przondo- and Drulisviruses, which feature two separate TSPs per virion, seem to have in common that the upstream encoded enzyme, e.g., ORF37 in phages K5-2 and K5-4, and ORF46 in phage KpV41, exhibits the conserved $Gp17_{T7}$-like N-terminal domain, which connects the proteins to the baseplate (Hsieh et al., 2017; Solovieva et al., 2018). However, this domain is apparently not present in the downstream encoded TSP, e.g., ORF38 in phages K5-2 and K5-4, and ORF55 in phage KpV41 (Hsieh et al., 2017; Solovieva et al., 2018). Thus, it remains unclear how the two enzymes are connected to the virion in Przondo- and Drulisviruses (**Figure 2**).

In addition to the podoviruses, several other bacteriophages of the *Myoviridae* and *Siphoviridae* families have been described infecting *K. pneumoniae*. Phage KP36, a member of the *Siphoviridae* family, genus Webervirus (T1virus), specifically infects K63 strains of *K. pneumoniae*. In this phage the active enzyme is encoded by gp50. It retains activity over a pH range from 4.0 to 7.0, but it is not temperature resistant, since the enzymatic activity is abolished at temperatures exceeding 45°C. Interestingly, the authors mentioned, that the *K. pneumoniae* capsular type K63 is structurally identical to the K42 CPS of *E.* coli. Hence, Gp50 is likely to be also active on certain *E. coli* (Majkowska-Skrobek et al., 2016). Phage KLPN1 is another KP36-like siphovirus, genus Webervirus. The phage produced plaques with expanding halos on type K2 capsular strains. Electron microscopy revealed that the tail fibers of this phage appear as elongated spherical structures. The baseplate resembles a rosette-like form with three "leaves." Based on amino acid sequence similarities ORF34 and ORF35 encode an endo-N-acetylneuraminidase/endosialidase domain. Experimental evidence on the function of these proteins is not available yet. Although the phage KLPN1 specifically infected K2 strains, it may well be that other capsular types are also infected by this phage due to the presence of two active enzymes (Hoyles et al., 2015).

The myovirus 0507-KN2-1 encodes a putative lyase (ORF96) that specifically cleaves the KN2 capsular type (Hsu et al., 2013). Based on genome sequence comparisons, this phage can be allocated to the Viunavirus genus. It forms small clear plaques with a large turbid halo. Probably the most curious myovirus that has been described to specifically interact with capsular antigens in *K. pneumoniae* is bacteriophage K64-1. K64-1 is a member of the *Myoviridae* family, Alcyoneusvirus genus that is currently not allocated to a particular subfamily. K64-1 infects ten different capsular types of *K. pneumoniae*. It encodes 11 different capsule degrading enzymes from which nine have been functionally characterized. Tail fiber structures in this phage are unique, as they appear as branching structures. It is likely that all encoded enzymes are present in the complex baseplate and tail fiber apparatus. The fine structure of these tail fibers is unknown so far (Pan et al., 2017).

The phage-encoded TSPs, which specifically cleave capsules of *K. pneumoniae*, have been applied in various set-ups to specifically control infections caused by the bacteria. In general, it seems that they retain their activity also *in vivo*. Decapsulation of *K. pneumoniae* rendered the bacteria sensitive to serum mediated killing, thereby significantly increasing survival of the infected rodents or of *Galleria mellonella* larvae, respectively (Lin et al., 2014; Majkowska-Skrobek et al., 2016; Majkowska-Skrobek et al., 2018; Pan et al., 2019; Wang et al., 2019). Furthermore, lyases do not seem to disturb other drugs, e.g., antibiotics, used to treat the infection (Majkowska-Skrobek et al., 2016).

Due to the high specificity of a TSP, pathogenic strains of *K. pneumonia* need to be isolated and typed in the clinic, before enzyme therapy can be applied. Mixed infections with strains exhibiting different capsular types are likely more difficult to treat, as long as the two different strains are not differentiated. If the enzyme is inactive on a particular strain, the bacteria cannot be controlled by the immune system. Therefore, rapid and cost-efficient typing methods are essential in order to choose the correct enzyme from a library.

As accurate typing of capsular antigens, either biochemically or genotypically, can be time consuming and laborious, "TSP-typing" would be specific, accurate, and easy. It seems that the purified enzymes even exhibit a greater specificity toward the capsular type than the native virion itself, rendering this technique advantageous compared to classical phage typing.

DECAPSULATED *Acinetobacter baumannii* ARE ATTENUATED *IN VIVO*

Health care acquired infections by bacteria of the *A. calcoaceticus* – *A. baumannii* (ACB) complex are increasing worldwide in hospital settings. The bacteria belong to the *Pseudomonadales* order and are therefore closely related to *Pseudomonas* spp. The high number of multi drug resistant strains and the capability of the bacteria to colonize catheters and other medical equipment, hinders effective control and prevention in the clinic. In *A. baumannii* 125 different capsular antigen types have been described (Arbatsky et al., 2018). However, only a few K-types, e.g., K1 and K45, have been identified as virulence factors so far. Like in *K. pneumonia,* the diversity of K-antigen structures has not yet been studied

biochemically, but genomically. A typing scheme for the ACB complex is not available yet, but strains of *A. baumannii* have been grouped into K-types. Some of these K-types were allocated to particular sequence types (ST).

Together with several highly similar viruses bacteriophage Fri1 represents an additional phage genus, Friunavirus, of the *Autographivirinae* subfamily. Friunaviruses encode a single TSP per virion. The enzymes again exhibit the N-terminal $Gp17_{T7}$-like domain for connection with the virion. In the two phages AS11 and AS12 the putative lyase is encoded by ORF 42 and ORF 45, respectively (Popova et al., 2017). From phage AB6 the purified enzyme (ORF 40) was functionally active on the tested phage host strain (Lai et al., 2016). However, a K-type specificity of AS11, AS12, and AB6 has not been reported yet.

Oliveira et al. (2017) isolated and characterized 12 phages, which infected species of the ACB complex. The isolated podoviruses exhibited high synteny in their genomes, although they have been isolated from distantly separated geographical regions, which spanned from America to Europe and Asia. The C-terminal pectate lyase domain of the TSP was often the only difference found among the viral genomes. All phage isolates belong to the *Autographivirinae*, Friunavirus genus. From phage P1, the authors characterized the function of the lyase. The enzyme exhibits the N-terminal $gp17_{T7}$-like domain. The C-terminal pectate lyase domain was cloned without the N-terminal domain and the authors proved its activity *in vitro*. In spotting tests it was functionally active even at concentrations of 0.1 μg/ml, and it retained its activity even after 2 years of storage at 4°C. As biochemical data on K-types are not available in *A. baumannii,* the authors linked the host range, with the genotype of the respective strains. Bacteriophages B3 and N1 specifically infected K2 strains of *A. baumannii*, while phages B1, B5, and B8 infected K9 strains. Phage B2 targeted a K44 strain. Interestingly, bacteriophages B4, B6, B7, P1 and P3 seem to be less specific, since they infected strains of different K-types. The authors, however, did not mention which strains and if two or more different K-types are infected by these phages. Based on the homologies of the capsular synthesis genes identified in the tested strains to glycosyltransferase sequences in the public databases, the authors hypothesized that the lyase of phages B3 and N1 may rely on pseudoaminic acid and glucopyranose residues in the capsule. The lyases of B1, B5, and B8 may bind to GalNAcA, while phages B4, B6, B7, P1 and P3 may have a preference for GlcNAc structures (Oliveira et al., 2017).

Another member of the *Podoviridae* family, phage Petty, was reported to infect both, strains of *A. baumannii* and *A. nosocomialis* (in total 4/40 strains tested). Unfortunately, the K-types of the respective strains were not mentioned in this study. Petty belongs to the genus Phikmvvirus. The TSP is encoded by gp39 and the protein was named Dpo1. Dpo1 also exhibits the N-terminal $gp17_{T7}$-like domain. The authors found that the enzymatic activity is enhanced by divalent cations (Hernandez-Morales et al., 2018). Liu et al. (2019) identified the TSP Dpo48 in phage IME200. The enzyme tolerates pH 5 – 9 and temperatures of 70°C. The K-type specificity of Dpo48 is still unknown (Liu et al., 2019). Recently, Oliveira et al. (2019b) characterized gp38 of bacteriophage B3, a member of the *Autographivirinae*. They found that it exhibits the N-terminal $gp17_{T7}$-like domain and that it is specific for K2-types. The enzyme is thermostable at 60°C (Oliveira et al., 2019b).

A K45/K30-specific TSP (gp69) was identified in bacteriophage B9, which belongs to the *Myoviridae* family (Oliveira et al., 2019a). Interestingly, based on bioinformatics and structure prediction this enzyme is composed of α-helices, and not of β-helices as usual. It remained stable at 80°C and retained its activity at a pH range from 5.0 to 9.0. The authors also compared the development of insensitive bacteria after prolonged incubation with the enzyme and the phage B9, respectively. They found that if bacteria were subjected to the enzyme alone and then re-isolated after incubation, they retained sensitivity. In contrast, bacteria subjected to the bacteriophage developed phage resistance. As a TSP does not kill the bacteria, but remove the capsule only, no selective pressure is applied on the bacteria *in vitro*. From this perspective, the development of resistance to TSPs might be underestimated.

The described TSPs were characterized not only *in vitro*, but also in various animal models *in vivo*. The interaction of the purified enzyme and the target bacteria was analyzed during infection. It seems that every tested enzyme renders the ACB bacteria sensitive to serum killing by the complement system and that infected animals either survive significantly longer, or can be even cured after infection in laboratory settings (Oliveira et al., 2017; Liu et al., 2019; Oliveira et al., 2019a,b). One TSP, Dpo1 of phage Petty, was also tested for its ability to degrade biofilms produced by *A. baumannii*. Although the enzyme removed some biofilm in a few tested strains, the removal amounted to only 20%. The authors concluded that although Dpo1 was active on the capsules of the tested strains, simple degradation of CPS may not be sufficient for removal of adhered *A. baumannii* cells. It is likely that Dpo1 is active against only one particular polysaccharide and *A. baumannii* may produce additional EPS polysaccharides or rely on other factors for biofilm formation (Hernandez-Morales et al., 2018). In addition to these experiments, the high specificity of the enzymes was once more shown to be very useful to establish a fast and reliable typing scheme for ACB complex bacteria.

TSP THERAPY RESCUED MICE INFECTED BY *Pasteurella multocida*

Pasteurella multocida is part of the oral microflora in many domesticated and agricultural animals. Capsular type A strains usually cause bovine hemorrhagic septicemia and avian cholera. In addition, the bacteria can cause oral diseases. Chen et al. (2018) expressed Dep-ORF8 of bacteriophage PHB02 (Teseptimavirus) recombinantly in *E. coli* and proved that the enzyme is capsular type A specific (Chen et al., 2018). The enzyme was also tested for its efficacy to control *P. multocida in vitro* and *in vivo*. If applied alone, it did not exhibit any detrimental effect on growth of the bacteria *in vitro*. In combination with serum, viable cell counts of *P. multocida* were reduced by 3.5–4.5 logs. Application of the enzyme *in vivo* did not reveal toxic

effects. From liver, spleen, kidneys, and lungs of Dep-ORF8 treated mice, an increase of eosinophils, basophiles or other pathological changes were not evident. If mice were infected with the pathogen and later treated with the enzyme, survival of the animals was significantly increased compared to the untreated control group (Chen et al., 2018). A closely related phage, PHB01 (Teseptimavirus), was reported to be capsular type D specific (Chen et al., 2019b). However, PHB01 could not infect every type D strain tested. The authors speculate that these strains may be phage resistant. The TSP of PHB01 was not characterized further yet.

TWO DIFFERENT DEPOLYMERASES DEGRADE THE CAPSULE IN *Bacillus subtilis*

In Gram-positive bacteria, CPS can also be chemically diverse. *Streptococcus pneumoniae* exhibits 98 different capsular serotypes (Paton and Trappetti, 2019). In *Staphylococcus aureus* 11 different capsular serotypes have been described (O'Riordan and Lee, 2004). The capsule contains mainly poly-N-acetylglucosamine. With respect to its function during biofilm formation, it is also termed polysaccharide intercellular adhesion (PIA) (Rohde et al., 2010; Wen and Zhang, 2015). *Bacillus anthracis*, *B. subtilis* or *S. pyogenes* also produce a capsule. However, these capsules belong to just one serotype. *S. pyogenes* produces a hyaluronic acid capsule, which is composed of glucuronic acid and *N*-acetylglucosamine repeating units. *Bacillus* spp. exhibits a rather unusual capsular polypeptide of γ-linked glutamate, e.g., poly-γ-glutamate (γ-PGA). Bacteriophage φNIT1, a member of the *Herelleviridae* family, Nitunavirus genus encodes a γ-PGA hydrolase (PghP) (Kimura and Itoh, 2003). The enzyme hydrolyses γ-PGA to oligopeptides, which are then converted to tri-, tetra-, and penta-γ-glutamates. Interestingly, PghP does not seem to be a structural protein of the φNIT1 virion. Instead, the enzyme is expressed at the end of the phages' infection cycle and is burst-released from the infected cells. It seems that *pghP* was acquired from a host organism. The structure of PghP was not determined yet. In addition to PghP, a second polysaccharide-degrading enzyme, an endo-levanase (LevP), was identified in φNIT1. LevP cleaves levan, an exopolysaccharide of *B. subtilis*. Again, it seems that also *levP* was acquired from a host organism. LevP is not a TSP, because similar levanases rather exhibit an N-terminal beta- propeller and a C-terminal beta-sandwich (Ernits et al., 2019). Apparently, PghP- and LevP-like proteins are also encoded in many other bacteriophages infecting *B. subtilis* (Ozaki et al., 2017).

EXTRACELLULAR POLYSACCHARIDE (EPS) DEGRADING TSPs

Extracellular polysaccharides (EPS) also add to the bacterial surface decoration (Limoli et al., 2015). Unlike CPS, EPS are not connected to the cell wall *per se*, but are secreted from the bacteria (Sachdeva et al., 2017). In general, EPS is considered as one of the major constituents in bacterial biofilms, where they mediate attachment and micro colony formation. Examples for bacterial EPS are alginate, Pel and Psl from *P. aeruginosa*, levan, colonic acid, bacterial cellulose from many phylogenetically different bacterial species, amylovoran from the plant pathogen *Erwinia amylovora*, *Vibrio* polysaccharides, or *B. subtilis* polysaccharides (Limoli et al., 2015). It should be noted that bacteria do not necessarily produce just one particular EPS, but rather a combination of different EPS at the same time. The ability to produce a biofilm, e.g., three-dimensional multilayer structures of bacteria embedded in an EPS matrix, seems to represent the most prominent form of microbial growth in nature. In a biofilm, bacteria are protected from desiccation, UV radiation, limited availability of nutrients, and antibiotics. Bacterial growth in a biofilm features the development of persister cells, which are resistant to environmental stresses and very difficult to eliminate. Absence of EPS decreases the ability of the bacteria to adhere to surfaces or tissues, affects colonization and therefore virulence in pathogenic bacteria.

IN THE FIRE BLIGHT PATHOGEN *Erwinia amylovora*, TSPs ENHANCE EFFICACY OF CAPSULE INDEPENDENT PHAGES

Erwinia amylovora is the causative agent of fire blight, a severe disease of *Rosaceae* plants. To prevent infection, streptomycin is usually applied during the flowering period. However, in some countries, use of streptomycin was banned recently. *E. amylovora* usually infects host blossoms via the stigma and invades the ovary. Later it spreads through the xylem vessels of an infected plant. In the xylem vessels *E. amylovora* produces high amounts of EPS, which leads to ooze formation, necrosis, and canker development. In *E. amylovora* the capsule is mainly composed of amylovoran and levan. Bacteriophage L1, a member of the *Autographivirinae*, genus Teseptimavirus (T7virus), exhibits Dpo_{L1}. The enzyme specifically cleaves amylovoran at the galactose backbone (Born et al., 2014). Any variation in the chemical structure of amylovoran has not been described yet and the majority of tested strains was sensitive to Dpo_{L1}. The enzyme was functionally characterized. It remained active at a pH range of 5.0–7.0 and featured a temperature optimum at 50°C (Born et al., 2014). The Dpo_{L1} encoding gene was later inserted into the genome of the capsule independent phage Y2, a myovirus. Infection of capsulated wild type bacteria by the recombinant phage Y2:dpo_{L1} revealed an improved efficacy and a more profound reduction of target bacteria compared to the parental phage (Born et al., 2017). Moreover, additional lyase encoding genes were identified in several other bacteriophages infecting *E. amylovora* such as the Zindervirus S2 (Knecht et al., 2018), many N4-like viruses (Thompson et al., 2019), Viunavirus Bue1 (Knecht et al., 2018), and in a giant jumbovirus RAY (Sharma et al., 2019). So far, only the enzymes of Bue1 and Gp76 of phage RAY have been preliminary characterized. The Bue1 enzyme did not exhibit amylovoran degrading activity (Knecht et al. unpublished results). The GP76 enzyme of phage RAY exhibited capsule degrading activity on closely related strains

of *Pantoea*, but not on the tested *Erwinia* host strains (Sharma et al., 2019). Future research will help to understand the function of these enzymes.

BIOFILMS OF *Pseudomonas aeruginosa* ARE DESTABILIZED BY ALGINATE-SPECIFIC TSPs

Pseudomonas aeruginosa is an opportunistic pathogen, which causes major problems in intensive care units. In the environment, the bacteria are typically associated with water and humid habitats. In many countries worldwide absence of *P. aeruginosa* is a microbiological criterion for the safety of drinking water. Depending on the national legislation, the bacteria must not be present in 100 or 300 ml samples, respectively. *P. aeruginosa* can cause severe wound infections and is typically associated with patients suffering from cystic fibrosis (CF). CF patients are prone to infection by mucoid strains, which are difficult to treat by antibiotics. The development of multiple drug resistance (MDR) in *P. aeruginosa* is another factor, which complicates therapy of infected patients. In addition, *P. aeruginosa* is a well known biofilm producer. Biofilms produced by the bacteria are typically thick, as *P. aeruginosa* can produce large amounts of alginate EPS (D-Mannuronate-L-Guluronate). When growing in the biofilm mode, *P. aeruginosa* can exhibit a more than 100-fold greater resistance toward antibiotics. Hence, as long as the bacteria do not develop MDR, TSP aided removal of the alginate EPS could render the bacteria more sensitive to antibiotics. To overcome MDR an increasing number of researchers aims at applying bacteriophages to control the pathogen. However, many *P. aeruginosa*-specific bacteriophages exhibit rather narrow host ranges and a selection of many different bacteriophages applied as a phage cocktail is needed for efficient control.

Glonti et al. (2010) described phage PT-6 (*Podoviridae*), that was biochemically characterized to lyse the alginate capsule of *P. aeruginosa in vitro* (Glonti et al., 2010). However, the genome sequence of phage PT-6 was not determined and a phylogenetic characterization has not been performed so far. Bacteriophage IME180 encodes a TSP in gene 2. Application of the enzyme in serum killing experiments enhanced inactivation of the treated bacteria. In addition, biofilms produced by *P. aeruginosa* could be successfully destroyed, but not completely eliminated by the enzyme (Mi et al., 2019).

Extracellular polysaccharides producing strains of *Pseudomonas putida* have also been controlled by bacteriophages and phage derived lyases. Cornelissen et al. (2011, 2012) identified a putative lyase in bacteriophages φ15 and AF, two members of the *Autographivirinae* subfamily. The authors applied φ15 to degrade biofilms of *P. putida*. As the phage mediated control of the biofilms was less profound than expected, the authors concluded that biofilm formation may even be a mechanism of phage resistance. The lyases were preliminarily studied, but activity on EPS was evident (Cornelissen et al., 2011; Cornelissen et al., 2012).

Judging from these studies it seems that removal of bacterial biofilms by application of lyases remains challenging and that more research is needed to better understand the limits. In natural habitats biofilms are likely produced by phylogenetically distinct bacteria. Hence, the EPS of a natural biofilm may be much more diverse than between different strains of a particular species. Given the high specificity of a lyase, a natural biofilm may not be affected by the action of a single enzyme. However, during infection of plants, animals and humans a particular strain of the pathogen dominates the intrinsic microflora. Hence, a single enzyme is very affective and can be applied as treatment. With the rise of multiple drug resistances in many different pathogenic bacteria and predominantly in the Gram-negatives, lyases represent a very promising treatment option.

LIPOPOLYSACCHARIDE DEGRADING TSPs

Lipopolysaccharide as another prominent polysaccharide has a high structural diversity, which defines many different serotypes in Gram-negative bacteria. The LPS is anchored in the bacterial outer membrane through the innermost part the lipid A, a phosphorylated diglucosamine. This lipid A is an endotoxin that causes inflammation in mammals after breakdown of the bacterial cell wall. In its core LPS contains the inner and outer core carbohydrates, e.g., KDO and heptoses, respectively. The core antigens are usually conserved in a particular bacterial species. The protruding O-antigen is composed of repeating units of 3–8 carbohydrates directly linked to the core oligosaccharide. It exhibits a great diversity, giving rise to 160 different O-antigens in *E. coli*, and more than 2500 different serotypes in *Salmonella*. Full length O-chains render a colony smooth, whereas truncated LPS molecules render a colony rough. Truncations in LPS can lead to significant attenuation in virulence and growth defects.

The interaction of TSPs with LPS are well studied in bacteriophages infecting *Salmonella enterica*. In *S. enterica,* typhoid and non-typhoid *Salmonella* are distinguished from each other. Typhoid fever is a severe infection of humans caused by *S.* Typhi or *S.* Paratyphi. These serotypes of *Salmonella enterica* are highly infectious and must not be mistaken for non-typhoid strains of *Salmonella* such as *S.* Typhimurium or *S.* Enteritidis. The latter serotypes cause Salmonellosis, a food borne infection of the gastro intestinal tract that leads to diarrhea and abdominal pain. Typhoid fever can directly spread from one patient to the other, while Salmonellosis is transmitted via contaminated food.

The TSP of bacteriophage P22, a temperate phage infecting *Salmonella*, is probably one of the best studied. P22 is a member of the *Podoviridae* family, Lederbergvirus genus and infects *Salmonella* serotypes sharing the trisaccharide repeating unit Man-Rha-Gal in the O-antigen. The TSP_{P22} destroys the O-antigen ligand by cleaving the glycosidic bond between rhamnose and galactose and is therefore an endorhamnosidase. Crystallization of the protein revealed that the epitope binding site is much larger than that of an antibody, explaining why the affinity of the protein to the O-antigen is much higher compared to antibodies. The binding site is located in the

central part of the beta-helix. The binding cleft accommodates all eight carbohydrate residues of two repeating units, reflecting an extensive contact surface. The active site of the enzyme was reported to be situated apart from the binding site (Steinbacher et al., 1996). Mutations of TSP_{P22} at amino acid position 331 (V331G, V331A) strongly affected O-antigen binding, while mutations at position 334 (A334V, A334I) affected O-antigen binding only slightly (Baxa et al., 1999). It was suggested that the destruction of the O-antigen is useful in order to facilitate detachment of progeny virions after the infection cycle (Steinbacher et al., 1996).

Waseh et al. (2010) applied TSP_{P22} to reduce *Salmonella* colonization in chicken. They found that TSP_{P22} agglutinates *Salmonella* at 4°C but not at higher temperatures of 42°C, e.g., at the chicken's body temperature. Oral administration of TSP_{P22} reduced *Salmonella* colonization in the chicken's gut and bacterial penetration into internal organs. Since motility seems to be implicated in colonization of host cells by bacteria, the authors analyzed the impact of TSP_{P22} on *Salmonella* motility. They found that spread of the bacteria was indeed significantly reduced, if TSP_{P22} was applied in soft agar plates incubated at 37°C (Waseh et al., 2010).

A very similar TSP was identified in the two bacteriophages Sf6 and HK620 (Chua et al., 1999; Freiberg et al., 2003; Barbirz et al., 2008). Both belong to the Lederbergvirus genus. Sf6 infects *Shigella flexneri*. The protein, again an endorhamnosidase, cleaves the tetrasaccharide repeat unit of the O-antigen in the Y serotype (Chua et al., 1999). In HK620, a coliphage, the TSP exhibits a highly similar secondary and tertiary structure compared to TSP_{P22} and TSP_{Sf6}, however at the C-terminus the amino acid sequence lacks homology. In fact, TSP_{HK620} is an endo-N-acetylglucosaminidase, which specifically cleaves the *E. coli* O18 antigen (Barbirz et al., 2008). All three proteins exhibit a conserved $pg17_{T7}$-like domain at the N-terminus, which connects the protein to the virion. Barbirz et al. (2008) reported a flexible linker between the N- and C-terminal domains in TSP_{HK620}. In addition, they found that the substrate-binding site of TSP_{HK620} and TSP_{P22} is on the face of the beta-helix, e.g., *intra*subunit, while in TSP_{Sf6} it is located between two helices, e.g., *inter*subunit (Barbirz et al., 2008; Leiman and Molineux, 2008). It is worth noting that substrate binding in highly conserved TSPs can be achieved in different manners.

Phage SP6, a Zindervirus, is phylogenetically closely related to bacteriophages K1E, and K1-5 (Scholl et al., 2002). However, SP6 predominantly infects *Salmonella*, while K1E and K1-5 are K-type specific coliphages (Leiman et al., 2007). The TSPs of SP6, however, do not recognize capsular antigens, but bind specifically to *Salmonella* LPS (Scholl et al., 2002). Like all members of the Zinderviruses, SP6 exhibits two TSPs, Gp46 and Gp47 (Gebhart et al., 2017; Tu et al., 2017). Both are connected to the baseplate via an adaptor protein, Gp37. Gp46 is an endorhamnosidase, which enables SP6 to infect *S.* Typhimurium and *S.* Enteritidis serotypes (Majkowska-Skrobek et al., 2016). The protein is functionally similar to TSP_{HK620}, TSP_{P22}, and TSP_{Sf6} and therefore shares a conserved C-terminus with these proteins, but it lacks the N-terminal $gp17_{T7}$-like domain, which connects TSP_{HK620}, TSP_{P22}, and TSP_{Sf6} to the baseplate (**Figure 2**).

The second TSP in SP6, Gp47 facilitates binding of the phage to *S.* Newport and *S.* Kentucky (Gebhart et al., 2017). The Gp46, Gp47, and Gp37 complex has a V-shaped structure. Only one TSP at a time binds to the host cell surface during adsorption. Hence, if *S.* Typhimurium is replaced by *S.* Newport, the entire V-shaped complex rotates in order to move the second TSP in a downward facing position. Thereby, the Gp46 tail spike undergoes a 60° upward rotation during adsorption, while the Gp47 tail spike undergoes a 60° downward rotation. Interestingly, SP6 does also infect rough *Salmonella*. This could be due to a general low affinity of the tail spikes for the core LPS further aiding adsorption (Tu et al., 2017). A highly similar tail spike architecture was described in bacteriophages K1E and K1-5 (Leiman et al., 2007).

Pseudomonas aeruginosa is the host bacterium of bacteriophage LKA1, a member of the *Autographivirinae*, Phikmvvirus genus. In *P. aeruginosa* two different types of LPS are produced. The A-band and the B-band. The A-band LPS contains a conserved O polysaccharide region composed of D-rhamnose (homopolysaccharide), while the B-band O-antigen (heteropolysaccharide) structure varies among the 20 O-serotypes of *P. aeruginosa* (Rocchetta et al., 1999). LKA1 is an O5-specific bacteriophage, which exhibits an O-specific polysaccharide lyase (Gp49). This lyase specifically binds and cleaves the B-band LPS (Olszak et al., 2017). Crystal structure of the TSP Gp49 suggests that the putative substrate binding and processing site is located on the face of the beta helix. The enzyme exhibits three domains. A typical N-terminal beta-helix, which binds and cleaves the substrate, a six-stranded beta-barrel insertion domain, which deepens the substrate binding groove and participates in the creation of the active site, and a C-terminal beta-sandwich, which could also be involved in substrate binding (Olszak et al., 2017). The Gp49 is stable at temperatures of 80°C and a 1-hour incubation at pH 6.0 or 12.0 reduced its activity by 50%.

The TSP Gp49 was further tested in virulence assays using the wax moth *Galleria mellonella* as a model system. Application of the TSP reduced virulence *in vivo* and the authors demonstrated enhanced sensitivity of treated bacteria to serum killing. Moreover, the activity of the antibiotics ciprofloxacin and gentamycin, was not affected. Finally, in contrast to $Dpo_{\phi 15}$, which specifically cleaves alginate (Cornelissen et al., 2011; Cornelissen et al., 2012), this enzyme caused biofilm degradation in the tested Pseudomonads. Hence, the authors concluded that LPS plays an important role for biofilm formation in *P. aeruginosa* (Olszak et al., 2017).

The *Vibrio cholerae* O139 infecting bacteriophage JA1 (*Podoviridae*) harbors a lyase which cleaves CPS between the GlcNAc and GalA residues. The authors discuss that the lyase may be useful for the generation of oligosaccharides, which could be effectively applied as CPS based vaccination. Since the CPS of *V. cholerae* is sensitive to acid, chemical treatment of CPS molecules could destruct epitopes that may be important to elicit protective immunity. The lyase in contrast to chemical treatment leaves these epitopes intact (Linnerborg et al., 2001).

The structure and function of the receptor-binding complex of bacteriophage CBA120, a member of the *Ackermannviridae* family, *Cvivirinae* subfamily, Kuttervirus genus was recently determined. CBA120 is an *E. coli* O157 infecting phage (Plattner et al., 2019). The production of Shiga Toxins (STX) makes infections with this particular type of *E. coli*, e.g., the Shiga Toxin producing *E. coli* (STEC), very severe. Released STX can cause kidney failure in infected patients. The disease, also referred to as hemolytic uremic syndrome (HUS), is treated with selected antibiotics, which do not enhance burst release of the toxin from the bacteria. If no antibiotic can be applied, only the symptoms can be treated, but not the cause of infection. Importantly, the production of STX is not restricted to O157, since many other O-serotypes of the bacteria, e.g., O26, O103, O104, O111, O145, and many more produce STX (Mir and Kudva, 2019).

In phage CBA120 four different TSPs, TSP1–TSP4, have been identified. TSP2 specifically binds and cleaves the O157 polysaccharide. Substrate-binding is performed in a cavity on the interface of two adjacent polypeptide chains. The enzyme then cleaves the O157 polysaccharide into Glc-GalNAc-Rha4NAc-Fuc tetrasaccharide subunits. Substrates of TSP1, TSP2, and TSP3 have been identified by bioinformatic analyses. It seems that prophage TSP sequences correlate with the O-antigen of the respective host bacterium. The analyses suggested that TSP1 might target *Salmonella enterica* serotype Minnesota or *Citrobacter freundii*. TSP3 and TSP4 seem to interact with *E. coli* O77 and O78, respectively. Indeed, infection of *S.* Minnesota, *E. coli* O77 and O78 by CBA120 could be demonstrated. The four TSPs are assembled in a branch-like structure that is attached to the baseplate of the phage. A very interesting finding was the identification of a $Gp10_{T4}$-like module in TSP2 and TSP4. Apparently, this particular module is needed to build up the complex branched architecture of the tail spikes (Plattner et al., 2019).

FUTURE PERSPECTIVES: PHAGE ENGINEERING

The highly conserved architecture of TSPs in different phage genera prompted researchers to genetically engineer and exchange the proteins to alter host ranges of the respective phages (Ando et al., 2015; Lai et al., 2016; Gebhart et al., 2017; Yosef et al., 2017). Since TSPs are connected to the virion via the highly conserved N-terminal $Gp17_{T7}$-like domain an exchange of the C-terminal enzymatically active domain was a straightforward approach. The presence of a flexible linker between the two domains may further allow optimizing exchanges of the C-terminal domain (Barbirz et al., 2008). Due to the high diversity in the primary structure, an exchange of a domain can be challenging, as it may not be clear at which amino acid position two different domains can be exchanged. Fortunately, phage tail spikes are more and more studied on the structural level, which provides a solid basis for future structure-guided TSP engineering.

Ando et al. (2015) applied a synthetic biology strategy to reprogram the host range of T3 and T7, respectively. The entire phage genomes were assembled from smaller genome fragments and cloned into yeast artificial chromosomes. In Gp17 the C-terminal domain was exchanged and synthetic phages were created. As expected the host ranges of $T3_{T7(gp17)}$ and $T7_{T3(gp17)}$ were swapped. These findings suggest, that the C-terminal domain of Gp17 defines the host range in Teseptimaviruses. Therefore, new host ranges can be conferred onto Tesetpimavirus scaffolds by engineering tail spikes. In addition, the technology was also used to redirect *E. coli* phage scaffolds to target pathogenic *Yersinia* and *Klebsiella* bacteria (Ando et al., 2015).

In another study, T7 was engineered for transduction of non-host bacteria applying a mutant lacking the tail genes gp 11, 12, and 17 (Kiro et al., 2013; Yosef et al., 2017). The deletion was complemented *in trans*. Therefore, homologs of the tail fiber genes from 15 different phages were cloned into plasmids. The plasmids also encoded an antibiotic resistance marker together with a T7-packaging signal. A phage propagation strain was transformed with the plasmid and then infected with the phage. The cell lysate contained virions encapsulating the T7 genome and virions encapsulating the plasmid at a ratio of ca. 1:1. The virions were used to transduce new host bacteria. Transductants were selected due to the plasmid encoded antibiotic marker. With this platform suitable TSPs for adsorption to new permissive host strains can be selected. Moreover, the efficiency of adsorption can be enhanced if the plasmid is subjected to a random mutagenesis followed by up to three panning rounds on a new permissive host strain (Yosef et al., 2017).

The TSPs of SP6 were used to replace the tail fiber gene of an R-type pyocin. R-type pyocins are bacteriocins, which feature a P2-like myoviral phage tail including baseplate and tail fibers, but lack the capsid and the genetic material. The bacteriocin is produced and burst-released by an infected bacterium. After release, the bacteriocin binds to its target bacterium through its tail fiber proteins. Then the cell membrane is punctured by a sheath contraction and insertion of the core. The target cell dies after depolarization of the cell membrane. Gebhart et al. demonstrated that a *Pseudomonas* specific R-type pyocin, e.g., R2, can be retargeted to strains of *S.* Kentucky and *S.* Newport if $Gp47_{SP6}$ was used to replace the native tail fiber protein of R2, and to strains of *S.* Typhimurium and *S.* Enteritidis, if $Gp46_{SP6}$ was used (Gebhart et al., 2017).

Lai et al. (2016) isolated and characterized two Friunaviruses, phage AB1 and AB6, which infected different strains of the host *A. baumannii*. The viruses exhibited a high degree of conservation, except for the lyase encoding gene. The author's exchanged $ORF41_{AB1}$ with $ORF40_{AB6}$ to generate the chimeric phage AB1tf6. As expected the host range of the chimeric phage was altered (Lai et al., 2016).

Due to the enormous progress in DNA sequencing technologies and recent developments in synthetic biology, engineering of bacteriophage genomes becomes a promising and powerful approach to optimize phage-based applications. For further reading recent review articles provide more detailed information on this matter (Chen et al., 2019a; Kilcher and Loessner, 2019).

In the context of the emerging antibiotic crises, novel approaches to tackle this crisis are urgently needed. As the structure and function of podoviral lyases is already well known, future research may explore on more complex baseplates and lyases in myo- and siphoviruses. Combining this fundamental research with the newest developments in synthetic biology, novel powerful antimicrobials such as engineered phages or optimized lyases, could be generated for future applications against life threatening bacteria.

AUTHOR CONTRIBUTIONS

All authors listed have made a substantial, direct and intellectual contribution to the work, and approved it for publication.

FUNDING

This work was funded by SNF grant 310030_156947/1 and CTI grant 18522.1 PFLS-LS.

REFERENCES

Ando, H., Lemire, S., Pires, D. P., and Lu, T. K. (2015). Engineering modular viral scaffolds for targeted bacterial population editing. *Cell Syst.* 1, 187–196. doi: 10.1016/j.cels.2015.08.013

Arbatsky, N. P., Shneider, M. M., Dmitrenok, A. S., Popova, A. V., Shagin, D. A., Shelenkov, A. A., et al. (2018). Structure and gene cluster of the K125 capsular polysaccharide from *Acinetobacter baumannii* MAR13-1452. *Int. J. Biol. Macromol.* 117, 1195–1199. doi: 10.1016/j.ijbiomac.2018.06.029

Barbirz, S., Muller, J. J., Uetrecht, C., Clark, A. J., Heinemann, U., and Seckler, R. (2008). Crystal structure of *Escherichia coli* phage HK620 tailspike: podoviral tailspike endoglycosidase modules are evolutionarily related. *Mol. Microbiol.* 69, 303–316. doi: 10.1111/j.1365-2958.2008.06311.x

Baxa, U., Steinbacher, S., Weintraub, A., Huber, R., and Seckler, R. (1999). Mutations improving the folding of phage P22 tailspike protein affect its receptor binding activity. *J. Mol. Biol.* 293, 693–701. doi: 10.1006/jmbi.1999.3165

Born, Y., Fieseler, L., Klumpp, J., Eugster, M. R., Zurfluh, K., Duffy, B., et al. (2014). The tail-associated depolymerase of *Erwinia amylovora* phage L1 mediates host cell adsorption and enzymatic capsule removal, which can enhance infection by other phage. *Environ. Microbiol.* 16, 2168–2180. doi: 10.1111/1462-2920.12212

Born, Y., Fieseler, L., Thony, V., Leimer, N., Duffy, B., and Loessner, M. J. (2017). Engineering of bacteriophages Y2::dpoL1-C and Y2::luxAB for efficient control and rapid detection of the fire blight pathogen, *Erwinia amylovora*. *Appl. Environ. Microbiol.* 83:e00341-17. doi: 10.1128/AEM.00341-17

Chen, Y., Batra, H., Dong, J., Chen, C., Rao, V. B., and Tao, P. (2019a). Genetic engineering of bacteriophages against infectious diseases. *Front. Microbiol.* 10:954. doi: 10.3389/fmicb.2019.00954

Chen, Y., Guo, G., Sun, E., Song, J., Yang, L., Zhu, L., et al. (2019b). Isolation of a T7-Like lytic *Pasteurella* bacteriophage vB_PmuP_PHB01 and its potential use in therapy against *Pasteurella multocida* infections. *Viruses* 11:E86. doi: 10.3390/v11010086

Chen, Y., Sun, E., Yang, L., Song, J., and Wu, B. (2018). Therapeutic application of bacteriophage PHB02 and its putative depolymerase against *Pasteurella multocida* capsular type A in mice. *Front. Microbiol.* 9:1678. doi: 10.3389/fmicb.2018.01678

Chua, J. E. H., Manning, P. A., and Morona, R. (1999). The *Shigella flexneri* bacteriophage Sf6 tailspike protein (TSP)/endorhamnosidase is related to the bacteriophage P22 TSP and has a motif common to exo- and endoglycanases, and C-5 epimerases. *Microbiology* 145, 1649–1659. doi: 10.1099/13500872-145-7-1649

Cornelissen, A., Ceyssens, P.-J., Krylov, V. N., Noben, J.-P., Volckaert, G., and Lavigne, R. (2012). Identification of EPS-degrading activity within the tail spikes of the novel *Pseudomonas putida* phage AF. *Virology* 434, 251–256. doi: 10.1016/j.virol.2012.09.030

Cornelissen, A., Ceyssens, P.-J., T'Syen, J., Van Praet, H., Noben, J.-P., Shaburova, O. V., et al. (2011). The T7-related *Pseudomonas putida* phage φ15 displays virion-associated biofilm degradation properties. *PLoS One* 6:e18597. doi: 10.1371/journal.pone.0018597

Cuervo, A., Pulido-Cid, M., Chagoyen, M., Arranz, R., Gonzalez-Garcia, V. A., Garcia-Doval, C., et al. (2013). Structural characterization of the bacteriophage T7 tail machinery. *J. Biol. Chem.* 288, 26290–26299. doi: 10.1074/jbc.M113.491209

Ernits, K., Eek, P., Lukk, T., Visnapuu, T., and Alamae, T. (2019). First crystal structure of an endo-levanase - the BT1760 from a human gut commensal *Bacteroides thetaiotaomicron*. *Sci. Rep.* 9:8443. doi: 10.1038/s41598-019-44785-0

Follador, R., Heinz, E., Wyres, K. L., Ellington, M. J., Kowarik, M., Holt, K. E., et al. (2016). The diversity of *Klebsiella pneumoniae* surface polysaccharides. *Microb. Genom.* 2:e000073. doi: 10.1099/mgen.0.000073

Freiberg, A., Morona, R., Van den Bosch, L., Jung, C., Behlke, J., Carlin, N., et al. (2003). The tailspike protein of *Shigella* phage Sf6 - A structural homolog of *Salmonella* phage p22 tailspike protein without sequence similarity in the beta-helix domain. *J. Biol. Chem.* 278, 1542–1548. doi: 10.1074/jbc.M205294200

Garcia-Doval, C., and van Raaij, M. J. (2012). Structure of the receptor-binding carboxy-terminal domain of bacteriophage T7 tail fibers. *Proc. Natl. Acad. Sci. U.S.A.* 109, 9390–9395. doi: 10.1073/pnas.1119719109

Gebhart, D., Williams, S. R., and Scholl, D. (2017). Bacteriophage SP6 encodes a second tailspike protein that recognizes *Salmonella enterica* serogroups C2 and C3. *Virology* 507, 263–266. doi: 10.1016/j.virol.2017.02.025

Glonti, T., Chanishvili, N., and Taylor, P. W. (2010). Bacteriophage-derived enzyme that depolymerizes the alginic acid capsule associated with cystic fibrosis isolates of *Pseudomonas aeruginosa*. *J. Appl. Microbiol.* 108, 695–702. doi: 10.1111/j.1365-2672.2009.04469.x

Guichard, J. A., Middleton, P. C., and McConnell, M. R. (2013). Genetic analysis of structural proteins in the adsorption apparatus of bacteriophage epsilon 15. *World J. Virol.* 2, 152–159. doi: 10.5501/wjv.v2.i4.152

Guo, Z. M., Huang, J., Yan, G. M., Lei, L. C., Wang, S., Yu, L., et al. (2017). Identification and characterization of Dpo42, a novel depolymerase derived from the *Escherichia coli* phage vB_EcoM_ECOO78. *Front. Microbiol.* 8:1460. doi: 10.3389/fmicb.2017.01460

Hallenbeck, P. C., Vimr, E. R., Yu, F., Bassler, B., and Troy, F. A. (1987). Purification and properties of a bacteriophage-induced endo-N-acetylneuraminidase specific for poly-alpha-2,8-sialosyl carbohydrate units. *J. Biol. Chem.* 262, 3553–3561.

Hernandez-Morales, A. C., Lessor, L. L., Wood, T. L., Migl, D., Mijalis, E. M., Cahill, J., et al. (2018). Genomic and biochemical characterization of acinetobacter podophage petty reveals a novel lysis mechanism and tail-associated depolymerase activity. *J. Virol.* 92:e01064-17. doi: 10.1128/JVI.01064-17

Hoyles, L., Murphy, J., Neve, H., Heller, K. J., Turton, J. F., Mahony, J., et al. (2015). *Klebsiella pneumoniae* subsp. pneumoniae-bacteriophage combination from the caecal effluent of a healthy woman. *PeerJ* 3:e1061. doi: 10.7717/peerj.1061

Hsieh, P.-F., Lin, H.-H., Lin, T.-L., Chen, Y.-Y., and Wang, J.-T. (2017). Two T7-like bacteriophages, K5-2 and K5-4, each encodes two capsule depolymerases: isolation and functional characterization. *Sci. Rep.* 7:4624. doi: 10.1038/s41598-017-04644-2

Hsu, C. R., Liao, C. H., Lin, T. L., Yang, H. R., Yang, F. L., Hsieh, P. F., et al. (2016). Identification of a capsular variant and characterization of capsular acetylation in *Klebsiella pneumoniae* PLA-associated type K57. *Sci. Rep.* 6:31946. doi: 10.1038/srep31946

Hsu, C. R., Lin, T. L., Pan, Y. J., Hsieh, P. F., and Wang, J. T. (2013). Isolation of a bacteriophage specific for a new capsular type of *Klebsiella pneumoniae* and characterization of its polysaccharide depolymerase. *PLoS One* 8:e70092. doi: 10.1371/journal.pone.0070092

Hu, X., Chen, Z., Xiong, K., Wang, J., Rao, X., and Cong, Y. (2017). Vi capsular polysaccharide: synthesis, virulence, and application. *Crit. Rev. Microbiol.* 43, 440–452. doi: 10.1080/1040841X.2016.1249335

Kilcher, S., and Loessner, M. J. (2019). Engineering bacteriophages as versatile biologics. *Trends Microbiol.* 27, 355–367. doi: 10.1016/j.tim.2018.09.006

Kimura, K., and Itoh, Y. (2003). Characterization of poly-gamma-glutamate hydrolase encoded by a bacteriophage genome: possible role in phage infection of *Bacillus subtilis* encapsulated with poly-gamma-glutamate. *Appl. Environ. Microbiol.* 69, 2491–2497. doi: 10.1128/aem.69.5.2491-2497.2003

Kiro, R., Molshanski-Mor, S., Yosef, I., Milam, S. L., Erickson, H. P., and Qimron, U. (2013). Gene product 0.4 increases bacteriophage T7 competitiveness by inhibiting host cell division. *Proc. Natl. Acad. Sci. U.S.A.* 110, 19549–19554. doi: 10.1073/pnas.1314096110

Knecht, L. E., Born, Y., Pothier, J. F., Loessner, M. J., and Fieseler, L. (2018). Complete genome sequences of *Erwinia amylovora* phages vB_EamP-S2 and vB_EamM-Bue1. *Microbiol. Resour. Announce.* 7:e00891-18. doi: 10.1128/MRA.00891-18

Lai, M.-J., Chang, K.-C., Huang, S.-W., Luo, C.-H., Chiou, P.-Y., Wu, C.-C., et al. (2016). The Tail associated protein of *Acinetobacter baumannii* phage ΦAB6 is the host specificity determinant possessing exopolysaccharide depolymerase activity. *PLoS One* 11:e0153361. doi: 10.1371/journal.pone.0153361

Latka, A., Maciejewska, B., Majkowska-Skrobek, G., Briers, Y., and Drulis-Kawa, Z. (2017). Bacteriophage-encoded virion-associated enzymes to overcome the carbohydrate barriers during the infection process. *Appl. Microbiol. Biotechnol.* 101, 3103–3119. doi: 10.1007/s00253-017-8224-6

Leiman, P. G., Battisti, A. J., Bowman, V. D., Stummeyer, K., Muhlenhoff, M., Gerardy-Schahn, R., et al. (2007). The structures of bacteriophages K1E and K1-5 explain processive degradation of polysaccharide capsules and evolution of new host specificities. *J. Mol. Biol.* 371, 836–849. doi: 10.1016/j.jmb.2007.05.083

Leiman, P. G., and Molineux, I. J. (2008). Evolution of a new enzyme activity from the same motif fold. *Mol. Microbiol.* 69, 287–290. doi: 10.1111/j.1365-2958.2008.06241.x

Limoli, D. H., Jones, C. J., and Wozniak, D. J. (2015). Bacterial extracellular polysaccharides in biofilm formation and function. *Microbiol. Spectr.* 3, 1–19. doi: 10.1128/microbiolspec.MB-0011-2014

Lin, H., Paff, M. L., Molineux, I. J., and Bull, J. J. (2017). Therapeutic application of phage capsule depolymerases against K1, K5, and K30 capsulated *E. coli* in mice. *Front. Microbiol.* 8:2257. doi: 10.3389/fmicb.2017.02257

Lin, H., Paff, M. L., Molineux, I. J., and Bull, J. J. (2018). Antibiotic therapy using phage depolymerases: robustness across a range of conditions. *Virus. Basel* 10:622. doi: 10.3390/v10110622

Lin, T. L., Hsieh, P. F., Huang, Y. T., Lee, W. C., Tsai, Y. T., Su, P. A., et al. (2014). Isolation of a bacteriophage and its depolymerase specific for K1 capsule of *Klebsiella pneumoniae*: implication in typing and treatment. *J. Infect. Dis.* 210, 1734–1744. doi: 10.1093/infdis/jiu332

Linnerborg, M., Weintraub, A., Albert, M. J., and Widmalm, G. (2001). Depolymerization of the capsular polysaccharide from *Vibrio cholerae* O139 by a lyase associated with the bacteriophage JA1. *Carbohydr. Res.* 333, 263–269. doi: 10.1016/S0008-6215(01)00159-8

Liu, Y. N., Mi, Z. Q., Mi, L. Y., Huang, Y., Li, P. Y., Liu, H. Y., et al. (2019). Identification and characterization of capsule depolymerase Dpo48 from *Acinetobacter baumannii* phage IME200. *PeerJ* 7:e6173. doi: 10.7717/peerj.6173

Majkowska-Skrobek, G., Łątka, A., Berisio, R., Maciejewska, B., Squeglia, F., Romano, M., et al. (2016). Capsule-targeting depolymerase, derived from Klebsiella KP36 phage, as a tool for the development of anti-virulent strategy. *Viruses* 8:324. doi: 10.3390/v8120324

Majkowska-Skrobek, G., Latka, A., Berisio, R., Squeglia, F., Maciejewska, B., Briers, Y., et al. (2018). Phage-borne depolymerases decrease *Klebsiella pneumoniae* resistance to innate defense mechanisms. *Front. Microbiol.* 9:2517. doi: 10.3389/fmicb.2018.02517

Mi, L., Liu, Y., Wang, C., He, T., Gao, S., Xing, S., et al. (2019). Identification of a lytic *Pseudomonas aeruginosa* phage depolymerase and its anti-biofilm effect and bactericidal contribution to serum. *Virus Genes* 55, 394–405. doi: 10.1007/s11262-019-01660-4

Mir, R. A., and Kudva, I. T. (2019). Antibiotic-resistant Shiga toxin-producing *Escherichia coli*: an overview of prevalence and intervention strategies. *Zoonoses Public Health* 66, 1–13. doi: 10.1111/zph.12533

Mushtaq, N., Redpath, M. B., Luzio, J. P., and Taylor, P. W. (2004). Prevention and cure of systemic *Escherichia coli* K1 infection by modification of the bacterial phenotype. *Antimicrob. Agents Chemother.* 48, 1503–1508. doi: 10.1128/aac.48.5.1503-1508.2004

Oliveira, H., Costa, A. R., Ferreira, A., Konstantinides, N., Santos, S. B., Boon, M., et al. (2019a). Functional analysis and antivirulence properties of a new depolymerase from a myovirus that infects *Acinetobacter baumannii* capsule K45. *J. Virol.* 93:e001163-8. doi: 10.1128/JVI.01163-18

Oliveira, H., Mendes, A., Fraga, A. G., Ferreira, A., Pimenta, A. I., Mil-Homens, D., et al. (2019b). K2 Capsule depolymerase is highly stable, is refractory to resistance, and protects larvae and mice from *Acinetobacter baumannii* sepsis. *Appl. Environ. Microbiol.* 85:e00934-19. doi: 10.1128/AEM.00934-19

Oliveira, H., Costa, A. R., Konstantinides, N., Ferreira, A., Akturk, E., Sillankorva, S., et al. (2017). Ability of phages to infect *Acinetobacter calcoaceticus-Acinetobacter baumannii* complex species through acquisition of different pectate lyase depolymerase domains. *Environ. Microbiol.* 19, 5060–5077. doi: 10.1111/1462-2920.13970

Olszak, T., Shneider, M. M., Latka, A., Maciejewska, B., Browning, C., Sycheva, L. V., et al. (2017). The O-specific polysaccharide lyase from the phage LKA1 tailspike reduces *Pseudomonas virulence*. *Sci. Rep.* 7:16302. doi: 10.1038/s41598-017-16411-4

O'Riordan, K., and Lee, J. C. (2004). Staphylococcus aureus capsular polysaccharides. *Clin. Microbiol. Rev.* 17, 218–234. doi: 10.1128/cmr.17.1.218-234.2004

Ozaki, T., Abe, N., Kimura, K., Suzuki, A., and Kaneko, J. (2017). Genomic analysis of Bacillus subtilis lytic bacteriophage varphiNIT1 capable of obstructing natto fermentation carrying genes for the capsule-lytic soluble enzymes poly-gamma-glutamate hydrolase and levanase. *Biosci. Biotechnol. Biochem.* 81, 135–146. doi: 10.1080/09168451.2016.1232153

Pan, Y. J., Lin, T. L., Chen, C. C., Tsai, Y. T., Cheng, Y. H., Chen, Y. Y., et al. (2017). Klebsiella phage phi K64-1 encodes multiple depolymerases for multiple host capsular types. *J. Virol.* 91:e02457-16. doi: 10.1128/JVI.02457-16

Pan, Y.-J., Lin, T.-L., Chen, Y.-Y., Lai, P.-H., Tsai, Y.-T., Hsu, C.-R., et al. (2019). Identification of three podoviruses infecting *Klebsiella* encoding capsule depolymerases that digest specific capsular types. *Microb. Biotechnol.* 12, 472–486. doi: 10.1111/1751-7915.13370

Paton, J. C., and Trappetti, C. (2019). *Streptococcus pneumoniae* capsular polysaccharide. *Microbiol. Spectr.* 7, 1–15. doi: 10.1128/microbiolspec.GPP3-0019-2018

Plattner, M., Shneider, M. M., Arbatsky, N. P., Shashkov, A. S., Chizhov, A. O., Nazarov, S., et al. (2019). Structure and function of the branched receptor-binding complex of bacteriophage CBA120. *J. Mol. Biol.* 431, 3718–3739. doi: 10.1016/j.jmb.2019.07.022

Popova, A. V., Lavysh, D. G., Klimuk, E. I., Edelstein, M. V., Bogun, A. G., Shneider, M. M., et al. (2017). Novel Fri1-like viruses infecting *Acinetobacter baumannii*-vB_AbaP_AS11 and vB_AbaP_AS12-characterization, comparative genomic analysis, and host-recognition strategy. *Viruses* 9:188. doi: 10.3390/v9070188

Rocchetta, H. L., Burrows, L. L., and Lam, J. S. (1999). Genetics of O-antigen biosynthesis in *Pseudomonas aeruginosa*. *Microbiol. Mol. Biol. Rev.* 63, 523–553.

Rohde, H., Frankenberger, S., Zahringer, U., and Mack, D. (2010). Structure, function and contribution of polysaccharide intercellular adhesin (PIA) to *Staphylococcus epidermidis* biofilm formation and pathogenesis of biomaterial-associated infections. *Eur. J. Cell Biol.* 89, 103–111. doi: 10.1016/j.ejcb.2009.k10.005

Sachdeva, S., Palur, R. V., Sudhakar, K. U., and Rathinavelan, T. (2017). *E. coli* group 1 capsular polysaccharide exportation nanomachinary as a plausible antivirulence target in the perspective of emerging antimicrobial resistance. *Front. Microbiol.* 8:70. doi: 10.3389/fmicb.2017.00070

Schmelcher, M., and Loessner, M. J. (2016). Bacteriophage endolysins: applications for food safety. *Curr. Opin. Biotechnol.* 37, 76–87. doi: 10.1016/j.copbio.2015.10.005

Scholl, D., Adhya, S., and Merril, C. R. (2002). Bacteriophage SP6 is closely related to phages K1-5, K5, and K1E but encodes a tail protein very similar to that of the distantly related P22. *J. Bacteriol.* 184, 2833–2836. doi: 10.1128/Jb.184.10.2833-2836.2002

Sharma, R., Pielstick, B. A., Bell, K. A., Nieman, T. B., Stubbs, O. A., Yeates, E. L., et al. (2019). A novel, highly related jumbo family of bacteriophages that were

isolated against *Erwinia*. *Front. Microbiol.* 10:1533. doi: 10.3389/fmicb.2019.01533

Solovieva, E. V., Myakinina, V. P., Kislichkina, A. A., Krasilnikova, V. M., Verevkin, V. V., Mochalov, V. V., et al. (2018). Comparative genome analysis of novel podoviruses lytic for hypermucoviscous *Klebsiella pneumoniae* of K1. K2, and K57 capsular types. *Virus Res.* 243, 10–18. doi: 10.1016/j.virusres.2017.09.026

Steinbacher, S., Baxa, U., Miller, S., Weintraub, A., Seckler, R., and Huber, R. (1996). Crystal structure of phage P22 tailspike protein complexed with *Salmonella* sp. O-antigen receptors. *Proc. Natl. Acad. Sci. U.S.A.* 93, 10584–10588. doi: 10.1073/pnas.93.20.10584

Stummeyer, K., Schwarzer, D., Claus, H., Vogel, U., Gerardy-Schahn, R., and Muhlenhoff, M. (2006). Evolution of bacteriophages infecting encapsulated bacteria: lessons from *Escherichia coli* K1-specific phages. *Mol. Microbiol.* 60, 1123–1135. doi: 10.1111/j.1365-2958.2006.05173.x

Thompson, D. W., Casjens, S. R., Sharma, R., and Grose, J. H. (2019). Genomic comparison of 60 completely sequenced bacteriophages that infect *Erwinia* and/or *Pantoea* bacteria. *Virology* 535, 59–73. doi: 10.1016/j.virol.2019.06.005

Thompson, J. E., Pourhossein, M., Waterhouse, A., Hudson, T., Goldrick, M., Derrick, J. P., et al. (2010). The K5 lyase KflA combines a viral tail spike structure with a bacterial polysaccharide lyase mechanism. *J. Biol. Chem.* 285, 23963–23969. doi: 10.1074/jbc.M110.127571

Tomlinson, S., and Taylor, P. W. (1985). Neuraminidase associated with coliphage E that specifically depolymerizes the *Escherichia coli* K1 capsular polysaccharide. *J. Virol.* 55, 374–378.

Tu, J. G., Park, T., Morado, D. R., Hughes, K. T., Molineux, I. J., and Liu, J. (2017). Dual host specificity of phage SP6 is facilitated by tailspike rotation. *Virology* 507, 206–215. doi: 10.1016/j.virol.2017.04.017

Wang, C., Li, P., Niu, W., Yuan, X., Liu, H., Huang, Y., et al. (2019). Protective and therapeutic application of the depolymerase derived from a novel KN1 genotype of *Klebsiella pneumoniae* bacteriophage in mice. *Res. Microbiol.* 170, 156–164. doi: 10.1016/j.resmic.2019.01.003

Waseh, S., Hanifi-Moghaddam, P., Coleman, R., Masotti, M., Ryan, S., Foss, M., et al. (2010). Orally administered P22 phage tailspike protein reduces *Salmonella* colonization in chickens: prospects of a novel therapy against bacterial infections. *PLoS One* 5:e0013904. doi: 10.1371/journal.pone.0013904

Wen, Z., and Zhang, J.-R. (2015). "Chapter 3 - bacterial capsules," in *Molecular Medical Microbiology* 2nd Edn, eds Y.-W. Tang, M. Sussman, D. Liu, I. Poxton, and J. Schwartzman, (Boston: Academic Press), 33–53. doi: 10.1016/b978-0-12-397169-2.00003-2

Yosef, I., Goren, M. G., Globus, R., Molshanski-Mor, S., and Qimron, U. (2017). Extending the host range of bacteriophage particles for DNA transduction. *Mol. Cell* 66, 721-728.e3. doi: 10.1016/j.molcel.2017.04.025

Yu, W.-L., Ko, W.-C., Cheng, K.-C., Lee, C.-C., Lai, C.-C., and Chuang, Y.-C. (2008). Comparison of prevalence of virulence factors for *Klebsiella pneumoniae* liver abscesses between isolates with capsular K1/K2 and non-K1/K2 serotypes. *Diagnos. Microbiol. Infect. Dis.* 62, 1–6. doi: 10.1016/j.diagmicrobio.2008.04.007

Conflict of Interest: The authors declare that the research was conducted in the absence of any commercial or financial relationships that could be construed as a potential conflict of interest.

frontiers in Microbiology

REVIEW
published: 10 January 2020
doi: 10.3389/fmicb.2019.02909

Microarray Strategies for Exploring Bacterial Surface Glycans and Their Interactions With Glycan-Binding Proteins

*María Asunción Campanero-Rhodes[1,2], Angelina Sa Palma[3], Margarita Menéndez[1,2] and Dolores Solís[1,2]**

[1] Instituto de Química Física Rocasolano, Consejo Superior de Investigaciones Científicas, Madrid, Spain, [2] Centro de Investigación Biomédica en Red de Enfermedades Respiratorias, Instituto de Salud Carlos III, Madrid, Spain, [3] UCIBIO, Department of Chemistry, Faculty of Science and Technology, NOVA University of Lisbon, Lisbon, Portugal

Bacterial surfaces are decorated with distinct carbohydrate structures that may substantially differ among species and strains. These structures can be recognized by a variety of glycan-binding proteins, playing an important role in the bacteria cross-talk with the host and invading bacteriophages, and also in the formation of bacterial microcolonies and biofilms. In recent years, different microarray approaches for exploring bacterial surface glycans and their recognition by proteins have been developed. A main advantage of the microarray format is the inherent miniaturization of the method, which allows sensitive and high-throughput analyses with very small amounts of sample. Antibody and lectin microarrays have been used for examining bacterial glycosignatures, enabling bacteria identification and differentiation among strains. In addition, microarrays incorporating bacterial carbohydrate structures have served to evaluate their recognition by diverse host/phage/bacterial glycan-binding proteins, such as lectins, effectors of the immune system, or bacterial and phagic cell wall lysins, and to identify antigenic determinants for vaccine development. The list of samples printed in the arrays includes polysaccharides, lipopoly/lipooligosaccharides, (lipo)teichoic acids, and peptidoglycans, as well as sequence-defined oligosaccharide fragments. Moreover, microarrays of cell wall fragments and entire bacterial cells have been developed, which also allow to study bacterial glycosylation patterns. In this review, examples of the different microarray platforms and applications are presented with a view to give the current state-of-the-art and future prospects in this field.

Keywords: bacterial glycans, microarrays, lectins, antibodies, immune system, vaccine development, bacterial interactions

OPEN ACCESS

Edited by:
Zuzanna Drulis-Kawa, University of Wrocław, Poland

Reviewed by:
Evguenii Vinogradov, National Research Council Canada, Canada
Anne Imberty, Centre National de la Recherche Scientifique (CNRS), France
Sheng-Ce Tao, Shanghai Jiao Tong University, China

***Correspondence:**
Dolores Solís
d.solis@iqfr.csic.es

Specialty section:
This article was submitted to Infectious Diseases, a section of the journal Frontiers in Microbiology

Received: *30 September 2019*
Accepted: *03 December 2019*
Published: *10 January 2020*

Citation:
Campanero-Rhodes MA, Palma AS, Menéndez M and Solís D (2020) Microarray Strategies for Exploring Bacterial Surface Glycans and Their Interactions With Glycan-Binding Proteins. Front. Microbiol. 10:2909. doi: 10.3389/fmicb.2019.02909

INTRODUCTION

The intricate network of glycans covering bacterial surfaces differs between Gram-negative and Gram-positive bacteria (**Figure 1**) (Salton and Kim, 1996). Gram-negative bacteria are enveloped by two cell membranes separated by a thin peptidoglycan layer, and display lipopolysaccharides (LPSs) embedded in the outer membrane. LPSs are anchored to the membrane through a highly

conserved lipid A moiety that is linked to a polysaccharide composed of an inner and outer core and an outermost chain built with repeating saccharide units, which is alluded to as O-chain or O-antigen (**Figure 1**, left part). Some Gram-negative bacteria, however, do not contain O-antigen chains in their LPS, which is therefore referred to as lipooligosaccharide (LOS). In contrast, Gram-positive bacteria only have one cell membrane that is covered by a thick peptidoglycan layer, and they usually display teichoic acids (TAs) anchored to the membrane (known as lipoteichoic acids or LTAs) or covalently bound to the peptidoglycan (known as wall teichoic acids or WTAs) (**Figure 1**, middle part). Common to several Gram-negative and -positive bacteria is the potential presence of cell surface glycoproteins and capsular polysaccharides. Mycobacteria can be considered apart from these two main groups as they display a unique envelope distinguished by a large cell wall complex formed by peptidoglycan covalently attached to arabinogalactan, which in turn is linked to long fatty acids (mycolic acids) that constitute the inner leaflet of the so-called mycomembrane (**Figure 1**, right part) (Jankute et al., 2015). Arabinomannan, lipoarabinomannan, phosphatidyl-myo-inositol-mannosides, phenolic glycolipids, and trehalose-containing lipids are other distinctive glycan structures of the mycobacterial envelope (**Figure 1**, right part). Overall, the repertoire of bacterial glycans shows a huge diversity in monosaccharide residues and linkage configurations, many of which are not found in the eukaryotic glycome (**Figure 2**) (Herget et al., 2008; Adibekian et al., 2011). The precise structure of these glycans may substantially differ among bacteria with the same cell surface architecture, and even among different strains of a given bacterial species. Moreover, some bacteria display very rare sugars, e.g., 3,6-dideoxyhexoses, which are found in a limited number of Enterobacteriaceae, or the 4,6-dideoxy sugar anthrose, distinctive of *Bacillus anthracis* (**Figure 2**). Thus, the specific glycans that decorate the bacterial surface can serve to typify strains.

Many bacterial glycans are immunogenic and have been used to develop vaccines against the respective bacteria. In addition, they may be recognized as "non-self" by host pattern-recognition receptors, including a variety of lectins of the innate immune system, for triggering defense mechanisms (Sukhithasri et al., 2013; Wesener et al., 2017; Casals et al., 2018). Not surprisingly, some bacteria camouflage from the host by displaying glycans that mimic the carbohydrate moieties of host cells. Moreover, recognition of such self-like glycans by host lectins may be exploited by the bacterium for down-regulating the innate immunity, or as stratagem for promoting attachment through lectin bridging of bacterial and host glycans. On the other hand, several bacteria bind directly to host glycans using surface-exposed adhesins (Moonens and Remaut, 2017), and in some cases these adhesins are also involved in the formation of bacterial microcolonies and biofilms through binding to glycans of neighbor cells or to secreted exopolysaccharides. Similarly, bacteriophages frequently target bacterial glycans for invading their hosts or to release the phage progeny. In addition, many bacterial hydrolases, e.g., those hydrolyzing the cell wall, are modular and contain carbohydrate-binding modules (CBMs) that bind to specific regions of the substrate to situate the catalytic domain at a position appropriate for cleavage. Furthermore, there is a specific class of plant receptors able to recognize bacterial oligosaccharides that operate as signaling molecules in plant−bacteria symbiosis. Thus, a broad variety of proteins from different life kingdoms recognize bacterial glycans and play important roles in the cross-talk of bacteria with their particular environment. Therefore, delineation of bacterial surface glycosignatures and assessment of their recognition by relevant glycan-binding proteins is crucial to understand, and when possible govern, the bacteria's behavior. To this aim, different microarray approaches have been developed.

The microarray technology emerged to meet the scientist's desire of a high-throughput analytical tool that enabled simultaneous analyses of a large number of biomolecular interactions using very small amounts of sample. The underlying concept was that a high local concentration of a given sample clustered in a miniature spot could enhance detection sensitivity. Prompted by the great success of DNA microarrays in gene expression profiling and related applications (Morley et al., 2004), protein (Zhu et al., 2001; Angenendt, 2005; Tao et al., 2008) and carbohydrate microarrays were also developed (Fukui et al., 2002; Blixt et al., 2004; Campanero-Rhodes et al., 2006), allowing high-throughput studies of protein expression and functionalities, including carbohydrate-mediated recognition events (Blumenschein et al., 2007; Campanero-Rhodes et al., 2007). Initially, most glycan libraries included in the arrays were mainly composed of mammalian-like structures, casting doubt on their value for exploring the binding preferences of proteins that recognize bacterial glycans. To overcome this limitation, growing efforts are being made to generate microarrays incorporating bacterial carbohydrate structures, ranging from small synthetic fragments to large natural polysaccharides.

Microarrays are frequently assembled on microscope glass slides coated or derivatized with a variety of reagents, depending on the nature of the samples to be immobilized (the probes) and the surface chemistry of choice (please see **Tables 1**, **2** for selected examples covered by this review). The binding of samples of interest (the targets) to the arrays is then assessed, typically using fluorescent detection systems that further enhance the sensitivity of the technique (**Figures 3**, **4**), although other methods have also been used for detection (**Figure 3** and **Table 1**).

This review gives different examples on the application of the microarray technology to explore bacterial surface glycans and their interactions with diverse glycan-binding proteins. Lectin and antibody microarrays have served to examine bacterial glycosignatures, facilitating bacteria identification and differentiation among strains, and to spot variations in glycan structures derived from changes in environmental conditions. In addition, they have been exploited for detection of bacteria in a diversity of samples, extending from sera to soils. Microarrays incorporating bacterial carbohydrate structures have proved to be useful for serodiagnosis of bacterial infections, identification of antigenic determinants for vaccine development, and mapping of epitopes recognized by bacteria-specific anti-carbohydrate antibodies. Moreover, they have served to identify bacterial ligands for lectins of the innate immune system and for bacterial

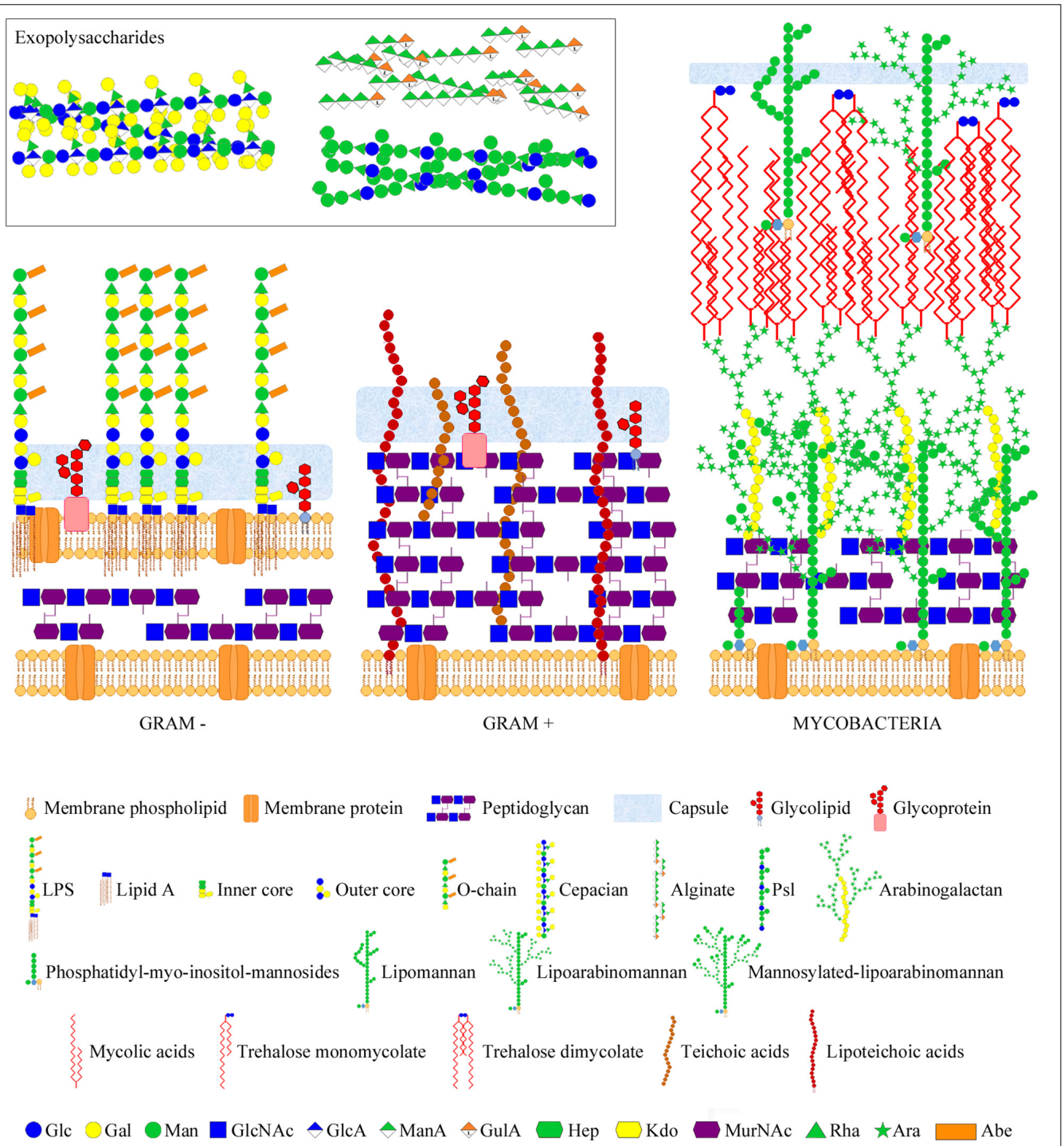

FIGURE 1 | Bacterial glycans and architecture of the cell wall of different bacterial groups. Gram-negative bacteria **(left part)** contain a thin peptidoglycan layer, sandwiched between two cell membranes, and display LPSs (composed of lipid A, inner and outer core, and O-chain) anchored to the outer membrane. Gram-positive bacteria **(middle part)** contain a thick peptidoglycan layer, covering the cell membrane, and usually display teichoic acids anchored to the membrane (lipoteichoic acids) or bound to the peptidoglycan. Gram-negative and -positive bacteria may also present cell surface glycolipids, glycoproteins, and a polysaccharide capsule. Moreover, they may also secret different polysaccharides (known as exopolysaccharides) into the external environment. Representative exopolysaccharide structures of cepacian (produced by *B. cepacia*), alginate, and Psl (produced by *P. aeruginosa*) are shown in the inset. Mycobacteria **(right part)** contain a large cell wall complex formed by peptidoglycan, arabinogalactan, and mycolic acids of the so-called mycomembrane, and display other distinctive glycan structures, such as lipomannan, lipoarabinomannan, phosphatidyl-myo-inositol-mannosides, and trehalose mycolates. Sugar residues are depicted using the Symbol Nomenclature for Glycans (SNFG) (Varki et al., 2015; Neelamegham et al., 2019).

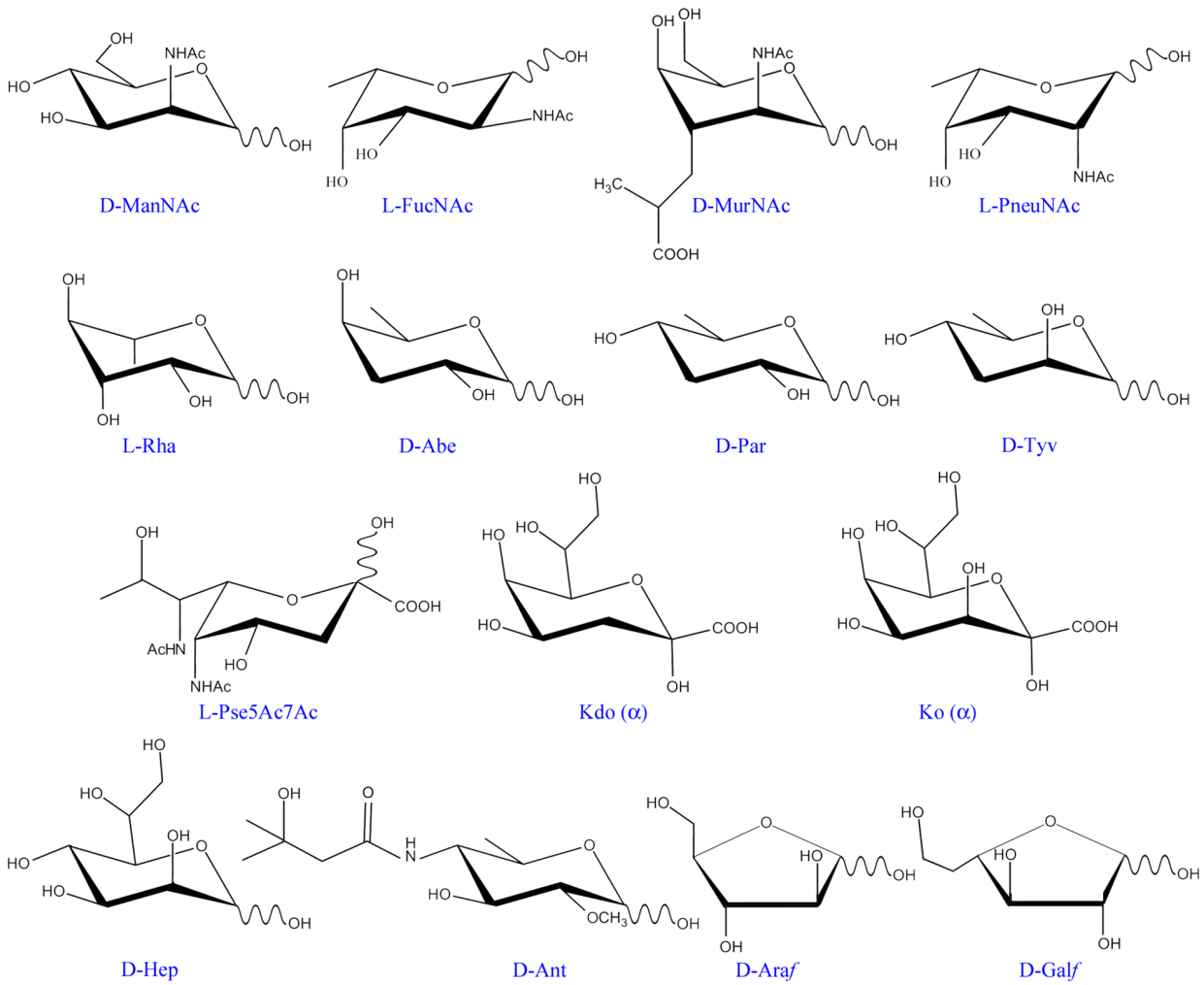

FIGURE 2 | Monosaccharide residues found in bacteria, but not in mammals. Only those monosaccharides mentioned in the text have been included. ManNAc, *N*-acetyl-mannosamine; FucNAc, *N*-acetyl-fucosamine; MurNAc, *N*-acetyl-muramic acid; PneuNAc; *N*-acetyl-pneumosamine; Rha, rhamnose; Abe, abequose; Par, paratose; Tyv, tyvelose; Pse5Ac7Ac, 5,7-di-*N*-acetyl pseudaminic acid; Kdo, 3-deoxy-D-manno-oct-2-ulosonic acid; Ko, D-glycero-D-talo-oct-2-ulosonic acid; Hep, L-glycero-D-mannoheptose; Ant, anthrose; Ara*f*, arabinofuranose; Gal*f*, galactofuranose.

and phagic proteins. Finally, microarrays of cell wall fragments and entire bacterial cells have been used to profile accessible carbohydrate structures on the bacterial surface, and to examine their interactions when they are displayed on the cell surface, thus preserving their natural arrangement, distribution, and density.

LECTIN MICROARRAYS FOR GLYCOPHENOTYPING OF BACTERIA

A diversity of lectin microarrays has been developed and applied to the analysis of the glycosylation profiles of different bacteria, also enabling differentiation among strains of a given bacterium, and to monitor variations in their glycosignatures associated with changes in culture conditions. These microarrays exploit the ability of lectins to selectively recognize specific carbohydrate structures on the bacterial surface. An example is the comparison of the binding patterns of *Escherichia coli* (laboratory strain DH5α), *Enterobacter cloacae*, *Staphyloccocus aureus* (Rosenbach), and *Bacillus subtilis* to an array of 16 lectins with various carbohydrate-binding specificities (Gao et al., 2010). A peculiarity of this study was the detection of bound bacteria using gold nanoparticles functionalized with *Griffonia simplicifolia* lectin II (GSL-II), which is specific for *N*-acetylglucosamine (GlcNAc, please see **Table 3** for detailed information on the binding specificities of model lectins mentioned in this review) and was shown to recognize the four bacteria, followed by silver deposition to enhance the resonance light scattering of the particles, finally used for quantitation (**Figure 3** and **Table 1**). Clearly different binding patterns were observed, with distinctive features for each bacterium. For example, whereas strong binding of *E. coli*, *E. cloacae*, and *B. subtilis* by the galactose (Gal)-specific agglutinins from *Ricinus communis* (RCA) and *Maackia amurensis* (MAA-I), and by the sialic acid-specific *M. amurensis*

TABLE 1 | Lectin and antibody microarrays used for glycophenotyping, differentiation, and detection of bacteria.

Printed probes	Slide surface chemistry[a]	Tested targets	Detection strategy	Detection technique	References
16 Lectins	Epoxy activated	*E. coli*, *E. cloacae*, *S. aureus*, *B. subtilis*	Lectin-conjugated gold nanoparticles followed by silver deposition	Resonance light scattering	Gao et al., 2010
15 Lectins	NHS activated polyacrylamide hydrogel coating	*S. aureus*	SYTO 60 labeling of bound bacteria	Fluorescence confocal microscopy	Liu et al., 2016
21/41 Lectins	NHS activated multi-component hydrogel coating	*E. coli* (4 strains)/*C. jejuni* (2 strains)	Bacteria labeled with SYTO 85/SYTOX Orange	Fluorescence scanning	Hsu et al., 2006 Kilcoyne et al., 2014
44 Lectins	Epoxysilane activated	*L. casei*, *L. paracasei* (16 strains)	Bacteria labeled with SYTOX Orange	Evanescent-field fluorescence scanning	Yasuda et al., 2011
8/15 Lectins + 2 Abs	Epoxy activated	*C. jejuni* LOS (3/8 strains)	LOS labeled with BODIPY	Fluorescence scanning	Semchenko et al., 2012a
ConA	ZnO nanorod arrays on fluorine-doped tin oxide glasses	*E. coli*	DAPI labeling of bound bacteria	Fluorescence microscopy	Zheng L. B. et al., 2017
3 Lectins + 3 sugars	Carbon nanotubes on gold electrodes	*E. coli* K12, *E. faecalis*, *S. mutans, S.* Typhi		Measurement of electronic resistance	Saucedo et al., 2018
Anti-*E. coli* O157:H7 Ab	Gold slides coated with biotin-labeled BSA + streptavidin (for printing of biotin-labeled Ab)	*E. coli* O157:H7	Fluorescein-labeled anti-*E. coli* O157:H7 Ab	Fluorescence microscopy	Gehring et al., 2006
6 Abs + 6 O-chain polysaccharides	Epoxy activated	*E. coli* (6 non-O157 STEC strains)	Alexa Fluor 555-labeled Abs	Fluorescence scanning	Hegde et al., 2013
7 Abs (pyrrole conjugates)	Gold-covered biochips (electrochemical arraying)	*E. coli* (15 STEC + 2 non-STEC strains)	Real-time monitoring of bacterial growth	SPR imaging	Mondani et al., 2016
35/66 Abs	Epoxy activated	*Salmonella enterica/ Streptococcus pneumoniae*	Bacteria labeled with Eosin Y/SYTO25	Fluorescence scanning	Cai et al., 2005 Marimon et al., 2010

[a] *Glass slides unless otherwise indicated; NHS, N-hydroxysuccinimide; SPR, surface plasmon resonance; Ab, antibody.*

lectin II (MAA-II) was observed, this was not the case for *S. aureus*, whose binding pattern was additionally characterized by the intensity of the signal for the fucose-specific *Aleuria aurantia* lectin (AAL). On the other hand, *B. subtilis* was distinguished by the binding signals for the lectins from *Erythrina cristagalli* (ECL) and, specially, *Datura stramonium* (DSL), while *E. coli* gave the strongest signal among the four bacteria tested for soybean agglutinin (SBA). Interestingly, signal intensities and binding patterns of *E. coli* and *S. aureus* appeared to change when these bacteria were grown in different culture media, suggesting variations in their surface glycans. An intriguing result of this study was the low signal observed for the binding of *S. aureus* by wheat germ agglutinin (WGA), particularly when compared with GSL-II as WGA also recognizes GlcNAc (see **Table 3**). Indeed, a later study of these authors using different procedures for lectin immobilization and detection of bacterial binding (specified in **Table 1**) showed comparable binding signals of the same *S. aureus* strain for WGA and GSL-II (Liu et al., 2016). This discrepancy could tentatively be explained by a different binding activity of printed WGA, possibly derived from the immobilization strategies employed, and draws attention to the importance of using appropriate internal controls of lectin activity.

Besides providing information on the glycosylation profiles of different bacteria, lectin microarrays can aid to differentiate strains of a given bacterium. This was first demonstrated by Hsu et al. (2006), who compared the lectin binding fingerprints of two closely related K12 *E. coli* strains (defective in O-chain synthesis) and of *E. coli* RS218, a neonatal meningitis pathogen. Using a panel of 21 lectins, whose binding activity was verified with fluorescently-labeled glycoprotein standards, clear differences in binding patterns and intensities were observed. In particular, the two K12-derived strains showed strong binding by GSL-II, WGA, and the α-*N*-acetylgalactosamine (α-GalNAc)-specific lectin from the snail *Helix pomatia* (HPA), but only one of them gave meaningful binding signals with four other lectins, suggesting the presence of different repertoires of surface glycan structures. This was even more evident for the pathogenic *E. coli* strain, which gave positive signals with 10 lectins of the panel. Since the invasiveness of *E. coli* RS218 was known to be growth dependent, the possibility that the lectin binding patterns could also change with growth was examined. A general decrease in the intensities of all the positive signals was observed when progressing from the lag phase to the stationary phase (Hsu et al., 2006), suggesting a possible correlation of glycosylation with invasion. Overall, the approach proved to be useful for distinguishing *E. coli* strains and monitoring dynamic alterations in the cell surface glycans.

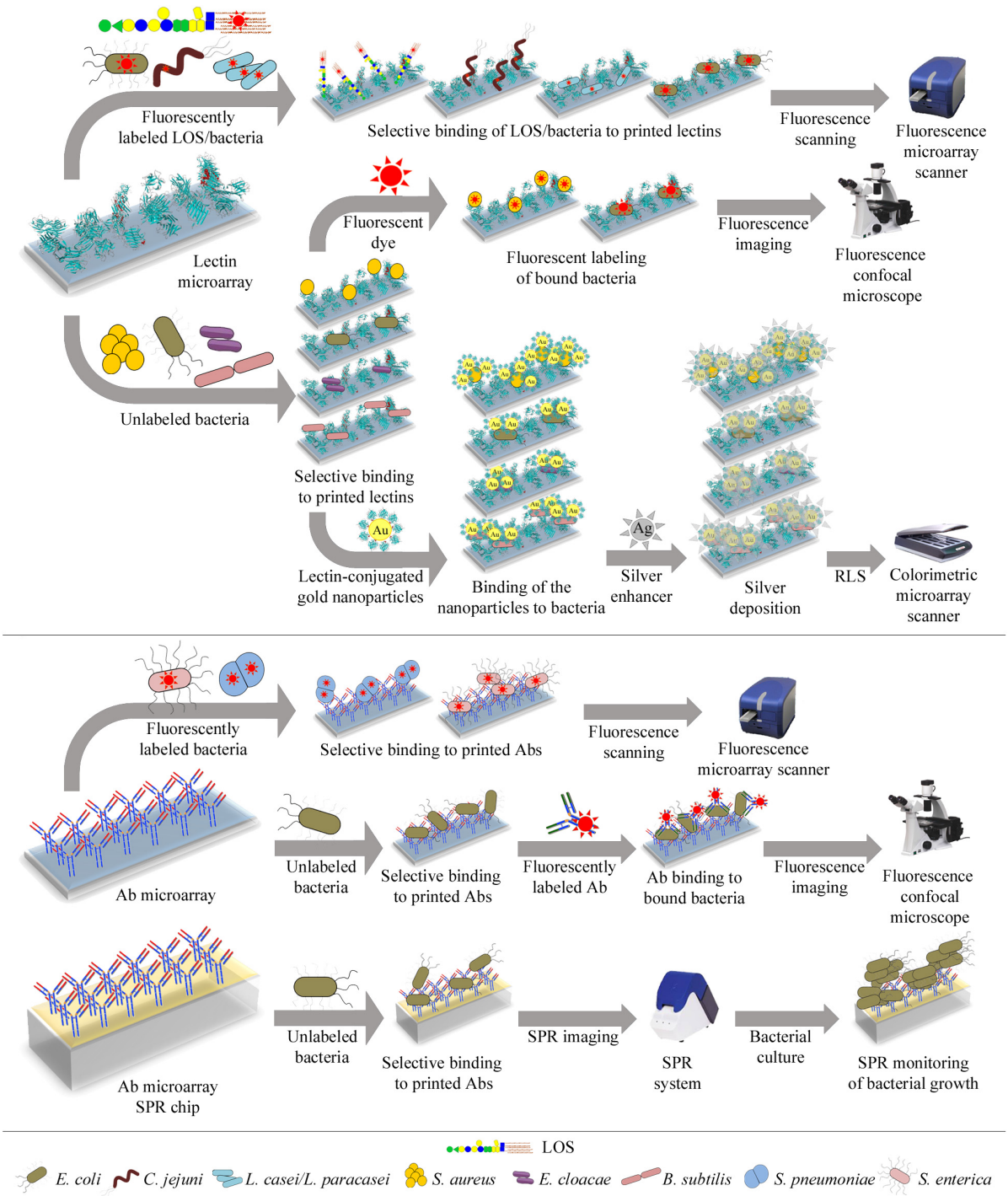

FIGURE 3 | Illustration of different lectin and antibody microarray approaches used for glycophenotyping, differentiation, and detection of bacteria. **Top panel**: Microarrays containing a collection of lectins with diverse carbohydrate-binding specificities can be incubated with fluorescently-labeled bacteria or LOS and bound targets directly quantified using a fluorescence microarray scanner **(upper row)**. Alternatively, the microarrays can be incubated with unlabeled bacteria and bound bacteria next labeled with a fluorescent dye, enabling detection by confocal microscopy **(middle row)**. Bound unlabeled bacteria can also be detected by incubation with gold nanoparticles conjugated to a lectin known to recognize the bacteria under study. The resonance light scattering (RLS) of the nanoparticles is then enhanced by deposition of silver and next measured using a colorimetric microarray scanner **(lower row)**. **Bottom panel**: Microarrays containing antibodies (Abs) raised against selected bacteria can be incubated with fluorescently-labeled bacteria and bound bacteria detected by fluorescence scanning **(upper row)**. The microarrays can also be incubated with unlabeled bacteria, followed by incubation with fluorescently-labeled anti-bacteria Abs, and bound Abs are next detected by confocal microscopy **(middle row)**. Finally, bacteria selectively bound by Abs arrayed on SPR (surface plasmon resonance) chips can be detected by monitoring their growth during on-chip culture, using SPR imaging **(lower row)**. Specific bacteria that have been tested using these different approaches are detailed in each case.

A similar approach was exploited to compare the lectin binding patterns of 16 *Lactobacillus casei/paracasei* strains indistinguishable from each other by 16S rRNA sequences (Yasuda et al., 2011). Using a panel of 44 lectins, a unique binding fingerprint was observed for 13 of these strains. Interestingly, half of the strains were bound by only one or two lectins, whereas the rest were recognized by multiple lectins with different carbohydrate-binding specificities, again pointing to a diversity of glycan structures. Thus, the assays enabled differentiation of strains, at the same time providing information on the carbohydrate determinants on the bacterial surface that are accessible for recognition.

Campylobacter jejuni is responsible for gastroenteritis in humans, while it is a commensal in chicken. A main difference between human and avian hosts is their core body temperature (37 and 42°C, respectively), what could be important for specific adaptation and ensuing pathogenesis or commensalism outcomes. In order to explore the effect of temperature on the surface glycans, two strains isolated from human hosts, the highly virulent *C. jejuni* 81-176 and the comparatively less invasive *C. jejuni* 81116, were cultured at 37 and 42°C and their lectin binding patterns were examined using a microarray comprising 41 lectins, whose binding activities were verified with fluorescently-labeled control glycoproteins (Kilcoyne et al., 2014). Distinctive hapten-inhibitable binding patterns for strains grown at 37°C were observed, being in general compatible with known structures of their surface glycans. For strain 81116 cultured at 42°C, an important decrease in the most intense binding signals was observed. These signals corresponded to lectins specific for Gal, lactose (Galβ(1-4)Glc), or GlcNAc, which are present in the LPS-like structure described in this strain, thus pointing to a decreased expression or alteration of this structure. In contrast, the changes in the lectin fingerprint of the virulent strain 81-176 grown at 42°C were more subtle, with only a subset of lectins showing small variations in binding intensity. This implied a relatively constant repertoire of glycan structures accessible for recognition. Based on the binding specificity of the lectins involved, these structures most probably include the capsular polysaccharide (CPS) and the LOS, which are known to play different roles in adhesion and invasion of epithelial cells as well as evasion of the immune system.

Campylobacter jejuni produces a variety of LOS structures that mimic mammalian gangliosides, what is thought to induce anti-ganglioside antibodies in the host and the subsequent development of neuropathies. A mixed lectin and antibody array was used to screen the LOS of *C. jejuni* strains for molecular mimicry (Semchenko et al., 2012a,b). First, a panel of 8 lectins, including cholera toxin subunit B (CTB), which binds ganglioside GM_1, together with two antibodies against gangliosides GM_1 and GM_2 as positive controls, were used to examine LOS preparations from strains 11168-O (known to mimic GM_1), 81-176 (GM_2 like), and 224 (unknown LOS type) (Semchenko et al., 2012b). Surprisingly, none of the LOS was bound by CTB, what could be due to a loss of lectin activity upon incorporation into the array, again stressing the importance of verifying the activity of printed lectins. The LOS from strain 11168-O gave strong binding signals for the Gal-specific agglutinins from *Arachis hypogaea* (PNA), *Viscum album* (VAA), and *Artocarpus integrifolia* (jacalin), in agreement with the presence of terminal Gal as found in GM_1, whereas a significantly lower binding by these lectins was observed for the LOS from strain 81-176, compatible with the absence of terminal Gal in its GM_2-like structure. In comparison, although the LOS from strain 224 was bound by the anti-GM_1 antibody, the binding signals for the Gal-specific lectins were equal to those observed for 81-176 rather than 11168-O. Using an extended array comprising 15 lectins, the binding patterns of the LOS from these three and five other uncharacterized *C. jejuni* strains were next examined (Semchenko et al., 2012a). Intriguingly, in this study no significant binding by VAA was observed for LOS 11168-O, indicating that, besides the procedure used for lectin printing, other factors, as, e.g., the activity of the specific lectin preparation employed, may affect the results. Based on the comparison of the antibody and lectin patterns of the uncharacterized LOSs with those of *C. jejuni* 11168-O- and 81-176-derived LOSs (with known GM_1- and GM_2-like structures, respectively), their terminal end structures were proposed. A parallel typing of LOS biosynthesis cluster, using a standard PCR method, revealed that the cluster type alone does not always allow prediction of the real LOS structure, highlighting the usefulness of the lectin microarray approach as complementary tool for evaluating the potential of clinical *C. jejuni* isolates to induce adverse autoimmune reactions.

The capture of bacteria by lectin arrays can also be exploited for detection of pathogenic bacteria in the clinical field as well as in the environmental or agri-food sectors. A ZnO nanorod array functionalized with concanavalin A (ConA), a mannose (Man)/glucose (Glc)-specific lectin from the legume *Canavalia ensiformis*, was employed for capturing *E. coli* (**Table 1**) and proved to work efficiently with reasonable detection limits and linear range (1.0×10^3 to 1.0×10^7 cfu mL^{-1}) even in complex samples, so it could be applied to the analysis of real samples (Zheng L. B. et al., 2017). More recently, a lectin and saccharide nano-chemiresistor array was used to detect *E. coli* K12, *Enterococcus faecalis, Streptococcus mutans,* and *Salmonella enterica* sv. Typhi (Saucedo et al., 2018). The array consisted in carbon nanotubes assembled on the surface of gold electrodes and functionalized with three lectins (ConA, PNA, and WGA) and three aminophenyl saccharides (Gal, Glc, and Man). After incubation with bacteria, changes in the electronic properties were monitored by measuring device resistance. *E. coli* and *S.* Typhi, both Gram-negative bacteria, gave noticeably different patterns, whereas for Gram-positive *E. faecalis* and *S. mutans* the patterns were more similar, although still clearly distinguishable. Detection was achieved at clinically relevant concentrations, indicating that an array with carefully chosen probes could be used as diagnostic tool.

ANTIBODY MICROARRAYS FOR DETECTION AND SEROTYPING OF BACTERIA

Bacterial surfaces display a variety of antigens that can be used for identification and typing of antigenically distinct strains.

Different microarrays incorporating O-antigen- or capsular-specific antibodies have been used to this aim. One example is the detection of Shiga-toxin producing *E. coli* (STEC), which is frequently identified as the pathogen responsible for food-illnesses and causes severe enteric infections such as diarrhea, hemorrhagic colitis, or even hemolytic uremic syndrome, a life-threatening complication. *E. coli* O157:H7 was the first enterohemorrhagic *E. coli* serotype detected in an outbreak in United States provoked by the consumption of contaminated burgers. The potential of antibody microarrays for detecting the bacterium was put forward by Gehring et al. (2006), who used a polyclonal anti-*E. coli* O157:H7 antibody printed onto microarray slides (**Table 1**) for capturing *E. coli* O157:H7 cells, in turn detected with fluorescently-labeled anti-*E. coli* O157:H7 antibody (sandwich fluorescent immunoassay, see **Figure 3**). A linear fluorescent response was observed from $\sim$3.0 $\times$ 10^6 to $\sim$9.0 $\times$ 10^7 cells/mL. A similar sandwich immunoassay was later used for identification of six other STEC serogroups, i.e., O26, O45, O103, O111, O121, and O145 (the top six non-O157 serogroups), which have been associated with 70–80% of non-O157 STEC-produced illnesses. Microarrays incorporating antibodies specific for one of these six O-antigens, along with the respective O-antigen polysaccharides as positive control, were tested for the binding of reference strains belonging to these serogroups and found to yield specific and reproducible signals at bacterial concentrations of 10^6 CFU/mL and above (Hegde et al., 2013). STEC can represent a serious threat to human health at very low contaminating levels (less than 100 CFU per sample), far below the limits of detection of this microarray approach and of other techniques commonly used. Consequently, a pre-enrichment step is always required. Several foods have been identified as potential sources of STEC, including tap water, but the main source and reservoir is beef. Indeed, a recent outbreak in United States has been associated with the consumption of ground beef contaminated with *E. coli* O103[1]. Therefore, the efficiency of the antibody microarray for serotyping contaminant non-O157 STEC in food was evaluated by testing ground beef samples enriched for 12 h after inoculation with 1–10 CFU of target serogroups, alone or in combination with one or two other serogroups (Hegde et al., 2013). All target groups were identified with no cross reactions, supporting the usefulness of the approach for the simultaneous detection of different STEC serogroups.

An antibody microarray approach for fast detection of O157 and the top six non-O157 STEC serogroups without the need of a pre-enrichment step was reported by Mondani et al. (2016). The approach was based on the on-chip culture of bacteria captured by the arrayed antibodies (**Figure 3**), and real-time monitoring of bacterial growth by surface plasmon resonance imaging (SPRi), a method previously found to be efficient for detecting *E. coli* O157:H7 at very low initial concentrations (Bouguelia et al., 2013; Mondani et al., 2014). Fifteen different strains belonging to the seven STEC serogroups, plus two non-STEC strains, were analyzed on SPR biochips presenting electrochemically arrayed antibodies against the target serogroups (**Table 1**). All STEC serogroups were successfully identified, even at initial concentrations in the range encountered in naturally contaminated samples (few CFU ml^{-1}), and no response was observed for the non-STEC strains. Moreover, *E. coli* O157:H7 was successfully detected in ground beef artificially contaminated with only few cells (5 CFU per 25 g). Thus, considering that detection of bacteria is carried out during enrichment, thereby reducing the processing time, the approach could be a faster alternative to other methods commonly used for detection of STEC in contaminated food.

Antibody microarrays have also proved to be useful for high-throughput serotyping of bacteria. As example, microarrays incorporating antisera against selected *Salmonella* O and H (flagellar proteins) antigens were efficient for serotyping *S. enterica* strains (Cai et al., 2005). Using 117 target strains, belonging to the top 20 commonly isolated and clinically relevant serotypes, and 73 non-target strains, this microarray approach successfully allowed one-step full or partial identification of 86 and 30 target strains, respectively, and exclusion of all non-target strains.

In the case of *Streptococcus pneumoniae,* the capsule is one of the major pathogenicity factors. Currently, 98 different serotypes, divided into 25 individual types and 21 serogroups, composed of two to eight serotypes with related capsular antigenic determinants that can be differentiated using factor (individual capsular antigen) antisera, have been identified. A microarray containing 66 different group-, type- and factor-specific antisera, with specificity for 83 of the 98 *S. pneumoniae* serotypes, was first tested with *S. pneumoniae* reference isolates of these 83 serotypes and found to correctly serotype 94% of the samples. Only 11 isolates within the same group were mistyped and for four samples a detectable signal was not obtained (Marimon et al., 2010). To test the utility of the microarray in clinical practice, 226 *S. pneumoniae* clinical isolates (106 invasive isolates and 120 randomly-selected non-invasive isolates) were next examined, in direct comparison to serotyping by latex agglutination followed by the Quellung reaction. Only for 7.1% of the isolates discrepant serotyping by the two methods was found. Moreover, for these isolates, PCR amplification of each capsular gene showed that only one isolate was misidentified by the microarray. Thus, the microarray approach proved to be an accurate serotyping technique and could be a valuable tool for pneumococcal epidemiological studies.

BACTERIAL GLYCAN ARRAYS FOR SERODIAGNOSIS OF BACTERIAL INFECTIONS

Exposure to bacterial antigens often induce the production of antibodies. A seminal study of Wang et al. (2002) demonstrated the usefulness of microbial glycan microarrays for detecting the presence in human serum of antibodies against several bacteria. An array incorporating a collection of carbohydrate-containing macromolecules, including 21 bacterial polysaccharides, was incubated with 1-µl human serum samples from normal individuals, and IgG and IgM antibodies captured in the

[1]https://www.cdc.gov/ecoli/2019/o103-04-19/index.html

TABLE 2 | Bacterial carbohydrate microarrays used for detection of bacteria-specific anti-carbohydrate antibodies and for recognition studies targeting diverse glycan binding proteins.

Printed probes	Immobilization strategy	Slide surface chemistry[a]	Tested targets	References
Synthetic structures of *C. difficile* CPS	Probes equipped with amino-linker	NHS activated	Human/mice sera, human feces[b], hybridoma supernatant	Oberli et al., 2011 Martin et al., 2013b Broecker et al., 2016a
Polysaccharides and synthetic structures of *S. pneumoniae* or carbapenem-resistant *K. pneumoniae* CPSs	Probes equipped with amino-linker	NHS activated	Human/mice/rabbit sera, mAbs	Geissner et al., 2016 Parameswarappa et al., 2016 Emmadi et al., 2017 Lisboa et al., 2017 Menova et al., 2018 Seeberger et al., 2017 Menova et al., 2018 Diago-Navarro et al., 2018
Synthetic structures of *M. tuberculosis* CPS arabinomannan	Probes coupled to BSA	Epoxy activated	Human/mice sera	Chen et al., 2016 Prados-Rosales et al., 2017
Library of bacterial CPSs	Direct adsorption of unmodified probes	Nitrocellulose	Human sera	Wang et al., 2002
S. enterica O-chains and synthetic substructures	Probes equipped with amino-linker	NHS activated	Rabbit *Salmonella* typing sera, human sera	Blixt et al., 2008
Library of LPS O-chains + core	Unmodified probes or equipped with amino-linker	NHS activated	Langerin, galectins 3, 4, 8, 9, Gp047	Feinberg et al., 2011 Stowell et al., 2014 Knirel et al., 2014 Javed et al., 2015
Library of synthetic LOS inner core structures	Probes equipped with amino-linker	Adipic acid dihydrazide-modified NHS activated	Human/mice sera, SP-D	Reinhardt et al., 2015 Reinhardt et al., 2016
Library of LPSs	Direct adsorption of unmodified probes	Nitrocellulose	Canine sera	Thirumalapura et al., 2005
Synthetic *M. tuberculosis* ManLAM or lipomannan structures	Probes equipped with thiol-linker	Maleimide-functionalized gamma amino propyl silane	Anti-ManLAM mAb, DC-SIGN	Chan et al., 2015 Leelayuwapan et al., 2017
Synthetic *C. difficile* LTA substructures	Probes equipped with amino-linker	NHS activated	Human sera, human feces[b]	Martin et al., 2013a Broecker et al., 2016b
Synthetic glycerol-based TA oligomers	Probes equipped with 2-aminobenzoic acid	Epoxy activated	Anti-*S. epidermidis* mAb, rabbit sera	van der Es et al., 2018
Synthetic peptidoglycan fragments	Probes equipped with amino-linker	Amorphous carbon with carboxylic acid surface	Peptidoglycan recognition protein PGRP-S	Wang et al., 2016
Natural and synthetic Nod factors, chitin oligosaccharides, and peptidoglycan-related compounds	Probes equipped with N-(2-aminoethyl)-4-(aminooxymethyl)benzamide linker	NHS activated	P60 autolysin, synthetic LysM domain	Maolanon et al., 2014 Sorensen et al., 2014
Library of glucan polysaccharide fragments	Neoglycolipids prepared by conjugation of probes to the aminolipids ADPH (reductive amination) or AOPE (oxime ligation)	Nitrocellulose	Anti-glucan mAbs, Dectin-1 DC-SIGN, DC-SIGNR, bacterial CBMs	Palma et al., 2006 Palma et al., 2015 Zhang et al., 2016 Li and Feizi, 2018
Cyclic β(1-2)-glucans	Probes embedded in a 3D matrix of a photoactive terpolymer	Nitrocellulose	DC-SIGN	Zhang et al., 2016
Synthetic fragments and derivatives of the tetrasaccharide of glycoprotein BclA from *B. anthracis* spores	Unmodified probes or equipped with thiol-linker	Photoactive phthalimide chromophores or maleimide-functionalized	Anti-*B. anthracis* spore Abs, anti-di/tetrasaccharide mAbs, cattle sera	Wang et al., 2007 Oberli et al., 2010 Tamborrini et al., 2011
Burkholderia pseudomallei CPS and LPS O-chain + core	Probes converted to glycosylamines by reductive amination	Epoxy activated	Human sera	Parthasarathy et al., 2006 Parthasarathy et al., 2008
Natural and synthetic *M. tuberculosis* polysaccharides	Unmodified probes or coupled to BSA	Epoxy activated	Human sera	Tong et al., 2005
M. tuberculosis lipid-linked glycans and polysaccharides	Unmodified probes	Nitrocellulose	Human ZG16p lectin	Hanashima et al., 2015

(Continued)

TABLE 2 | Continued

Printed probes	Immobilization strategy	Slide surface chemistry[a]	Tested targets	References
Library of synthetic *M. tuberculosis* representative structures	Probes equipped with amino-linker and coupled to BSA	Epoxy activated	DC-SIGN, DC-SIGNR, Dectin-2, langerin, MGR, mannose receptor, mincle	Zheng R. B. et al., 2017
Library of diverse synthetic bacterial structures	Probes equipped with amino- or thiol-linker	NHS/epoxy activated or maleimide-functionalized	MAbs, human sera, DC-SIGN, *B. cenocepacia* lectins A and C-Ct[c]	Geissner et al., 2019
Library of bacterial PSs, CPSs, and LPSs	Unmodified probes or equipped with amino-linker	NHS activated	Human sera, mice/rabbit Abs, galectins 3, 4, 8, langerin, intelectin-1	Stowell et al., 2014 Wesener et al., 2015 Hanske et al., 2017

[a]*Glass slides unless otherwise indicated;* [b]*Supernatant of human feces;* [c]*C-terminal domain of B. cenocepacia lectin C; NHS, N-hydroxysuccinimide; ADPH, N-aminoacetyl-N-(9-anthracenylmethyl)-1,2-dihexadecyl-sn-glycero-3-phosphoethanolamine; AOPE, 1,2-dihexadecyl-sn-glycero-3-phosphoethanolamine; MGR, macrophage galactose receptor; Ab, antibody.*

array were independently detected using the respective anti-human IgG/IgM secondary antibodies (see **Figure 4** for a schematic representation of different strategies used for fluorescent detection of target binding to bacterial carbohydrate microarrays). IgM binding to pneumococcus type 27 and different *Klebsiella* polysaccharides was spotted, and the repertoire of bacterial polysaccharides recognized by IgG antibodies was broader, also including *E. coli* types K92 and K100, group B meningococcus, *Haemophilus influenzae* type A, and 5 different pneumococcus types. These results questioned the traditional belief that naturally occurring anti-polysaccharide antibodies were mainly of IgM type, and demonstrated that the proposed system was efficient for detecting specific antibodies in human serum. Moreover, a microarray containing a panel of nine LPS preparations isolated from different bacteria, including *Francisella tularensis*, was later found to be efficient for detecting anti-*F. tularensis* LPS antibodies in tularemia-positive canine serum samples (Thirumalapura et al., 2005), while more focused arrays containing capsular and O-antigen saccharides from different strains of *Burkholderia mallei* and/or *Burkholderia pseudomallei* successfully detected specific antibodies in the serum of human patients infected with these bacteria (Parthasarathy et al., 2006, 2008). Altogether, these studies revealed the potential of bacterial glycan microarrays for the serological diagnosis of bacterial infections.

Different types of bacterial glycans have been included in the arrays (**Table 2**), essentially depending on the specific bacterium under study. For example, several *Salmonella* serogroups are characterized by displaying O-antigens containing 3,6-dideoxy-D-ribo- (paratose, abbreviated Par, serogroup A), -D-xylo- (abequose, abbreviated Abe, serogroup B), or -D-arabino- (tyvelose, abbreviated Tyv, serogroup D) hexose residues (**Figure 2**), α(1-3)-linked to a common Manα(1-4)Rhaα(1-3)Gal main chain (Rha standing for rhamnose). A microarray including synthetic di-, tri-, and tetrasaccharide glycosides based on these regions was tested with group-specific anti-*Salmonella* rabbit sera, showing a rather selective IgG binding to the respective O-antigens (Blixt et al., 2008). Based on the high specificity observed for the disaccharides Tyvα(1-3)Manα, Parα(1-3)Manα, and Abeα(1-3)Manα, their ability to detect *Salmonella*-specific antibodies in the serum of patients infected with *S. enterica* sv. Enteritidis (serogroup D) or *S. enterica* sv. Typhimurium (serogroup B) was examined in comparison to healthy controls. The first group of patients showed significantly elevated levels of antibodies against Tyvα(1-3)Manα, whereas the second group showed high reactivity toward Abeα(1-3)Manα, in both groups Parα(1-3)Manα giving only background signals. Therefore, O-antigen specific microarrays could be a suitable tool for serodiagnosis of *Salmonella* infections.

Mycobacteria display surface glycoconjugates very different from those of most other bacteria (**Figure 1** right part). Tong et al. (2005) developed a multiplexed assay for serodiagnosis of tuberculosis based on a microarray containing 54 antigens of different classes, i.e., fractions of *Mycobacterium tuberculosis* cells and culture fluid, oligosaccharides conjugated to bovine serum albumin (BSA), purified LPSs and polysaccharides, and recombinant antigens. The goal was to identify antigens, or combinations thereof, allowing discrimination between culture-positive pulmonary tuberculosis patients, culture-negative patients with other pulmonary diseases, and healthy individuals. The authors found that a BSA conjugate containing the branched structure Araβ(1-2)Araα(1-3)[Araβ(1-2)Araα(1-5)]Araα(1-5)Ara of the cell wall glycolipid lipoarabinomannan (LAM, **Figure 5**), on its own, discriminated with good specificity and sensitivity between tuberculosis and non-tuberculosis sera, pointing out the applicability of LAM in serological tests.

BACTERIAL GLYCAN ARRAYS FOR IDENTIFICATION OF NOVEL VACCINE CANDIDATES

Development of efficient vaccines to prevent bacterial infections can be facilitated by microarray-assisted identification of bacterial structures inducing an immune response and analysis of the specific epitopes recognized by vaccine-elicited protective antibodies. In tuberculosis patients, for example, antibody responses to LAM and to the related capsular polysaccharide arabinomannan (AM) correlate strongly, suggesting that AM is the immunogenic portion of LAM. A microarray containing a panel of 12 synthetic AM fragments, coupled to BSA, was used to assess the reactivity of IgG antibodies in the sera of 30 healthy

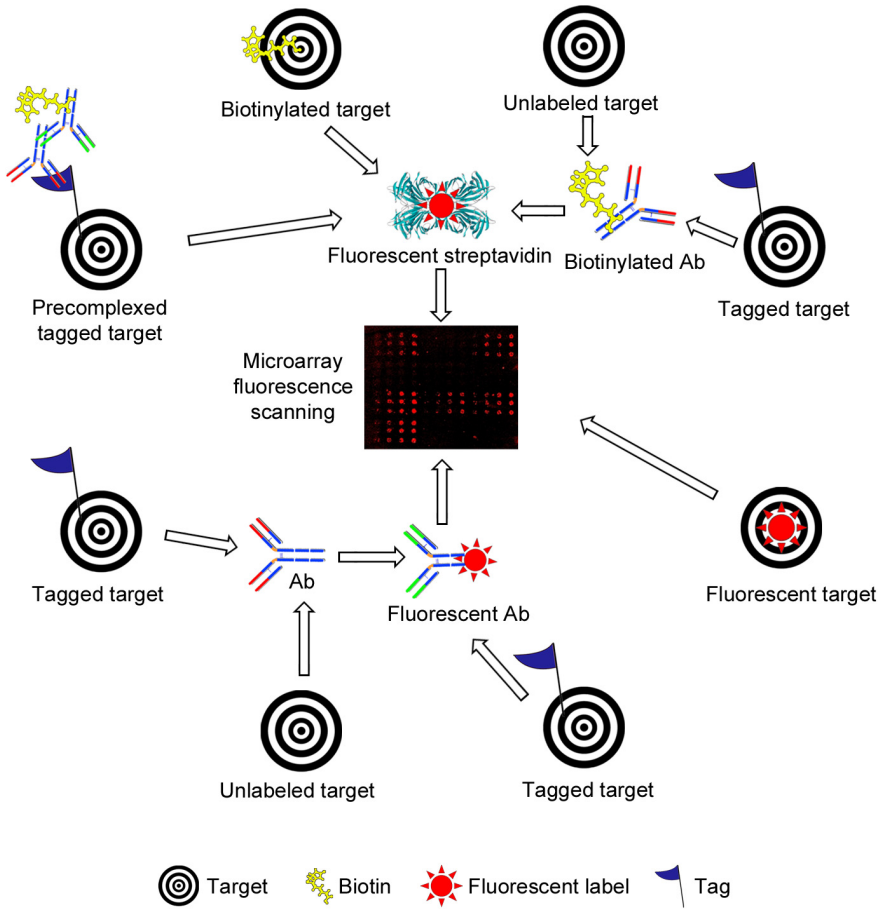

FIGURE 4 | Schematic representation of different strategies used for fluorescence-based detection of lectin and antibody (Ab) binding to bacterial carbohydrate and whole cell microarrays. The simplest setup involves incubation with a fluorescently labeled target **(lower right side)**. A common strategy is the use of biotinylated targets, which are next detected by incubation with fluorescently labeled streptavidin **(upper part)**. The targets may carry other tags (e.g., His- or Fc-tags), and detection then has involved the use of biotinylated or unlabeled Abs, followed by incubation with streptavidin or with a biotinylated secondary Ab, as appropriate. Pre-complexing tagged targets with primary and secondary Abs has been exploited to reduce the number of incubation steps and/or to increase the sensitivity of detection. Alternatively, tagged targets have been detected by incubation with a fluorescent or unlabeled Ab, the latter followed by incubation with a fluorescent secondary Ab **(lower part)**. Finally, the binding of unlabeled targets has been monitored using biotinylated or unlabeled primary Abs followed by fluorescently labeled streptavidin or secondary Abs. In all cases, the final step involves the scanning of fluorescence signals.

M. tuberculosis-uninfected adults before and after primary or secondary vaccination with the licensed bacillus Calmette-Guerin (BCG) vaccine (Chen et al., 2016). In both vaccination groups, sera obtained 4 and 8 weeks after vaccination had significantly higher levels of AM-specific IgGs, although heterogeneous binding patterns to the microarray-printed AM fragments were observed. Interestingly, increased IgG titers correlated with enhanced BCG phagocytosis, particularly with IgG reactivity to three particular AM epitopes that contained at least two Man residues. Overall, the results suggested that AM-specific IgGs contribute to the defense against mycobacterial infection in humans. Moreover, immunization with AM-protein conjugates was also found to contribute to protection against infection (Prados-Rosales et al., 2017). In detail, immunization of mice with a 20 kDa AM fraction conjugated to *M. tuberculosis* Ag85b or to protective antigen from *B. anthracis* resulted in elevated levels of AM-specific antibodies able to stain *M. tuberculosis* cells, as observed by electron microscopy. To gain insight into the AM epitopes recognized by the antibodies, the binding of immune sera to a microarray including 30 BSA-conjugated synthetic AM fragments (representative of the mannan backbone, branched arabinan, and terminal Man residues) was examined. Binding to a diversity of fragments was observed, the most prevalent being linear or branched arabinan structures. Importantly, immunized mice next infected with the bacterium had lower bacterial loads in lungs and spleen and lived longer than control mice, with a marked reduction in mycobacterial dissemination. Thus, the humoral arabinan-targeted response elicited by the AM-protein conjugates can importantly contribute to the outcome of mycobacterial infection, suggesting that AM could be a good candidate for developing new vaccines against *M. tuberculosis*.

The glycan chain of the *B. anthracis* exosporium glycoprotein BclA, which decorates the surface of *B. anthracis* spores, also

contains a unique tetrasaccharide structure consisting of 2-*O*-methyl-4-(3-hydroxy-3-methylbutamido)-4,6-dideoxy-Glc (termed anthrose and abbreviated Ant, **Figure 2**) β(1-3)-linked to Rhaα(1-3)Rhaα(1-2)Rha. A microarray including synthetic fragments and derivatives of this tetrasaccharide was examined for the binding of pooled rabbit polyclonal anti-anthrax spore IgG antibodies, revealing the presence of antibodies binding to anthrose-containing tri- and tetrasaccharides (Wang et al., 2007). Thus, the glycan chain of BclA appeared to be immunogenic and could be employed to develop novel vaccines targeting anthrax spores. In fact, mice immunization with the tetrasaccharide or with Antβ(1-3)Rha was later proved to elicit an antibody response, enabling the generation of monoclonal IgGs (Oberli et al., 2010). The binding specificity of several anti-tetrasaccharide and anti-disaccharide monoclonal antibodies (mAbs) was examined by microarray screening using a series of synthetic mono- to tetrasaccharides equipped with different anthrose side chain appendages. The anti-disaccharide mAbs recognized all the structures with intact anthrose, including anthrose monosaccharides, whereas the anti-tetrasaccharide mAbs required at least two Rha units as well as the terminal anthrose for tight binding. Although small modifications of the anthrose side chain only significantly affected anti-tetrasaccharide mAb binding, a drastic chain truncation abolished binding for all mAbs. Altogether, the results demonstrated that anthrose is the primary recognition unit. Interestingly, an anthrose-deficient *B. anthracis* lineage was identified in cattle from West Africa (Tamborrini et al., 2011), where anthrax is highly endemic and the majority of vaccines for cattle are based on live spores from an anthrose-positive strain. Thus, the spread of anthrose-deficient strains in this region could be an escape strategy of *B. anthracis*.

Microarrays containing synthetic structures based on TAs have also proved to be efficient for detecting anti-TA antibodies in serum (**Table 2**). A library of compounds comprising the most common glycerol phosphate backbone with 15 monomers in length, decorated by α-Glc, α-GlcN (glucosamine) or α-GlcNAc residues at various positions of the main chain (**Figure 5**), was interrogated for the binding of a mouse anti-*Staphylococcus epidermidis* mAb, serum obtained from rabbits immunized with *E. faecalis* LTA, and rabbit serum raised against a BSA-TA conjugate (van der Es et al., 2018). Clearly different IgG/IgM binding patterns were observed, unveiling selective recognition of specific TA epitopes and posing that TA-based vaccination strategies could be possible. Indeed, the potential of LTA glycans as vaccine candidates to protect from *Clostridium difficile* infections was previously proposed. This bacterium contains an unusual LTA phosphodiester-linked repeating unit with the sequence -6)GlcNAcα(1-3)[P6]-GlcNAcα(1-2)GroA (GroA being glyceric acid) (**Figure 5**). A microarray-printed synthetic dimer of this repeating unit was used to assess the binding of IgG antibodies in the serum of *C. difficile*-infected patients, unveiling recognition in six out of 12 tested samples and thereby suggesting that this epitope could be a relevant *C. difficile* antigen (Martin et al., 2013a). In a later study (Broecker et al., 2016b), a conjugate of the dimer and the carrier protein CRM_{197}, a constituent of licensed vaccines, was used to immunize mice, and antibody responses in serum were followed using microarrays containing the dimer as well as monomers of the repeating unit with one or two phosphorylated GlcNAc residues. The results revealed that the conjugate elicited anti-LTA antibodies for which the minimal epitope for recognition was the repeating unit. Importantly, sera of immunized mice significantly opsonized all *C. difficile* strains and clinical isolates investigated. Moreover, colonization by *C. difficile* in immunized mice orally challenged with live bacteria was reduced compared with control mice. Thus, *C. difficile* LTA glycans emerged as potential vaccine candidates.

Two different *C. difficile* CPSs, named PS-I and PS-II, were also found to be antigenic and immunogenic. Both CPSs are present in a hypervirulent *C. difficile* strain responsible for outbreaks in North America and Europe. PS-I has a branched pentaglycosyl phosphate repeating unit [-4)Rhaα(1-3)Glcβ(1-4)[Rhaα(1-3)]Glcα(1-2)Glcα(1-P], while PS-II has a branched hexaglycosyl phosphate repeating unit [-6)Glcβ(1-3)GalNAcβ(1-4)Glcα(1-4)[Glcβ(1-]GalNAcβ(1-3)Manα(1-P] (**Figure 5**) (Ganeshapillai et al., 2008). First, the non-phosphorylated PS-II hexasaccharide was synthesized, conjugated to CRM_{197}, and used to immunize mice (Oberli et al., 2011). Binding assays to the microarray-printed hexasaccharide showed the presence of specific IgG antibodies in the serum of immunized mice, indicating that the hexasaccharide was immunogenic. Moreover, specific IgA antibodies were detected in the feces of patients with *C. difficile* infection (Oberli et al., 2011; Martin et al., 2013b), suggesting that PS-II could be an antigenic determinant in humans. The non-phosphorylated PS-I pentasaccharide, together with mono-, di-, and tri-saccharide substructures thereof, were also synthesized and used for microarray screening of specific IgAs in feces and IgGs in serum of *C. difficile*-infected patients, in comparison to other patients and healthy controls. Variable antibody levels were detected in all groups, indicating that these structures represent biologically relevant epitopes. The main antigenic determinant of the pentasaccharide was explored by examining the binding to the arrays of sera of mice immunized with a PS-I pentasaccharide-CRM_{197} conjugate and of mAbs generated from such sera using the hybridoma technique (Broecker et al., 2016a), revealing that the disaccharide Rhaα(1-3)Glc, which is found twice in the pentasaccharide, is a minimal size epitope. Therefore, a simple disaccharide could be a valid target for developing novel vaccination approaches against *C. difficile*. Compared to the disaccharide, a construct displaying five disaccharide units showed noticeably tighter binding (about five orders of magnitude) to the mAbs and elicited in mice an IgG response more specific for larger glycans (Broecker et al., 2016a), thus limiting cross-reaction with structurally related glycans.

The antigenic CPS determinants of different *S. pneumoniae* serotypes were also investigated using a similar strategy, i.e., synthesis of the repeating unit and substructures thereof, construction of microarrays incorporating these synthetic structures, and screening of relevant sera for detection of recognized structures, often complemented with immunization of mice or rabbits with CRM_{197}-conjugates of selected structures and subsequent microarray-assisted evaluation of serum antibodies and mAbs. Clearly distinct determinants were

identified in each case. Thus, in serotype 2 the GlcAα(1-6)Glcα(1-2) branch (GlcA being glucuronic acid) was found to be an important substructure of the hexasaccharide repeating unit (Emmadi et al., 2017), while in serotype 7F the two side chains that decorate the linear tetrasaccharide backbone, i.e., Galβ(1- and GlcNAcα(1-2)Rhaα(1-, played a key role (Menova et al., 2018). Gal modification with a pyruvate ketal in the linear tetrasaccharide unit of serotype 4 was observed to be an important determinant, although pyruvate-independent epitopes were also unveiled (Geissner et al., 2016), whereas in the serotype 5 pentasaccharide unit the rare aminosugar *N*-acetyl-L-pneumosamine (PneuNAc, **Figure 2**) together with branched *N*-acetyl-L-fucosamine (FucNAc) were essential for antibody recognition and avidity (Lisboa et al., 2017). These findings could be of relevance for designing efficient synthetic glycoconjugate vaccines against *S. pneumoniae*.

In contrast to the above listed serotypes containing tetra- to hexasaccharide units, the repeating unit of *S. pneumoniae* serotype 3 CPS consists only of a disaccharide. Therefore, in this case, besides the respective disaccharide and monosaccharide units, one tetrasaccharide (comprising two repeating units) and two different trisaccharides with shifted sequences were synthesized and used in the microarray screening of two mAbs raised against serotype 3 CPS (Parameswarappa et al., 2016).

FIGURE 5 | Selected examples of representative structures printed in bacterial carbohydrate microarrays. The repeating unit of *Enterococcus faecalis* LTA is shown as representative of a glycerol phosphate LTA backbone. Bacterial β(1-2)-linked cyclic glucans can occur in unsubstituted form or substituted at Glc C6 with anionic groups (e.g., succinyl in *B. abortus*). The structure shown for NTHi LOS corresponds to the major glycoform of strain 375. Because of space limitations, the structure of the O-chain of *K. pneumoniae* LPS is shown below the structure of the LPS core. Unless specifically indicated, sugar units are D-stereoisomers in pyranoside form. Sugars in furanoside form are labeled with the *f* suffix. GroA, glyceric acid; Gro, glycerol; GalA, galacturonic acid; P, phosphate; PEtN, phosphoethanolamine; OAc, *O*-acetyl; PCho, phosphorylcholine.

The results showed that the tetrasaccharide was bound better than the smaller structures. Moreover, a tetrasaccharide-CRM_{197} conjugate was found to elicit opsonophagocytic antibodies in mice and confer protection against serotype 3 in a model of pneumococcal pneumonia (Parameswarappa et al., 2016), thus validating the usefulness of the approach.

The CPS of carbapenem-resistant *Klebsiella pneumoniae* has also been explored for their antigenic potential using a similar strategy. A CRM_{197}-conjugate of the hexasaccharide repeating unit proved to be immunogenic in mice and rabbits, and elicited antibodies able to promote phagocytosis of the bacterium (Seeberger et al., 2017). CPSs have also been used to develop vaccines against different invasive serogroups of *Neisseria meningitidis*. However, in the case of meningococcal serogroup B, vaccines based on non-capsular antigens are needed because its capsule consists of autoantigenic α(2-8)-linked polysialic acid. As an alternative, the antigenic potential of the inner core structure of *N. meningitidis* LOS (**Figure 5**) was examined (Reinhardt et al., 2015). A library of species-specific mono- to tetrasaccharide structures was synthesized and used for microarray-assisted screening of human sera. Strong IgG binding to the tetrasaccharide GlcNAcα(1-2)Hepα(1-3)Hepα(1-5)Kdoα (Hep denoting L-glycero-D-mannoheptose, and Kdo denoting 3-deoxy-D-manno-oct-2-ulosonic acid), which is the conserved LPS inner core structure of all *N. meningitidis* immunotypes, and to the related trisaccharide lacking Kdo was observed, while binding to Hepα(1-3)Hepα(1-5)Kdoα was only weak, revealing the importance of the distal GlcNAc for recognition. Immunization of mice with a tetrasaccharide-CRM_{197} conjugate elicited an antibody response against the tetrasaccharide. Of note, mice serum antibodies bound to cells of a broad collection of *N. meningitidis* strains, and the binding to a LPS-free mutant was significantly lower, demonstrating the accessibility of the LPS inner core on the cell surface. Interestingly, epitope mapping using the microarray-printed library of synthetic structures revealed that, unlike human serum antibodies, Kdo was the immuno-dominant residue for the mice antibodies. A possible explanation posed by the authors is the presence in mouse germline antibodies of an inherited binding pocket specific for Kdo. In that case, mice might not be the best model to evaluate the synthetic Kdo-containing tetrasaccharide as potential vaccine candidate. Moreover, it is likely that in this structure the Kdo residue is much more exposed than in *N. meningitidis* cells, shed membrane vesicles, or fragments from opsonized bacteria that predictably elicited the antibodies detected in human serum.

BACTERIAL GLYCAN ARRAYS FOR TESTING ANTIBODIES WITH DIAGNOSTIC OR THERAPEUTIC POTENTIAL

Besides aiding in the identification of vaccine candidates, bacterial glycan microarrays have helped to dissect the binding specificities of mAbs obtained for diagnostic or therapeutic purposes. An example is the antibody-based detection of tuberculosis biomarkers, which can form the basis of an inexpensive point-of-care diagnostic test. A suitable biomarker is the Man-capped form of LAM that is found in the blood, sputum, and urine of the patients. A high affinity recombinant antibody found to interact only with array-printed synthetic carbohydrates containing linear α(1-2)Man linkages, as present in LAM caps, was shown to bind pathogenic mycobacterial species and demonstrated improved sensitivity in the detection of tuberculosis over standard diagnostic methodologies, particularly when urine and serum clinical specimens were tested combinedly (Chan et al., 2015).

On the other hand, immunotherapy using antibodies targeting bacterial surface polysaccharides could be a valuable alternative for fighting infections produced by antibiotic-resistant bacteria, such as carbapenem-resistant *K. pneumoniae*. Two mAbs displaying distinct binding patterns to a microarray containing its CPS repeating unit and fragments thereof were found to be protective against the most virulent clinical strains of this bacterium, promoting their killing and preventing the spread of infection in a murine model (Diago-Navarro et al., 2018). Thus, they can be considered candidates for an antibody-based approach to treat patients infected with carbapenem-resistant *K. pneumoniae*, for which therapeutic options are scarce.

BACTERIAL GLYCAN ARRAYS FOR IDENTIFICATION OF LIGANDS FOR LECTINS OF THE INNATE IMMUNE SYSTEM

While the antibody-mediated (acquired) immune response requires time to develop after an antigenic challenge, the innate immune response is immediate and it does not require previous exposure to the pathogen, thus being the first line of defense against infection. A variety of lectins that recognize specific glycans on pathogens' surfaces make an important contribution to innate immune protection. The use of microarrays incorporating bacterial glycan structures has greatly facilitated the identification of ligands and dissection of glycotopes recognized by these lectins (see **Figure 6** for schematic representation of lectins of the innate immune system cited in this review).

The value of the approach was demonstrated in a study by Palma et al. (2006) on the assignment of carbohydrate-binding specificity for Dectin-1, the major receptor of the innate immune system on leucocytes against fungal pathogens. The binding of Dectin-1 to a microarray containing 187 neoglycolipids, prepared by reductive amination from selected fractions of *Saccharomyces cerevisiae*, *Alcaligenes faecalis* and *Umbilicaria papulosa* glucan polysaccharides, and from other diverse glycans including many mammalian type glycans, was examined. Remarkably, exclusive binding of Dectin-1 to 10-mer or longer β(1-3)-linked gluco-oligosaccharides, as present in *A. faecalis* glucan curdlan, was detected. This strict requirement of long β(1-3)-linked chains for binding was confirmed in a later study, in which a total of 153 gluco-oligosaccharide neoglycolipids from plant, fungal, and

bacterial glucan polysaccharides were prepared by oxime-ligation (Palma et al., 2015). In contrast, the innate immune receptor DC-SIGN (dendritic cell-specific ICAM-3-grabbing nonintegrin) exhibited a broad binding profile, which included recognition of linear β(1-2)-gluco-oligosaccharides derived from the cyclic β(1-2)-glucan of *Brucella abortus* (Palma et al., 2015). Using a focused (1-2)-glucan array, binding of the closely related endothelial cell receptor DC-SIGNR (also named L-SIGN) and of serum mannose-binding protein to linear α and β(1-2)-gluco-oligosaccharides was also observed, although showing distinct lectin-specific binding patterns and differing influence of linkage configuration and chain length (Zhang et al., 2016). Moreover, DC-SIGN was found to recognize intact forms of cyclic *B. abortus* β(1-2)-glucan (**Figure 5**) printed on microarrays using an appropriate immobilization strategy (**Table 2**). Of note, linear and circular β(1-2)-linked glucans are produced and secreted by different Proteobacteria and are thought to be involved in biofilm formation, interactions with the host, and modulation of immune cells activities. Overall, these studies evidenced that although these four C-type (Ca^{2+}-dependent) lectins of the innate immune system, i.e., Dectin-1, DC-SIGN, DC-SIGNR, and mannose-binding protein, recognize glucans, their fine binding specificities are noticeably different.

Analogous observations were made when the binding patterns of several membrane C-type lectin receptors to an array of mycobacterial glycans were compared. As mentioned above, mycobacteria display unusual surface glycoconjugates. In addition to AM and LAM, they comprise phosphatidyl-myo-inositol mannosides, phenolic glycolipids, glycopeptidolipids, trehalose mycolates, trehalose-containing LOSs, and capsular α-glucans (**Figure 1**, right part). An array containing 60 chemically synthesized glycans, representing all these classes of mycobacterial structures, was screened with a panel of seven human C-type lectins as well as with bovine mincle (Zheng R. B. et al., 2017), all of them found on the surface of macrophages and/or dendritic cells. No ligands were identified for the macrophage galactose receptor, consistent with its specificity for GalNAc, which was absent from the array. Appropriate ligands were neither present for blood dendritic cell antigen 2 (BDCA-2). Although in this case the primary binding site does bind Man, additional contacts with a Gal residue at a secondary site are known to be required for high-affinity binding. In contrast, DC-SIGN strongly bound to LAM cap structures containing Man residues without a clear preference for particular types of glycans, and it was apparently able to bind internal Man residues. Binding of DC-SIGN to several LAM core structures, possibly inaccessible in the cell wall, and to a phosphatidyl-myo-inositol derivative with terminal Manα(1-2)Man was also detected. Interestingly, a different study revealed binding to array-printed mycobacterial phosphatidylinositol mono- and di-mannosides of the human soluble lectin ZG16p (Hanashima et al., 2015), putting forward a possible involvement of this lectin in the gastrointestinal immune system. The mannose receptor, present on macrophages and sinusoidal endothelial cells, was found to recognize several LAM cap and core structures (Zheng R. B. et al., 2017). However, its binding pattern clearly differed from that of DC-SIGN, as the presence of terminal Man residues was a main factor for recognition. Indeed, the mannose receptor bound to several glycans bearing a single terminal Man, including a phenolic glycolipid. Three other Man-specific lectins, DC-SIGNR, Dectin-2 (from macrophages and dendritic cells), and langerin (present on Langerhans cells), also showed preferential binding to ligands containing exposed Man, although distinctive recognition patterns were visible (Zheng R. B. et al., 2017). For example, langerin bound ligands bearing single terminal Man residues, in addition to more complex LAM structures, whereas Dectin-2 and DC-SIGNR showed a more restricted binding profile, with predominant recognition of Manα(1-2)Man-containing structures. In striking contrast, bovine mincle, found in macrophages and other antigen-presenting cells, bound to a distinct set of mycobacterial glycans containing trehalose (Glcα(1-1)αGlc), independently on variations in substituents, including additions to the 4- or 6-hydroxyl groups of one of the Glc residues. Thus, there was a clear non-overlap between mycobacterial ligands for mincle and for the other Man-specific receptors tested, which also showed distinctive binding preferences.

In a different study, DC-SIGN was also found to interact with the α(1-6)-mannan backbone of lipomannan, another important glycolipid of the *M. tuberculosis* cell wall (**Figure 1**, right part). Comparison of DC-SIGN binding to array-printed mannans containing 7, 13, and 19 α(1-6)-linked Man units revealed a clear preference for the longer chains (Leelayuwapan et al., 2017), again indicating that this receptor is able to bind internal Man residues. Moreover, binding of DC-SIGN to other microbial glycans was recently observed using a microarray containing 120 synthetic bacterial structures out of over 300 structures (Geissner et al., 2019). In addition to a *M. tuberculosis* AM hexasaccharide displaying terminal Man, DC-SIGN was found to recognize *N*-acetyl-mannosamine (ManNAc)-terminating oligosaccharides based on the CPS of *S. pneumoniae* serotypes 4 and 9. Furthermore, binding to several structures with terminal Hep, based on the LPS inner core of *H. influenzae*, *N. meningitidis, Proteus* sp., and *Yersinia pestis*, was also detected, with α(1-2)- (*H. influenzae,* **Figure 5**) and α(1-3)- (*N. meningitidis* and *Proteus*) linked Hep being more efficiently bound than α(1-7)-linked Hep (*Y. pestis*). These results further highlighted the plasticity of DC-SIGN's binding site for accommodating Man-related structures, even bearing substituents at positions 2 (as in ManNAc) or 6 (as in Hep), thereby allowing this receptor to recognize a broad range of microbial ligands.

The ability of human langerin to recognize bacterial glycans different from those displayed by mycobacteria was explored using a microarray containing a collection of 48 bacterial polysaccharides obtained by mild acid hydrolysis of diverse LPSs (O-chain and core) (Feinberg et al., 2011). Langerin bound to *E. coli* and *Shigella boydii* polysaccharides containing Manα(1-2)Man units, indicating that this is an important glycotope for langerin recognition. However, binding to these structures was not detected in a later study using an extended microarray, comprising over 300 bacterial

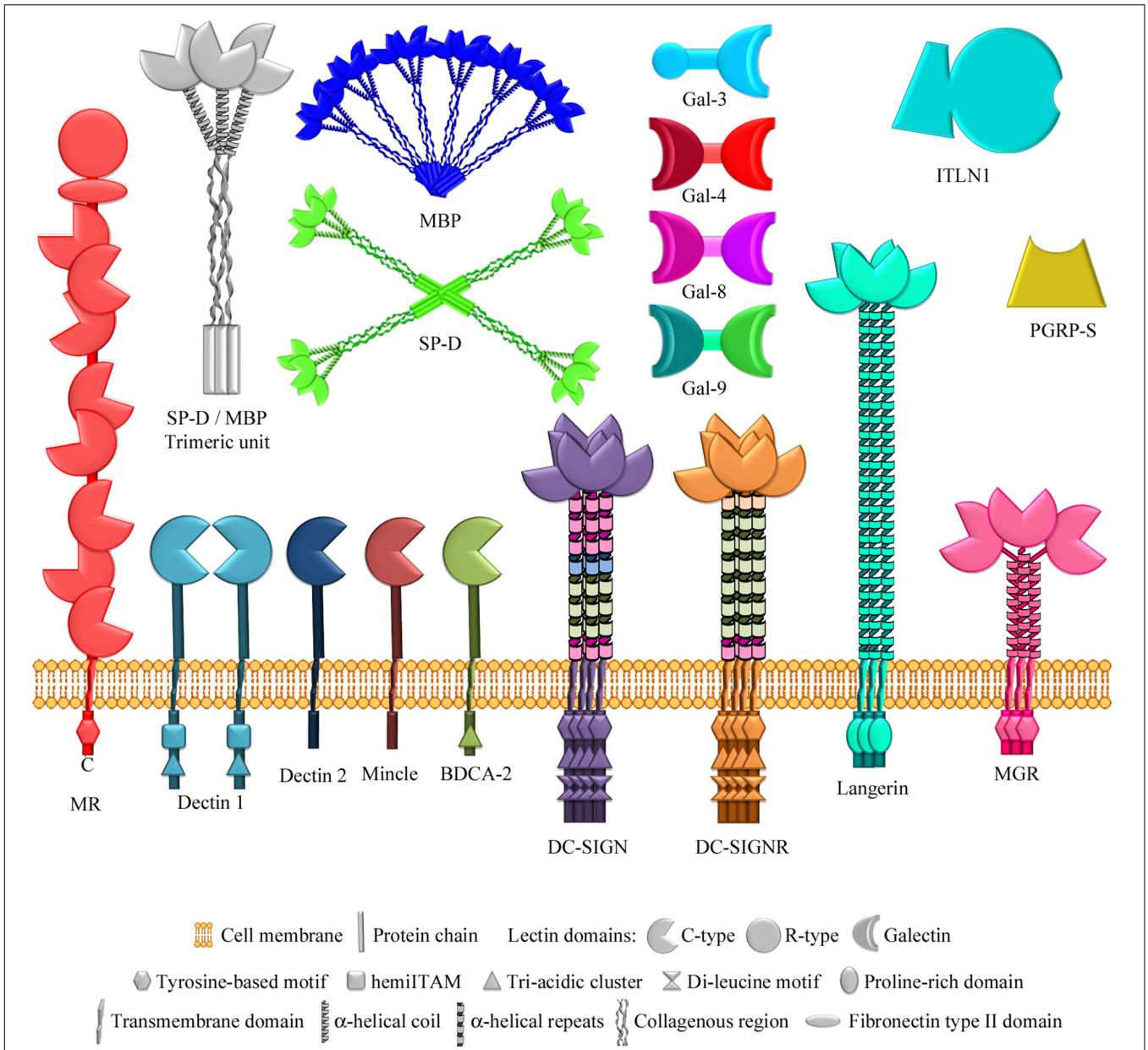

FIGURE 6 | Lectins of the innate immune system examined using bacterial glycan microarrays. The lectins studied comprise several multimodular membrane receptors that contain C-type carbohydrate-recognition domains (Solís et al., 2015) in addition to other non-lectin domains, specified in each case. The mannose receptor also contains an R-type lectin domain. Soluble lectins examined also include two C-type lectins of the collectin family (so called because they contain a collagenous region), which form different multimeric structures based on similar trimeric units. Other soluble lectins studied are different members of the galectin family, belonging to the chimera type (containing one carbohydrate-recognition domain) and tandem-repeat type (containing two different carbohydrate-recognition domains) structural subgroups, intelectin-1 (a member of the X-type lectin family), and a peptidoglycan recognition protein. MR, mannose receptor; BDCA-2, blood dendritic cell antigen 2; DC-SIGN, dendritic cell-specific ICAM-3-grabbing nonintegrin; DC-SIGNR, endothelial cell DC-SIGN homolog; MGR, macrophage galactose receptor; SP-D, surfactant protein D; MBP, serum mannose-binding protein; Gal-3/4/8/9, galectins 3/4/8/9; ITLN1, intelectin-1; PGRP-S, short peptidoglycan recognition protein.

polysaccharides, intact LPSs, and CPSs from a broad range of Gram-negative and -positive bacteria [microbial glycan microarray of the Consortium for Functional Glycomics (CFG)[2]]. Here, only weak binding signals were observed for some non-Man-containing *Shigella* and *Yersinia* antigens, whereas robust binding to yeast mannan was found (Hanske et al., 2017). Unfortunately, as none of these structures were tested in the previous microarray, it is not possible to compare the relative binding intensities obtained in these two studies. Therefore, a further analysis of the binding

[2]http://www.functionalglycomics.org

of human langerin to the spotted *E. coli*, *Shigella*, and *Yersinia* antigens is required. In contrast, despite exhibiting structurally and thermodynamically identical binding to Man and Manα(1-2)Man, murine langerin recognized a broad set of oligosaccharides with highly heterogeneous structures, what could be due to the presence in the murine form of a secondary site, adjacent to the canonic binding site and able to establish interactions with large glycans (Hanske et al., 2017). This interspecies variability could be the result of distinct evolutionary pressures imposed by the different expression patterns of murine and human langerins and their exposure to microbes.

The above-mentioned collections of 48 and 300 bacterial glycans were also used to examine the binding of three members of the galectin family belonging to two different structural subgroups, i.e., galectin 3 (of chimera type), and galectins 4 and 8 (of tandem-repeat-type) (**Figure 6**). Galectins are a family of lectins widely expressed in epithelial and immune cells and involved, among many other biological phenomena, in inflammation and immunity. In the 48-glycan array, a unique selectivity for the O antigen of *Providencia alcalifaciens* O5 was observed. Importantly, binding of the three galectins to the intact bacterium resulted in loss of viability, demonstrating the utility of the microarray to unveil host−bacteria interactions of functional significance (Stowell et al., 2014). Further analysis of galectin binding to the expanded set of 300 bacterial glycans revealed recognition of a diversity of species presenting mammalian-like carbohydrate determinants, as *K. pneumoniae*, *E. coli*, *P. alcalifaciens*, *Proteus vulgaris,* and *S. pneumoniae* (Stowell et al., 2014). These results demonstrated the ability of galectins to target bacteria displaying self-like antigens. In striking contrast, intelectin-1, a member of the X-type lectin family suspected to be involved in innate immunity, bound in this extended array to ligands containing β-linked galactofuranose, saccharide residues with D-glycerol-1-phosphate substituents, Hep, D-glycero-D-talo-oct-2-ulosonic acid, or Kdo residues, which are widely distributed in bacteria but are not found in mammalian glycans (Wesener et al., 2015). These two studies beautifully illustrate the complementarity in the recognition of self-like and non-self bacterial glycan epitopes by soluble lectins of the innate immune system.

Besides, the binding of tandem-repeat type galectins 4, 8, and 9 to a different microarray incorporating a collection of nearly 150 polysaccharides obtained by mild acid degradation of LPSs from six different bacteria genera (*Escherichia*, *Shigella*, *Salmonella*, *Cronobacter*, *Proteus*, and *Pseudomonas*) was examined (Knirel et al., 2014). Although galectins are characterized by a canonical β-galactoside-binding ability, several β-galactoside-containing polysaccharides with no forbidden substituents at the Gal moieties were not recognized by these galectins. Moreover, binding to non-βGal polysaccharides was detected. Keeping in mind that natural polysaccharides are heterogeneous and may contain minor populations that could account for the observed behavior, this study put forward the binding of galectins to non-canonical determinants.

Surfactant protein D (SP-D) is a different soluble lectin of the innate immune system known to recognize LPSs of several Gram-negative bacteria, triggering agglutination and phagocytosis. SP-D belongs to the C-type collectin family and binds to the LPS inner core Hep constituent. To get insights into the influence of adjacent residues and Hep linkages, the binding of SP-D to a glycan array containing 12 different synthetic inner core structures was examined (Reinhardt et al., 2016). Preferred binding to ligands containing tri-Hep terminal sequences over shorter substructures was observed, the presence of an internal Kdo having no detrimental effect on the recognition. However, replacement of the external Hep moiety by GlcNAc resulted in decreased binding. Moreover, a slight preference for terminal α(1-2)- over α(1-7)-linked Hep was observed. Overall, the results demonstrated SP-D binding to LPS inner core structures present in, e.g., *H. influenzae*, *Enterobacteriaceae*, *Proteus*, or *N. meningitidis*.

Other mammalian effectors of the immune system recognize bacterial cell wall peptidoglycans and activate antimicrobial defense systems, as, e.g., the so called peptidoglycan recognition proteins (PGRPs). However, the recognized motifs are poorly characterized. A series of peptidoglycan fragments consisting of MurNAcβ(1-4)GlcNAc (MG, MurNAc standing for *N*-acetylmuramic acid), $(MurNAc\beta(1\text{-}4)GlcNAc)_2$ (MGMG), or $(GlcNAc\beta(1\text{-}4)MurNAc)_2$ (GMGM), conjugated to di- (L-Ala-D-isoGln), tri- (L-Ala-D-isoGln-L-Lys), or tetrapeptides (L-Ala-D-isoGln-L-Lys-D-Ala), were tested for the binding of human PGRP-S (PGRP short, also known as PGRP 1) (Wang et al., 2016). In accordance with previous data, PGRP-S showed a preference for GMGM conjugates with tri- and tetra-peptides over the dipeptide. In addition, PGRP-S was also found to bind MGMG sequences, again with preference for tri- and tetrapeptide-containing structures. Although this could indicate that peptide length is important for recognition, as interpreted by the authors, the possibility that the Lys residue at position 3 of the tri-/tetra-peptides could be specifically involved in the binding should not be excluded.

In summary, a range of microarrays incorporating diverse bacterial glycans, from large collections to more focused libraries of a specific glycan type or bacterial origin (**Table 2**), have been selectively used to investigate the binding behavior of different lectins of the innate immune system, unveiling a repertoire of complementary recognition profiles and broad to very strict binding specificities, depending on the particular lectin.

BACTERIAL GLYCAN ARRAYS FOR THE STUDY OF LIGANDS RECOGNIZED BY BACTERIAL AND PHAGIC GLYCAN BINDING PROTEINS

Bacteria frequently use surface-exposed lectins to bind to host glycans that serve as docking points for adhesion, and different glycan microarray platforms mainly built with mammalian

glycan libraries have been used to get insights into their mode of binding and potential ligands (Flannery et al., 2015; Poole et al., 2018) or to evaluate bacterial adhesion and the efficiency of antiadhesive compounds (Kalograiaki et al., 2018a). In addition, some of these lectins are involved in the formation of bacterial microcolonies and biofilms through binding to glycans present on the surface of neighbor cells or to secreted exopolysaccharides. This is the case for several lectins from *Pseudomonas aeruginosa* and *Burkholderia cepacia* species, two bacteria that can even form mixed biofilms (Elias and Banin, 2012). The binding specificity of *P. aeruginosa* lectins PA-IL and PA-IIL (also referred to as LecA and LecB) and of *B. cenocepacia* lectins A and C (designated BC2L-A and BC2L-C) was investigated using glycan arrays from the Consortium for Functional Glycomics. Despite PA-IIL and BC2L-A are closely related Man-binding lectins, PA-IIL was found to show preference for fucosylated oligosaccharides (Marotte et al., 2007), while BC2L-A only bound to oligomannose glycans (Lameignere et al., 2008). Interestingly, screening of the two separate carbohydrate-recognition domains of BC2L-C revealed binding of the N-terminal domain to fucosylated oligosaccharides and of the C-domain to Man-terminated glycans (Sulak et al., 2011), thus combining in one single lectin binding properties similar to those of PA-IIL and BC2L-A. In contrast, PA-IL showed a high specificity for terminal α-Gal, with preference for Galα(1-4)Gal-terminating structures (Blanchard et al., 2008). Although the arrays tested were based on mammalian glycan structures, binding of these lectins to similar sugar epitopes in bacterial glycans, as, e.g., in the Gal- and Man-rich exopolysaccharide of *P. aeruginosa* (Psl), could be extrapolated. In addition, PA-IIL, BC2L-A, and BC2L-C could recognize Hep residues of LPSs, as described above for the Man-specific innate immune lectins DC-SIGN and SP-D. Indeed, binding of BC2L-A to Hep mono- and disaccharides, and Hep-containing oligo- and polysaccharides was later confirmed using a combination of NMR spectroscopy, X-ray crystallography, and calorimetry techniques (Marchetti et al., 2012). Moreover, binding of BC2L-A and the C-domain of BC2L-C to microarray-printed Man or Hep terminating bacterial glycans has very recently reported, this study unveiling a preference of both lectins for α(1-6)- over α(1-2)-linked Hep (Geissner et al., 2019). All in all, a study of the binding patterns to appropriate bacterial glycan arrays would certainly be of great help to identify the precise structures recognized by the bacterial lectins. This in turn will facilitate the design of new antibacterial agents able to interfere with microcolony and biofilm formation.

Many bacterial glycoside hydrolases contain non-catalytic CBMs that target the enzyme to specific regions on its substrate and promote hydrolysis. A finely tuned selectivity in carbohydrate recognition was demonstrated in a study on the binding of six bacterial glucan-binding CBMs to the collection of 153 gluco-oligosaccharide neoglycolipids described in the preceding section (Palma et al., 2015). The analysis confirmed known binding preferences, with distinct CBM-specific profiles and differing influence of oligosaccharide sequence and length, and also revealed novel binding specificities including recognition of bacterial glycans. For example, CBM41 from *Thermotoga maritima* pullulanase showed the predicted binding to α(1-4)-gluco-oligosaccharides, and the presence of α(1-6)-linked Glc was found to be better tolerated at an internal position than at the non-reducing end. Binding of CBM11 from *Clostridium thermocellum* endoglucanase was in agreement with its selectivity toward Glcβ(1-4)Glcβ(1-4)Glcβ(1-3)Glc, although only heptasaccharide and longer chains were bound, suggesting that chain length is important for recognition. In the case of CBM4-2 from *T. maritima* laminarinase, which showed preferential binding to linear β(1-3)-glucans, a minimum chain length of four units was required, while for two CBMs from *Cellvibrio mixtus* cellulase (CBM32-2) and *Bacillus halodurans* laminarinase (CBM6), showing prominent binding to linear β(1-2)- and β(1-3)-, as well as branched β(1-3/6)-oligosaccharides, binding to di- and tri-saccharide structures could be detected. Finally, CBM6-2 from *C. mixtus* endoglucanase 5A, which contains two binding clefts with different specificity, exhibited the broadest recognition profile, including binding to linear β(1-2)-gluco-oligosaccharides derived from the cyclic β(1-2)-glucan of *B. abortus*, not reported previously for this CBM. This study demonstrated the effectiveness of the microarray as a tool for probing recognition of short as well as long bacterial glucans.

A different module present in bacterial peptidoglycan hydrolases is the Lysin Motif (LysM) domain. This is a widespread domain, found in proteins from viruses to mammals, that recognizes polysaccharides containing GlcNAc residues, as present in the bacterial cell wall peptidoglycan or in chitin, the main constituent of fungal cell walls. Furthermore, plant receptors containing LysM domains recognize lipochitin oligosaccharides that are synthesized by nitrogen fixing bacteria to be used as signaling molecules (Nod factors) in legume–rhizobium symbiosis. A microarray containing a series of natural and synthetic Nod factors, chitin oligosaccharides, and peptidoglycan-related compounds was developed to investigate interactions involving LysM domain-containing proteins (Maolanon et al., 2014). Analysis of the binding to the array of P60, an autolysin of *Listeria monocytogenes* that hydrolyzes the cell wall peptidoglycan and is essential for bacterial virulence, revealed recognition of chitin oligosaccharides of $\geq$ 5 GlcNAc units and selective binding to some Nod factors, in particular those containing a C18:1 lipid chain. Interestingly, a chemically synthesized LysM domain of the Nod factor receptor 5 from the legume *Lotus japonicas* was also found to show preference for Nod factors with C18:1 lipid chains (Sorensen et al., 2014). Thus, the bacterial and plant LysM domains appeared to exhibit a similar dependence on the lipid structure, hinting at a possible role of the lipid moiety in the binding of LysM domains to Nod factors.

Bacteriophages also exploit recognition of specific bacterial glycan motifs for invading their hosts. An example is the lytic phage NCTC 12673, which recognizes the capsular polysaccharide of only a limited number of *C. jejuni* isolates, thereby conferring the phage its high host specificity. In addition, NCTC 12673 contains a putative binding protein, Gp047, with a much broader host-binding range than the phage, being capable of binding to multiple *C. jejuni* and

Campylobacter coli strains. This protein was found to recognize flagellin decorated with acetamidino-modified pseudaminic acid. However, it did not bind any of the structures printed in the 48-glycan array mentioned before, not even to glycans of *P. aeruginosa* containing acetimidoyl groups, thus evidencing the specific requirement for recognition of the acetamidino modification on pseudaminic acid (Javed et al., 2015). The authors proposed that Gp047 could be released from phage-infected bacteria and bind to flagella of neighboring *C. jejuni* cells, thereby reducing their motility and assisting in the next round of infection.

BACTERIA MICROARRAYS FOR EXAMINING BACTERIAL SURFACE GLYCANS AND THEIR RECOGNITION BY GLYCAN-BINDING PROTEINS

The potential of microarrays incorporating natural or synthetic bacterial glycan structures for exploring the recognition of bacteria by carbohydrate-binding proteins is evidently limited by the library of probes included in the array. If the particular carbohydrate structure recognized by the protein is not present in the array, the analysis may be misinterpreted as a lack of binding to a given bacterium. On the other hand, the presentation of the glycan probes in the array in an accessible and clustered (high density) form may substantially differ from their natural arrangement and accessibility on the bacterial surface. Therefore, the possibility that the results do not correlate with the real bacteria−receptor interplay does exist and poses a challenge to the design of microarray-based strategies. Moreover, synergistic operative interactions of the glycan-binding proteins with other cell surface molecules cannot be evaluated. Therefore, besides assessing recognition of isolated bacterial components by glycan-binding proteins for identification of ligand candidates, analysis of binding to bacterial supramolecular structures and entire cells is needed.

An example is the study of the recognition of the bacterial peptidoglycan by the cell wall-binding domain of the endolysin Cpl-7, which is encoded by the pneumococcal Cp-7 bacteriophage (Bustamante et al., 2017). Cpl-7 is composed of a catalytic domain with muramidase activity and a cell wall-binding domain (C-Cpl-7) made up of three CW_7 repeats. Although these repeats have only been characterized in two other endolysins, they are present in many putative cell wall hydrolase sequences, suggesting that they target a conserved element of the bacterial cell wall. Inspection of the mode of binding of peptidoglycan fragments to C-Cpl-7 using a combination of X-ray crystallography, saturation transfer difference NMR spectroscopy (STD-NMR), and docking studies, unveiled GlcNAcβ(1-4)MurNAc-L-Ala-D-isoGln as the minimal recognized fragment and the involvement, among other contacts, of a fully conserved arginine residue in hydrogen bonding with the GlcNAc moiety. Binding assays of C-Cpl-7 to cell wall fragments from the laboratory *S. pneumoniae* strain R6, grown in choline- or ethanolamine-containing media (i.e., with choline- or ethanolamine-containing TAs), printed on nitrocellulose-coated glass slides, confirmed recognition of the pneumococcal cell wall independently of the choline or ethanolamine decoration of TAs (Bustamante et al., 2017). Moreover, upon substitution in the three repeats of the mentioned arginine residue by alanine, what did not alter the protein structure, a decrease of around 50% in the intensity of the binding signals was observed. These results suggested that the mode of binding to the complex peptidoglycan layer is likely to be analogous to that defined for the small glycopeptide studied.

As endolysins break down the cell wall from the inside of bacteria to release the phage progeny, the use of cell wall fragments to investigate endolysins' recognition of the bacterial peptidoglycan (or of TAs) is indicated. However, the interaction of glycan-binding proteins with bacterial surface glycans should be better explored using microarray-printed entire cells. This approach was used to detect antibodies against cell surface antigens (Thirumalapura et al., 2006). Microarrays containing inactivated *E. coli*, *F. tularensis*, *K. pneumoniae*, *S.* Typhimurium, *E. faecalis*, *S. aureus*, *S. epidermidis*, *Streptococcus pyogenes*, and *L. monocytogenes* cells were tested for the binding of mAbs against *F. tularensis* O-antigen, *Salmonella* O-antigen (B group), *S. aureus* peptidoglycan, and *L. monocytogenes*. Specific recognition of the respective bacteria was demonstrated with no meaningful cross-reactions. To assess the utility of the approach for antibody detection in clinical samples, seven canine serum samples from clinical cases of tularemia and positive for *F. tularensis* antibodies, along with six canine serum samples negative for *F. tularensis* antibodies, were comparatively tested. Significantly higher levels of anti-*F. tularensis* antibodies were detected in tularemia positive samples compared to negative samples (Thirumalapura et al., 2006). In addition, variable levels of antibodies against the other bacteria were also observed, showing that simultaneous detection of different anti-bacteria antibodies was possible.

More recently, bacteria microarrays have proved to be useful for exploring the presence of carbohydrate structures on bacterial surfaces (Campanero-Rhodes et al., 2015; Kalograiaki et al., 2016, 2018b). *K. pneumoniae* O1:K2 strain 52145, a clinically relevant serotype, was first used as model bacterium (Campanero-Rhodes et al., 2015). This strain displays a Gal-containing O-chain (**Figure 5**) and a CPS built by a branched Glc/Man-based tetrasaccharide repeating unit, which are glycan structures commonly found in isolates from *K. pneumoniae*-infected individuals. By testing the binding of a panel of 10 lectins of known binding specificities to array-printed *K. pneumoniae* 52145 cells, the accessibility for lectin recognition of Gal- and Man/Glc-containing structures on the bacterial surface was confirmed. A series of isogenic mutants lacking the capsule, the LPS O-chain and/or the major outer membrane protein OmpA, printed in parallel, helped to dissect the specific structures recognized by those lectins giving meaningful binding signals toward the wild type strain. A strong preference of the Gal-specific lectins RCA and PNA (**Table 3**) for non-capsulated and O-chain-containing strains was evident, pointing to the O-chain as the primary recognized epitope. In the case of the Man/Glc-specific lectin ConA, the results indicated that the CPS was not

TABLE 3 | Binding specificities of model lectins mentioned in this review.

Lectin	Abbreviation	Source	Monosaccharide	Sugar-binding preferences
Concanavalin A	ConA	*Canavalia ensiformis* seeds	Man/Glc	α-Methyl-mannopyranoside > α-Man > α-Glc > α-GlcNAc
Wheat germ agglutinin	WGA	*Triticum vulgaris*	GlcNAc	$[GlcNAc]_3$, $[GlcNAc]_2$, GlcNAc. It may bind Neu5Ac, but not Neu5Gc
Griffonia simplicifolia lectin II	GSL-II	*Griffonia simplicifolia* seeds	GlcNAc	Terminal α- or β-GlcNAc residues
Datura stramonium lectin	DSL	*Datura stramonium* seeds	GlcNAc	β(1-4)-linked GlcNAc oligomers: Chitotriose > chitobiose > GlcNAc. Also LacNAc and LacNAc oligomers
Peanut agglutinin	PNA	*Arachis hypogaea* peanuts	Gal	Galβ(1-3)GalNAc (T-antigen), Lac
Ricinus communis agglutinin	RCA-I, RCA_{120}	*Ricinus communis* seeds	Gal	Terminal β-Gal. Galβ(1-4)Glc >> Galβ(1-3)Glc. GalNAc is a very poor inhibitor
Viscum album agglutinin	VAA	*Viscum album* leaves	Gal	Terminal β-Gal
Artocarpus integrifolia lectin	Jacalin	*Artocarpus integrifolia* seeds	Gal	Galβ(1-3)GalNAc (T-antigen), non-, mono- or di-sialylated
Erythrina cristagalli lectin	ECL	*Erythrina cristagalli* seeds	Gal	Lac, LacNAc
Soybean agglutinin	SBA	*Glycine max* seeds	GalNAc/Gal	Terminal α- or β-linked GalNAc and to a lesser extent Gal residues
Helix pomatia agglutinin	HPA	*Helix pomatia* albumin gland	GalNAc	α-GalNAc over β-GalNAc. Weakly α-Gal
Aleuria aurantia lectin	AAL	*Aleuria aurantia* mushrooms	Fuc	Fuc α(1-6)-linked to GlcNAc or α(1-3)-linked to LacNAc related structures
Maackia amurensis lectin I	MAL-I	*Maackia amurensis* seeds	Gal	Galβ(1-4)GlcNAc
Maackia amurensis lectin II	MAL-II	*Maackia amurensis* seeds	Neu5Ac	Neu5Acα(2-3)Galβ(1-3)GalNAc

Man, mannose; Glc, glucose; GlcNAc, N-acetylglucosamine; Gal, galactose; GalNAc, N-acetylgalactosamine; Fuc, fucose; Neu5Ac, N-acetylneuraminic acid; Neu5Gc, N-glycolylneuraminic acid; LacNAc, N-acetyllactosamine; Lac, lactose.

the main recognized structure, as there was no preference for capsulated over non-capsulated strains. Importantly, for all the lectins the binding signals were reduced down to background levels when the binding assays were carried out in the presence of their specific haptens, thereby proving that lectin binding was carbohydrate mediated. Therefore, other glycan structures different from the CPS were apparently recognized by ConA.

The efficiency of bacteria microarrays for exploring the presence of surface glycans of bacteria not presenting CPS and O-antigen-containing LPS was next demonstrated using non-typeable *H. influenzae* (NTHi) as model (Kalograiaki et al., 2016). Binding assays to microarray-printed NTHi strain 375 (hereafter referred to as NTHi375) with a panel of 19 lectins revealed positive and hapten-inhibitable signals for Gal-, Glc-, and sialic acid-specific lectins, indicating the presence on the bacterial surface of carbohydrate structures specifically recognized by the lectins. Analysis of lectin binding to a set of isogenic mutant strains expressing sequentially truncated LOS supported the notion that the LOS could be a target for most lectins. Interestingly, LOS truncation had disparate consequences on the binding of the Gal-specific lectins VAA and RCA (**Table 3**). In particular, the absence of the Galα(1-4)Galβ epitope from the chain extension linked to the distal manno-heptose of the Hep trisaccharide inner core (**Figure 5**) resulted in decreased binding of VAA but had no significant effect on the binding of RCA, suggesting that RCA might not bind this LOS. Indeed, a follow up study using microarrays containing the purified LOS showed only marginal binding of RCA as opposed to strong binding of VAA, which was drastically reduced for a truncated LOS lacking Galα(1-4)Galβ (Kalograiaki et al., 2018c). In striking contrast, RCA bound strongly to the microarray-printed LOS from the capsule-deficient *H. influenzae* laboratory strain RdKW20, whose major glycoform displays terminal Galβ(1-4)Glc at the distal Hep extension, while, although ∼19% of this LOS bears terminal Galα(1-4)Galβ, VAA bound only weakly. In-depth analysis of the LOS epitopes recognized by RCA and VAA in each case, using STD-NMR experiments assisted by molecular dynamics simulations, revealed that RCA bound the RdKW20 LOS glycoform displaying terminal Galβ(1-4)Glcβ, whereas VAA recognized the Galα(1-4)Galβ(1-4)Glcβ epitope (**Figure 5**) in NTHi375 LOS but not in RdKW20 LOS, what could be due to different conformational preferences of the branch and ensuing presentation of the epitope. Binding assays to wild type and selected mutant/transformed whole bacterial cells ran in parallel revealed that, besides the LOS, other carbohydrate structures on the bacterial surface serve as lectin ligands, and highlighted the impact of the specific display of cell surface components on lectin binding, stressing the importance of examining binding to entire bacterial cells (Kalograiaki et al., 2018c).

Having proved the utility of bacteria microarrays for exploring the presence of carbohydrate structures on the surface of the model NTHi375 strain, the glycosignatures of five other NTHi clinical isolates from otitis media and COPD (chronic obstructive pulmonary disease) patients and from pediatric healthy carriers were examined (Kalograiaki et al., 2016). Different lectin-binding fingerprints were observed, consistent with the known inter-strain heterogeneity of *H. influenzae* LOS, which is linked to variable outcomes with the host, i.e., colonization, persistence, or acute infection. Again, RCA and VAA exhibited different binding patterns, supporting that these two lectins recognize different ligands on the NTHi surface. At any rate, the results evidenced the availability on

the bacterial surface of Man/Glc, Gal, and sialic acid residues that could be recognized by lectins of the innate immune system with the appropriate carbohydrate-binding specificity. Indeed, analysis of the binding of SP-D, galectin-8, and Siglec-14, which exhibit Man/Glc, Gal, and sialic acid binding specificities, respectively, to the array-printed NTHi clinical isolates revealed lectin- and strain-specific recognition (Kalograiaki et al., 2016), providing the first experimental evidence for direct binding of SP-D to NTHi and also demonstrating binding of galectin-8 and Siglec-14 to NTHi strains other than NTHi2019, previously reported (Angata et al., 2013; Stowell et al., 2014). Overall, the microarray analysis afforded information on the glycosignatures of the tested bacteria and detected recognition by host receptors, providing semiquantitative data on binding avidity.

OTHER APPLICATIONS OF LECTIN, ANTIBODY, AND BACTERIAL GLYCAN MICROARRAYS

The main focus of this review was the description of microarray strategies for exploring the presence of glycans on bacterial surfaces and their interactions with a diversity of glycan-binding proteins. Still, other interesting microarray approaches that could be of value to the microbiologist community deserve to be mentioned.

A first example is the use of a sandwiched microarray platform for testing the efficiency of antibiotics on *S. aureus* growth (Liu et al., 2016). A lectin-hydrogel microarray was employed for capturing bacteria, and a matching drug-laden polyacrylamide microarray was then used for building microchambers between the two microarrays, in which live bacteria were co-cultured with antibiotics. Minimum inhibitory concentrations obtained in this way for four well-known antibiotics were in agreement with reported values.

Antibody microarrays have been used for detecting bacteria in a diversity of samples, covering from water to rocks. For example, *E. coli* O157:H7, *S.* Typhimurium, and *Legionella pneumophila,* which are responsible for water-borne infections, were detected in water using a flow-through chemiluminescence microarray approach (Wolter et al., 2008; Karsunke et al., 2009). A method for fast detection of clinically relevant levels of *S. Enteritidis* in blood, based on monitoring of bacterial growth by SPRi, has also been reported (Templier et al., 2017). The method was claimed to be of value for detecting bloodstream bacterial infections (bacteremia) using blood volumes similar to those used in standard analyses. Moreover, microarrays containing collections of up to 300 antibodies have been used for environmental monitoring of bacteria, in, e.g., aquatic ecosystems (Blanco et al., 2015), or even detection of "signs of life" in solid samples, including sediments, rocks, and subsoil samples, especially those from extreme environments such as the hypersaline Atacama subsurface (Parro et al., 2011) or the permafrost from the antarctical Deception Island (Blanco et al., 2012). Although most of the antibodies used in these studies did not explicitly target bacterial glycan structures, as they were raised against whole bacterial cells, in some cases detection of bacterial exopolysaccharides, LTAs, and peptidoglycans was demonstrated (Rivas et al., 2008; Parro et al., 2011; Blanco et al., 2012; Puente-Sánchez et al., 2014). Of note, the successful results obtained with these arrays supported their utility for planetary exploration, as, e.g., the search for life in Mars.

Regarding carbohydrate microarrays, a singular approach involving binding assays of purified bacterial glycans to microarray-printed host glycans was used to examine host–bacteria glycan–glycan interactions. Numerous interactions of LOS/LPSs isolated from *C. jejuni*, *H. influenzae*, *S.* Typhimurium, and *Shigella flexneri* with the printed probes were detected (Day et al., 2015). Moreover, cell assays demonstrated that adherence of bacteria to host cells could be inhibited with either host or bacterial glycans, indicating that the observed glycan−glycan interactions could importantly contribute to the binding of bacteria to host cells. As mentioned before, the potential of carbohydrate microarrays for exploring recognition events is limited by the library of probes used for building the arrays, what is frequently restricted by the laborious procedures required for obtaining well-defined glycan structures. Engineered phages displaying specific oligosaccharides, named "glycophages," have been put forward as an alternative (or complement) to the commonly used glycan libraries of natural and/or synthetic origin (Çelik et al., 2015). In particular, microarray-printed phages displaying the *P. aeruginosa* O11 O-antigen were successfully recognized by serum antibodies against this O-antigen, which did not bind to other glycophages in the array displaying O-antigen polysaccharides from *C. jejuni, Campylobacter lari*, *E. coli* O78, *E. coli* O148, *F. tularensis*, or *Shigella dysenteriae*, demonstrating the applicability of the approach. A key advantage of glycophages is that they can be produced in bacteria in large quantities and isolated easily from bacterial supernatants.

CONCLUDING REMARKS

As illustrated in this review, the number and diversity of applications of the microarray technology grow continuously, offering novel and complementary high-throughput tools for bacteria-related studies in multiple areas, from basic science to the clinical or food safety fields and even environmental exploration. Still, several advances are required to maximize the potential of this technology. For example, the binding specificity of microarray-printed lectins has been typically investigated using eukaryotic glycans as ligand candidates. Therefore, their ability to recognize sugar residues and structures exclusively found in bacteria is not known in most cases and should be thoroughly examined. Production of recombinant lectins with engineered binding specificities would definitely facilitate a wider and more selective coverage of bacterial glycans. Regarding antibody microarrays, the quality and cross-reactivity of anti-carbohydrate antibodies are important issues to tackle. In addition, increased sensitivity is required to enable their use as routine tool for detection of contaminating bacteria in real-world samples. Expansion of bacterial glycan libraries through improved methods for isolation and structural characterization or chemical/enzymatic synthesis or by exploiting novel alternatives, as the above-mentioned "glycophages," would

enhance the potential of carbohydrate microarrays for exploring recognition events. Common to all types of microarrays is the need of better tools to analyze data and to establish functional correlations, e.g., between bacterial glycosignatures and virulence. These and other developments leading to a greater simplicity and accessibility to this technique will surely broaden its applications in bacterial glycobiology and related areas.

AUTHOR CONTRIBUTIONS

MC-R reviewed the literature, prepared the figures and tables, and edited the manuscript. AP and MM contributed to literature search and edited the manuscript. DS conceived the review, contributed to literature search, and wrote the manuscript.

FUNDING

This work was financed by the Spanish Ministry of Economy and Competitiveness (Grant BFU2015-70052-R), the Spanish Ministry of Science, Innovation, and Universities, the Spanish State Research Agency, the European Regional Development Fund (RTI2018-099985-B-I00, MCIU/AEI/FEDER, UE), the CIBER of Respiratory Diseases (CIBERES), an initiative from the Spanish Institute of Health Carlos III (ISCIII), the Fundação para a Ciência e a Tecnologia (FCT-MCTES), Portugal (Grants PTDC/QUI-QUI/112537/2009, PTDC/BIA-MIB/31730/2017, and IF/00023/2012), and the Applied Molecular Biosciences Unit (UCIBIO) (Financed by FCT-MCTES, UID/Multi/04378/2013/2019).

ACKNOWLEDGMENTS

AP thanks Professor Ten Feizi and past and present members of the Glycosciences Laboratory, in particular Wengang Chai, Yan Liu, Yibing Zhang and Hongtao Zhang, for their collaboration in the establishment of the neoglycolipid-based glucan oligosaccharide microarrays cited in this review.

REFERENCES

Adibekian, A., Stallforth, P., Hecht, M. L., Werz, D. B., Gagneux, P., and Seeberger, P. H. (2011). Comparative bioinformatics analysis of the mammalian and bacterial glycomes. *Chem. Sci.* 2, 337–344. doi: 10.1093/glycob/cwu092

Angata, T., Ishii, T., Motegi, T., Oka, R., Taylor, R. E., Soto, P. C., et al. (2013). Loss of Siglec-14 reduces the risk of chronic obstructive pulmonary disease exacerbation. *Cell. Mol. Life Sci.* 70, 3199–3210. doi: 10.1007/s00018-013-1311-7

Angenendt, P. (2005). Progress in protein and antibody microarray technology. *Drug Discov. Today* 10, 503–511. doi: 10.1016/S1359-6446(05)03392-1

Blanchard, B., Nurisso, A., Hollville, E., Tetaud, C., Wiels, J., Pokorna, M., et al. (2008). Structural basis of the preferential binding for globo-series glycosphingolipids displayed by *Pseudomonas aeruginosa* lectin I. *J. Mol. Biol.* 383, 837–853. doi: 10.1016/j.jmb.2008.08.028

Blanco, Y., Prieto-Ballesteros, O., Gómez, M. J., Moreno-Paz, M., García-Villadangos, M., Rodríguez-Manfredi, J. A., et al. (2012). Prokaryotic communities and operating metabolisms in the surface and the permafrost of Deception Island (Antarctica). *Environ. Microbiol.* 14, 2495–2510. doi: 10.1111/j.1462-2920.2012.02767.x

Blanco, Y., Quesada, A., Gallardo-Carreño, I., Aguirre, J., and Parro, V. (2015). CYANOCHIP: an antibody microarray for high-taxonomical-resolution cyanobacterial monitoring. *Environ. Sci. Technol.* 49, 1611–1620. doi: 10.1021/es5051106

Blixt, O., Head, S., Mondala, T., Scanlan, C., Huflejt, M. E., Alvarez, R., et al. (2004). Printed covalent glycan array for ligand profiling of diverse glycan binding proteins. *Proc. Natl. Acad. Sci. U.S.A.* 101, 17033–17038. doi: 10.1073/pnas.0407902101

Blixt, O., Hoffmann, J., Svenson, S., and Norberg, T. (2008). Pathogen specific carbohydrate antigen microarrays: a chip for detection of *Salmonella* O-antigen specific antibodies. *Glycoconj J.* 25, 27–36. doi: 10.1007/s10719-007-9045-0

Blumenschein, T. M. A., Friedrich, N., Childs, R. A., Saouros, S., Carpenter, E. P., Campanero-Rhodes, M. A., et al. (2007). Atomic resolution insight into host cell recognition by *Toxoplasma gondii*. *Embo. J.* 26, 2808–2820. doi: 10.1038/sj.emboj.7601704

Bouguelia, S., Roupioz, Y., Slimani, S., Mondani, L., Casabona, M. G., Durmort, C., et al. (2013). On-chip microbial culture for the specific detection of very low levels of bacteria. *Lab Chip* 13, 4024–4032. doi: 10.1039/c3lc50473e

Broecker, F., Hanske, J., Martin, C. E., Baek, J. Y., Wahlbrink, A., Wojcik, F., et al. (2016a). Multivalent display of minimal *Clostridium difficile* glycan epitopes mimics antigenic properties of larger glycans. *Nat. Commun.* 7:11224. doi: 10.1038/ncomms11224

Broecker, F., Martin, C. E., Wegner, E., Mattner, J., Baek, J. Y., Pereira, C. L., et al. (2016b). Synthetic lipoteichoic acid glycans are potential vaccine candidates to protect from *Clostridium difficile* Infections. *Cell Chem. Biol.* 23, 1014–1022. doi: 10.1016/j.chembiol.2016.07.009

Bustamante, N., Iglesias-Bexiga, M., Bernardo-García, N., Silva-Martín, N., García, G., Campanero-Rhodes, M. A., et al. (2017). Deciphering how Cpl-7 cell wall-binding repeats recognize the bacterial peptidoglycan. *Sci. Rep.* 7:16494. doi: 10.1038/s41598-017-16392-4

Cai, H. Y., Lu, L., Muckle, C. A., Prescott, J. F., and Chen, S. (2005). Development of a novel protein microarray method for serotyping *Salmonella enterica* strains. *J. Clin. Microbiol.* 43, 3427–3430. doi: 10.1128/Jcm.43.7.3427-3430.2005

Campanero-Rhodes, M. A., Childs, R. A., Kiso, M., Komba, S., Le Narvor, C., Warren, J., et al. (2006). Carbohydrate microarrays reveal sulphation as a modulator of siglec binding. *Biochem. Biophys. Res. Commun.* 344, 1141–1146. doi: 10.1016/j.bbrc.2006.03.223

Campanero-Rhodes, M. A., Llobet, E., Bengoechea, J. A., and Solís, D. (2015). Bacteria microarrays as sensitive tools for exploring pathogen surface epitopes and recognition by host receptors. *Rsc Adv.* 5, 7173–7181. doi: 10.1039/c4ra14570d

Campanero-Rhodes, M. A., Smith, A., Chai, W. G., Sonnino, S., Mauri, L., Childs, R. A., et al. (2007). N-glycolyl GM1 ganglioside as a receptor for simian virus 40. *J. Virol.* 81, 12846–12858. doi: 10.1128/jvi.01311-07

Casals, C., Campanero-Rhodes, M. A., García-Fojeda, B., and Solís, D. (2018). The role of collectins and galectins in lung innate immune defense. *Front. Immunol.* 9:1998. doi: 10.3389/fimmu.2018.01998

Çelik, E., Ollis, A. A., Lasanajak, Y., Fisher, A. C., Gür, G., Smith, D. F., et al. (2015). Glycoarrays with engineered phages displaying structurally diverse oligosaccharides enable high-throughput detection of glycan-protein interactions. *Biotechnol. J.* 10, 199–209. doi: 10.1002/biot.201400354

Chan, C. E., Götze, S., Seah, G. T., Seeberger, P. H., Tukvadze, N., Wenk, M. R., et al. (2015). The diagnostic targeting of a carbohydrate virulence factor from *M.Tuberculosis*. *Sci. Rep.* 5:10281. doi: 10.1038/srep10281

Chen, T., Blanc, C., Eder, A. Z., Prados-Rosales, R., Souza, A. C., Kim, R. S., et al. (2016). Association of human antibodies to arabinomannan with enhanced mycobacterial opsonophagocytosis and intracellular growth reduction. *J. Infect. Dis.* 214, 300–310. doi: 10.1093/infdis/jiw141

Day, C. J., Tran, E. N., Semchenko, E. A., Tram, G., Hartley-Tassell, L. E., Ng, P. S. K., et al. (2015). Glycan:glycan interactions: high affinity biomolecular interactions that can mediate binding of pathogenic bacteria to host cells. *Proc. Natl. Acad. Sci. U.S.A.* 112, E7266–E7275. doi: 10.1073/pnas.1421082112

Diago-Navarro, E., Motley, M. P., Ruiz-Pérez, G., Yu, W., Austin, J., Seco, B. M. S., et al. (2018). Novel, broadly reactive anticapsular antibodies against

carbapenem-resistant *Klebsiella pneumoniae* protect from infection. *mBio* 9:e91-18. doi: 10.1128/mBio.00091-18

Elias, S., and Banin, E. (2012). Multi-species biofilms: living with friendly neighbors. *Fems Microbiol. Rev.* 36, 990–1004. doi: 10.1111/j.1574-6976.2012.00325.x

Emmadi, M., Khan, N., Lykke, L., Reppe, K., Parameswarappa, S. G., Lisboa, M. P., et al. (2017). A *Streptococcus pneumoniae* Type 2 oligosaccharide glycoconjugate elicits opsonic antibodies and is protective in an animal model of invasive Pneumococcal disease. *J. Am. Chem. Soc.* 139, 14783–14791. doi: 10.1021/jacs.7b07836

Feinberg, H., Taylor, M. E., Razi, N., McBride, R., Knirel, Y. A., Graham, S. A., et al. (2011). Structural basis for langerin recognition of diverse pathogen and mammalian glycans through a single binding site. *J. Mol. Biol.* 405, 1027–1039. doi: 10.1016/j.jmb.2010.11.039

Flannery, A., Gerlach, J. Q., Joshi, L., and Kilcoyne, M. (2015). Assessing bacterial interactions using carbohydrate-based microarrays. *Microarrays* 4, 690–713. doi: 10.3390/microarrays4040690

Fukui, S., Feizi, T., Galustian, C., Lawson, A. M., and Chai, W. (2002). Oligosaccharide microarrays for high-throughput detection and specificity assignments of carbohydrate-protein interactions. *Nat. Biotechnol.* 20, 1011–1017. doi: 10.1038/nbt735

Ganeshapillai, J., Vinogradov, E., Rousseau, J., Weese, J. S., and Monteiro, M. A. (2008). *Clostridium difficile* cell-surface polysaccharides composed of pentaglycosyl and hexaglycosyl phosphate repeating units. *Carbohydrate Res.* 343, 703–710. doi: 10.1016/j.carres.2008.01.002

Gao, J., Liu, D., and Wang, Z. (2010). Screening lectin-binding specificity of bacterium by lectin microarray with gold nanoparticle probes. *Anal. Chem.* 82, 9240–9247. doi: 10.1021/ac1022309

Gehring, A. G., Albin, D. M., Bhunia, A. K., Reed, S. A., Tu, S. I., and Uknalis, J. (2006). Antibody microarray detection of *Escherichia coli* O157 : H7: quantification, assay limitations, and capture efficiency. *Anal. Chem.* 78, 6601–6607. doi: 10.1021/ac0608467

Geissner, A., Pereira, C. L., Leddermann, M., Anish, C., and Seeberger, P. H. (2016). Deciphering antigenic determinants of *Streptococcus pneumoniae* Serotype 4 capsular polysaccharide using synthetic oligosaccharides. *ACS Chem. Biol.* 11, 335–344. doi: 10.1021/acschembio.5b00768

Geissner, A., Reinhardt, A., Rademacher, C., Johannssen, T., Monteiro, J., Lepenies, B., et al. (2019). Microbe-focused glycan array screening platform. *Proc. Natl. Acad. Sci. U.S.A.* 116, 1958–1967. doi: 10.1073/pnas.1800853116

Hanashima, S., Gotze, S., Liu, Y., Ikeda, A., Kojima-Aikawa, K., Taniguchi, N., et al. (2015). Defining the Interaction of Human Soluble Lectin ZG16p and Mycobacterial Phosphatidylinositol Mannosides. *Chembiochem* 16, 1502–1511. doi: 10.1002/cbic.201500103

Hanske, J., Schulze, J., Aretz, J., McBride, R., Loll, B., Schmidt, H., et al. (2017). Bacterial polysaccharide specificity of the pattern recognition receptor langerin is highly species-dependent. *J. Biol. Chem.* 292, 862–871. doi: 10.1074/jbc.M116.751750

Hegde, N. V., Praul, C., Gehring, A., Fratamico, P., and DebRoy, C. (2013). Rapid O serogroup identification of the six clinically relevant Shiga toxin-producing *Escherichia coli* by antibody microarray. *J. Microbiol. Methods* 93, 273–276. doi: 10.1016/j.mimet.2013.03.024

Herget, S., Toukach, P. V., Ranzinger, R., Hull, W. E., Knirel, Y. A., and von der Lieth, C. W. (2008). Statistical analysis of the bacterial carbohydrate structure data base (BCSDB): characteristics and diversity of bacterial carbohydrates in comparison with mammalian glycans. *BMC Struct. Biol.* 8:35. doi: 10.1186/1472-6807-8-35

Hsu, K. L., Pilobello, K. T., and Mahal, L. K. (2006). Analyzing the dynamic bacterial glycome with a lectin microarray approach. *Nat. Chem. Biol.* 2, 153–157. doi: 10.1038/nchembio767

Jankute, M., Cox, J. A., Harrison, J., and Besra, G. S. (2015). Assembly of the mycobacterial cell wall. *Annu. Rev. Microbiol.* 69, 405–423. doi: 10.1146/annurev-micro-091014-104121

Javed, M. A., van Alphen, L. B., Sacher, J., Ding, W., Kelly, J., Nargang, C., et al. (2015). A receptor-binding protein of *Campylobacter jejuni* bacteriophage NCTC 12673 recognizes flagellin glycosylated with acetamidino-modified pseudaminic acid. *Mol. Microbiol.* 95, 101–115. doi: 10.1111/mmi.12849

Kalograiaki, I., Abellán-Flos, M., Fernández, L. A., Menéndez, M., Vincent, S. P., and Solís, D. (2018a). Direct evaluation of live uropathogenic *Escherichia coli* adhesion and efficiency of antiadhesive compounds using a simple microarray approach. *Anal. Chem.* 90, 12314–12321. doi: 10.1021/acs.analchem.8b04235

Kalograiaki, I., Campanero-Rhodes, M. A., Proverbio, D., Euba, B., Garmendia, J., Aastrup, T., et al. (2018b). Bacterial surface glycans: microarray and QCM strategies for glycophenotyping and exploration of recognition by host receptors. *Methods Enzymol.* 598, 37–70. doi: 10.1016/bs.mie.2017.06.011

Kalograiaki, I., Euba, B., Fernández-Alonso, M. D. C., Proverbio, D., St Geme, J. W. III, Aastrup, T., et al. (2018c). Differential recognition of *Haemophilus influenzae* whole bacterial cells and isolated lipooligosaccharides by galactose-specific lectins. *Sci. Rep.* 8:16292. doi: 10.1038/s41598-018-34383-x

Kalograiaki, I., Euba, B., Proverbio, D., Campanero-Rhodes, M. A., Aastrup, T., Garmendia, J., et al. (2016). Combined bacteria microarray and quartz crystal microbalance approach for exploring glycosignatures of nontypeable *Haemophilus influenzae* and recognition by host lectins. *Anal. Chem.* 88, 5950–5957. doi: 10.1021/acs.analchem.6b00905

Karsunke, X. Y., Niessner, R., and Seidel, M. (2009). Development of a multichannel flow-through chemiluminescence microarray chip for parallel calibration and detection of pathogenic bacteria. *Anal. Bioanal. Chem.* 395, 1623–1630. doi: 10.1007/s00216-009-2905-7

Kilcoyne, M., Twomey, M. E., Gerlach, J. Q., Kane, M., Moran, A. P., and Joshi, L. (2014). *Campylobacter jejuni* strain discrimination and temperature-dependent glycome expression profiling by lectin microarray. *Carbohydr Res.* 389, 123–133. doi: 10.1016/j.carres.2014.02.005

Knirel, Y. A., Gabius, H. J., Blixt, O., Rapoport, E. M., Khasbiullina, N. R., Shilova, N. V., et al. (2014). Human tandem-repeat-type galectins bind bacterial non-betaGal polysaccharides. *Glycoconj J.* 31, 7–12. doi: 10.1007/s10719-013-9497-3

Lameignere, E., Malinovska, L., Slavikova, M., Duchaud, E., Mitchell, E. P., Varrot, A., et al. (2008). Structural basis for mannose recognition by a lectin from opportunistic bacteria *Burkholderia cenocepacia*. *Biochem. J.* 411, 307–318. doi: 10.1042/bj20071276

Leelayuwapan, H., Kangwanrangsan, N., Chawengkirttikul, R., Ponpuak, M., Charlermroj, R., Boonyarattanakalin, K., et al. (2017). Synthesis and immunological studies of the lipomannan backbone glycans found on the surface of *Mycobacterium tuberculosis*. *J. Org. Chem.* 82, 7190–7199. doi: 10.1021/acs.joc.7b00703

Li, Z., and Feizi, T. (2018). The neoglycolipid (NGL) technology-based microarrays and future prospects. *FEBS Lett.* 592, 3976–3991. doi: 10.1002/1873-3468.13217

Lisboa, M. P., Khan, N., Martin, C., Xu, F. F., Reppe, K., Geissner, A., et al. (2017). Semisynthetic glycoconjugate vaccine candidate against *Streptococcus pneumoniae* serotype 5. *Proc. Natl. Acad. Sci. U.S.A.* 114, 11063–11068. doi: 10.1073/pnas.1706875114

Liu, X., Lei, Z., Liu, D. J., and Wang, Z. X. (2016). Development of a sandwiched microarray platform for studying the interactions of antibiotics with *Staphylococcus aureus*. *Anal. Chim. Acta* 917, 93–100. doi: 10.1016/j.aca.2016.02.038

Maolanon, N. N., Blaise, M., Sorensen, K. K., Thygesen, M. B., Cló, E., Sullivan, J. T., et al. (2014). Lipochitin oligosaccharides immobilized through oximes in glycan microarrays bind LysM proteins. *Chembiochem* 15, 425–434. doi: 10.1002/cbic.201300520

Marchetti, R., Malinovska, L., Lameignere, E., Adamova, L., de Castro, C., Cioci, G., et al. (2012). *Burkholderia cenocepacia* lectin A binding to heptoses from the bacterial lipopolysaccharide. *Glycobiology* 22, 1387–1398. doi: 10.1093/glycob/cws105

Marimon, J. M., Monasterio, A., Ercibengoa, M., Pascual, J., Prieto, I., Simón, L., et al. (2010). Antibody microarray typing, a novel technique for *Streptococcus pneumoniae* serotyping. *J. Microbiol. Methods* 80, 274–280. doi: 10.1016/j.mimet.2010.01.011

Marotte, K., Sabin, C., Preville, C., Moume-Pymbock, M., Wimmerova, M., Mitchell, E. P., et al. (2007). X-ray structures and thermodynamics of the interaction of PA-IIL from *Pseudomonas aeruginosa* with disaccharide derivatives. *ChemMedChem* 2, 1328–1338. doi: 10.1002/cmdc.200700100

Martin, C. E., Broecker, F., Eller, S., Oberli, M. A., Anish, C., Pereira, C. L., et al. (2013a). Glycan arrays containing synthetic *Clostridium difficile* lipoteichoic acid oligomers as tools toward a carbohydrate vaccine. *Chem. Commun.* 49, 7159–7161. doi: 10.1039/c3cc43545h

Martin, C. E., Broecker, F., Oberli, M. A., Komor, J., Mattner, J., Anish, C., et al. (2013b). Immunological evaluation of a synthetic *Clostridium difficile*

oligosaccharide conjugate vaccine candidate and identification of a minimal epitope. *J. Am. Chem. Soc.* 135, 9713–9722. doi: 10.1021/ja401410y

Menova, P., Sella, M., Sellrie, K., Pereira, C. L., and Seeberger, P. H. (2018). Identification of the minimal glycotope of *Streptococcus pneumoniae* 7F capsular polysaccharide using synthetic oligosaccharides. *Chemistry* 24, 4181–4187. doi: 10.1002/chem.201705379

Mondani, L., Delannoy, S., Mathey, R., Piat, F., Mercey, T., Slimani, S., et al. (2016). Fast detection of both O157 and non-O157 shiga-toxin producing *Escherichia coli* by real-time optical immunoassay. *Lett. Appl. Microbiol.* 62, 39–46. doi: 10.1111/lam.12503

Mondani, L., Roupioz, Y., Delannoy, S., Fach, P., and Livache, T. (2014). Simultaneous enrichment and optical detection of low levels of stressed *Escherichia coli* O157:H7 in food matrices. *J. Appl. Microbiol.* 117, 537–546. doi: 10.1111/jam.12522

Moonens, K., and Remaut, H. (2017). Evolution and structural dynamics of bacterial glycan binding adhesins. *Curr. Opin. Struct. Biol.* 44, 48–58. doi: 10.1016/j.sbi.2016.12.003

Morley, M., Molony, C. M., Weber, T. M., Devlin, J. L., Ewens, K. G., Spielman, R. S., et al. (2004). Genetic analysis of genome-wide variation in human gene expression. *Nature* 430, 743–747. doi: 10.1038/nature02797

Neelamegham, S., Aoki-Kinoshita, K., Bolton, E., Frank, M., Lisacek, F., Lutteke, T., et al. (2019). Updates to the symbol nomenclature for glycans guidelines. *Glycobiology* 29, 620–624. doi: 10.1093/glycob/cwz045

Oberli, M. A., Hecht, M. L., Bindschadler, P., Adibekian, A., Adam, T., and Seeberger, P. H. (2011). A possible oligosaccharide-conjugate vaccine candidate for *Clostridium difficile* is antigenic and immunogenic. *Chem. Biol.* 18, 580–588. doi: 10.1016/j.chembiol.2011.03.009

Oberli, M. A., Tamborrini, M., Tsai, Y. H., Werz, D. B., Horlacher, T., Adibekian, A., et al. (2010). Molecular analysis of carbohydrate-antibody interactions: case study using a *Bacillus anthracis* tetrasaccharide. *J. Am. Chem. Soc.* 132, 10239–10241. doi: 10.1021/ja104027w

Palma, A. S., Feizi, T., Zhang, Y., Stoll, M. S., Lawson, A. M., Díaz-Rodríguez, E., et al. (2006). Ligands for the beta-glucan receptor, Dectin-1, assigned using "designer" microarrays of oligosaccharide probes (neoglycolipids) generated from glucan polysaccharides. *J. Biol. Chem.* 281, 5771–5779. doi: 10.1074/jbc.M511461200

Palma, A. S., Liu, Y., Zhang, H., Zhang, Y., McCleary, B. V., Yu, G., et al. (2015). Unravelling glucan recognition systems by glycome microarrays using the designer approach and mass spectrometry. *Mol. Cell Prot.* 14, 974–988. doi: 10.1074/mcp.M115.048272

Parameswarappa, S. G., Reppe, K., Geissner, A., Menova, P., Govindan, S., Calow, A. D. J., et al. (2016). A semi-synthetic oligosaccharide conjugate vaccine candidate confers protection against *Streptococcus pneumoniae* Serotype 3 Infection. *Cell Chem. Biol.* 23, 1407–1416. doi: 10.1016/j.chembiol.2016.09.016

Parro, V., de Diego-Castilla, G., Moreno-Paz, M., Blanco, Y., Cruz-Gil, P., Rodríguez-Manfredi, J. A., et al. (2011). A microbial oasis in the hypersaline Atacama subsurface discovered by a life detector chip: implications for the search for life on Mars. *Astrobiology* 11, 969–996. doi: 10.1089/ast.2011.0654

Parthasarathy, N., DeShazer, D., England, M., and Waag, D. M. (2006). Polysaccharide microarray technology for the detection of *Burkholderia pseudomallei* and *Burkholderia mallei* antibodies. *Diagn. Microbiol. Infect. Dis.* 56, 329–332. doi: 10.1016/j.diagmicrobio.2006.04.018

Parthasarathy, N., DeShazer, D., Peacock, S. J., Wuthiekanun, V., England, M. J., Norris, S. L., et al. (2008). Application of polysaccharide microarray technology for the serodiagnosis of *Burkholderia pseudomallei* infection (melioidosis) in humans. *J. Carbohydr. Chem.* 27, 32–40. doi: 10.1080/07328300802030761

Poole, J., Day, C. J., von Itzstein, M., Paton, J. C., and Jennings, M. P. (2018). Glycointeractions in bacterial pathogenesis. *Nat. Rev. Microbiol.* 16, 440–452. doi: 10.1038/s41579-018-0007-2

Prados-Rosales, R., Carreño, L., Cheng, T., Blanc, C., Weinrick, B., Malek, A., et al. (2017). Enhanced control of *Mycobacterium tuberculosis* extrapulmonary dissemination in mice by an arabinomannan-protein conjugate vaccine. *PLoS Pathog.* 13:e1006250. doi: 10.1371/journal.ppat.1006250

Puente-Sánchez, F., Moreno-Paz, M., Rivas, L. A., Cruz-Gil, P., García-Villadangos, M., Gómez, M. J., et al. (2014). Deep subsurface sulfate reduction and methanogenesis in the Iberian Pyrite Belt revealed through geochemistry and molecular biomarkers. *Geobiology* 12, 34–47. doi: 10.1111/gbi.12065

Reinhardt, A., Wehle, M., Geissner, A., Crouch, E. C., Kang, Y., Yang, Y., et al. (2016). Structure binding relationship of human surfactant protein D and various lipopolysaccharide inner core structures. *J. Struct. Biol.* 195, 387–395. doi: 10.1016/j.jsb.2016.06.019

Reinhardt, A., Yang, Y., Claus, H., Pereira, C. L., Cox, A. D., Vogel, U., et al. (2015). Antigenic potential of a highly conserved *Neisseria meningitidis* lipopolysaccharide inner core structure defined by chemical synthesis. *Chem. Biol.* 22, 38–49. doi: 10.1016/j.chembiol.2014.11.016

Rivas, L. A., García-Villadangos, M., Moreno-Paz, M., Cruz-Gil, P., Gómez-Elvira, J., and Parro, V. (2008). A 200-antibody microarray biochip for environmental monitoring: searching for universal microbial biomarkers through immunoprofiling. *Anal. Chem.* 80, 7970–7979. doi: 10.1021/ac8008093

Salton, M. R. J., and Kim, K. S. (1996). "Structure," in *Medical Microbiology*, ed. S. Baron, (Galveston, TX: University of Texas).

Saucedo, N. M., Gao, Y. N., Pham, T., and Mulchandani, A. (2018). Lectin- and saccharide-functionalized nano-chemiresistor arrays for detection and identification of pathogenic bacteria infection. *Biosens. Basel* 8:63. doi: 10.3390/bios8030063

Seeberger, P. H., Pereira, C. L., Khan, N., Xiao, G., Diago-Navarro, E., Reppe, K., et al. (2017). A semi-synthetic glycoconjugate vaccine candidate for carbapenem-resistant *Klebsiella pneumoniae*. *Angew Chem. Int. Engl.* 56, 13973–13978. doi: 10.1002/anie.201700964

Semchenko, E. A., Day, C. J., Moutin, M., Wilson, J. C., Tiralongo, J., and Korolik, V. (2012a). Structural heterogeneity of terminal glycans in *Campylobacter jejuni* lipooligosaccharides. *PloS one* 7:e40920. doi: 10.1371/journal.pone.0040920

Semchenko, E. A., Moutin, M., Korolik, V., Tiralongo, J., and Day, C. J. (2012b). Lectin array analysis of purified lipooligosaccharide: a method for the determination of molecular mimicry. *J. Glycomics Lipidomics* 2:103. doi: 10.4172/2153-0637.1000103

Solís, D., Bovin, N. V., Davis, A. P., Jiménez-Barbero, J., Romero, A., Roy, R., et al. (2015). A guide into glycosciences: how chemistry, biochemistry and biology cooperate to crack the sugar code. *Biochim. Biophys. Acta Gen. Sub.* 1850, 186–235. doi: 10.1016/j.bbagen.2014.03.016

Sorensen, K. K., Simonsen, J. B., Maolanon, N. N., Stougaard, J., and Jensen, K. J. (2014). Chemically synthesized 58-mer LysM domain binds lipochitin oligosaccharide. *Chembiochem* 15, 2097–2105. doi: 10.1002/cbic.201402125

Stowell, S. R., Arthur, C. M., McBride, R., Berger, O., Razi, N., Heimburg-Molinaro, J., et al. (2014). Microbial glycan microarrays define key features of host-microbial interactions. *Nat. Chem. Biol.* 10, 470–476. doi: 10.1038/nchembio.1525

Sukhithasri, V., Nisha, N., Biswas, L., Kumar, V. A., and Biswas, R. (2013). Innate immune recognition of microbial cell wall components and microbial strategies to evade such recognitions. *Microbiol. Res.* 168, 396–406. doi: 10.1016/j.micres.2013.02.005

Sulak, O., Cioci, G., Lameignere, E., Balloy, V., Round, A., Gutsche, I., et al. (2011). *Burkholderia cenocepacia* BC2L-C is a super lectin with dual specificity and proinflammatory activity. *PLoS Pathog.* 7:e1002238. doi: 10.1371/journal.ppat.1002238

Tamborrini, M., Bauer, M., Bolz, M., Maho, A., Oberli, M. A., Werz, D. B., et al. (2011). Identification of an African *Bacillus anthracis* lineage that lacks expression of the spore surface-associated anthrose-containing oligosaccharide. *J. Bacteriol.* 193, 3506–3511. doi: 10.1128/JB.00078-11

Tao, S. C., Li, Y., Zhou, J., Qian, J., Schnaar, R. L., Zhang, Y., et al. (2008). Lectin microarrays identify cell-specific and functionally significant cell surface glycan markers. *Glycobiology* 18, 761–769. doi: 10.1093/glycob/cwn063

Templier, V., Livache, T., Boisset, S., Maurin, M., Slimani, S., Mathey, R., et al. (2017). Biochips for direct detection and identification of bacteria in blood culture-like conditions. *Sci. Rep.* 7:9457. doi: 10.1038/s41598-017-10072-z

Thirumalapura, N. R., Morton, R. J., Ramachandran, A., and Malayer, J. R. (2005). Lipopolysaccharide microarrays for the detection of antibodies. *J. Immunol. Methods* 298, 73–81. doi: 10.1016/j.jim.2005.01.004

Thirumalapura, N. R., Ramachandran, A., Morton, R. J., and Malayer, J. R. (2006). Bacterial cell microarrays for the detection and characterization of antibodies against surface antigens. *J. Immunol. Methods* 309, 48–54. doi: 10.1016/j.jim.2005.11.016

Tong, M., Jacobi, C. E., van de Rijke, F. M., Kuijper, S., van de Werken, S., Lowary, T. L., et al. (2005). A multiplexed and miniaturized serological tuberculosis assay identifies antigens that discriminate maximally between TB

and non-TB sera. *J. Immunol. Methods* 301, 154–163. doi: 10.1016/j.jim.2005.04.004

van der Es, D., Berni, F., Hogendorf, W. F. J., Meeuwenoord, N., Laverde, D., van Diepen, A., et al. (2018). Streamlined synthesis and evaluation of teichoic acid fragments. *Chemistry* 24, 4014–4018. doi: 10.1002/chem.201800153

Varki, A., Cummings, R. D., Aebi, M., Packer, N. H., Seeberger, P. H., Esko, J. D., et al. (2015). Symbol Nomenclature for graphical representations of glycans. *Glycobiology* 25, 1323–1324. doi: 10.1093/glycob/cwv091

Wang, D., Carroll, G. T., Turro, N. J., Koberstein, J. T., Kovac, P., Saksena, R., et al. (2007). Photogenerated glycan arrays identify immunogenic sugar moieties of *Bacillus anthracis* exosporium. *Proteomics* 7, 180–184. doi: 10.1002/pmic.200600478

Wang, D., Liu, S., Trummer, B. J., Deng, C., and Wang, A. (2002). Carbohydrate microarrays for the recognition of cross-reactive molecular markers of microbes and host cells. *Nat. Biotechnol.* 20, 275–281. doi: 10.1038/nbt0302-275

Wang, N., Hirata, A., Nokihara, K., Fukase, K., and Fujimoto, Y. (2016). Peptidoglycan microarray as a novel tool to explore protein-ligand recognition. *Biopolymers* 106, 422–429. doi: 10.1002/bip.22807

Wesener, D. A., Dugan, A., and Kiessling, L. L. (2017). Recognition of microbial glycans by soluble human lectins. *Curr. Opin. Struct. Biol.* 44, 168–178. doi: 10.1016/j.sbi.2017.04.002

Wesener, D. A., Wangkanont, K., McBride, R., Song, X., Kraft, M. B., Hodges, H. L., et al. (2015). Recognition of microbial glycans by human intelectin-1. *Nat. Struct. Mol. Biol.* 22, 603–610. doi: 10.1038/nsmb.3053

Wolter, A., Niessner, R., and Seidel, M. (2008). Detection of *Escherichia coli* O157:H7, *Salmonella typhimurium*, and *Legionella pneumophila* in water using a flow-through chemiluminescence microarray readout system. *Anal. Chem.* 80, 5854–5863. doi: 10.1021/ac800318b

Yasuda, E., Tateno, H., Hirabayashi, J., Iino, T., and Sako, T. (2011). Lectin microarray reveals binding profiles of *Lactobacillus casei* strains in a comprehensive analysis of bacterial cell wall polysaccharides. *Appl. Environ. Microbiol.* 77, 4539–4546. doi: 10.1128/AEM.00240-11

Zhang, H., Palma, A. S., Zhang, Y., Childs, R. A., Liu, Y., Mitchell, D. A., et al. (2016). Generation and characterization of beta1,2-gluco-oligosaccharide probes from *Brucella abortus* cyclic beta-glucan and their recognition by C-type lectins of the immune system. *Glycobiology* 26, 1086–1096. doi: 10.1093/glycob/cww041

Zheng, L. B., Wan, Y., Qi, P., Sun, Y., Zhang, D., and Yu, L. M. (2017). Lectin functionalized ZnO nanoarrays as a 3D nano-biointerface for bacterial detection. *Talanta* 167, 600–606. doi: 10.1016/j.talanta.2017.03.007

Zheng, R. B., Jégouzo, S. A. F., Joe, M., Bai, Y., Tran, H. A., Shen, K., et al. (2017). Insights into interactions of mycobacteria with the host innate immune system from a novel array of synthetic mycobacterial glycans. *ACS Chem. Biol.* 12, 2990–3002. doi: 10.1021/acschembio.7b00797

Zhu, H., Bilgin, M., Bangham, R., Hall, D., Casamayor, A., Bertone, P., et al. (2001). Global analysis of protein activities using proteome chips. *Science* 293, 2101–2105. doi: 10.1126/science.1062191

Conflict of Interest: The authors declare that the research was conducted in the absence of any commercial or financial relationships that could be construed as a potential conflict of interest.

frontiers in Microbiology

ORIGINAL RESEARCH
published: 20 March 2020
doi: 10.3389/fmicb.2020.00397

Binding of Phage-Encoded FlaGrab to Motile *Campylobacter jejuni* Flagella Inhibits Growth, Downregulates Energy Metabolism, and Requires Specific Flagellar Glycans

*Jessica C. Sacher[1], Asif Shajahan[2], James Butcher[3], Robert T. Patry[2,4], Annika Flint[3], David R. Hendrixson[5], Alain Stintzi[3], Parastoo Azadi[2] and Christine M. Szymanski[1,2,4]**

[1] Department of Biological Sciences, University of Alberta, Edmonton, AB, Canada, [2] Complex Carbohydrate Research Center, University of Georgia, Athens, GA, United States, [3] Ottawa Institute of Systems Biology, University of Ottawa, Ottawa, ON, Canada, [4] Department of Microbiology, University of Georgia, Athens, GA, United States, [5] Department of Microbiology, University of Texas Southwestern Medical Center, Dallas, TX, United States

OPEN ACCESS

Edited by:
Felipe Cava,
Umeå University, Sweden

Reviewed by:
Orhan Sahin,
Iowa State University, United States
Christopher James Day,
Griffith University, Australia

***Correspondence:**
Christine M. Szymanski
cszymans@uga.edu

Specialty section:
This article was submitted to Infectious Diseases, a section of the journal Frontiers in Microbiology

Received: *02 November 2019*
Accepted: *26 February 2020*
Published: *20 March 2020*

Citation:
Sacher JC, Shajahan A, Butcher J, Patry RT, Flint A, Hendrixson DR, Stintzi A, Azadi P and Szymanski CM (2020) Binding of Phage-Encoded FlaGrab to Motile Campylobacter jejuni Flagella Inhibits Growth, Downregulates Energy Metabolism, and Requires Specific Flagellar Glycans. Front. Microbiol. 11:397. doi: 10.3389/fmicb.2020.00397

Many bacterial pathogens display glycosylated surface structures that contribute to virulence, and targeting these structures is a viable strategy for pathogen control. The foodborne pathogen *Campylobacter jejuni* expresses a vast diversity of flagellar glycans, and flagellar glycosylation is essential for its virulence. Little is known about why *C. jejuni* encodes such a diverse set of flagellar glycans, but it has been hypothesized that evolutionary pressure from bacteriophages (phages) may have contributed to this diversity. However, interactions between *Campylobacter* phages and host flagellar glycans have not been characterized in detail. Previously, we observed that Gp047 (now renamed FlaGrab), a conserved *Campylobacter* phage protein, binds to *C. jejuni* flagella displaying the nine-carbon monosaccharide 7-acetamidino-pseudaminic acid, and that this binding partially inhibits cell growth. However, the mechanism of this growth inhibition, as well as how *C. jejuni* might resist this activity, are not well-understood. Here we use RNA-Seq to show that FlaGrab exposure leads *C. jejuni* 11168 cells to downregulate expression of energy metabolism genes, and that FlaGrab-induced growth inhibition is dependent on motile flagella. Our results are consistent with a model whereby FlaGrab binding transmits a signal through flagella that leads to retarded cell growth. To evaluate mechanisms of FlaGrab resistance in *C. jejuni,* we characterized the flagellar glycans and flagellar glycosylation loci of two *C. jejuni* strains naturally resistant to FlaGrab binding. Our results point toward flagellar glycan diversity as the mechanism of resistance to FlaGrab. Overall, we have further characterized the interaction between this phage-encoded flagellar glycan-binding protein and *C. jejuni*, both in terms of mechanism of action and mechanism of resistance. Our results suggest that *C. jejuni* encodes as-yet unidentified mechanisms for generating flagellar glycan diversity, and point to phage proteins as exciting lenses through which to study bacterial surface glycans.

Keywords: bacteriophages, *Campylobacter jejuni*, flagella, protein glycosylation, pseudaminic acid, mass spectrometry, motility, bacterial surface structures

INTRODUCTION

Targeting bacterial virulence without threatening essential cellular processes is a strategy that can help minimize antimicrobial resistance (Heras et al., 2015). Many bacterial pathogens display glycosylated surface structures that promote virulence in human and animal hosts, making these structures attractive drug targets (Szymanski and Wren, 2005). However, understanding the role and diversity of bacterial surface glycans has lagged behind other fields of biology, due in part to a lack of a predictable code for their synthesis, difficulties in characterizing the detected glycans, and a lack of appropriate reagents with specificity for bacterial glycans, which are much more diverse at the monosaccharide level than those found in eukaryotes.

Campylobacter jejuni causes severe diarrheal disease around the world (Bolton, 2015) and has been associated with human growth stunting in low-resource settings (Amour et al., 2016). *C. jejuni* relies on glycosylated flagella to colonize the gastrointestinal epithelium of humans and animals (Guerry, 2007). Its flagellin proteins (FlaA and FlaB) are among the most heavily glycosylated bacterial proteins known (Logan, 2006), with up to 10% of their molecular weight due to glycans (Guerry and Szymanski, 2008). Unlike some other flagellated bacterial pathogens, such as *Pseudomonas aeruginosa,* whose flagella assemble with or without glycosylation (Schirm et al., 2004), flagellar glycosylation is essential to *C. jejuni* flagellar filament biogenesis, and is thus essential for its motility and virulence (Goon et al., 2003; Logan, 2006). The importance of glycosylated flagella to *C. jejuni* is further illustrated by the fact that it devotes approximately 3% of its small, 1.6-Mb genome to genes associated with flagellar glycosylation, and that two of its three sigma factors are devoted to regulating flagellar biosynthesis and glycosylation (Logan, 2006). Given the importance of flagellar glycosylation to *C. jejuni* virulence and the high proportion of genetic resources it devotes to this process, understanding *C. jejuni* flagellar glycosylation has a high likelihood of generating key insights toward better controlling this pathogen.

Campylobacter species glycosylate their flagella with two major nonulosonic acids (nine-carbon sugars): pseudaminic acid (5,7-diacetamido-3,5,7,9-tetradeoxy-L-*glycero*-α-L-*manno*-nonulosonic acid, also known as Pse5Ac7Ac or Pse) and legionaminic acid (5,7-diamino-3,5,7,9-tetradeoxy-D-*glycero*-D-*galacto*-nonulosonic acid, also known as Leg5Ac7Ac or Leg), both of which have a molecular mass of ∼316 Da. In addition, several derivatives of these glycans have been identified on *C. jejuni* flagella to date. The genetic and biochemical pathways for biosynthesis of many of these glycans have been studied extensively in *C. jejuni* and *Campylobacter coli;* this has primarily been done by analyzing trypsin-digested flagella by mass spectrometry (MS) and by analyzing nucleotide-activated flagellar glycan precursors in the cytoplasm of defined mutants using MS and nuclear magnetic resonance (NMR) spectroscopy (Guerry et al., 1990, 1991, 2006; Thibault et al., 2001; Logan et al., 2002; Goon et al., 2003; Schirm et al., 2003, 2005; Szymanski et al., 2003; McNally et al., 2006, 2007; Schoenhofen et al., 2006; Guerry, 2007; Ewing et al., 2009; Howard et al., 2009). However, these methods are technically demanding, expensive, and time-intensive, and thus the already impressive repertoire of *Campylobacter* flagellar glycans has come from the analysis of only a few strains. Furthermore, linking genotype with phenotype in this organism, especially in the context of flagellar biogenesis and modification, is complicated by the presence of phase-variable polynucleotide tracts in genes encoding glycosylation enzymes. This leads to frequent on/off switching of genes (∼1/1,000 generations) due to slipped-strand mispairing during DNA replication (Lango-Scholey et al., 2016). For example, *C. jejuni* 11168, the first genome-sequenced strain of the species, harbors poly-deoxyguanosine (poly-G) tracts in at least 28 of its genes (Parkhill et al., 2000; Lango-Scholey et al., 2016), 10 of which are found within its ∼50-gene flagellar glycosylation locus (Hitchen et al., 2010). Given these challenges, much of the diversity in *Campylobacter* flagellar glycans, as well as the mechanisms that drive this diversity, remain unknown.

Bacteriophages (phages), viruses specific for bacteria, commonly target bacterial surface structures, many of which are glycosylated (Simpson et al., 2015). It follows that evolutionary pressure from phages has likely contributed to driving the diversity in bacterial surface glycans. *Campylobacter* phages are known to recognize host cells by binding to glycosylated surface structures, such as flagella (Baldvinsson et al., 2014) and capsular polysaccharide (CPS) (Sørensen et al., 2011; Gencay et al., 2018); however, these interactions have not been characterized in detail. Previously, we observed that Gp047 (now renamed FlaGrab), a conserved *Campylobacter* phage protein (Javed et al., 2014), binds to *C. jejuni* flagella displaying the nine-carbon monosaccharide 7-acetamidino-pseudaminic acid (Pse5Ac7Am) (Javed et al., 2015a), and that this binding inhibits cell growth (Javed et al., 2015b). However, the mechanism of this growth inhibition, as well as how *C. jejuni* might resist this activity, are not well-understood.

The aim of this study was to better characterize the interaction between phage-encoded FlaGrab and *C. jejuni* cells from two perspectives: (1) how FlaGrab exerts its growth inhibitory activity, and (2) how cells are able to resist this activity. We hypothesized that FlaGrab binding to *C. jejuni* flagella would create increased drag that would signal cells to alter gene expression in a way that would slow cell growth. To test this, we used RNA-Seq to observe changes in gene expression in response to FlaGrab, and examined the role of flagellar motility in FlaGrab activity. We hypothesized that *C. jejuni* might resist FlaGrab activity by displaying flagellar glycans different from those expressed by FlaGrab-susceptible strains. To test this, we used transmission electron microscopy and immunogold labeling to analyze whether *C. jejuni* strains resistant to FlaGrab activity evaded binding by the protein. To understand the mechanism by which strains were able to evade binding, we examined the flagellar glycosylation genetic loci and used mass spectrometry to characterize the flagellar glycans of FlaGrab-resistant strains. Our results show that FlaGrab binding to motile *C. jejuni* flagella leads to changes in expression of energy metabolism genes, and that cells resistant to this binding display altered flagellar glycans.

MATERIALS AND METHODS

Bacterial Growth Conditions

C. jejuni strains were grown on NZCYM (Difco) agar, supplemented with 50 μg/mL kanamycin where needed, at 37°C under microaerobic conditions (85% N_2, 10% CO_2, 5% O_2). *E. coli* was grown on LB agar supplemented with 50 μg/mL kanamycin where needed. The list and sources of bacterial strains used in this study are given in **Table 1**.

Expression and Purification of FlaGrab and Its Derivatives

FlaGrab was expressed as an N-terminal glutathione-S-transferase (GST) fusion protein as described previously (Kropinski et al., 2011). CC-FlaGrab [the C-terminal quarter of FlaGrab, previously shown to harbor the growth inhibitory activity (Javed et al., 2015b)] and NC-FlaGrab [the N-terminal quarter of FlaGrab, previously shown to retain no growth inhibitory activity (Javed et al., 2015b)] were expressed in *E. coli* BL21 as GST-fused proteins and purified as described previously (Javed et al., 2013), with the exception that proteins were eluted in 10 mM reduced L-glutathione, 50 mM HEPES, and 1 mM DTT at pH 9.0. The list of plasmids used in this study are listed in **Table 1**.

Total RNA Extraction

Cells were harvested from overnight NZCYM plate cultures, pelleted and washed once in NZCYM broth and set to an OD_{600} of 0.05 (2×10^8 CFU/mL) in 20 mL NZCYM broth in 125-mL Erlenmeyer flasks. Cells were grown under microaerobic conditions with agitation at 200 rpm. After 4.5 h incubation, CC-FlaGrab was added to a final concentration of 25 μg/mL. As negative controls, 6 mL HEPES buffer or 6 mL NC-FlaGrab were used. Flasks were incubated 30 min before the entire contents of each was harvested and the RNA stabilized using 0.1 volumes of ice cold 10% buffered phenol in 100% ethanol (Palyada et al., 2004). Total RNA was extracted from each sample using a hot phenol method as previously described (Palyada et al., 2004). Genomic DNA was removed from the samples using RNAse-free DNAse I (Epicenter) (37°C for 30 min) and cleaned using the Zymo RNA Clean & Concentrator. PCR was used to confirm the absence of residual DNA and the DNase treatment was repeated until the absence of genomic DNA was confirmed. Total RNA quality was assessed using an Agilent Bioanalyzer and RNA was stored at −80°C until further use. This experiment was done in biological triplicate, with the exception of the NC-FlaGrab control, which was done only once.

TABLE 1 | List of bacterial strains and plasmids used in this study.

Name	Source	References
C. jejuni NCTC 11168 (MP21)	Human enteropathy	Gundogdu et al., 2007
C. jejuni NCTC 12567	Chicken	McNally et al., 2007
C. jejuni NCTC 12660	Chicken	Frost et al., 1999
C. jejuni NCTC 12661	Pigeon	Frost et al., 1999
C. jejuni NCTC 12664	Chicken	Frost et al., 1999
C. jejuni NCTC 11168 Δ*cj1295*	*C. jejuni* NCTC 11168 (MP21)	This work
C. jejuni 11168 Δ*motA*	*C. jejuni* 11168 (MP21)	This work
C. jejuni 11168 Δ*motB*	*C. jejuni* 11168 (MP21)	This work
pGEX_*ccgp047*	Expression construct of GST-fused CC-Gp047 (CC-FlaGrab) in pGEX 6P-2	Javed et al., 2013
pGEX_*ncgp047*	Expression construct of GST-fused NC-Gp047 (NC-FlaGrab) in pGEX 6P-2	Javed et al., 2013
pDRH3330 (pUC19::*motA*-cat-*rpsL*)	*motA* mutagenesis construct	Beeby et al., 2016
pDRH3331 (pUC19::*motB*-cat-*rpsL*)	*motB* mutagenesis construct	Beeby et al., 2016

RNA Sequencing

Samples were subsequently depleted of rRNA using the RiboZero Bacterial kit according to the manufacturer's instructions and rRNA depletion was confirmed using the Agilent Bioanalyzer RNA 6000 Pico Kit. The Ion Total RNA-seq kit was used to construct strand-specific barcoded sequencing libraries according to the manufacturer's instructions. Following library construction, each library was quality-checked and quantified using the Bioanalyzer High Sensitivity DNA kit. Once all libraries were completed, they were pooled together in equimolar amounts and were templated using the Ion PI Hi-Q kit. The templated beads were sequenced on an Ion Torrent Proton using the Ion PI Hi-Q sequencing 200 kit on a single Proton V2 chip.

The raw sequencing reads were demultiplexed by the Ion Torrent suite software and mapped to the 11168 genome using STAR (Love et al., 2014). The raw demultiplexed sequencing reads have been deposited at the NCBI SRA archive under accession number PRJNA580017. Reads aligning to coding regions were counted using HT-seq using the default settings (Dobin et al., 2013). DESeq2 was used to identify differentially expressed transcripts between the control and CC-FlaGrab treated cells. Genes with a false discovery rate (FDR)-corrected $p < 0.05$ were considered differentially expressed. We also conducted gene set enrichment analysis (GSEA) on *C. jejuni* Kyoto Encyclopedia of Genes and Genomes (KEGG) pathways using the generally applicable gene set enrichment (GAGE) method (Luo et al., 2009) with a minimum FDR cutoff of <0.1 (Love et al., 2014).

Generation of *motA, motB,* and *cj1295* Mutants

To generate *motA* and *motB* mutants, *C. jejuni* 11168 was transformed by natural transformation with the pDRH3330 (*motA*) or pDRH3331 (*motB*) mutation constructs published by Beeby et al. (2016). To generate a *cj1295* mutant, *C. jejuni* 11168 was naturally transformed with the *cj1295* mutation construct (p1295) described by Hitchen et al. (2010).

For natural transformation of mutant constructs, an overnight culture of *C. jejuni* cells was streaked onto BHI containing 2% yeast extract (BHIY), grown for 6 h under the conditions described above, and harvested into PBS. Cells were washed

once in PBS, resuspended in 250 μL PBS, spotted (20–30 × 10-μL spots) onto pre-warmed (37°C) BHIY plates and allowed to absorb into agar ∼5 min. p1295 DNA (20 μg/mL in water) was spotted (∼10-μL spots) atop each spot of cell suspension and allowed to dry ∼5 min. Plates were incubated for 12–16 h, then the contents of the plates were harvested and spread or streaked across 4–6 BHI plates containing 50 μg/mL kanamycin. Plates were incubated until colonies appeared (3–5 days). Isolated colonies were patched onto kanamycin-containing BHI plates and grown overnight prior to confirmation of successful mutagenesis by colony PCR (OneTaq, NEB) using gene-specific primers (Hitchen et al., 2010; Beeby et al., 2016). This protocol has been deposited into Protocols.io (dx.doi.org/10.17504/protocols.io.magc2bw).

Immunogold Labeling and Transmission Electron Microscopy

Immunogold labeling and transmission electron microscopy was done as described previously (Javed et al., 2015a), with some exceptions. Briefly, *C. jejuni* cells (OD_{600} = 3.0) were harvested from a plate of overnight growth in NZCYM broth, incubated with Formvar-coated copper grids for 45 min, washed 1 × 3 min with PBS, then fixed by incubating in 2.5% paraformaldehyde in PBS for 20 min. Grids were then washed 3 × 3 min with PBS, incubated in blocking solution (PBS containing 5% bovine serum albumin and 0.05% Tween) for 35 min, then in freshly purified GST-tagged FlaGrab (0.2 mg/mL diluted 1:25 in blocking solution) for 45 min. Grids were then washed 3 × 3 min in blocking solution, incubated in a rabbit anti-FlaGrab antibody solution (diluted 1:50 in blocking solution) for 45 min, washed 3 × 3 min as above, and incubated in a solution of goat anti-rabbit IgG (whole molecule) conjugated to 10-nm gold particles (Sigma, diluted 1:50 in blocking solution) for 45 min. Finally, grids were sequentially washed (3 × 3 min each) with blocking solution, PBS, and distilled water, then air-dried on Whatman filter paper overnight. All steps were done at room temperature. Grids were examined using a transmission electron microscope (JEOL JEM1011; JEOL, Inc., Peabody, MA, USA). Images were captured using a high contrast 2k × 2k mid-mount digital camera (Advanced Microscopy Techniques, Corp., Woburn, MA, USA). This protocol has been deposited into Protocols.io (dx.doi.org/10.17504/protocols.io.mv5c686).

FlaGrab Growth Clearance Assay

Bacterial growth clearance was tested by spotting phage protein onto a freshly inoculated bacterial suspension using the overlay agar method described previously, with some modifications (Javed et al., 2015b). Briefly, overnight bacterial cultures were harvested in NZCYM broth and set to an OD_{600} of 0.35. A 5-mL aliquot of this suspension was transferred to a standard sized empty Petri dish and incubated at 37°C without shaking for 4 h under microaerobic conditions. The suspension was then set to an OD_{600} of 0.5, and 200 μL of this was mixed with 5 mL sterile 0.6% molten NZCYM agar at 45°C. This suspension was poured onto the surface of a pre-warmed (37°C) NZCYM plate containing 1.5% agar. Plates were allowed to solidify for 15 min and then 10 μL UV-sterilized FlaGrab or CC-FlaGrab solution (0.91–1.3 mg/mL in 10 mM reduced L-glutathione, 50 mM Tris, 1 mM DTT, pH 9.0) was spotted onto the agar surface and allowed to completely soak into the agar before inverting the plate and incubating at 37°C under microaerobic conditions. Zones of growth clearance were observed after 18–24 h.

Sequence Alignments and Analysis

Nucleic acid sequence information for *cj1293-cj1342* (the flagellar glycosylation locus in 11168) for strains 11168, 12567, 12660, 12661, and 12664 was obtained from NCBI (Gundogdu et al., 2007; Sacher et al., 2018a,b). Nucleotide and amino acid sequence alignments and phylogenetic trees were generated using Geneious version 8 [http://www.geneious.com (Kearse et al., 2012)]. Alignment figures were generated using T-Coffee (Di Tommaso et al., 2011) and Boxshade (http://sourceforge.net/projects/boxshade/). Black shading indicates the consensus sequence, gray shading indicates similar residues.

Preparation of Cell-Free Flagella for MS

Cell-free flagella were prepared for MS as described previously with some modifications (Javed et al., 2015a). Briefly, bacterial growth was harvested from 20 to 40 NZCYM agar plates, washed with PBS and resuspended in 100–150 mL PBS and stored up to 7 days at −80°C. Cells were thawed by vortexing and flagella were sheared from cells using a Polytron homogenizer for 6 × 30 s (allowing 30 s incubation on ice between rounds) at max rpm on ice. Cells were then removed by centrifugation at 8,700 × g for 20 min at 4°C. To collect flagellar filaments, the resulting supernatant was ultracentrifuged at 207,870 × g, 4°C for 1.5 h using 6 × 30-mL tubes (Beckman). Pellets were washed 3 times by resuspending each pellet in 20 mL distilled water and ultracentrifuging again as above, giving a total of 4 × 1.5 h ultracentrifuge runs. After washing, pellets were resuspended and pooled into a total of 1 ml distilled water and incubated at −20°C until use.

Flagellin Protease Digestion

First, 100 μg of flagella protein sample was dissolved in 25 μL of digestion buffer [50 mM aqueous ammonium bicarbonate (NH_4HCO_3) buffer]. Then, 25 μL of dithiothreitol (DTT) solution (25 mM) was added to the samples and incubated at 45°C for 45 min. Subsequently, carbamidomethylation was performed by adding 25 μL of iodoacetamide (IAA) solution (90 mM) and incubating at room temperature for 45 min in the dark. The sample was then dialyzed against double distilled water and lyophilized. Flagellin was digested by adding 12.5 μL sequencing-grade trypsin (Promega, 0.4 μg/μL) and incubating at 37°C for 12 h. The digest was desalted by C18 solid phase extraction cartridges and then dried under a speed vacuum. The peptides and glycopeptides were subsequently re-dissolved in 0.1% formic acid in water and stored at −30°C until analysis by nano-LC-MS/MS.

Nano-LC-MS/MS Acquisition

Desalted flagellin digests were analyzed on an Orbitrap Fusion Tribrid mass spectrometer (Thermo Scientific) equipped with a nanospray ion source and connected to a Dionex binary solvent system. Pre-packed nano-LC columns (15 cm in length, 75 μm in internal diameter) filled with 3 μm C18 material were used for chromatographic separation of glycoprotein digests. Precursor ion scanning was performed at 120,000 resolution in an Orbitrap analyzer, and precursors at a time frame of 3 s were selected for subsequent fragmentation using higher energy collision dissociation (HCD) at a normalized collision energy of 28 and collision-induced dissociation (CID) at an energy of 35. The threshold for triggering an MS/MS event was set to 500 counts. The fragment ions were analyzed on an Orbitrap after HCD and CID fragmentation at a resolution of 30,000. Charge state screening was enabled, and precursors with unknown charge state or a charge state of +1 were excluded (positive ion mode). Dynamic exclusion was enabled with an exclusion duration of 10 sec.

MS Data Analysis

The LC-MS/MS spectra of the tryptic digest of proteins were searched against the FlaA and FlaB protein sequence of the respective strains in FASTA format using Byonic 2.3 software with trypsin as the digestion enzyme. Carbamidomethylation of cysteine and oxidation of methionine were selected as variable modifications. Glycan modifications such as Pse5Ac7Ac (m/z = 316.12705), Pse5Ac7Am (m/z = 315.14304), DMGA-Pse5Ac7Ac (m/z = 390.16383), and DMGA-Pse5Ac7Am (m/z = 389.17981) were used as variable modifications on serines/threonines. The LC-MS/MS spectra were analyzed manually for the glycopeptide fragmentation on HCD and CID with the support of Xcalibur software. To identify glycans, the spectra of the glycopeptides were evaluated for glycan neutral loss patterns, oxonium ions, and glycopeptide fragmentations. Unknown derivatives of pseudaminic acid were identified based on the presence of oxonium ions and neutral losses on the spectra of glycopeptides bearing glycosylation sites.

RESULTS

FlaGrab-Treated Cells Upregulate Membrane Proteins and Downregulate TCA Cycle Genes

To determine the mechanism of FlaGrab growth inhibition of *C. jejuni* 11168 cells, we sequenced total mRNA (RNA-seq) from cells incubated with CC-FlaGrab [the C-terminal quarter of FlaGrab, previously shown to possess the growth inhibitory activity (Javed et al., 2015b)] for 30 min and compared their transcriptomic profiles with cells incubated with buffer. As an additional negative control, we extracted RNA from buffer-exposed cells and from cells exposed to NC-FlaGrab (the N-terminal quarter of FlaGrab, previously shown to retain no growth inhibitory activity). PCA plot analysis of all samples showed that the NC-FlaGrab clustered with the buffer controls, suggesting that FlaGrab only impacts gene expression when capable of binding to host targets (**Figure S1**).

Incubating *C. jejuni* 11168 with CC-FlaGrab altered the expression of genes encoding energy metabolism enzymes, membrane proteins, and periplasmic proteins (**Figure 1** and **Table 2**). Upregulated genes include *omp50,* which encodes a major *C. jejuni* porin and phosphotyrosine kinase also known as Cjtk (Corcionivoschi et al., 2012). Other upregulated genes include *cj1169c* (a periplasmic protein-encoding gene upstream of *omp50*); *cj0037c* (cccC), which encodes cytochrome C (Guccione et al., 2017); *dsbI*, which encodes a disulfide bond forming protein; *tlp4,* which encodes a chemotaxis receptor; *metB*, which encodes a methionine biosynthesis enzyme; and *cj0761*, which encodes a hypothetical protein. Downregulated genes include *sdhAB* (*mrfAB*), which are misannotated as succinate dehydrogenases but are likely to encode methylmenaquinol:fumarate reductases, which function in the tricarboxylic acid (TCA) cycle (Weingarten et al., 2009; Kassem et al., 2014; Guccione et al., 2017). Other downregulated genes include *cj0426,* which encodes an ABC transporter ATP binding protein, the downstream gene *cj0427*, *rpmF*, which encodes a 50s ribosomal protein, and *cj0911* and *cj1485c,* which encode hypothetical periplasmic proteins. KEGG pathway analysis showed that several categories were enriched in the downregulated genes upon CC-FlaGrab exposure, including the

TABLE 2 | Differentially expressed *C. jejuni* 11168 genes upon CC-FlaGrab treatment.

Gene	Annotation	Fold change	*p*-value[a]
omp50 (cjtk)	50 kDa outer membrane protein precursor, phosphotyrosine kinase[b]	2.39	< 0.01
cj0037c (cccC)	Putative cytochrome C	2.22	< 0.01
dsbI	Disulphide bond formation protein	1.98	< 0.01
cj0761	Hypothetical protein Cj0761	1.83	< 0.01
cj1169c	Putative periplasmic protein	1.79	< 0.01
tlp4	Putative methyl-accepting chemotaxis signal transduction protein	1.62	< 0.01
metB	Putative *O*-acetylhomoserine (thiol)-lyase	1.44	0.05
cj0426	Putative ABC transporter ATP-binding protein	−1.41	0.04
cj0911	Putative periplasmic protein	−1.44	0.03
sdhA (mrfA)	Possible methylmenaquinol:fumarate reductase (TCA cycle)[c]	−1.45	0.05
sdhB (mrfB)	Possible methylmenaquinol:fumarate reductase (TCA cycle)[c]	−1.53	0.02
rpmF	50S ribosomal protein L32	−1.58	0.01
cj1485c	Putative periplasmic protein	−1.68	0.01
cj0427	Hypothetical protein Cj0427	−1.74	< 0.01

[a] *For each gene, fold change in expression post CC-FlaGrab treatment is listed followed by the FDR-adjusted p-value in brackets.*
[b] *Genbank annotation updated according to Corcionivoschi et al. (2012).*
[c] *Genbank annotation updated according to Kassem et al. (2014).*

TABLE 3 | Statistically significant downregulated KEGG pathways following *C. jejuni* 11168 exposure to CC-FlaGrab.

Significantly downregulated KEGG pathways[a]	*p*-value
cje00020 Citrate cycle (TCA cycle)	0.001
cje01200 Carbon metabolism	0.006
cje00190 Oxidative phosphorylation	0.019
cje03010 Ribosome	0.019
cje01130 Biosynthesis of antibiotics	0.019
cje01120 Microbial metabolism in diverse environments	0.019
cje00650 Butanoate metabolism	0.020

[a]*Differentially expressed host genes for each condition were subjected to gene set enrichment analysis (GSEA) on annotated Kyoto Encyclopedia of Genes and Genomes (KEGG) pathways using GAGE with an FDR cutoff of <0.1.*

TCA cycle, carbon metabolism, and oxidative phosphorylation pathways (**Table 3**).

FlaGrab Binding to Flagellar Motor Mutants Δ*motA* and Δ*motB* Does Not Cause Growth Inhibition

We next sought to understand how FlaGrab binding to bacterial flagella might lead to the observed effects on cell physiology. The proton motive force is hypothesized to power *C. jejuni* flagellar rotation through the MotA and MotB stator proteins, as in many other motile bacteria (Blair and Berg, 1990; Hosking et al., 2006; Morimoto et al., 2010; Kojima et al., 2018). Since flagellar motility is reduced upon FlaGrab binding (Javed et al., 2015a), we hypothesized that the cell might sense increased FlaGrab-induced flagellar stiffness and increase proton flow through the flagellar motor channel to compensate for this inhibition of flagellar rotation. This increased proton flow might in turn disrupt the electron transport chain (as proposed by Flint et al., 2014), which could prompt cells to respond by altering transcription of energy metabolism pathways. We predicted that if this were true, flagellar motility mutants, such as **Δ***motA* and **Δ***motB*, which do not express functional flagellar motors, would resist FlaGrab-induced clearing (Beeby et al., 2016; Ribardo et al., 2019). To test this, we generated insertional mutants in each of **Δ***motA* and **Δ***motB* in *C. jejuni* 11168 and confirmed that these mutants were non-motile (**Figure S2**). We then tested their binding and susceptibility to FlaGrab. We used immunogold labeling and transmission electron microscopy to show that binding to these mutants occurred to wild type levels (**Figure 2**), but when we tested growth inhibition of the **Δ***motA* and **Δ***motB* mutants using a soft agar spot assay, we found that FlaGrab was unable to clear the growth of these mutants (**Figure 2**, inset). This result supported our hypothesis that flagellar function is required for FlaGrab-mediated growth inhibition.

Some *C. jejuni* Strains Display Reduced Susceptibility to FlaGrab-Induced Growth Inhibition

To better understand the mechanisms by which *C. jejuni* may resist FlaGrab growth inhibition, we sought to identify strains resistant to this activity. We identified four *C. jejuni* strains, 12567, 12660, 12661, and 12664, which were naturally reduced in their ability to be cleared by FlaGrab and CC-FlaGrab compared to 11168 (Javed et al., 2013) (**Table 4**). Strain 12567 was cleared to near-11168 levels, while strain 12664 was not cleared. Strain 12660 displayed reduced clearing, and strain 12661 was generally not cleared, although one biological replicate of this strain was cleared well. Motility of these strains did not correlate with susceptibility to FlaGrab-induced clearance; most strains displayed similar motility to 11168, with the exception of 12661, which was significantly less motile (49%, $p = 0.008$) than 11168 (**Figure S3**).

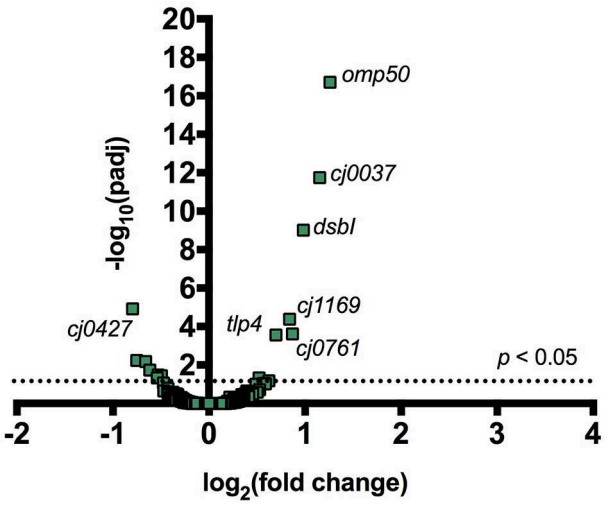

FIGURE 1 | Addition of CC-FlaGrab to *C. jejuni* 11168 cells leads to changes in gene expression. For all transcribed *C. jejuni* 11168 genes, the negative log of the FDR-adjusted *p*-value is plotted against the $\log_2$ fold change in transcription following CC-FlaGrab treatment compared with buffer-treated controls.

C. jejuni Strains Resistant to FlaGrab-Induced Growth Inhibition Also Display Reduced FlaGrab Binding

We hypothesized that reduced FlaGrab clearing would correlate with reduced binding. To test this, we probed cells with immunogold-labeled FlaGrab and examined them using transmission electron microscopy. We found that 12567 displayed robust FlaGrab binding (**Figure 3**), while 12660 displayed intermediate levels of binding. Interestingly, we found that biological replicates of 12661 showed either no binding or robust binding to FlaGrab ($n = 2$ each). Finally, we observed a complete lack of FlaGrab binding to 12664. Although neither the growth inhibition assay nor the immunogold-labeling assay provides quantitative results, the level of growth inhibition observed for these strains appeared to correlate with the levels of FlaGrab binding to the strains. These results suggested that reduced FlaGrab binding may explain the observed resistance to FlaGrab achieved by these strains.

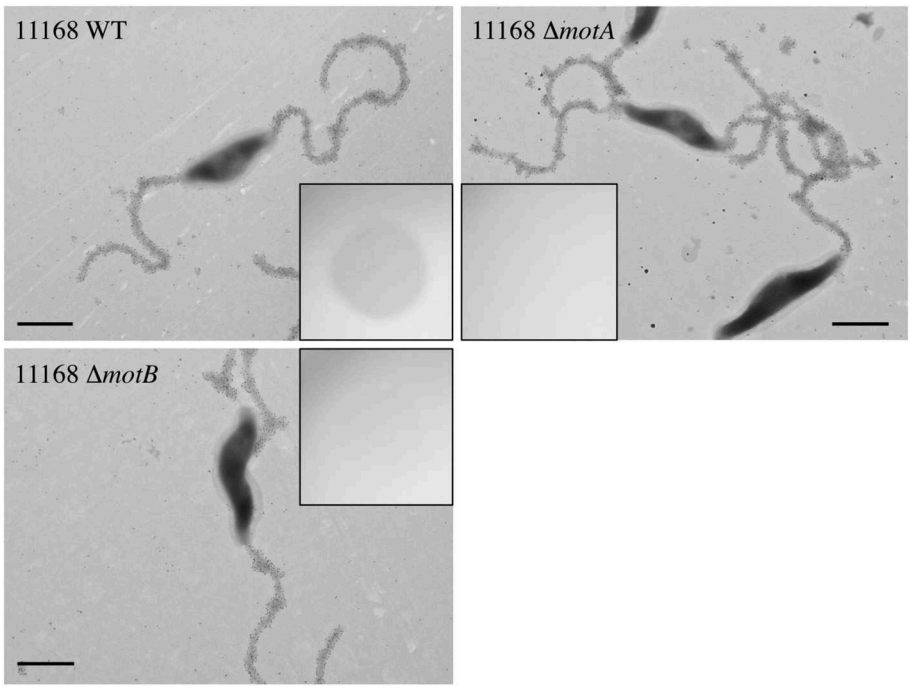

FIGURE 2 | *C. jejuni* 11168 wild type, Δ*motA* mutant, and Δ*motB* mutant cells are similarly bound by CC-FlaGrab, as shown by immunogold labeling with FlaGrab-specific antibodies and transmission electron microscopy. **(Inset)** Only wild type cell growth is cleared by CC-FlaGrab, as shown by digital images of overnight growth on soft agar overlay plates following spotting with equal concentrations of CC-FlaGrab. All images are representative of experiments done in duplicate. Scale bars represent 800 nm.

TABLE 4 | Growth clearance of *C. jejuni* strains by FlaGrab and CC-FlaGrab.

Strain	FlaGrab growth clearance[a]		CC-FlaGrab growth clearance[a]	
C. jejuni NCTC 11168	+++	+++	++	+
C. jejuni 12567	+	++	+	-
C. jejuni NCTC 12660	+	+	+	-
C. jejuni NCTC 12661	-	-	++	-
C. jejuni NCTC 12664	-	-	-	-

[a]*Degree of growth clearance following spotting of full-length FlaGrab or CC-FlaGrab on growing C. jejuni cells and overnight incubation. Clearing was scored visually. (+ + +) = very clear, (++) = slightly clear, (+) = very faint clearing, (-) = no clearing. Each column represents a separate biological replicate.*

C. jejuni Strains Resistant to FlaGrab Binding Encode all Genes Required for Biosynthesis and Transfer of Pse5Ac7Am

We next sought to understand how cells achieved altered levels of FlaGrab binding. As we previously showed that FlaGrab requires Pse5Ac7Am for binding to *C. jejuni* 11168 flagella (Javed et al., 2015a), we hypothesized that strains displaying reduced levels or differing patterns of FlaGrab binding would express different levels of Pse5Ac7Am on their flagella. Pse5Ac7Ac is synthesized by the sequential action of PseB, PseC, PseH, PseG, PseI, and PseF (Logan, 2006). Pse5Ac7Am is formed by adding the Am group to Pse5Ac7Ac by PseA (Guerry et al., 2006). Pse5Ac7Ac and Pse5Ac7Am are then transferred to flagellin in the cytoplasm by the action of separate transferases: PseE transfers Pse5Ac7Ac, while PseD transfers Pse5Ac7Am (Karlyshev et al., 2002; Karlyshev and Wren, 2005; Guerry et al., 2006). *C. jejuni* and *C. coli* require Pse5Ac7Ac biosynthesis for flagellar biogenesis (Goon et al., 2003), and all strains examined here are flagellate, and thus, we predicted that all strains would encode the genes required for Pse5Ac7Ac synthesis and transfer onto Fla protein subunits. However, we hypothesized that 12664, which is unable to bind FlaGrab, would encode a non-functional version of a gene involved in Pse5Ac7Am biosynthesis and/or transfer (i.e., *pseA* and/or *pseD*). We hypothesized that 12661, which we found to variably bind FlaGrab, might express a phase-variable version of one or both of these genes. To test these hypotheses, we analyzed the sequenced genomes for these strains (Sacher et al., 2018a,b) and examined the region spanning *cj1293-cj1343,* which was previously established as the flagellar glycosylation locus in *C. jejuni* 11168 (Parkhill et al., 2000).

In terms of gene content, we found a high degree of similarity at the flagellar glycosylation loci of all five strains (**Figure 4**). Compared to 11168, which encodes 47 genes in this locus, we found that 12567, 12660, and 12664 had between 46–48 genes, while 12661 encodes only 40. This is in contrast to *C. jejuni* 81–176, another well-characterized strain, which encodes only 24 of the 47 flagellar glycosylation genes encoded by 11168 (Guerry et al., 2006). Notably, we found that similarly to 11168,

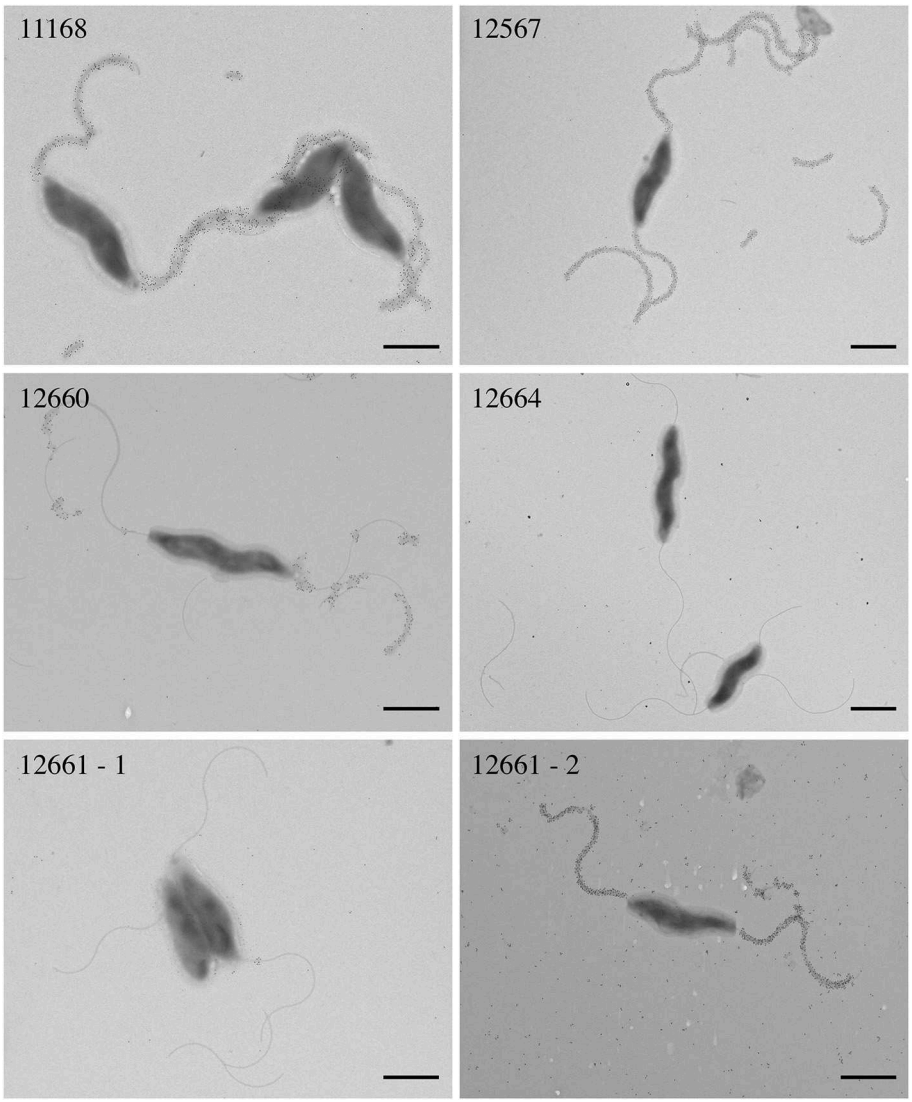

FIGURE 3 | Transmission electron microscopy with immunogold labeling using CC-FlaGrab followed by anti-FlaGrab antibodies and then immunogold-conjugated secondary antibodies to probe *C. jejuni* strains. From top left: strains *C. jejuni* 11168, 12567, 12660, 12664, 12661-1, and 12661-2. Strain 12661 is depicted twice to show the two phenotypes that were observed with this strain. Scale bars represent 800 nm.

all four strains (12567, 12660, 12661, and 12664) encoded copies of all genes required for Pse5Ac7Ac and Pse5Ac7Am synthesis and transfer.

Strain-Level Differences in FlaGrab Binding Correlate With Differences in PseD Sequence

We next examined whether amino acid sequence differences in PseA or PseD encoded by 12661 or 12664 could explain the observed differences in FlaGrab binding to these strains, since these proteins are the only two genes known to be required for Pse5Ac7Am display on flagella (the known FlaGrab receptor) in 11168 that are not required for flagellar filament biogenesis (Guerry et al., 2006). At the protein level, we found that PseA was upwards of 98.7% identical among strains, but that PseD diverged among strains (**Figure S4A**). PseD sequences from 11168, 12567, and 12660 were upwards of 96.9% identical to one another, but sequences from 12661 and 12664 were only 79.6–83.4% identical to PseD from 11168, 12567, and 12660. PseD sequences from 12661 and 12664 were 93.6% identical to one another. Most of the sequence divergence occurred within the third quarter of the PseD amino acid sequence. The fact that the two strains observed to express the most substantial reduction in FlaGrab binding grouped apart from the other strains based on their PseD sequence supported the hypothesis that changes in PseD sequence might explain the reduced FlaGrab binding of strains 12661 and 12664.

C. jejuni 12661 Encodes a 25-Nucleotide Insertion Containing a Poly-G Tract in *pseD*

The fact that FlaGrab binding to 12661 flagella occurred variably, while 12664 displayed a consistent lack of FlaGrab binding, pointed to the existence of differences in Pse5Ac7Am expression between these strains. This prompted us to more closely examine the nucleotide sequence identity of *pseD* from these two strains, which led us to discover a 25-nt insertion near the 5′ end of *pseD* in 12661 that is not present in any of the other strains (**Figure 5**). Interestingly, this insertion included a 9-G homopolymeric (poly-G) tract. Homopolymeric tracts are commonly signs of phase-variability in bacterial genes, and have been implicated in *C. jejuni* phage-host interactions (Coward et al., 2006; Sørensen et al., 2012). We analyzed the raw Illumina MiSeq reads from our whole genome sequence analysis of 12661 (Sacher et al., 2018b), and indeed found variability in the number of Gs at this locus, supporting the notion that this strain could encode a phase-variable version of *pseD* (data not shown).

FlaGrab Pressure Does Not Select for *pseD*-Off Variants in 12661 Under Our Conditions

To test the hypothesis that slipped-strand mispairing in *pseD* drives variation in 12661 binding to FlaGrab, we first amplified

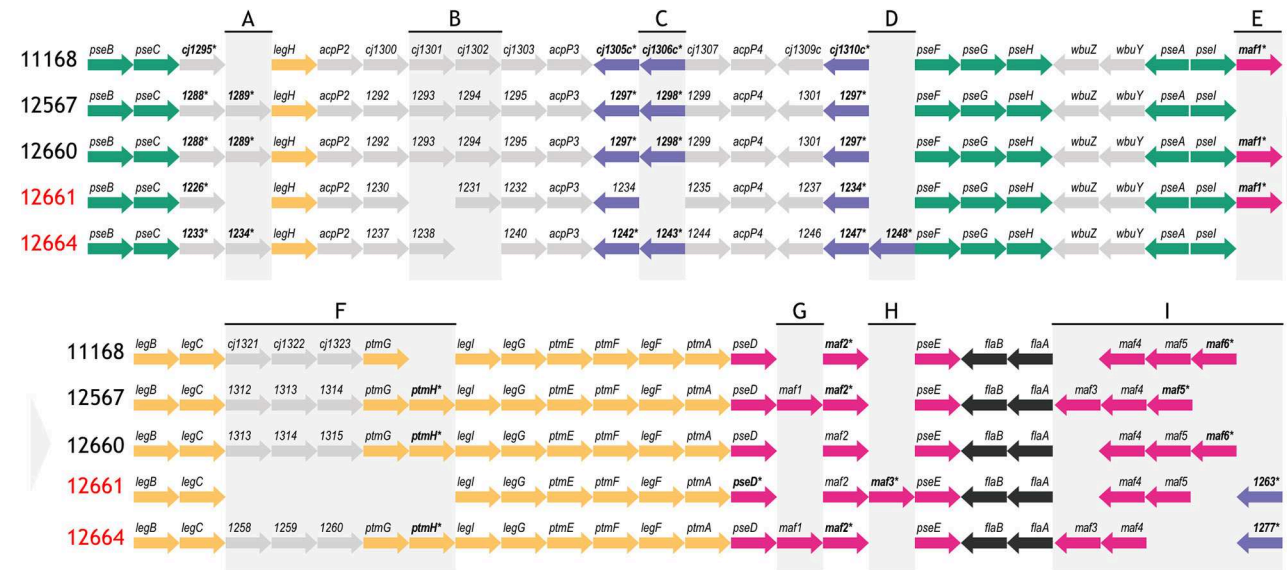

FIGURE 4 | Schematic depicting the flagellar glycosylation loci of strains *C. jejuni* 12567, 12660, 12661 and 12664, as compared to *C. jejuni* 11168. Strain names indicated in red refer to strains that either variably (12661) or consistently (12664) showed a lack of FlaGrab binding by immunogold/TEM. Asterisks/bolded genes contain a phase-variable poly-G tract. Colors represent genes involved in the same biological pathway (green: *pse* biosynthesis, yellow: *leg* biosynthesis, black: flagellar filament biosynthesis) or genes within the same family according to predicted function (purple: DUF2920 domain-containing genes, pink: *maf* genes). Other genes are indicated in gray. **(A)–(I)** are used to indicate regions of heterogeneity in gene content between strains, which are referred to in the text. Arrow direction indicates direction of transcription. Gene lengths are not to scale. Pseudogenes are not depicted.

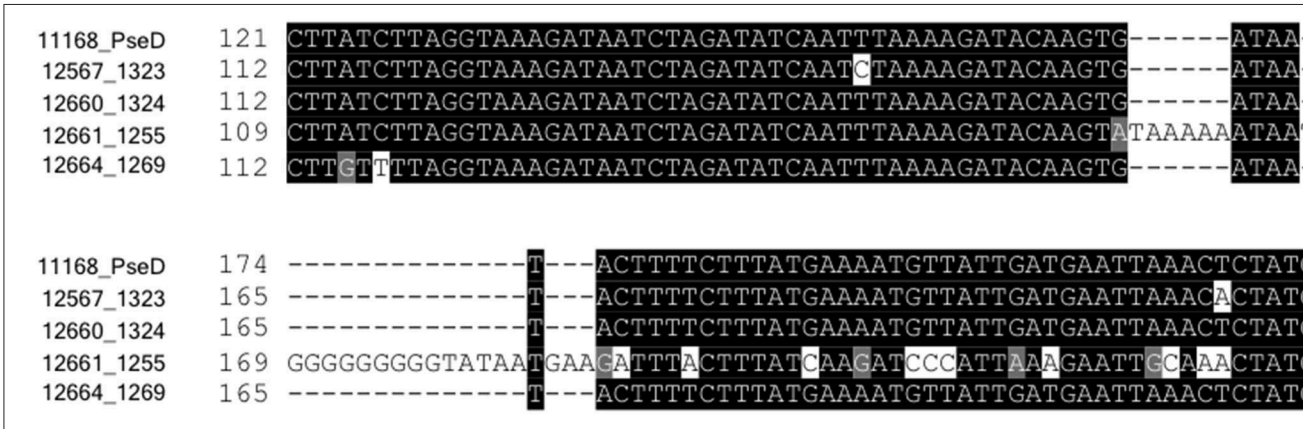

FIGURE 5 | Strain 12661 harbors a poly-G tract-containing insertion in *pseD* that is not present in strains 11168, 12567, 12660, or 12664. Nucleotide sequence alignment of an internal region of *pseD* for all strains showing the 25 inserted nucleotides in strain 12661, nine of which make up a poly-G tract.

the *pseD* region from five single colony isolates, then from a mixed population of cells, and then from purified genomic DNA, all in the absence of FlaGrab, and assessed poly-G tract lengths using Sanger sequencing. To ensure the region we were amplifying was *pseD* and not a homologous sequence, since *C. jejuni* strains tend to encode 6–7 highly similar *maf* (motility associated factor, including *pseD*) genes at the flagellar glycosylation locus, we designed our primers to amplify a region anchored within *ptmA*, the gene directly upstream of *pseD*. We found that in all cases, the poly-G tract in *pseD*_12661 was in the "on" (9 Gs) state, suggesting in-frame expression of PseD (data not shown). We next sought to determine whether FlaGrab binding would provide a pressure for the strain to phase-vary its *pseD*. We grew 12661 in the presence of FlaGrab and amplified *pseD* from 12661 within and outside the spot of FlaGrab-induced clearing using colony PCR followed by Sanger sequencing. Sequence analysis of amplicons derived from FlaGrab-exposed cells ($n = 2$ sections) and FlaGrab-unexposed cells ($n = 3$ sections) showed that the poly-G tract remained phased-on in each case, with no apparent secondary peaks underneath the primary nucleotide identified at each location (data not shown). From this, we concluded that under the conditions tested, FlaGrab pressure does not select for off-switching of *pseD* in *C. jejuni* 12661.

C. jejuni Strains 12661 and 12664 Display Flagellar Glycan Profiles Distinct From One Another and From 11168

Along with the differences in *pseD* sequence observed in 12661 and 12664, we wanted to determine whether these strains, which displayed reduced FlaGrab binding, displayed flagellar glycans distinct from 11168, which displays robust FlaGrab binding. To test this, we used high-resolution liquid chromatography with tandem mass spectrometry (LC-MS/MS) to identify and compare the glycans present on trypsin-digested flagella isolated from 12661 (in its non-FlaGrab-binding state), 12664 and 11168. We hypothesized that we would see reduced levels (or a complete absence) of Pse5Ac7Am on 12661 and 12664 flagella compared with 11168, and we surmised that other glycans would instead be present on the flagella of 12661 and 12664.

To verify our methodology, we first examined 11168 flagellar glycans. In agreement with Ulasi et al. (2015), we detected four glycopeptides: ^{180}ISTSGEVQFTLK^{191}, ^{204}VVISTSVGTGLGALADEINK^{223}, ^{339}DILISGSNLSSAGFGATQF^{357}, and ^{464}TTAFGVK^{470}, and identified several glycoforms for each (**Figures 6**, **7**) (Ulasi et al., 2015). Also in agreement with Ulasi et al. and others, we detected oxonium ions corresponding to Pse5Ac7Ac (m/z = 317.13), Pse5Ac7Am (m/z = 316.15), dimethylglyceric acid (DMGA)-Pse5Ac7Ac (m/z = 391.16), and DMGA-Pse5Ac7Am (m/z = 390.18) (Logan et al., 2009; Zampronio et al., 2011; Ulasi et al., 2015). We also compared the relative glycan abundances at each location by comparing the relative peak intensities between the analyzed glycopeptides. We observed that for all four peptides, 3.81–16.44% of the glycan content corresponded to Pse5Ac7Ac, while 56.39–69.89% corresponded to Pse5Ac7Am or its Leg derivative, 2.64–10.41% corresponded to DMGA-Pse5Ac7Ac, and 12.01–23.65% corresponded to DMGA-Pse5Ac7Am (**Figure 7**).

We next sought to analyze 12661 flagellar peptides. To confirm the non-FlaGrab-binding state of the 12661 population used for MS, we performed FlaGrab immunogold labeling/TEM on the same cell preparation as used to prepare flagella for MS, and confirmed that the protein did not bind to flagella in that preparation (data not shown). Our MS analysis of trypsin-digested 12661 flagellin resulted in the detection of the four glycopeptides described for 11168, ^{180}ISTSGEVQFTLK^{191}, ^{204}VVISTSVGTGLGALADEINK^{223}, ^{339}DILISGSNLSSAGFGATQF^{357}, and ^{464}TTAFGVK^{470} (**Figure 8**). On all four peptides, we detected oxonium ions of m/z = 317.13 (**Figure 8A**), which corresponds to Pse5Ac7Ac. Also on all four peptides, we detected an oxonium ion of m/z = 332.15 (**Figure 8B**), which does not correspond to any known *Campylobacter* flagellar glycan, but based on the addition of 15 Da to the mass of Pse5Ac7Ac, may represent the addition of an amine group to this glycan (the proposed structure is depicted in **Figure 8B**, inset). Notably, we did not detect oxonium ions corresponding to Pse5Ac7Am, DMGA-Pse5Ac7Ac or DMGA-Pse5Ac7Am. In terms of relative glycan content, we observed that for the first three peptides, glycans corresponding to Pse5Ac7Ac made up 9.78–30.31% of the glycan content, while the remaining 69.69–90.22% of the glycan content corresponded to the unknown glycan of m/z = 332.15 (**Figure 7**). However, the ^{464}TTTFGVK^{470} peptide displayed the opposite trend, with 83.00% of the glycan content corresponding to Pse5Ac7Ac and 17.00% corresponding to the unknown glycan of m/z = 332.15.

We next analyzed 12664 flagellin. We detected the first three glycopeptides described above, but not the ^{464}TTAFGVK^{470} peptide, so its glycan profile could not be determined (**Figures 7**, **9**). Interestingly, upon analysis of the three glycopeptides detected, we detected oxonium ions of m/z = 316.15, which corresponds to Pse5Ac7Am. Also on all three glycopeptides, we detected an unknown glycan of m/z = 331.16. Based on the addition of 15 Da to the mass of Pse5Ac7Am, this may represent the addition of an amine group to this glycan (the proposed structure is depicted in **Figure 9B**, inset). In addition, in this strain, as for 12661 but not for 11168, we did not detect the DMGA derivatives DMGA-Pse5Ac7Ac or DMGA-Pse5Ac7Am. In terms of glycan content, the glycan corresponding to Pse5Ac7Am was 43.86–58.60% abundant across the three detected glycopeptides, while the unknown glycan of m/z = 331 was 41.40–56.14% abundant. Also, the glycan corresponding to Pse5Ac7Ac was 3.17% abundant on the ^{204}VVISTSVGTGLGALVEEINK^{223} peptide only, but was not detected on the others.

FlaGrab Binding to *C. jejuni* 11168 Flagellar Glycans Does Not Require Dimethylglyceric Acid (DMGA)

To rule out the possibility that the absence of DMGA-Pse5Ac7Am was the reason for the lack of FlaGrab binding in 12664 and 12661, we sought to determine whether FlaGrab binding to Pse5Ac7Am requires DMGA in 11168. Hitchen et al.

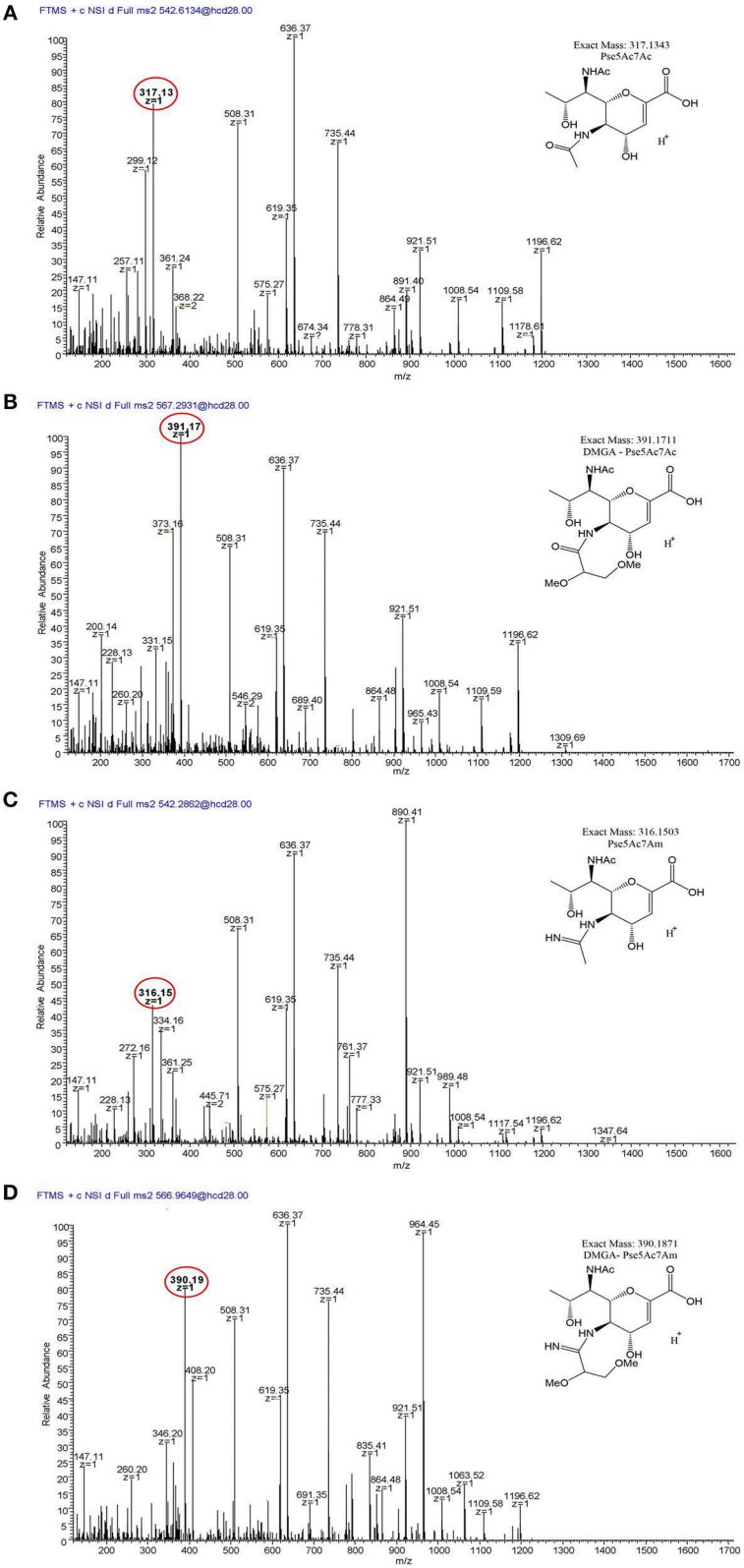

FIGURE 6 | LC/MS-MS fragmentation spectra of trypsin-digested *C. jejuni* 11168 flagellar glycopeptide ^{180}ISTSGEVQFTLK^{191}. **(A)** ^{180}ISTSGEVQFTLK^{191} + Pse5Ac7Ac (oxonium ion m/z = 317.13); **(B)** ^{180}ISTSGEVQFTLK^{191} + Pse5Ac7Am (oxonium ion m/z = 316.15); **(C)**, ^{180}ISTSGEVQFTLK^{191} + DMGA-Pse5Ac7Ac (oxonium ion m/z = 391.17); **(D)** ^{180}ISTSGEVQFTLK^{191} + DMGA-Pse5Ac7Am (oxonium ion m/z=390.19). Oxonium ions are circled, and proposed structures of monosaccharides are shown.

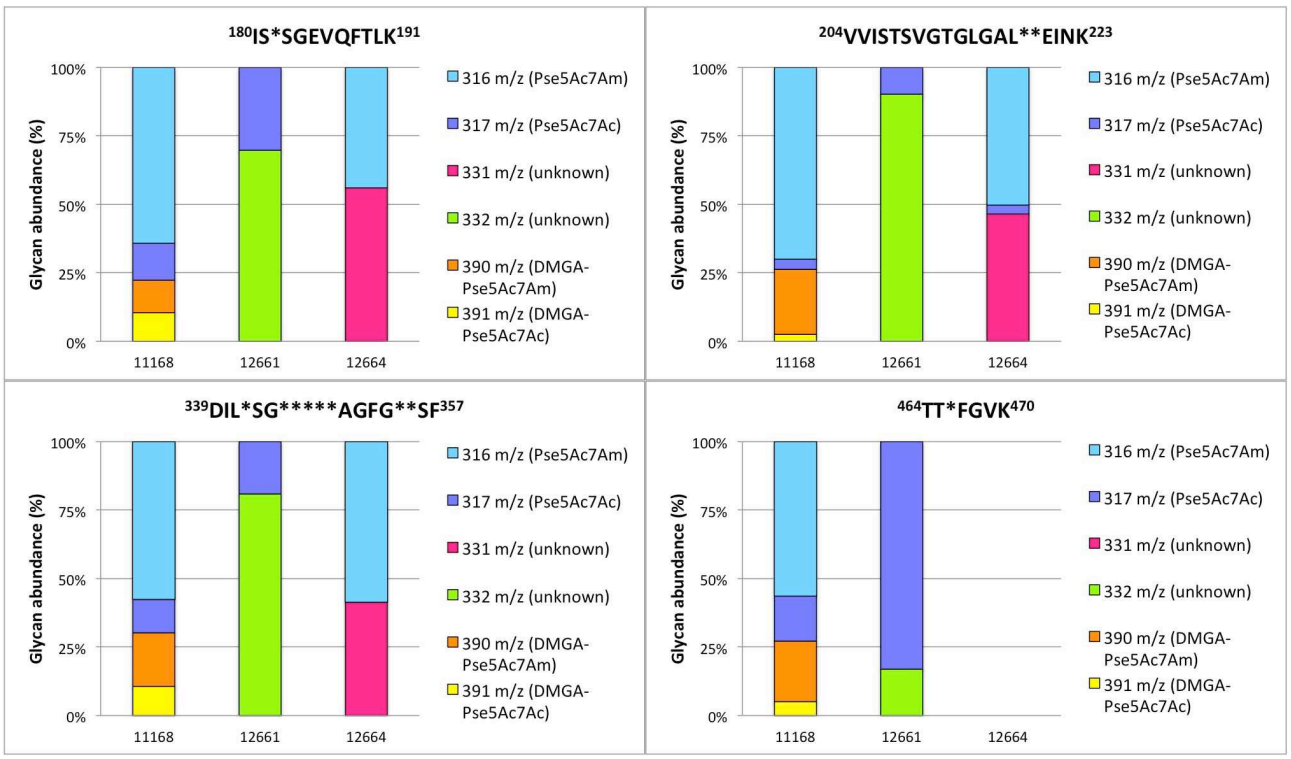

FIGURE 7 | Percent relative abundance of flagellar glycans presented by *C. jejuni* 11168, 12661, and 12664 for four detected *C. jejuni* FlaA/FlaB peptides as determined by LC-MS/MS. In 12664, the peptide ^{464}TTAFGVK^{470} was not detected, and thus no bar is depicted.

(2010) have shown that a *cj1295* mutant in *C. jejuni* 11168 is unable to synthesize DMGA-Pse5Ac7Ac or DMGA-Pse5Ac7Am (Hitchen et al., 2010). We therefore generated a *cj1295* mutant in 11168 and used immunogold labeling/TEM to test whether FlaGrab binding still occurred in this strain. We found no difference in FlaGrab binding between the *cj1295* mutant and wild type cells (**Figure 10**), suggesting that DMGA is not required for FlaGrab binding to Pse5Ac7Am.

Differences in 11168, 12661, and 12664 Gene Content at the Flagellar Glycosylation Locus Are Primarily Among *maf* and DUF2920-Containing Genes

To gain insight into the genetic basis for the observed differences in flagellar glycans detected on 11168, 12661, and 12664 flagella, we examined the differences in gene content at the flagellar glycosylation locus of each strain. In particular, we hypothesized that 12661 and 12664 would encode genes in this locus not encoded by 11168 that might explain their display of unknown glycans of m/z = 332 and 331 glycans, respectively. Notably, the m/z value for each unknown glycan represents a gain of ∼15 Da relative to the other glycan detected for that strain (m/z = 317 and 316, respectively), suggesting that an amine group (NH_2, 16 Da) might substitute for a hydrogen atom on the glycan detected in each case. We therefore examined the genes within the flagellar glycosylation locus that were only present in 12661 and 12664 to see if any had homology to an aminotransferase, but did not identify any aminotransferase homologs.

To identify candidate genes that might be involved in the synthesis of the unknown glycans of m/z = 332 and 331, we examined other differences in gene content at the flagellar glycosylation locus between 12664, 12661, and 11168. We noted strain-specific differences in *maf* gene content and in distribution of poly-G tracts among these genes. Differences in *maf* genes were particularly noteworthy, as paralogues of these (*pseD, pseE*) are known to be involved in pseudaminic acid transfer to flagellin in *Campylobacter*. For instance, strain 12664 lacks the motility associated factor *maf5* (*cj1341c*), while *maf6* (*cj1342c*) is missing from both 12664 and 12661 (**Figure 4**, Region I). As well, the poly-G tract in *maf2* is uniquely absent in 12661. We also noted differences in the number, location, and presence/absence of poly-G tracts in genes containing a DUF2920 domain (DUF = domain of unknown function) (**Figure 4**, Regions C, D, and I). In 12664, we noted the unique presence of the DUF2920-containing gene *CJ12664_1248* downstream of the identically-annotated *cj1310c* (**Figure 4**, Region D). In addition, we found that 12664 encodes another DUF2920-containing gene, *CJ12664_1277*, just upstream of *maf4* (*cj1340c*) (**Figure 4**, Region I), and we found that 12661 also encoded this second DUF2920-containing gene (*CJ12661_1263*). However, strain 12661 is also missing the DUF2920-containing gene *cj1306* (**Figure 4**, Region C). While strains 11168 and 12664 encode a poly-G tract in *cj1305c*, another

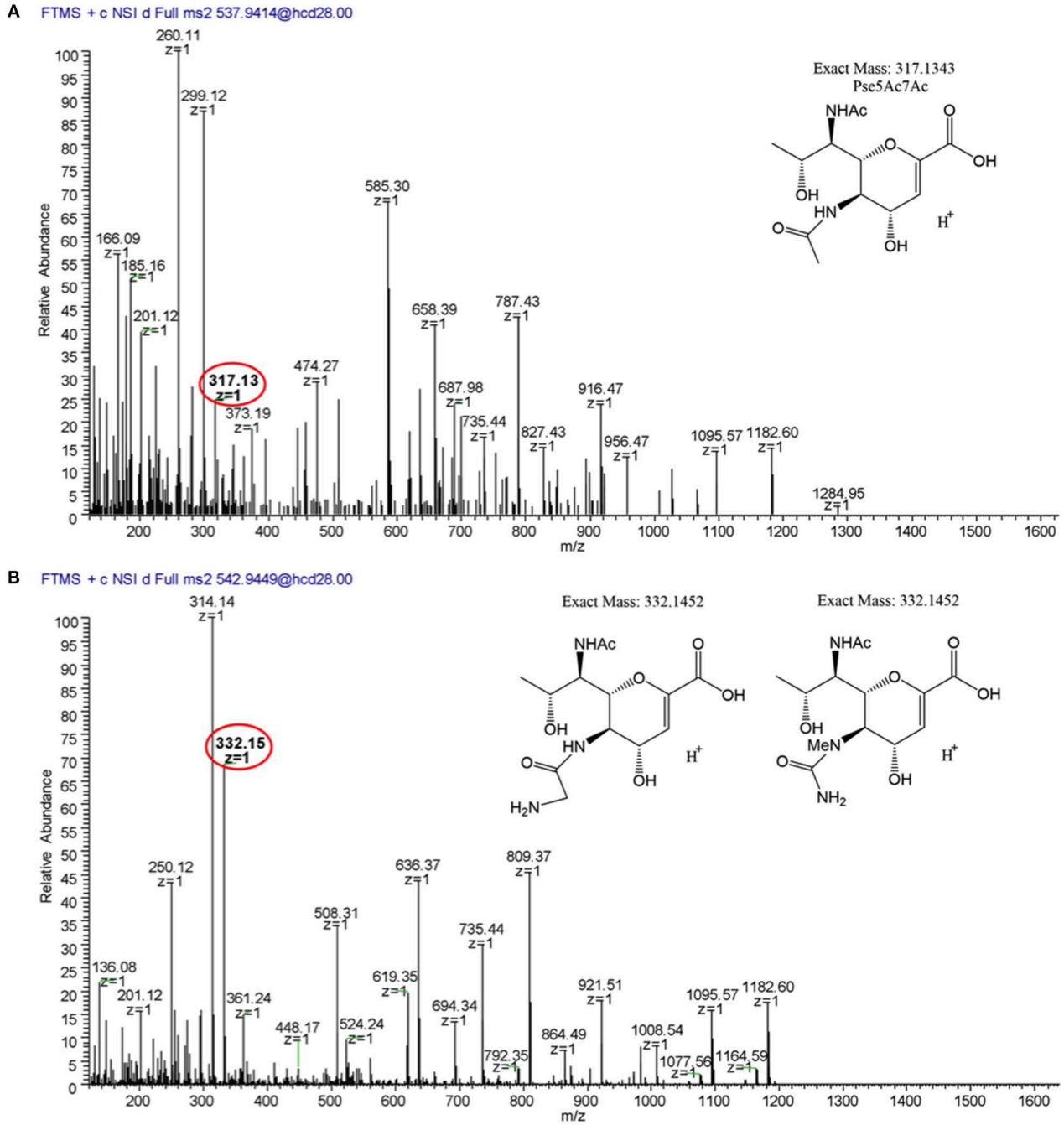

FIGURE 8 | LC/MS-MS fragmentation spectra of trypsin-digested *C. jejuni* 12661 flagellar glycopeptide ^{180}ISSSGEVQFTLK^{191}. **(A)** MS^2 spectrum of ^{180}ISSSGEVQFTLK^{191} + a glycan of oxonium ion m/z = 317.13 ($C_{13}H_{21}O_7N_2^+$), **(B)** MS^2 spectrum of ^{180}ISSSGEVQFTLK^{191} + a glycan of oxonium ion m/z = 332.15 ($C_{13}H_{22}O_7N_3^+$). Oxonium ions are circled, and proposed structures of monosaccharides are shown.

DUF2920-containing gene, this poly-G tract is disrupted in strain 12661. Outside of *maf* and DUF2920-containing genes, strain 12664 also uniquely lacks the *fkbH* domain-containing gene *cj1302* (**Figure 4**, Region B) (it is present as a pseudogene), and 12661 uniquely lacks *cj1301,* which is annotated as an epimerase (**Figure 4**, Region B).

DISCUSSION

In this study, we sought to understand how FlaGrab, a protein encoded by all *C. jejuni* phages characterized to date (Javed et al., 2014), inhibits the growth of *C. jejuni* 11168 by binding to its flagella, and to understand how some strains of *C. jejuni*

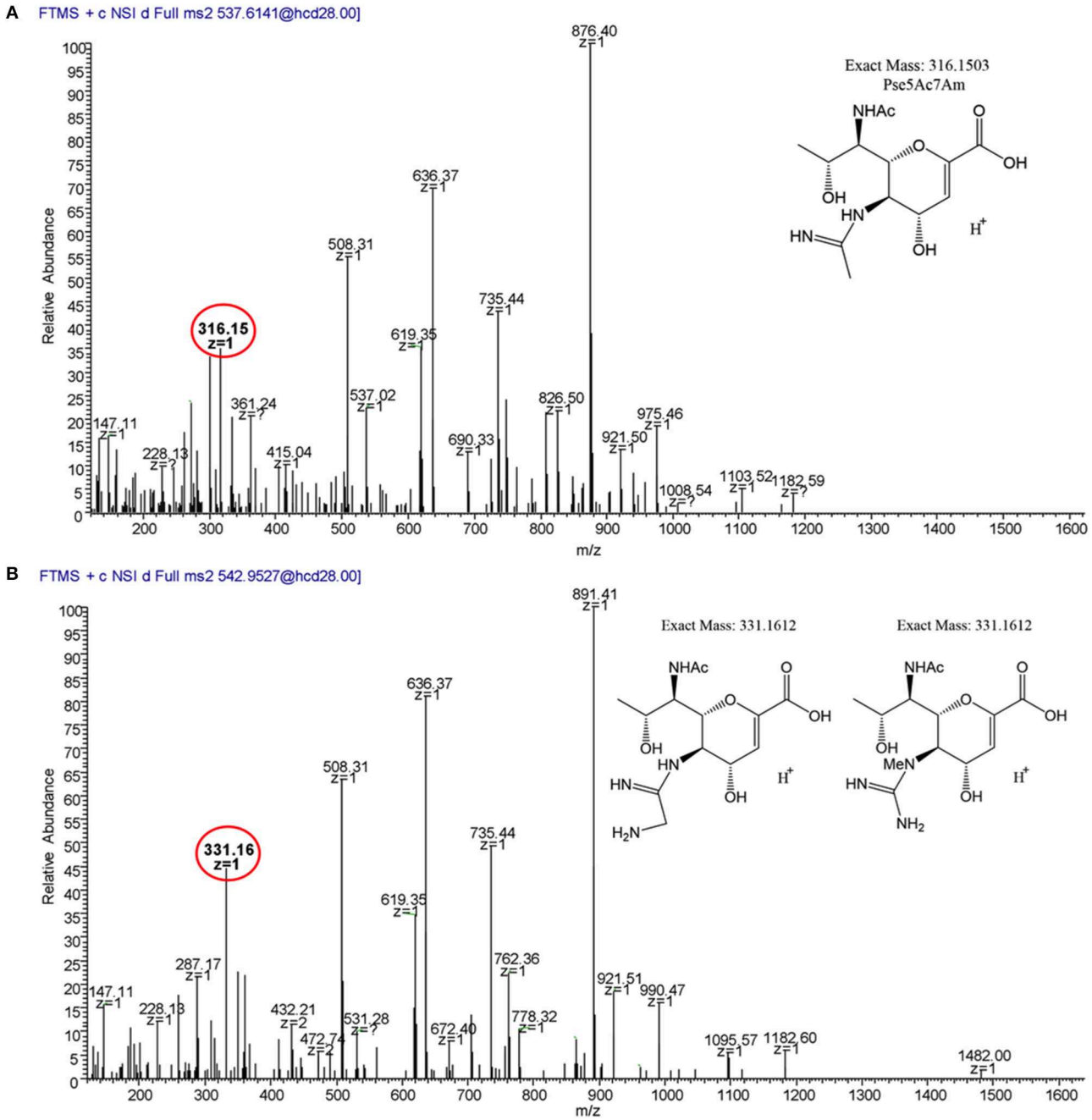

FIGURE 9 | MS^2 fragmentation spectra of trypsin-digested *C. jejuni* 12664 flagellar glycopeptide ^{180}ISSSGEVQFTLK^{191}. **(A)** MS^2 spectrum of ^{180}ISSSGEVQFTLK^{191} + a glycan of oxonium ion m/z = 316.15 ($C_{13}H_{22}O_6N_3^+$); **(B)** MS^2 spectrum of ^{180}ISSSGEVQFTLK^{191} + a glycan of oxonium ion m/z = 331.16 ($C_{13}H_{23}O_6N_4^+$). Oxonium ions are circled, and proposed structures of monosaccharides are shown.

are able to resist this effect (Sacher, 2018). Ultimately, our goal was to gain insight into how phage pressures might contribute to *C. jejuni* flagellar glycan diversity and complexity by studying susceptibility and resistance to a phage protein with both an inhibitory effect on cells and a specificity for certain surface-exposed glycans.

First, we examined the growth inhibitory effect that resulted from FlaGrab binding to *C. jejuni* flagella. Other organisms, such as *Bacillus subtilis*, have been shown to alter biofilm-related gene expression in response to flagellar contact with a surface (which could be recapitulated through binding by flagella-specific antibodies) (Cairns et al., 2013; Belas, 2014).

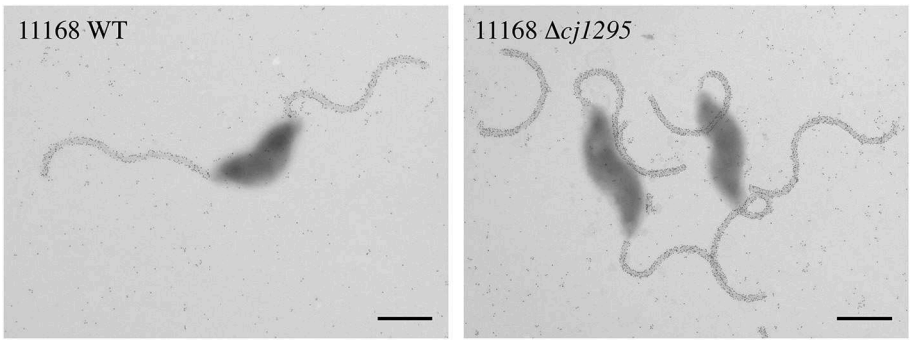

FIGURE 10 | Transmission electron micrographs of FlaGrab-labeled *C. jejuni* 11168 and 11168Δ*cj1295*. Images are representative of experiments done in duplicate. Scale bars represent 800 nm.

Therefore, we hypothesized that FlaGrab binding to *C. jejuni* flagella might inhibit flagellar rotation, which might in turn send a signal through the flagella that would alter gene expression in a way that would reduce cellular growth rate. As *C. jejuni* has previously been shown to alter its protein expression during biofilm association (Kalmokoff et al., 2006), we surmised that it might have evolved a mechanism of sensing and responding to surface contact, and that FlaGrab binding might be stimulating such a pathway. To test whether *C. jejuni* gene expression was altered in response to FlaGrab binding, we analyzed total gene expression changes in cells treated with the C-terminal (binding) component of FlaGrab, CC-FlaGrab, by RNA-seq. We found that genes involved in the TCA cycle, oxidative phosphorylation, and carbon metabolism were downregulated upon FlaGrab treatment, reflecting an overall metabolic downshift that is not surprising in light of the reduced growth observed. Interestingly, the pattern of FlaGrab-induced altered gene expression we have observed in *sdhA* (*mrfA*) and *sdhB* (*mrfB*) is mirrored by the gene expression changes observed by Guccione et al. (2017) in response to aerobic growth of *C. jejuni* (Guccione et al., 2017). One can speculate that FlaGrab may induce a mild form of oxidative stress on exposed cells. In support of this notion, we previously observed that *C. jejuni* 11168 upregulates expression of oxidative stress response genes in response to infection by phage NCTC 12673, the phage from which the FlaGrab protein described here originates (Sacher et al., 2018c). Further work into understanding the connection between phage infection, oxidative stress and oxidative stress response in *C. jejuni* is merited.

We next sought to examine the mechanism by which FlaGrab might lead to the observed effects on cells. *C. jejuni* flagellar rotation is hypothesized to be driven by proton motive force through the MotA and MotB stator proteins, as in many other motile bacteria (Chaban et al., 2018), and altered proton flow has been shown to increase flagellar torque in other bacteria (Lele et al., 2013). In addition, *C. jejuni* cells are known to modulate their swimming speed according to viscosity (Szymanski et al., 1995). We therefore hypothesized that FlaGrab binding, which occurs all along the length of the flagella of susceptible *C. jejuni* cells, might lead cells to sense increased drag, which might induce the flagellar motor complex to increase proton flow through the motor channel to compensate. This increased proton flow would presumably disrupt proton motive force homeostasis in the cell, perhaps due to electron leakage across the electron transport chain, as has been proposed by Flint et al., which could explain the observed growth inhibition (Flint et al., 2014). To begin to examine this hypothesis, we tested whether FlaGrab could inhibit the growth of *motA* or *motB* mutants, which have a "paralyzed" flagellar phenotype as they each lack a key element of the flagellar motor (Ribardo et al., 2019). We predicted that these mutants would be bound, but not cleared by FlaGrab. Consistent with our prediction, we found that *motA* and *motB* mutants were both completely resistant to FlaGrab growth inhibition, and yet FlaGrab binding was normal, suggesting that clearance activity does indeed require flagellar motor function. Further work is required to demonstrate that FlaGrab binding to functional flagella indeed alters proton flow, and to determine whether this disruption is sufficient to explain the observed growth inhibition. Still, our results are consistent with a model whereby FlaGrab binding to flagella is "mechanosensed" by the cell through detection of increased drag on rotating flagella.

Next, we wanted to understand the mechanisms by which *C. jejuni* might resist FlaGrab activity. To do this, we identified two *C. jejuni* strains with reduced susceptibility to FlaGrab-induced growth inhibition, 12661 and 12664. We first sought to determine whether a lack of motility might explain their resistance. Strain 12664 displayed similar motility levels to 11168, suggesting that a lack of motility was not the reason for its FlaGrab resistance. However, 12661 was 49% less motile, which could explain part of this strain's reduced susceptibility to FlaGrab activity. We next sought to examine the levels of FlaGrab binding to 12664 and 12661. We determined that both strains exhibited reduced FlaGrab binding, suggesting that FlaGrab resistance may be a consequence of reduced expression of the FlaGrab receptor (Pse5Ac7Am). Interestingly, strain 12661 was variably susceptible to both FlaGrab-induced growth inhibition and binding, while strain 12664 was consistently FlaGrab-resistant. These results suggested that each strain had evolved to avoid FlaGrab binding in its own way, and suggested that 12661 might encode a phase-variable version of a gene required for FlaGrab receptor expression.

We next wanted to further elucidate how *C. jejuni* 12661 and 12664 each escaped FlaGrab binding. We hypothesized that these strains might avoid FlaGrab binding either by not encoding Pse5Ac7Am at all, by encoding mechanisms of downregulating or off-switching their Pse5Ac7Am expression, or by expressing other glycans able to render Pse5Ac7Am unrecognizable to FlaGrab. We first compared the genes each strain encoded at the flagellar glycosylation locus with 11168, and found that both 12661 and 12664 encode full-length copies of all genes known to be required for Pse5Ac7Am synthesis and display on flagella (Logan et al., 2008). However, we found that strains 12661 and 12664 clustered separately from FlaGrab-binding strains, such as 11168, according to their PseD sequence (**Figure S4**). PseD is considered to be responsible for Pse5Ac7Am transfer onto *C. jejuni* flagellin, as Pse5Ac7Am accumulated in the cytosol but was not detected on the flagella of a *pseD* mutant in *C. jejuni* strain 81–176 (Guerry et al., 2006; McNally et al., 2006). It is plausible that the observed sequence differences in PseD in strains 12661 and 12664 might lead to changes in the ability of PseD to transfer Pse5Ac7Am that could explain the reduced FlaGrab binding to these two strains. Further work into understanding the active site of PseD, as well as the predicted effects of the observed sequence differences on its function, are merited. Interestingly, *pseD* polymorphisms have recently been implicated in *C. jejuni* persistence in humans: in a study by Crofts et al., a single *C. jejuni* strain was used to infect several volunteers, and whole genome sequencing of isolates from subjects who experienced severe and/or recurrent infections revealed an enrichment of *pseD* gene variants (Crofts et al., 2018). Further understanding of PseD function and the factors contributing to selection of variants, particularly as they relate to phage-host interactions (which are understudied in mammalian systems), may thus yield important data, and should be pursued in the future.

We next set out to explain why strain 12661 was variably bound by FlaGrab. The simplest explanation was phase variation at either *pseA* or *pseD,* as these are the two *C. jejuni* genes known to be involved in Pse5Ac7Am display that can be disrupted without abolishing flagellar filament biogenesis (Guerry et al., 2006). Phase variation is common in *C. jejuni,* and has been implicated in *C. jejuni* phage-host interactions (Coward et al., 2006; Sørensen et al., 2012). Interestingly, we found that 12661 expressed a poly-G-tract-containing version of *pseD,* while the other strains did not. However, we did not observe phase variation at this locus, even when cells were exposed to FlaGrab. Therefore, we concluded that variation in *pseD* was not the explanation for the variable FlaGrab binding phenotype we observed.

To determine whether FlaGrab-resistant strains expressed less Pse5Ac7Am, we analyzed the flagellar glycans of these strains compared to 11168. We found that the oxonium ion corresponding to Pse5Ac7Am, the known receptor for FlaGrab, was not identified on 12661 flagella, suggesting that this strain's resistance to FlaGrab was indeed mediated by the loss of this glycan. Conversely, flagella from strain 12664 did produce an oxonium ion with a mass to charge ratio consistent with Pse5Ac7Am. It is likely that this glycan corresponds not to Pse5Ac7Am, but instead to Leg5Am7Ac, a glycan of the same mass known to be displayed on *C. coli* VC167 flagella (McNally et al., 2007), which we have shown to be insufficient for FlaGrab binding (Javed et al., 2015a). In support of this explanation, strain 12664 encodes the genes (*cj1321–1325/6*) previously shown by Howard et al. (2009) to be involved in Leg5Am7Ac synthesis (Howard et al., 2009), while strain 12661 does not. Unfortunately, our efforts to obtain sufficient quantities of cytoplasmic nucleotide-activated sugars from 12664 to conclusively identify the glycan using NMR have thus far been unsuccessful. Of note, if 12664 does express Leg5Am7Ac and not Pse5Ac7Am, it would still call to question why Pse5Ac7Am is not also present. Although *C. coli* VC167 has been observed only to express Leg5Am7Ac and not Pse5Ac7Am, this strain only encodes the genes for the former (McNally et al., 2007), while strain 12664 encodes all genes required for both glycans (McNally et al., 2007). If both glycans are present on 12664 flagella, an alternate explanation for the lack of FlaGrab binding could be that the unknown glycan of m/z = 331 shields the FlaGrab binding epitope. Further work into understanding the mechanism behind the lack of FlaGrab binding in this strain is on-going.

As both 12661 and 12664 flagella lacked any oxonium ions corresponding to the DMGA-containing sugars found on 11168 flagella, we wanted to rule out the possibility that DMGA-Pse5Ac7Am was the required glycan for FlaGrab binding. We mutagenized *cj1295* in *C. jejuni* 11168, as this gene was shown to be responsible for DMGA-Pse5Ac7Ac and DMGA-Pse5Ac7Am synthesis in this strain (Hitchen et al., 2010). Since we observed no difference in FlaGrab binding to 11168 compared to the *cj1295* mutant, we concluded that DMGA is not part of the receptor required for FlaGrab binding to flagella.

During this study, we identified two novel glycan masses expressed on *C. jejuni* flagella: oxonium ions of m/z = 332 and 331. As these m/z ratios are equal to 317 + 15 and 316 + 15, we propose that they correspond to Pse5Ac7Ac and Pse5Ac7Am (or their legionaminic acid equivalents) with the addition of an amine group (NH_2, 16 Da) in place of a hydrogen atom. We sought to identify candidate genes within the flagellar glycosylation loci that might be involved in the synthesis of the novel glycans we identified. Compared with 11168, the main differences we observed were in number and location of *maf* and DUF2920-containing genes. Phenotypes have been identified for some of the *maf* genes in *C. jejuni,* including *pseD, pseE*, and *maf4* (involved in Pse5Ac7Am transfer to flagellin, Pse5Ac7Ac transfer to flagellin, and CO_2 or $C_2H_2O_2$ transfer to Pse5Ac7Ac, respectively), but the role of most *maf* genes is unknown (Karlyshev et al., 2002; van Alphen et al., 2008). As for DUF2920 genes, even less is known about their function (Guerry et al., 2006). While it is possible that strain-specific *maf* and DUF2920 gene content could be responsible for the diversity in flagellar glycan expression we have uncovered here, it will undoubtedly be challenging to parse the roles of each in *C. jejuni* flagellar glycosylation. Nonetheless, our results point to these gene families as attractive targets for future studies.

CONCLUSIONS

We have gained new insights into the mechanism of *C. jejuni* growth clearance by the conserved phage-encoded protein FlaGrab. Our results are consistent with a model whereby FlaGrab binds cells and transmits a mechanical signal through the flagella, which leads to slower cell growth. We also characterized the mechanism of FlaGrab resistance of two *C. jejuni* strains, and found that resistance was due to evasion of FlaGrab binding by altering flagellar glycan display through strain-specific mechanisms. We found that both strains display a different modified glycan not previously observed on *Campylobacter* flagella, and that the number and organization of *maf* and DUF2920-containing genes constitute the main differences at the flagellar glycosylation locus between FlaGrab-susceptible and -resistant strains. Together our results add to our understanding of the interactions between *C. jejuni* surface glycans and a conserved glycan-specific phage protein, and highlight unexplored diversity in *C. jejuni* flagellar glycosylation.

DATA AVAILABILITY STATEMENT

The datasets generated for this study can be found in the NCBI SRA archive #PRJNA580017.

AUTHOR CONTRIBUTIONS

JS designed and performed experiments, analyzed the data, and wrote the manuscript. ASh performed the mass spectrometry experiments and analyzed the data. RP performed microscopy and motility experiments. AF performed RNA sequencing. JB analyzed the RNA-Seq data. JB, ASt, PA, and DH provided materials and guidance, and analyzed the data. CS supervised and funded the project, analyzed the data, and edited the manuscript.

FUNDING

JS is a recipient of an NSERC Alexander Graham Bell Canada Graduate Student Scholarship. CS is an Alberta Innovates Strategic Chair in Bacterial Glycomics. Research in ASt laboratory was supported by CIHR grant MOP#84224. The glycan analysis was supported by US Department of Energy Grants DE-SC0015662 and NIH Grants S10OD018530 and P41GM103490 to PA. Research in DH's laboratory was supported by NIH grant R01AI065539.

ACKNOWLEDGMENTS

We thank Dennis Linton for the *cj1295* mutagenesis construct, Cory Wenzel for helpful discussions, and Jan Zheng for help in creating **Figure 4**. This work was adapted from work published in JS's doctoral thesis (Sacher, 2018).

SUPPLEMENTARY MATERIAL

The Supplementary Material for this article can be found online at: https://www.frontiersin.org/articles/10.3389/fmicb.2020.00397/full#supplementary-material

REFERENCES

Amour, C., Gratz, J., Mduma, E., Svensen, E., Rogawski, E. T., McGrath, M., et al. (2016). Epidemiology and impact of campylobacter infection in children in 8 low-resource settings: results from the MAL-ED study. *Clin. Infect. Diseases: An Off. Publ. Infect. Diseases Soc. Am.* 63, 1171–1179. doi: 10.1093/cid/ciw542

Baldvinsson, S. B., Holst Sørensen, M. C., Vegge, C. S., Clokie, M. R. J., and Brøndsted, L. (2014). *Campylobacter jejuni* motility is required for infection of the flagellotropic bacteriophage F341. *Appl. Environ. Microbiol.* 80, 7096–7106. doi: 10.1128/AEM.02057-14

Beeby, M., Ribardo, D., Brennan, C., Ruby, E., Jensen, G., and Hendrixson, D. (2016). Diverse high-torque bacterial flagellar motors assemble wider stator rings using a conserved protein scaffold. *Proc. Natl. Acad. Sci. U.S.A.* 113, E1917–E1926. doi: 10.1073/pnas.1518952113

Belas, R. (2014). Biofilms, flagella, and mechanosensing of surfaces by bacteria. *Trends Microbiol.* 22, 517–527.doi: 10.1016/j.tim.2014.05.002

Blair, D. F., and Berg, H. C. (1990). The MotA protein of *E. coli* is a proton-conducting component of the flagellar motor. *Cell* 60, 439–449. doi: 10.1016/0092-8674(90)90595-6

Bolton, D. J. (2015). Campylobacter virulence and survival factors. *Food Microbiol.* 48, 99–108. doi: 10.1016/j.fm.2014.11.017

Cairns, L. S., Marlow, V. L., Bissett, E., Ostrowski, A., and Stanley-Wall, N. R. (2013). A mechanical signal transmitted by the flagellum controls signalling in *Bacillus subtilis*. *Mol. Microbiol.* 90, 6–21. doi: 10.1111/mmi.12342

Chaban, B., Coleman, I., and Beeby, M. (2018). Evolution of higher torque in *Campylobacter*-type bacterial flagellar motors. *Sci. Rep.* 8:97. doi: 10.1038/s41598-017-18115-1

Corcionivoschi, N., Alvarez, L. J., Sharp, T., Strengert, M., Alemka, A., Mantell, J., et al. (2012). Mucosal reactive oxygen species decrease virulence by disrupting *Campylobacter jejuni* phosphotyrosine signaling. *Cell Host Microbe* 12, 47–59. doi: 10.1016/j.chom.2012.05.018

Coward, C., Grant, A. J., Swift, C., Philp, J., Towler, R., Heydarian, M., et al. (2006). Phase-variable surface structures are required for infection of *Campylobacter jejuni* by bacteriophages. *Appl. Environ. Microbiol.* 72, 4638–4647. doi: 10.1128/AEM.00184-06

Crofts, A. A., Poly, F. M., Ewing, C. P., Kuroiwa, J. M., Rimmer, J. E., Harro, C., et al. (2018). *Campylobacter jejuni* transcriptional and genetic adaptation during human infection. *Nat. Microbiol.* 3:494. doi: 10.1038/s41564-018-0133-7

Di Tommaso, P., Moretti, S., Xenarios, I., Orobitg, M., Montanyola, A., Chang, J., et al. (2011). T-coffee: a web server for the multiple sequence alignment of protein and RNA sequences using structural information and homology extension. *Nucleic Acids Res.* 39, W13–W17. doi: 10.1093/nar/gkr245

Dobin, A., Davis, C. A., Schlesinger, F., Drenkow, J., Zaleski, C., Jha, S., et al. (2013). STAR: ultrafast universal RNA-seq aligner. *Bioinformatics* 29, 15–21. doi: 10.1093/bioinformatics/bts635

Ewing, C. P., Andreishcheva, E., and Guerry, P. (2009). Functional characterization of flagellin glycosylation in *Campylobacter jejuni* 81-176. *J. Bacteriol.* 191, 7086–7093. doi: 10.1128/JB.00378-09

Flint, A., Sun, Y., Butcher, J., Stahl, M., Huang, H., and Stintzi, A. (2014). Phenotypic screening of a targeted mutant library reveals *Campylobacter jejuni* defenses against oxidative stress. *Infect. Immun.* 82, 2266–2275. doi: 10.1128/IAI.01528-13

Frost, J. A., Kramer, J. M., and Gillanders, S. A. (1999). Phage typing of *Campylobacter jejuni* and *Campylobacter coli* and its use as an adjunct to serotyping. *Epidemiol. Infect.* 123:S095026889900254X. doi: 10.1017/S095026889900254X

Gencay, Y. E., Sørensen, M. C. H., Wenzel, C. Q., Szymanski, C. M., and Brøndsted, L. (2018). Phase variable expression of a single phage receptor in *Campylobacter*

jejuni NCTC12662 influences sensitivity toward several diverse CPS-dependent phages. *Front. Microbiol.* 9:82. doi: 10.3389/fmicb.2018.00082

Goon, S., Kelly, J. F., Logan, S. M., Ewing, C. P., and Guerry, P. (2003). Pseudaminic acid, the major modification on *Campylobacter* flagellin, is synthesized via the Cj1293 gene. *Mol. Microbiol.* 50, 659–671. doi: 10.1046/j.1365-2958.2003.03725.x

Guccione, E. J., Kendall, J. J., Hitchcock, A., Garg, N., White, M. A., Mulholland, F., et al. (2017). Transcriptome and proteome dynamics in chemostat culture reveal how *Campylobacter jejuni* modulates metabolism, stress responses and virulence factors upon changes in oxygen availability. *Environ. Microbiol.* 19, 4326–4348. doi: 10.1111/1462-2920.13930

Guerry, P. (2007). *Campylobacter* flagella: not just for motility. *Trends Microbiol.* 15, 456–461. doi: 10.1016/j.tim.2007.09.006

Guerry, P., Alm, R. A., Power, M. E., Logan, S. M., and Trust, T. J. (1991). Role of two flagellin genes in *Campylobacter* motility. *J. Bacteriol.* 173, 4757–4764. doi: 10.1128/JB.173.15.4757-4764.1991

Guerry, P., Ewing, C. P., Schirm, M., Lorenzo, M., Kelly, J., Pattarini, D., et al. (2006). Changes in flagellin glycosylation affect *Campylobacter* autoagglutination and virulence. *Mol. Microbiol.* 60, 299–311. doi: 10.1111/j.1365-2958.2006.05100.x

Guerry, P., Logan, S. M., Thornton, S., and Trust, T. J. (1990). Genomic organization and expression of *Campylobacter* flagellin genes. *J. Bacteriol.* 172, 1853–1860. doi: 10.1128/JB.172.4.1853-1860.1990

Guerry, P., and Szymanski, C. M. (2008). Campylobacter sugars sticking out. *Trends in Microbiol.* 16, 428–435. doi: 10.1016/j.tim.2008.07.002

Gundogdu, O., Bentley, S. D., Holden, M. T., Parkhill, J., Dorrell, N., and Wren, B. W. (2007). Re-annotation and re-analysis of the campylobacter jejuni NCTC11168 genome sequence. *BMC Genomics* 8:162. doi: 10.1186/1471-2164-8-162

Heras, B., Scanlon, M. J., and Martin, J. L. (2015). Targeting virulence not viability in the search for future antibacterials. *Br. J. Clin. Pharmacol.* 79, 208–215. doi: 10.1111/bcp.12356

Hitchen, P., Brzostek, J., Panico, M., Butler, J. A., Morris, H. R., Dell, A., et al. (2010). Modification of the *Campylobacter jejuni* flagellin glycan by the product of the Cj1295 homopolymeric-tract-containing gene. *Microbiology* 156, 1953–1962. doi: 10.1099/mic.0.038091-0

Hosking, E. R., Vogt, C., Bakker, E. P., and Manson, M. D. (2006). The *Escherichia coli* MotAB proton channel unplugged. *J. Mol. Biol.* 364, 921–937. doi: 10.1016/j.jmb.2006.09.035

Howard, S. L., Jagannathan, A., Soo, E. C., Hui, J. P. M., Aubry, A. J., Ahmed, I., et al. (2009). *Campylobacter jejuni* glycosylation island important in cell charge, legionaminic acid biosynthesis, and colonization of chickens. *Infect. Immun.* 77, 2544–2556. doi: 10.1128/IAI.01425-08

Javed, M. A., Ackermann, H. W., Azeredo, J., Carvalho, C. M., Connerton, I., Evoy, S., et al. (2014). A suggested classification for two groups of *Campylobacter* myoviruses. *Arch. Virol.* 159, 181–190. doi: 10.1007/s00705-013-1788-2

Javed, M. A., Poshtiban, S., Arutyunov, D., Evoy, S., and Szymanski, C. M. (2013). Bacteriophage receptor binding protein based assays for the simultaneous detection of *Campylobacter jejuni* and *Campylobacter coli*. *PLoS ONE* 8:e69770. doi: 10.1371/journal.pone.0069770

Javed, M. A., Sacher, J. C., van Alphen, L. B., Patry, R. T., and Szymanski, C. M. (2015b). A flagellar glycan-specific protein encoded by *Campylobacter phages* inhibits host cell growth. *Viruses*. 7, 6661–6674. doi: 10.3390/v7122964

Javed, M. A., van Alphen, L. B., Sacher, J., Ding, W., Kelly, J., Nargang, C., et al. (2015a). A receptor-binding protein of *Campylobacter jejuni* bacteriophage NCTC 12673 recognizes flagellin glycosylated with acetamidino-modified pseudaminic acid. *Mol. Microbiol.* 95, 101–115. doi: 10.1111/mmi.12849

Kalmokoff, M., Lanthier, P., Tremblay, T. L., Foss, M., Lau, P. C., Sanders, G., et al. (2006). Proteomic analysis of *Campylobacter jejuni* 11168 biofilms reveals a role for the motility complex in biofilm formation. *J. Bacteriol.* 188, 4312–4320. doi: 10.1128/JB.01975-05

Karlyshev, A. V., Linton, D., Gregson, N. A., and Wren, B. W. (2002). A novel paralogous gene family involved in phase-variable flagella-mediated motility in *Campylobacter jejuni*. *Microbiology* 148, 473–480. doi: 10.1099/00221287-148-2-473

Karlyshev, A. V., and Wren, B. W. (2005). Development and application of an insertional system for gene delivery and expression in *Campylobacter jejuni*. *Appl. Environ. Microbiol.* 71, 4004–4013. doi: 10.1128/AEM.71.7.4004-4013.2005

Kassem, I. I., Khatri, M., Sanad, Y. M., Wolboldt, M., Saif, Y. M., Olson, J. W., et al. (2014). The impairment of methylmenaquinol:fumarate reductase affects hydrogen peroxide susceptibility and accumulation in *Campylobacter jejuni*. *MicrobiologyOpen* 3, 168–181. doi: 10.1002/mbo3.158

Kearse, M., Moir, R., Wilson, A., Stones-Havas, S., Cheung, M., Sturrock, S., et al. (2012). Geneious basic: an integrated and extendable desktop software platform for the organization and analysis of sequence data. *Bioinformatics* 28, 1647–1649. doi: 10.1093/bioinformatics/bts199

Kojima, S., Kojima, C., Takao, M., Almira, G., Kawahara, I., Sakuma, M., et al. (2018). The helix rearrangement in the periplasmic domain of the flagellar stator B subunit activates peptidoglycan binding and ion influx. *Structure* 26, 59–598.e5. doi: 10.1016/j.str.2018.02.016

Kropinski, A. M., Arutyunov, D., Foss, M., Cunningham, A., Ding, W., Singh, A., et al. (2011). Genome and proteome of *Campylobacter jejuni* bacteriophage NCTC 12673. *Appl. Environ. Microbiol.* 77, 8265–8271. doi: 10.1128/AEM.05562-11

Lango-Scholey, L., Aidley, J., Woodacre, A., Jones, M. A., and Bayliss, C. D. (2016). High throughput method for analysis of repeat number for 28 phase variable loci of campylobacter jejuni strain NCTC11168. *PLoS ONE* 11. doi: 10.1371/journal.pone.0159634

Lele, P. P., Hosu, B. G., and Berg, H. C. (2013). Dynamics of mechanosensing in the bacterial flagellar motor. *Proc. Natl. Acad. Sci.* 110, 11839–11844. doi: 10.1073/pnas.1305885110

Logan, S. M. (2006). Flagellar glycosylation - a new component of the motility repertoire? *Micrbiology*. 152(Pt 5), 1249–1262.doi: 10.1099/mic.0.28735-0

Logan, S. M., Hui, J. P., Vinogradov, E., Aubry, A. J., Melanson, J. E., Kelly, J. F., et al. (2009). Identification of novel carbohydrate modifications on *Campylobacter jejuni* 11168 flagellin using metabolomics-based approaches. *FEBS J.* 276, 1014–1023. doi: 10.1111/j.1742-4658.2008.06840.x

Logan, S. M., Kelly, J. F., Thibault, P., Ewing, C. P., and Guerry, P. (2002). Structural heterogeneity of carbohydrate modifications affects serospecificity of *Campylobacter* flagellins. *Mol. Microbiol.* 46, 587–597. doi: 10.1046/j.1365-2958.2002.03185.x

Logan, S. M., Schoenhofen, I. C., and Guerry, P. (2008). "O-linked flagellar glycosylation in *Campylobacter*," in *Campylobacter, 3rd Edn.*, eds I. Nachamkin, C. M. Szymanski, and M. J. Blaser (Washington, DC: ASM Press), 471–481.

Love, M. I., Huber, W., and Anders, S. (2014). Moderated estimation of fold change and dispersion for RNA-seq data with DESeq2. *Genome Biol.* 15:550. doi: 10.1186/s13059-014-0550-8

Luo, W., Friedman, M. S., Shedden, K., Hankenson, K. D., and Woolf, P. J. (2009). GAGE: generally applicable gene set enrichment for pathway analysis. *BMC Bioinformatics* 10:161. doi: 10.1186/1471-2105-10-161

McNally, D. J., Aubry, A. J., Hui, J. P., Khieu, N. H., Whitfield, D., Ewing, C. P., et al. (2007). Targeted metabolomics analysis of *Campylobacter coli* VC167 reveals legionaminic acid derivatives as novel flagellar glycans. *J. Biol. Chem.* 282, 14463–14475. doi: 10.1074/jbc.M611027200

McNally, D. J., Hui, J. P. M., Aubry, A. J., Mui, K. K. K., Guerry, P., Brisson, J. R., et al. (2006). Functional characterization of the flagellar glycosylation locus in *Campylobacter jejuni* 81-176 using a focused metabolomics approach. *J. Biol. Chem.* 281, 18489–18498. doi: 10.1074/jbc.M603777200

Morimoto, Y. V., Che, Y., Minamino, T., and Namba, K. (2010). Proton-conductivity assay of plugged and unplugged MotA/B proton channel by cytoplasmic pHluorin expressed in *Salmonella*. *FEBS Lett.* 584, 1268–1272. doi: 10.1016/j.febslet.2010.02.051

Palyada, K., Threadgill, D., and Stintzi, A. (2004). Iron acquisition and regulation in *Campylobacter jejuni*. *J. Bacteriol.* 186, 4714–4729. doi: 10.1128/JB.186.14.4714-4729.2004

Parkhill, J., Wren, B. W., Mungall, K., Ketley, J. M., Churcher, C., Basham, D., et al. (2000). The genome sequence of the food-borne pathogen *Campylobacter jejuni* reveals hypervariable sequences. *Nature.* 403, 665–668. doi: 10.1038/35001088

Ribardo, D. A., Kelley, B. R., Johnson, J. G., and Hendrixson, D. R. (2019). A chaperone for the stator units of a bacterial flagellum. *mBio* 10:e01732-19. doi: 10.1128/mBio.01732-19

Sacher, J. C. (2018). *Insights Into the Role of the Flagellar Glycosylation System in* Campylobacter jejuni *Phage-Host Interactions*. Doctoral thesis, University of Alberta, Edmonton, AB, Canada.

Sacher, J. C., Flint, A., Butcher, J., Blasdel, B., Reynolds, H. M., Lavigne, R., et al. (2018a). Transcriptomic analysis of the *Campylobacter jejuni* response to T4-like phage NCTC 12673 infection. *Viruses.* 10:332. doi: 10.3390/v10060332

Sacher, J. C., Yee, E., Szymanski, C. M., and Miller, W. G. (2018b). Complete genome sequence of *Campylobacter jejuni* strain 12567, a livestock-associated clade representative genome. *Announcements*. 6:e00513-18. doi: 10.1128/genomeA.00513-18

Sacher, J. C., Yee, E., Szymanski, C. M., and Miller, W. G. (2018c). Complete genome sequences of three *Campylobacter jejuni* phage-propagating strains genome. *Announcements*. 6:e00514-18. doi: 10.1128/genomeA.00514-18

Schirm, M., Arora, S. K., Verma, A., Vinogradov, E., Thibault, P., Ramphal, R., et al. (2004). Structural and genetic characterization of glycosylation of type A flagellin in pseudomonas aeruginosa. *J. Bacteriol.* 186, 2523–2531. doi: 10.1128/JB.186.9.2523-2531.2004

Schirm, M., Schoenhofen, I. C., Logan, S. M., Waldron, K. C., and Thibault, P. (2005). Identification of unusual bacterial glycosylation by tandem mass spectrometry analyses of intact proteins. *Anal. Chem.* 77, 7774–7782. doi: 10.1021/ac051316y

Schirm, M., Soo, E. C., Aubry, A. J., Austin, J., Thibault, P., and Logan, S. M. (2003). Structural, genetic and functional characterization of the flagellin glycosylation process in helicobacter pylori. *Mol. Microbiol.* 48, 1579–1592. doi: 10.1046/j.1365-2958.2003.03527.x

Schoenhofen, I. C., McNally, D. J., Vinogradov, E., Whitfield, D., Young, N. M., Dick, S., et al. (2006). Functional characterization of dehydratase/aminotransferase pairs from *Helicobacter* and *Campylobacter*: enzymes distinguishing the pseudaminic acid and bacillosamine biosynthetic pathways. *J. Biol. Chem.* 281, 723–732. doi: 10.1074/jbc.M511021200

Simpson, D. J., Sacher, J. C., and Szymanski, C. M. (2015). Exploring the interactions between bacteriophage-encoded glycan binding proteins and carbohydrates. *Curr. Opin. Struct. Biol.* 34, 69–77. doi: 10.1016/j.sbi.2015.07.006

Sørensen, M. C. H., van Alphen, L. B., Fodor, C., Crowley, S. M., Christensen, B. B., Szymanski, C. M., et al. (2012). Phase variable expression of capsular polysaccharide modifications allows *Campylobacter jejuni* to avoid bacteriophage infection in chickens. *Front. Cell. Infect. Microbiol.* 2:11. doi: 10.3389/fcimb.2012.00011

Sørensen, M. C. H., van Alphen, L. B., Harboe, A., Li, J., Christensen, B. B., Szymanski, C. M., et al. (2011). Bacteriophage F336 recognizes the capsular phosphoramidate modification of *Campylobacter jejuni* NCTC11168. *J. Bacteriol.* 193, 6742–6749. doi: 10.1128/JB.05276-11

Szymanski, C. M., King, M., Haardt, M., and Armstrong, G. D. (1995). *Campylobacter jejuni* motility and invasion of Caco-2 cells. *Infect. Immun.* 63, 4295–4300.

Szymanski, C. M., Logan, S. M., Linton, D., and Wren, B. W. (2003). *Campylobacter* – a tale of two protein glycosylation systems. *Trends Microbiol.* 11, 233–238. doi: 10.1016/S0966-842X(03)00079-9

Szymanski, C. M., and Wren, B. W. (2005). Protein glycosylation in bacterial mucosal pathogens. *Nat. Rev. Microbiol.* 3, 225–237. doi: 10.1038/nrmicro1100

Thibault, P., Logan, S. M., Kelly, J. F., Brisson, J. R., Ewing, C. P., Trust, T. J., et al. (2001). Identification of the carbohydrate moieties and glycosylation motifs in *Campylobacter jejuni* flagellin. *J. Biol. Chem.* 276, 34862–34870. doi: 10.1074/jbc.M104529200

Ulasi, G. N., Creese, A. J., Hui, S. X., Penn, C. W., and Cooper, H. J. (2015). Comprehensive mapping of O-glycosylation in flagellin from *Campylobacter jejuni* 11168: a multienzyme differential ion mobility mass spectrometry approach. *Proteomics* 15, 2733–2745. doi: 10.1002/pmic.201400533

van Alphen, L. B., Wuhrer, M., Bleumink-Pluym, N. M. C., Hensbergen, P. J., Deelder, A. M., and van Putten, J. P. M. (2008). A functional *Campylobacter jejuni* maf4 gene results in novel glycoforms on flagellin and altered autoagglutination behaviour. *Microbiology* 154, 3385–3397. doi: 10.1099/mic.0.2008/019919-0

Weingarten, R. A., Taveirne, M. E., and Olson, J. W. (2009). The dual-functioning fumarate reductase is the sole succinate: quinone reductase in *Campylobacter jejuni* and is required for full host colonization. *J. Bacteriol.* 191:5292. doi: 10.1128/JB.00166-09

Zampronio, C. G., Blackwell, G., Penn, C. W., and Cooper, H. J. (2011). Novel glycosylation sites localized in *Campylobacter jejuni* flagellin FlaA by liquid chromatography electron capture dissociation tandem mass spectrometry. *J. Proteome Res.* 10, 1238–1245. doi: 10.1021/pr101021c

Conflict of Interest: The authors declare that the research was conducted in the absence of any commercial or financial relationships that could be construed as a potential conflict of interest.

frontiers in Microbiology

ORIGINAL RESEARCH
published: 24 September 2020
doi: 10.3389/fmicb.2020.510638

In vitro Analysis of O-Antigen-Specific Bacteriophage P22 Inactivation by *Salmonella* Outer Membrane Vesicles

*Mareike S. Stephan[1], Nina K. Broeker[1], Athanasios Saragliadis[2], Norbert Roos[2], Dirk Linke[2] and Stefanie Barbirz[1]**

[1]Physical Biochemistry, Department for Biochemistry and Biology, University of Potsdam, Potsdam, Germany, [2]Department of Biosciences, University of Oslo, Oslo, Norway

Bacteriophages use a large number of different bacterial cell envelope structures as receptors for surface attachment. As a consequence, bacterial surfaces represent a major control point for the defense against phage attack. One strategy for phage population control is the production of outer membrane vesicles (OMVs). In Gram-negative host bacteria, O-antigen-specific bacteriophages address lipopolysaccharide (LPS) to initiate infection, thus relying on an essential outer membrane glycan building block as receptor that is constantly present also in OMVs. In this work, we have analyzed interactions of *Salmonella* (*S.*) bacteriophage P22 with OMVs. For this, we isolated OMVs that were formed in large amounts during mechanical cell lysis of the P22 S. Typhimurium host. *In vitro*, these OMVs could efficiently reduce the number of infective phage particles. Fluorescence spectroscopy showed that upon interaction with OMVs, bacteriophage P22 released its DNA into the vesicle lumen. However, only about one third of the phage P22 particles actively ejected their genome. For the larger part, no genome release was observed, albeit the majority of phages in the system had lost infectivity towards their host. With OMVs, P22 ejected its DNA more rapidly and could release more DNA against elevated osmotic pressures compared to DNA release triggered with protein-free LPS aggregates. This emphasizes that OMV composition is a key feature for the regulation of infective bacteriophage particles in the system.

Keywords: bacteriophage, bacterial outer membrane vesicles, O-antigen, bacterial membrane fractionation, *Salmonella*, lipopolysaccharide

OPEN ACCESS

Edited by:
Felipe Cava,
Umeå University, Sweden

Reviewed by:
Konstantin Anatolievich Miroshnikov, Institute of Bioorganic Chemistry (RAS), Russia
Jose A. Bengoechea, Queen's University Belfast, United Kingdom

****Correspondence:***
Stefanie Barbirz
barbirz@uni-potsdam.de

Specialty section:
This article was submitted to Infectious Diseases, a section of the journal Frontiers in Microbiology

Received: *07 November 2019*
Accepted: *26 August 2020*
Published: *24 September 2020*

Citation:
Stephan MS, Broeker NK, Saragliadis A, Roos N, Linke D and Barbirz S (2020) In vitro Analysis of O-Antigen-Specific Bacteriophage P22 Inactivation by Salmonella Outer Membrane Vesicles. Front. Microbiol. 11:510638. doi: 10.3389/fmicb.2020.510638

INTRODUCTION

Bacteriophages are ubiquitous in the microbial world and major players in many bacterial ecosystems. Here, they perform a variety of life styles, with prophages or mature phage particles as prominent examples of prevalent phage states (Feiner et al., 2015). Key event in a phage's life cycle is the interaction with host surface receptors to initiate infection of the bacterial host. If this step is successful, the resulting genome transfer to the bacterial cytosol will open the route for a plethora of phage genome functions inside the host cell (Salmond and Fineran, 2015; Erez et al., 2017; Rostol and Marraffini, 2019). Diverse bacterial cell surface structures serve as bacteriophage receptors (Silva et al., 2016). Besides protein-based phage receptors,

glycan structures, the major building blocks of the bacterial envelope, represent a very important and structurally diverse phage receptor class (Pires et al., 2016; Latka et al., 2017). Phages do not only exploit glycans to start cell entry (Wang et al., 2019) but also may alter these structures to prevent superinfection (Kintz et al., 2015). In turn, bacteria constantly modify their surface composition to escape from phage attack (Rostol and Marraffini, 2019).

O-antigen-specific phages are specialists that use lipopolysaccharide (LPS) as an essential receptor for infection initiation in Gram-negative hosts (Broeker and Barbirz, 2017). These tailed phages link recognition and enzymatic processing of the O-polysaccharide to a so far unknown membrane interaction step that leads to conformational rearrangements in the tail and subsequent particle opening *in vitro* (Andres et al., 2010, 2012; Broeker et al., 2018, 2019). *In vivo*, full genome transfer additionally requires other factors like outer membrane (OM) proteins or a membrane potential (Leavitt et al., 2013; Parent et al., 2014). *In vitro*, purified and protein-free LPS alone is sufficient to inactivate O-antigen-specific phages, because binding to membrane-mimicking LPS aggregates can trigger DNA release from the capsid (Broeker et al., 2019). *In vitro* studies furthermore revealed that the kinetics of this process were dependent on the architecture of the tail, but not on the chemical composition of the O-antigen receptor. Moreover, to control phage populations and to achieve superinfection exclusion, O-antigen-specific phages may modify the O-antigen structure of their host cell (Susskind et al., 1974; Cenens et al., 2015).

In response to bacteriophage attack, bacteria control the number of phage particles in their environment in multiple ways, and, in turn, phages respond by own strategies to overcome bacterial defense (Doron et al., 2018; Vidakovic et al., 2018; Rostol and Marraffini, 2019). Among the large number of defense mechanisms determining the ecosystem in which bacteria and phages coexist, as a matter of fact, the host surface is a critical point for bacteriophage entry control (Leon and Bastias, 2015). For example, O-antigen phase variations may result in mixed bacterial populations and an increased resistance to phage attack (Seed et al., 2012; Schmidt et al., 2016). Moreover, like all living cells, bacteria can also shed outer membrane vesicles (OMVs; Schwechheimer and Kuehn, 2015). In OMVs, bacteria may control the content of bacteriophage surface receptors and thus exploit this extracellular material as buffer against phage attack (Manning and Kuehn, 2011; Biller et al., 2014; Reyes-Robles et al., 2018).

The ubiquitous budding of spherical OM structures is highly conserved in both pathogenic and non-pathogenic Gram-negative bacteria (Bai et al., 2014; Celluzzi and Masotti, 2016; Guerrero-Mandujano et al., 2017). OMVs are composed of OMs, containing LPS, phospholipids and OM proteins, and soluble periplasmic components like DNA and proteins. OMVs function in bacterial communication, cell wall remodeling, horizontal gene transfer, defense, and pathogenicity (Mashburn and Whiteley, 2005; Bonnington and Kuehn, 2016; Crispim et al., 2019); their composition may thus differ from that of OM and periplasm (Schwechheimer et al., 2013; Kim et al., 2018; Malge et al., 2018). The size of the vesicles depends on the given strain but generally ranges from 50 to 250 nm in diameter (Beveridge, 1999). Vesiculation is induced as response to different stress factors, like the presence of antimicrobial or toxic particles or unfavorable environmental conditions, for example, nutrient deficiency or elevated temperatures (Loeb, 1974; Manning and Kuehn, 2011; Schwechheimer et al., 2013; Bai et al., 2014). Host cell OMVs can bind and rapidly remove free phage particles from a solution and effectively reduce phage activity (Manning and Kuehn, 2011; Biller et al., 2014; Parent et al., 2014; Reyes-Robles et al., 2018). However, the mechanisms of this interaction, that is time-resolved observation of the all involved steps on a molecular level, have not been studied in detail so far.

In this work, we have analyzed *Salmonella* phage P22 in the presence of OMV prepared from its host, *Salmonella enterica* ssp. *enterica* sv. Typhimurium (S. Typhimurium). Podovirus P22 is an O-antigen-specific, transducing phage with a short, non-contractile tail. P22 is a well-established model system for studying DNA transduction, *Salmonella* genetics, and lysogeny (Prevelige, 2006; Casjens and Grose, 2016). P22 uses LPS as its receptor, and tailspike protein (TSP)-mediated cleavage of the O-antigen part then positions the phage particle on the cell surface, where the particle opens (Andres et al., 2010). *In vivo*, genome transfer is mediated by a set of P22 ejection proteins that contribute to forming a channel-like structure that provides access to the cytosol by bridging the cell wall (Wang et al., 2019). *In vitro*, purified protein-free LPS aggregates mimicking the OM were sufficient to elicit DNA release into the solution (Andres et al., 2010). We wanted to extend this *in vitro* system to a more complex receptor system and have analyzed dynamics of DNA release from phage P22 in the presence of OMVs. We used large-scale OMV preparations to obtain sufficient material for fluorescence spectroscopy studies (Thein et al., 2010). Our *in vitro* analyses show that OMVs efficiently rendered P22 phage particles non-infective. OMV-triggered P22 phages ejected their DNA more rapidly than LPS-triggered P22 phages. However, and in contrast to pure LPS preparations, when triggered by OMVs, only a subfraction of these phages also injected their DNA into the vesicles.

MATERIALS AND METHODS

Materials and Bacterial Strains

Yo-Pro®-1 iodide was obtained from Invitrogen (Thermo Fisher Scientific Life Technologies, Darmstadt, Germany), and Purpald® (4-Amino-3-hydrazino-5-mercapto-1,2,4-triazole and 4-Amino-5-hydrazino-1,2,4-triazole-3-thiol) was obtained from Sigma Aldrich (Merck KGaA, Darmstadt, Germany). The standard buffer in all experiments was 10 mM Tris–HCl and 4 mM $MgCl_2$, pH 7.6. *Salmonella* strains S. Typhimurium AroA::Tn10 iroBC::kan (LPS and vesicle preparation) and S. Typhimurium DB 7136 LT2 (phage propagation) were from our laboratory collections (Tindall et al., 2005). The hypervesiculating strain S. Typhimurium ATCC 14028 MvP2390 was provided by Prof. Dr. Michael Hensel (University Osnabrück). Preparation of LPS has been described previously (Andres et al., 2010). LPS was quantified in all OMV samples by the Purpald® assay, and the protein content of OMV

was determined with bicinchoninic acid (BCA; Smith et al., 1985; Lee and Tsai, 1999). PEG 8000 was purchased from Roth (Carl Roth GmbH, Karlsruhe, Germany). All other chemicals used were of analytic grade and double-distilled water was used throughout.

Preparation of Outer Membrane Vesicles From Cell Lysates

OMVs present after mechanical cell lysis were prepared according to Thein et al. (2010). Briefly, S. Typhimurium AroA::Tn10 iroBC::kan were grown in LB medium supplemented with 50 μg ml^{-1} kanamycin overnight at 37°C. After cell harvest, cells were incubated with 0.1 mg ml^{-1} lysozyme and 10 μg ml^{-1} DNase I on ice and lysed with French press. Membranes were collected by centrifugation at 75,400 × *g* for 30 min at 4°C and suspended in standard buffer. For OMV purification with sucrose density gradients ("OMV Suc"), total membranes were loaded on a three-step sucrose density gradient (3 ml 75% w/v, 5 ml 50% w/v, and 3 ml 25% w/v) and centrifuged at 250,000 × *g* for 12 to 16 h at 4°C to separate inner membrane (IM) and OM fractions. The OM accumulated at the 50/75% sucrose interface. The harvested OM fraction was diluted in water, collected at 30,000 × *g* (30 min) and stored at 4°C. Alternatively, OMVs were obtained by selective detergent solubilization ("OMV Det"). For this, the total membranes after French press lysis were incubated with 1% N-lauroylsarcosine and centrifuged at 30,000 × *g* for 30 min at 4°C to solubilize the IM. To wash OMV, they were suspended in water, collected at 30,000 × *g* (30 min) and stored at 4°C.

Preparation of Outer Membrane Vesicles Naturally Budded Into *Salmonella* Culture Supernatants

Hypervesiculating S. Typhimurium ATCC 14028 MvP2390 were grown in LB medium supplemented with 50 μg ml^{-1} kanamycin at 37°C to an $OD_{600\ nm}$ of 1.5. Cells and cell debris were removed by two subsequent centrifugation steps at 4000 × *g* (15 min each, 4°C). The supernatant was filtered twice on Whatman cellulose acetate 0.45 μm and 0.20 μm (GE Healthcare Europe GmbH, Freiburg, Germany), and OMVs ("OMV budded") were collected from the filtrate at 38,500 × *g* (3 h, 4°C) and stored in phosphate-buffered saline (PBS) at 4°C.

Electron Microscopy

EM images were recorded on a JEOL JEM1400-Plus transmission electron microscope (TEM). Staining methods for Gram-negative bacteria samples have been described (Grin et al., 2011). Samples were loaded on Formvar-coated copper grids, stained with 1% (w/v) uranyl acetate and embedded in 1% (w/v) uranyl acetate and 0.4% (w/v) methyl cellulose.

Interaction Studies of Phage Particles With LPS and OMVs

Plaque-Forming Assay

The plaque-forming assay monitors the decrease of infectious particles due to co-incubation with LPS or OMV. 5 × 10^3 pfu ml^{-1} P22 bacteriophages were incubated with 2.5 μg ml^{-1} LPS or OMV LPS equivalents in standard buffer at 37°C. After different incubation times, 100 μl were taken, mixed with warm soft agar, and plated on thin LB agar plates. After overnight incubation at 37°C, the plaques were counted and plaque-forming units (pfu ml^{-1}) were determined. As control, P22 bacteriophages were incubated with buffer only.

DNA Ejection Monitored by Yo-Pro Fluorescence

Bacteriophage P22 DNA ejection was followed by fluorescence spectroscopy as described before (Andres et al., 2010). OMVs for these experiments were prepared with the sucrose gradient method (OMV Suc). Briefly, 4 × 10^9 pfu ml^{-1} P22 bacteriophages were incubated at 37°C with 10 μg ml^{-1} LPS or OMV LPS equivalents in the presence of 1.1 μM Yo-Pro®-1 iodide. The fluorescence signal was detected at 509 nm after excitation at 491 nm. After 170 min, DNase I was added to a final concentration of 10 μg ml^{-1}. Curves were corrected for Yo-Pro phage staining in presence of O-antigen-depleted OMVs. Curves were fitted to a monoexponential function as described before (Andres et al., 2010; Chiaruttini et al., 2010).

$$F_t = F_{\max} \cdot \left(1 - e^{-k_{open} t}\right) \quad (1)$$

F_t Fluorescence signal at time point t

F_{max} maximum signal amplitude

k_{open} reaction rate constant of phage particle opening

t time

For ejection experiments with PEG 8000, osmotic pressures at 37°C were calculated from the PEG weight fraction according to the empirical polynomial (Parsegian et al., 1986):

$$\Pi(atm) = -1.29\,G^2T + 140G^2 + 4G$$

G Converted PEG weight percent (w) concentration:

$$G = \frac{w}{100 - w}$$

T Temperature (°C)

RESULTS

Preparation and Characterization of S. Typhimurium Outer Membrane Vesicles

To investigate differences in preparation of OMVs and to study the effects of altered vesicle characteristics on bacteriophage interactions, different preparation protocols were employed (**Table 1**). Gram-negative bacteria shed OMVs in culture supernatants; however, the low concentrations usually require large preparation scales to obtain sufficient amounts for quantitative functional analyses. We therefore generated OMV samples by accumulation of OMs after mechanical lysis of S. Typhimurium cells. Either IMs and OMs were separated on sucrose density gradients or IMs were solubilized by detergents to collect the OM fraction by centrifugation (Thein et al., 2010). Moreover, and for comparison, we isolated OMVs from culture supernatant

TABLE 1 | Preparation methods for OMVs from S. Typhimurium.

OMV sample[a]	Membrane preparation	Enzyme treatment	Separation of IM and OM	Vesicle diameter[b]	Protein/ LPS ratio[c]
OMV Det	Membrane accumulation	DNase I and lysozyme treatment	Solubilization of inner membrane	50–100 nm	0.178
OMV Det*	Membrane accumulation	---	Solubilization of inner membrane	50–425 nm	0.244
OMV Suc	Membrane accumulation	DNase I and lysozyme treatment	Sucrose density gradient	25–125 nm	0.174
Budded OMV	Naturally budded vesicles	---	---	25–100 nm	0.936

[a]*Det, detergent method; Suc, sucrose gradient method.*
[b]*Determined by electron microscopy and dynamic light scattering (***Supplementary Figure S1***).*
[c]*BCA and Purpald assay.*

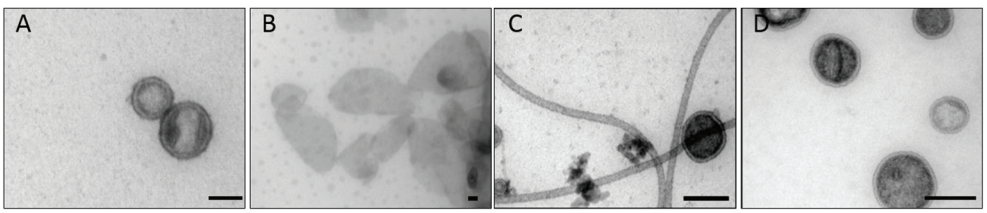

FIGURE 1 | Transmission electron microscopy of *Salmonella* Typhimurium outer membrane vesicles (OMVs). **(A)** OMV Det, **(B)** OMV Det*, **(C)** budded OMV, **(D)** OMV Suc. The bar represents 50 nm.

filtrates of the hypervesiculating S. Typhimurium strain MvP2390 that is defective in Braun's lipoprotein (Dramsi et al., 2008).

Electron microscopy analysis showed that with all preparation methods, samples were obtained with spherical vesicles of 50–100 nm diameter (**Figure 1**). Stokes radii measured by dynamic light scattering confirmed these OMV size distributions (**Supplementary Figure S1**). To obtain homogeneously round-shaped vesicles from membrane accumulation, we noticed that a pre-lysis treatment of cells with DNase I and lysozyme was mandatory, because otherwise only large and irregular membrane aggregates were formed (**Figure 1B** and **Supplementary Figure S2**). The vesicles' protein: LPS ratio was calculated from analyses with BCA and Purpald assays, respectively (**Table 1**). In contrast, IM fractions that could be isolated from sucrose gradients contained notably less vesicle-like structures (**Supplementary Figure S3**). OMVs from membrane accumulation contained typical OM markers, like OM proteins and LPS (**Supplementary Figure S3**). SDS-PAGE with glycan staining confirmed that they contained LPS with a typical O-antigen chain length distribution (**Supplementary Figure S4**). Hence, LPS in OMVs could be quantified with the Purpald assay. Furthermore, co-expression of a fluorescently labeled OmpA-mCherry construct as OM marker protein showed that it was located in the OMV fraction after membrane accumulation and sucrose density gradient separation (**Supplementary Figure S3**).

The budded OMVs from culture supernatants showed an increased protein content compared to OMVs collected by membrane accumulation and also a different protein composition as estimated from SDS-PAGE analysis (**Supplementary Figure S5**). As shown earlier, under typical growth conditions, naturally budded *Salmonella* OMVs contain an increased amount of cytosolic proteins (Bai et al., 2014), which may account for the elevated protein content. Moreover, EM images of our samples revealed flagella-like structures that apparently had co-purified with the OMVs. In principle, it would be also possible that additional periplasmic proteins are present in the lumen of these naturally budded vesicles or that they display increased amounts of OM proteins (Volgers et al., 2018). However, the small yield of these OMVs isolated from culture supernatants impeded a further detailed proteomic analysis.

Interaction of Vesicles With Bacteriophage P22

Transmission electron microscopy showed that P22 bacteriophages interact with OMVs. After overnight incubation at 37°C, the uranyl acetate stain reveals the OM structure as a bright ring enclosing the vesicle lumen that appeared in a darker, "negative" stain (**Figure 2**). All OMV preparations showed vesicles being bound by phages. Phages either showed intense staining of the capsid shell or a lighter appearance of their capsids, which we assign to DNA-ejected and non-ejected particles, respectively. Phages were attached to the vesicle surface with their tail apparatus (arrows in **Figure 2**), but at the given resolution, differences in the tail conformation of ejected and non-ejected phages cannot be verified. As a rough estimate from manual image inspection, we found about 25% of the vesicles with bound phage (**Supplementary Figure S6**). A quantitative analysis would require cryo-EM sample preparation and variation of the phage-OMV ratio to estimate proportions of bound and ejected versus bound and non-ejected phages (Parent et al., 2014; Reyes-Robles et al., 2018).

To further validate irreversible binding and inactivation of phage P22 by OMVs, we analyzed P22-OMV mixtures

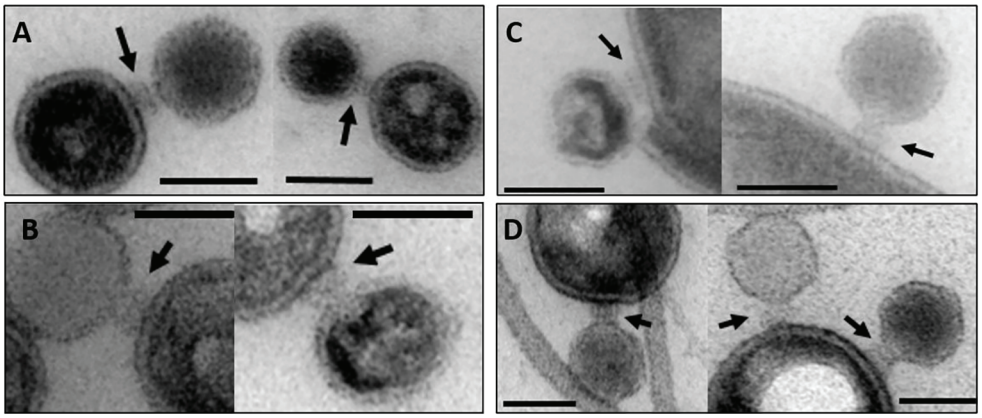

FIGURE 2 | Transmission electron microscopy images of OMV incubated with bacteriophage P22. The arrows point to the phage's baseplate. The bar represents 50 nm. **(A)** OMV Suc, **(B)** OMV Det, **(C)** OMV Det*, **(D)** budded OMV (*cf*. **Table 1** for description of different OMV samples).

for their ability to form plaques on the P22 S. Typhimurium host. With prolonged incubation times, we found that the plaque-forming units in the presence of membrane preparation-derived OMVs were reduced rapidly to less than 5% of the initial value (**Figure 3**). Interestingly, the inactivation of P22 by OMVs was well comparable to that found by a purified, protein-free LPS sample; accordingly, we assume that the proteins present in the OMVs did not influence the phage inactivation. Rather, as previously described, the isolated LPS receptor is a sufficient inhibitor to inactivate the O-antigen-specific P22 phage (Broeker and Barbirz, 2017; Broeker et al., 2019). However, whereas inactivation profiles for OMVs obtained from OM and LPS were highly similar, budded OMVs obtained from culture supernatants showed a much slower inactivation effect on phage P22, with about 25% of active phage particles remaining after 6 h of incubation. This might be related to their increased protein content, probably reducing the number and altering the distribution of surface-accessible LPS receptors, resulting in a slower decrease of infective, unbound phage particles. Flagella contaminations in this preparation might additionally have affected their capacity for phage inactivation.

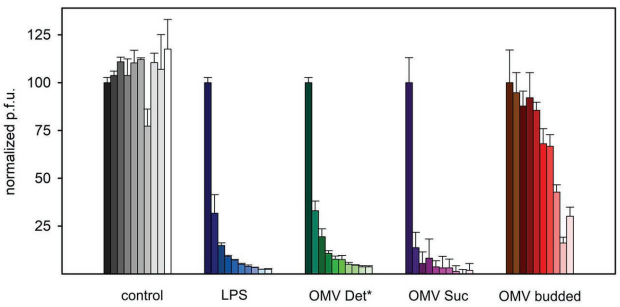

FIGURE 3 | Reduction of P22 plaque formation on S. Typhimurium in the presence of LPS or OMV. 8×10^4 P22 bacteriophages were incubated with 2.5 μg ml^{-1} LPS or 2.5 μg ml^{-1} OMV LPS equivalents at 37°C before analysis of plaque-forming units on S. Typhimurium. Increasing incubation times shown as fading colors: 0, 5, 10, 20, 30, 45, 60, 90, 120, 180, and 240 min. For characteristics of different OMV types *cf*. **Table 1**. Error bars represent results from three technical replicates.

P22 Bacteriophage Particle Opening Analysis With Vesicles

Lysis and plaque-forming assays only show irreversible binding and inactivation of phage P22, but no information is obtained whether inactivated bacteriophage P22 particles have lost their DNA upon contact with OMVs. Moreover, from negative stain EM analyses, neither quantitative amounts of ejected phage nor dynamics of the DNA ejection process were accessible. We therefore monitored DNA ejection of bacteriophage P22 with a fluorescence ejection assay that has been described previously (Andres et al., 2010, 2012; Broeker et al., 2018, 2019). In this assay, purified host LPS is mixed with the bacteriophage. This triggers opening of the phage capsid and release of DNA in the surrounding solution that contains the fluorescent DNA-intercalating dye Yo-Pro. This leads to a rapid and intense fluorescence signal increase with increasing phage DNA concentrations in solution. In contrast, in the absence of LPS, phage particles remain intact and only show a weak background fluorescent signal, because the dye Yo-Pro has weak affinity to the highly condensed DNA inside the phage capsids. As a consequence, O-antigen-specific phages only show a DNA ejection signal when triggered with an intact LPS, whereas O-polysaccharide or lipid A alone or rough LPS do not elicit DNA release (Andres et al., 2010). For P22, as for other phages, monoexponential kinetic ejection profiles were measured with this method that describes the rate-limiting phage particle opening step (Chiaruttini et al., 2010; Andres et al., 2012).

Co-incubation of P22 phage and OMVs in the presence of Yo-Pro resulted in a monoexponential increase of the fluorescence signal, reaching a plateau after about 170 min (**Figure 4**). Neither OMVs alone nor a control in which phage was incubated with OMVs that lack the phage O-antigen receptor showed a notable fluorescence signal increase. Hence, the fluorescence increase in the presence of OMVs monitors phage DNA liberated

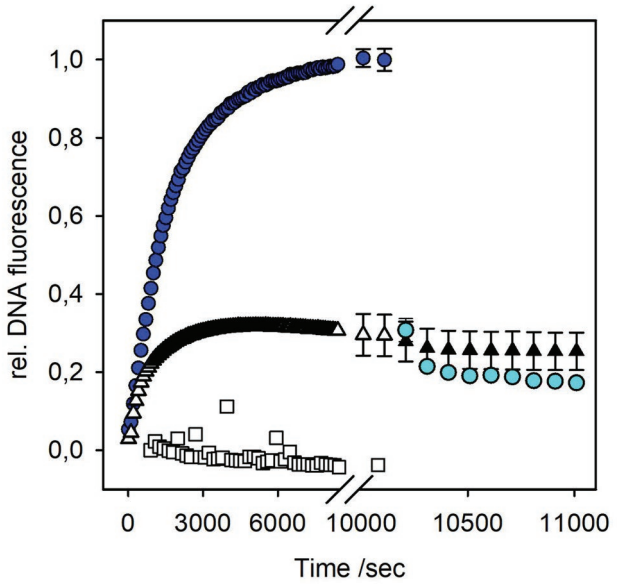

FIGURE 4 | DNA release from bacteriophage P22 triggered by OMV or LPS. Incubation of 4 × 10^9 pfu/ml P22 phages at 37°C in the presence of a fluorescent DNA-binding dye (1 μM Yo-Pro) with 10 μg ml^{-1} LPS (blue circles) or OMVs (white triangles; 10 μg ml^{-1} LPS equivalents, see Materials and Methods). Rate constants for phage particle opening were calculated from monoexponential fluorescence increase to $k_{open,LPS}$ = 5.89 ± 0.01 × 10^{-4} s^{-1}, and $k_{open,OMV}$ = 10.00 ± 0.01 × 10^{-4} s^{-1}, respectively (Chiaruttini et al., 2010). After 170 min, DNase I (10 μg ml^{-1}) was added to the ejected phages, either LPS-triggered (cyan circles) or OMV-triggered (black triangles). Plot shows mean values of three technical replicates. For clarity, only every tenth point was plotted and exemplary error bars are given for the last points of the ejection curves and for data in presence of DNase I only. Plots with all error bars can be found in **Supplementary Figure S9**. As an O-antigen-free control, 10 μg ml^{-1} OMV LPS equivalents were incubated overnight with 10 μg ml^{-1} P22TSP at 37°C prior to the ejection experiment (white squares).

from the phage capsids. We monitored similar DNA release profiles from phage P22 with all OMVs irrespective of their source and purification protocol (**Supplementary Figure S7**). However, the naturally budded OMVs contained protein impurities and were available only at an overall poor yield (see above). In all fluorescence experiments, we therefore worked with OMVs obtained from accumulated membranes with the sucrose gradient method (*cf.* Materials and Methods).

To check whether phages ejected their DNA into the vesicles or into the solution, we added DNase I after the ejection signal had reached a plateau. If DNA is free in solution, nucleotides produced by DNase I will no longer intercalate with Yo-Pro, resulting in a decrease of the fluorescence signal (Andres et al., 2010). However, the fluorescence signal obtained from P22 DNA ejection in the presence of OMVs did not decrease (**Figure 4**). Apparently, when triggered by OMVs, all DNA ejected from phage was not accessible to DNase I, because it was protected either inside the vesicles or inside the phage capsids.

The plaque-forming assay showed that OMVs can rapidly inactivate phage particles in solution. To check whether all phages in the fluorescence experiment were associated with OMVs, we added free LPS to the mixtures 170 min after the reaction was started. If at this time point a significant amount of phage particles had remained free in solution, a signal increase due to DNA release upon phage interactions with the newly added free LPS receptor should be observed. However, we did not observe any further signal increase upon LPS addition (**Supplementary Figure S8**). This result is in agreement with the plaque-forming assay where OMV rapidly cleared off phage particles from the solution. We therefore conclude that all P22 phage particles in the fluorescent assay were rapidly and irreversibly associated with OMVs and could no longer interact with newly added LPS.

In the fluorescence assay, the OMV concentration was calculated as LPS units determined with the Purpald test to be able to compare OMV-triggered phage ejection profiles with those triggered with purified LPS. Comparison of kinetic constants for DNA ejection triggered either by LPS or OMVs showed that particle opening velocities with OMVs were increased about 2-fold relative to LPS (**Figure 4**). However, only about 30% of the signal amplitude were reached compared to phages triggered with a pure LPS sample. Even if we increased OMV concentrations 3-fold, we did not observe an increase in the amount of ejected DNA (**Supplementary Figure S8**). This means that only a part of the phage particles have lost their DNA in the presence of OMVs, in contrast to purified LPS, in presence of which all particles completely exposed their DNA to the solution (Andres et al., 2010).

OMVs used in the fluorescence experiments were prepared from accumulated OMs after French press cell lysis. We cannot fully exclude the idea that a part of the OMVs obtained by this method might be inverse, i.e., with the LPS at the inside and the phospholipid part at the outside. O-antigen-specific phage P22 would not bind to a vesicle with O-antigen chains on the inside and not eject its DNA and would thus remain inert against the inside-out vesicle fraction. OMVs in this study were quantified *via* their LPS concentration. We did not find an increase in DNA ejection when we increased the OMV concentration from 10 μg ml^{-1} LPS to 30 μg ml^{-1} LPS (**Supplementary Figure S8**). This means that at 10 μg ml^{-1} LPS OMV concentration, all phage particles in the system can interact with the OMVs. If a part of the vesicles were inside out, we should observe an increase in ejected phages because with increased OMV concentration, more phage O-antigen receptors become exposed. Moreover, we enzymatically removed the O-antigen from the vesicle surface by incubation with purified P22 tailspike protein prior to exposing them to phage P22. The resulting O-antigen-depleted vesicles could not trigger DNA ejection from phage P22 (**Supplementary Figure S8**). From these controls, we conclude that the fluorescence signal observed in our experiments is exclusively related to a phage interaction with vesicles that expose LPS on the outside.

DNA Ejection in the Presence of Polyethylene Glycol (PEG)

Protein-free, highly pure LPS preparations that are present as aggregates free in solution could trigger particle opening in all P22 phages present in a reaction. However, for P22 DNA

ejection triggered by OMVs, only about 30% of DNA signal was obtained. Moreover, this signal was not accessible to DNase I. These findings imply two scenarios for P22 DNA ejection in the presence of OMV, either (i) 30% of the particles have completely ejected their DNA, whereas for the remaining fraction no DNA release occurs, or (ii) all particles have released their DNA, but only to about 30%. To distinguish between these two situations, we analyzed DNA release from phage P22 in the presence of increasing PEG concentrations. It has been shown previously for siphovirus λ that DNA ejection is driven by the intra-capsid osmotic pressure and that at increasing osmotic pressures, less DNA could leave the λ capsids (Evilevitch et al., 2003, 2005). Also for P22, it was shown that at increasing osmotic pressures and when triggered with LPS and OM proteins, part of its DNA remained in the phage capsid and was protected from DNase cleavage (Jin et al., 2015).

We therefore analyzed the DNA fluorescence increase in the presence of different concentrations of PEG 8000, when P22 was mixed with OMVs (**Figure 5A**). At 15% (3.58 atm) PEG, we obtained about 40% of the initial signal. This shows that an external osmotic pressure could effectively reduce DNA ejection from vesicle-associated phages. However, earlier work showed that, at this osmotic pressure (3.58 atm), still around 70% of the P22 DNA could leave the capsid when triggered with LPS or a mixture of LPS and the outer membrane protein OmpA (Jin et al., 2015). Hence, P22 triggered by OMVs ejected less DNA at increased external osmotic pressures, illustrating that OMVs represent an OM receptor system different from pure LPS or OM protein–LPS mixtures. Furthermore, the notable effect also of lower PEG concentrations on DNA release confirms that only about 30% of the P22 particles are actively ejecting their DNA in the presence of OMVs. At 5% PEG (0.46 atm), we already observed a signal decrease to 70% (**Supplementary Figure S10**). If all particles in the system were actively releasing only a part of their DNA, these low osmotic pressures would not elicit a pronounced effect on ejection because the initial release of only a small fraction of DNA is also possible against elevated osmotic pressures.

It was shown for other systems that at higher PEG concentrations, the DNA ejection can be completely stopped (Evilevitch et al., 2003; Jin et al., 2015). However, in our fluorescence setup, we could not further increase PEG concentrations, as this resulted in high signal-to-noise ratio and large standard deviations. This was probably due to vesicle solubility hampered by PEG or slow equilibration of the mixtures in the viscous solution. At an osmotic pressure of 6.77 atm (20% PEG), we can thus only estimate that P22 was able to still release about 20% of its DNA. Moreover, and as described above, also in the presence of PEG, it was not possible to notably reduce the DNA signal by the addition of DNase. Again, we assume that the DNA was injected into the vesicle lumen, impeding quantification of DNA that had remained in the phage capsid at the given PEG concentration by DNA accessibility.

As DNA protection from DNase inside the P22 capsid upon ejection against increasing osmotic pressures had only been accessed on agarose gels before (Jin et al., 2015), we also analyzed purely LPS-triggered DNA release in the presence of PEG with time-resolved Yo-Pro fluorescence (**Figure 5**). Interestingly, we found that much lower osmotic pressures could completely halt DNA ejection from phage P22 than it was reported in the previous work. Already at 15% PEG (3.58 atm), nearly no free DNA was detectable in the solution and was protected from DNase cleavage, indicating that DNA release from phage P22 had come to a nearly complete stop. We assume that this different result might be due to our different LPS preparation method that ensured the complete absence of even minute contaminations of other OM components like proteins or phospholipids.

In summary, our results confirmed that irrespectively of the triggering system, either OMVs or LPS, particle opening and DNA egress from P22 are driven by osmotic pressure

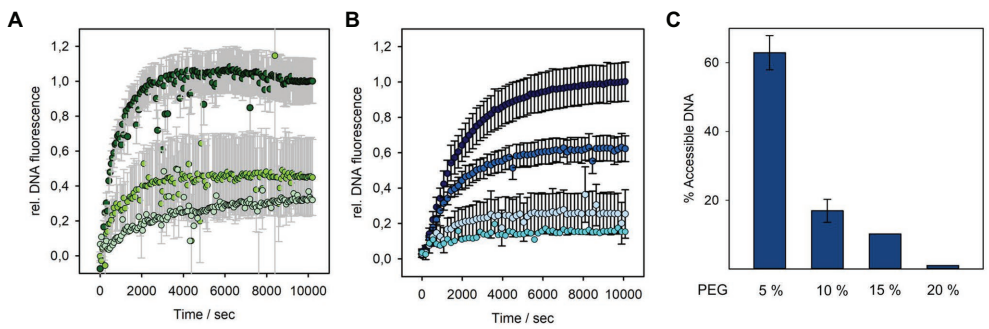

FIGURE 5 | DNA release from bacteriophage P22 triggered by OMV or LPS at different solution osmotic pressures. Incubation of 4×10^9 pfu/ml P22 phages at 37°C in the presence of a fluorescent DNA-binding dye (1.1 μM Yo-Pro) and increasing PEG 8000 concentrations with **(A)** OMV (10 μg ml^{-1} LPS equivalents) at 0% PEG (dark green, 0 atm), 15% PEG (grass green, 3.58 atm), or 20% PEG (pale green, 6.77 atm) or **(B)** 10 μg ml^{-1} LPS at 0% PEG (dark blue, 0 atm), 5% PEG (medium blue, 0.46 atm), 15% PEG (light blue, 3.58 atm), or 20% PEG (cyan, 6.77 atm; in brackets: osmotic pressure of the solution at 37°C, see Materials and Methods). Plots with error bars show mean values of three technical replicates. Values at 20% PEG are estimates from single measurements. Only every 10th data point was plotted. LPS curves in **(B)** had notably smaller error bars (black) than the OMV curves in (**A**; error bars plotted in gray for clarity). **(C)** DNA remaining accessible to DNase I after LPS-triggered DNA release from phage P22 at different PEG concentrations. Percentage values after DNase I incubation were calculated relative to the maximal DNase accessible fluorescence amplitude at 0% PEG (see **Supplementary Figure S10** for the measured fluorescence signals and ejection curves at more PEG concentrations).

inside the capsid. Moreover, whereas with LPS, 100% of the phages can eject, with OMV, an inert fraction of about 70% remains, which is unable to liberate its DNA.

DISCUSSION

Host infection of O-antigen-specific bacteriophages is initiated by the binding of phage particles to LPS. Degradation or deacetylation of the polysaccharide anchors the phage irreversibly to the cell surface, presumably in a defined distance to ensure proper spatial positioning for building a membrane-spanning infection apparatus (Andres et al., 2010; Broeker and Barbirz, 2017; Prokhorov et al., 2017; Wang et al., 2019). It is characteristic for O-antigen-specific phages that *in vitro* preparations of LPS render them non-infectious because they elicit particle opening and DNA release (Andres et al., 2012; Broeker et al., 2018, 2019). In contrast, neither O-polysaccharide alone nor lipid A or rough-type LPS with short O-antigen chains is sufficient to trigger particle opening. Apparently, the membrane-like character of LPS preparations that form multilamellar aggregates in solution is a prerequisite to trigger irreversible rearrangements in the phage tail apparatus, ultimately leading to DNA ejection (Richter et al., 2011). However, to also release P22's ejection proteins, the presence of OM proteins is necessary, illustrating that LPS-triggered DNA release only covers a subset of the initial phage infection steps (Parent et al., 2014). In this work, we have investigated the interactions of the O-antigen-specific bacteriophage P22 with OMVs that present LPS and other OM components in a defined way to the phage.

OMV Composition and Structure Is Highly Dependent on the Formation Process

OMVs are small vesicles with the same membrane organization as found in the Gram-negative OM, i.e., an inner leaflet of phospholipids and an outer LPS layer (Whitfield and Trent, 2014). OMVs thus resemble the OM to a much higher extent as compared to pure LPS aggregates. From this, it naturally follows that vesicles can be active in controlling bacteriophages in a bacterial population, and although these interactions have been unambiguously observed before with electron microscopy, they have so far only been addressed by a few studies (Manning and Kuehn, 2011; Biller et al., 2014; Parent et al., 2014; Reyes-Robles et al., 2018). One major drawback is the difficulty to obtain enough OMV material from culture supernatants (Thein et al., 2010). We therefore used OM fractions where the vesicles were formed during cell lysis. As a matter of fact, OMV composition, especially with respect to the protein content, is highly dependent on the conditions under which the vesicles are formed. During a natural budding event, bacterial cells control the OMV protein load, for example in response to nutrient availability in the medium or to distribute antibiotic resistance factors like β-lactamases (Bai et al., 2014; Kim et al., 2018). Moreover, the size of budded vesicles is dictated by the strain of origin, formation mechanism, and LPS and protein composition (Deatherage et al., 2009; Kulp and Kuehn, 2010; Schwechheimer and Kuehn, 2015; Toyofuku et al., 2019).

We have used different techniques to obtain vesicles from OM preparations. Here, the formation of vesicles from the enriched OM is driven by hydrophobic effects and leaflet asymmetry (Park et al., 2015; Rozycki and Lipowsky, 2015). We found that DNaseI and lysozyme treatment were important prerequisites to obtain OMVs with size and shape similar to naturally budded OMVs. This emphasizes that inefficient separation of IMs and OMs most probably resulted in contamination with IM components. In the accumulated OM fraction this hence changed membrane thickness and resulted in large and irregular vesicle size. Moreover, the separation method, i.e., either sucrose gradient or detergent treatment, can influence the extent of residual IM contaminations in OMVs, as well as the protein content (Thein et al., 2010). Accordingly, we observed differences in the protein pattern in OMVs prepared *via* sucrose gradient or with detergent, although the total protein content was approximately the same. All quantitative bacteriophage-OMV interaction fluorescence analyses in this work were thus carried out with OMVs prepared by a single technique, i.e., the sucrose gradient method. We are aware that OMVs obtained from different preparation methods might show different results. Even more, to further address OMV function in bacterial control of bacteriophage populations, naturally budded vesicles should be tested, for which large-scale preparations have also been reported (Hsia et al., 2016). Nevertheless, we claim that our reductionist *in vitro* system can add insight into bacteriophage interactions with their O-antigen receptors when part of a more complex membrane system as present in OMVs.

Bacteriophage P22 OMV Interactions Clearly Differ From Interactions With Isolated LPS Receptors

OMVs produced from bacteriophage P22's S. Typhimurium host act as a decoy for phage particles. Like free LPS aggregates, incubation with OMV preparations rapidly reduced the number of infective particles in the solution. Phages that are in contact with OMVs in the majority were not primed for genome transfer. Rather, they were inactivated, mostly by simply binding and blocking the phage on the OMV by a so far unknown mechanism and, to a smaller extent, by genome loss as shown in this and other studies. Differences in the decrease of infective particle numbers were found with OMVs from different preparations. In particular, the naturally budded OMVs isolated from culture supernatants reduced infective P22 particle numbers to a lesser extent compared to OMVs prepared from OM fractions. It is important to note here that in the experiment, all OMV samples were adjusted to the same LPS content. However, lacking proteome characterization of budded OMVs, we can only speculate whether they contained a different OM protein decoration that interfered with LPS receptor accessibility or influenced the membrane curvature. Moreover, additional periplasmic proteins inside the OMVs could have slowed down P22 inactivation, for example, by increasing the osmotic pressure in the vesicle lumen. Also, if these OMVs presented less LPS on their surface, TSP cleavage of the O-antigen receptor might compete with irreversible phage attachment (Broeker et al., 2019) and prevent phage inactivation. During P22 isolation, OMVs

were not pulled down together with the phage, in contrast to podovirus Sf6 that co-purified with OMVs through interactions with OmpA and OmpC (Parent et al., 2014).

In vitro fluorescence analyses have been used regularly to monitor DNA ejection from phages triggered with their isolated receptors, either OM proteins or LPS, in bulk or on a single particle level (Mangenot et al., 2005; Andres et al., 2010, 2012; Chiaruttini et al., 2010; Gonzalez-Garcia et al., 2015; Broeker et al., 2019). In these experimental setups, a DNA-specific dye fluorescence increase is observed due to DNA release from a capsid-confined state into a more relaxed state in the solution. For P22 it was shown that particles open and eject about 80% of their DNA content when triggered with LPS (Andres et al., 2010). The kinetic profile of this process is conserved in other podovirus systems analyzed with the same method, but different LPS receptors (Broeker et al., 2018). This reflects that the rate-limiting particle opening step most probably involves rearrangements in conserved parts of the podovirus tail assembly.

In this work, we have now used OMVs to trigger *in vitro* particle opening of bacteriophage P22 and could monitor time-resolved DNA release with a DNA-sensitive fluorescence stain. This is in contrast to cryo-EM analyses that compared end points of ejection by quantifying phages that had lost their DNA (Reyes-Robles et al., 2018). Phage-released DNA in the presence of OMVs was fully protected from DNase degradation, in contrast to the DNA released with pure LPS in solution. This indicates that OMVs and the phage were intimately linked in a stable complex where DNA ejection was exclusively targeted to the vesicle lumen. Similarly, EM images of bacteriophage-bound OMVs of the marine cyanobacterium *Prochlorococcus* suggested that DNA transfer into the vesicle lumen had taken place, as the tail of the myovirus was contracted and the capsid was empty (Biller et al., 2014). Our fluorescence bulk kinetic study typically monitored approximately 10^9 P22 particles, of which only about 30% ejected their DNA upon contact with OMVs. Also for other phages, cryo-EM imaging and quantification showed that a majority of particles had retained their DNA inside the capsid when bound to OMVs, for example, *Vibrio cholerae* phages in up to 90% of all particles imaged (Reyes-Robles et al., 2018). This fraction is similar to what was found with cryo-EM for OMV-bound *Shigella* podovirus Sf6 (Parent et al., 2014). So far, we have failed with attempts to physically separate the OMV-phage P22 complexes to individually analyze the vesicles' DNA content after phage contact. Similar problems had also been reported before for OMVs binding to bacteriophage T4 (Manning and Kuehn, 2011). Apparently, it is difficult to find solubilization conditions that either address the OMV or the phage without affecting the integrity of the other. Moreover, irreversible phage attachment to OMVs might already destabilize the phage even if it has not released its DNA.

Our experiments furthermore showed that, compared to using pure LPS as receptor for triggering DNA release from phage P22, the fluorescence signal obtained with OMV receptors went into saturation twice as fast. In OMVs, P22 now encountered a more complex membrane system compared to LPS. LPS has a unique solution behavior, forming multilamellar aggregates that presumably mimic membrane-like structures addressed by the phage *in vitro*, but do not represent all characteristics of the OM heterobilayer (Andres et al., 2010; Richter et al., 2011). In OMVs in contrast, OM proteins are present that might in a so far unknown way accelerate the phage particle opening step and the subsequent DNA release. This becomes evident especially when analyzing P22 at elevated osmotic pressures. In this work, we showed that DNA release triggered by highly pure LPS lacking OM proteins already ceased at external osmotic pressures of about 3.6 atm. However, it has been shown earlier that in the presence of OM proteins at this osmotic pressure, P22 still released a fraction of its DNA (Jin et al., 2015). Moreover, OM proteins enabled the release of P22's ejection proteins, in contrast to LPS alone. Our actual DNA ejection studies are in line with these findings. P22 in the presence of OMVs at 6.8 atm osmotic pressure still showed partial DNA loss, emphasizing that progression of DNA release from the phage particle is intimately coupled to the receptor type. For P22, it was shown that this can be pure LPS aggregates, a combination of LPS and OM proteins or OMVs. We note that in comparison of the present study with the one cited above (Parent et al., 2014), the latter showed no difference in fractional DNA release between samples triggered with LPS alone or with a mixture of OmpA and LPS. As a reason for this ambiguity, we assume that different LPS preparation protocols may have resulted in incomplete OM protein removal. In summary, the new results emphasize the critical role of OM composition for phage control. Bacteria might exploit this by adjusting their OMV contents in response to phage attack.

Our *in vitro* experiments again illustrate that all energy needed for DNA release from bacteriophages is already stored in the system (Keller et al., 2017). The phage genome is highly confined inside the capsid, packaged against the DNA intramolecular electrostatic repulsion forces by an ATP-hydrolysis-driven motor (Smith et al., 2001). Accordingly, increasing external osmotic pressures can counteract genome liberation (Evilevitch et al., 2003). For siphovirus λ with a long, non-contractile tail, an internal capsid pressure of about 20 atm was estimated that was dependent on the relationship of genome length and capsid size (Grayson et al., 2006). However, external factors were shown to significantly influence the genome ejection characteristics of λ, illustrating the complex behavior of the DNA polyelectrolyte both inside the capsid and when transferred into the solution (Evilevitch, 2018). Also, the osmotic status of OMVs interacting with phage P22 might play a role in the observed DNA release process. If OMVs had a significant turgor, for example, due to their luminal protein content, the amount of DNA release from P22 would be insensitive to low osmotic pressures in the surrounding solution. However, also with OMVs, we observed that the amount of ejected DNA decreased with increasing PEG solution concentrations. This indicates (i) that presumably no osmotic pressure existed in the OMVs and (ii) that ejecting P22 particles could transfer substantial amounts of DNA inside the vesicles. As already discussed above, we could not directly quantify how much DNA remained inside the phage capsid and how much was translocated into the vesicle lumen. Nevertheless,

the notable effect of low PEG concentrations on the ejection signal shows that more than 30% of the DNA must have left the capsid on the level of an individually ejecting phage, in agreement with cryo-EM studies with other phage systems (Parent et al., 2014; Reyes-Robles et al., 2018). Hence, the reduced signal amplitude observed in fluorescence curves obtained with OMVs is due to a reduced number of particles actively ejecting when compared to particles triggered with free LPS. In the future, this bulk study-derived hypothesis needs further evaluation to understand molecular details of OMV-mediated bacteriophage inhibition.

CONCLUSION

Bacteriophage P22 *in vitro* particle opening studies with OMVs revealed that the action of the LPS receptor on the phage is modulated when LPS is part of a more complex OM system. Although OMVs could also effectively reduce the number of infective particles, inactivation was not driven by DNA release from all particles as observed with pure LPS fragments. Rather, a remarkable amount of phages did not eject their DNA. The mechanism of this OMV-driven bacteriophage inactivation remains to be elucidated and may be steered by different OMV properties. For example, vesicular curvature and protein decoration result in enhanced membrane tension and variable membrane thickness, respectively (Wu et al., 2014; Huang et al., 2017). Also, the presence of OM proteins as co-receptors influences the phage interactions (Parent et al., 2014). Moreover, multiple binding of P22 phages on small vesicles may induce mutual obstruction between the phages, prohibiting the DNA ejection. Importantly, we found that a preparation of naturally budded vesicles showed a much smaller capacity to inhibit the phage compared to the fraction obtained during mechanical cell lysis. This emphasizes that vesicle composition is a major control point for their function as phage blocking agents. From a more general point of view, if bacteria shed OMVs to block a phage population, they might employ a mechanism to inhibit substantial DNA liberation into the OMVs. As OMVs may also act in gene transfer, bacteria thus avoid another route with which phage genes could enter the bacterial cell. Further analyses will elucidate how the biochemical composition and properties of OMVs are linked to bacteriophage population regulation in a given functional context.

DATA AVAILABILITY STATEMENT

All datasets generated for this study are included in the article/**Supplementary Material**.

AUTHOR CONTRIBUTIONS

SB, DL, NR, and NB conceptualized the study and methodology. MS, NR, and AS performed the experiments. MS, NR, NB, and SB evaluated and visualized the data. MS, SB, DL, and AS wrote the manuscript. SB, DL, AS, NR, and NB supervised the study. SB and DL acquired funding. All authors contributed to the article and approved the submitted version.

FUNDING

This project was funded by a short-term exchange grant of the German Academic Exchange Service to SB (PPP 57345139) and the Research Council of Norway to DL (RCN 267434). MS is funded by the International Max Planck Research School on Multiscale Biosystems.

ACKNOWLEDGMENTS

We thank Antje Hofgaard, Jens Wohlmann, and Martin Wolff for assistance with electron microscopy and dynamic light scattering, respectively. We thank Mandy Schietke for excellent technical support.

SUPPLEMENTARY MATERIAL

The Supplementary Material for this article can be found online at: https://www.frontiersin.org/articles/10.3389/fmicb.2020.510638/full#supplementary-material

OMV size distributions from dynamic light scattering (**Supplementary Figure S1**), additional TEM images (**Supplementary Figures S2**, **S3**, and **S6**) and characterization of OMVs (**Supplementary Figures S3–S5**) as well as additional DNA ejection curves (**Supplementary Figures S7–S9**) can be found in the **Supplementary Data Sheet 1**.

REFERENCES

Andres, D., Hanke, C., Baxa, U., Seul, A. t., Barbirz, S., and Seckler, R. (2010). Tailspike interactions with lipopolysaccharide effect DNA ejection from phage P22 particles in vitro. *J. Biol. Chem.* 285, 36768–36775. doi: 10.1074/jbc.M110.169003

Andres, D., Roske, Y., Doering, C., Heinemann, U., Seckler, R., and Barbirz, S. (2012). Tail morphology controls DNA release in two Salmonella phages with one lipopolysaccharide receptor recognition system. *Mol. Microbiol.* 83, 1244–1253. doi: 10.1111/j.1365-2958.2012.08006.x

Bai, J., Kim, S. I., Ryu, S., and Yoon, H. (2014). Identification and characterization of outer membrane vesicle-associated proteins in *Salmonella enterica* serovar Typhimurium. *Infect. Immun.* 82, 4001–4010. doi: 10.1128/Iai.01416-13

Beveridge, T. J. (1999). Structures of gram-negative cell walls and their derived membrane vesicles. *J. Bacteriol.* 181, 4725–4733. doi: 10.1128/JB.181.16.4725-4733.1999

Biller, S. J., Schubotz, F., Roggensack, S. E., Thompson, A. W., Summons, R. E., and Chisholm, S. W. (2014). Bacterial vesicles in marine ecosystems. *Science* 343, 183–186. doi: 10.1126/science.1243457

Bonnington, K. E., and Kuehn, M. J. (2016). Outer membrane vesicle production facilitates LPS Remodeling and outer membrane maintenance in Salmonella during environmental transitions. *mBio* 7:e01532–16. doi: 10.1128/mBio.01532-16

Broeker, N. K., and Barbirz, S. (2017). Not a barrier but a key: how bacteriophages exploit host's O-antigen as an essential receptor to initiate infection. *Mol. Microbiol.* 105, 353–357. doi: 10.1111/mmi.13729

Broeker, N. K., Kiele, F., Casjens, S. R., Gilcrease, E. B., Thalhammer, A., Koetz, J., et al. (2018). In vitro studies of lipopolysaccharide-mediated DNA release of podovirus HK620. *Viruses* 10:289. doi: 10.3390/v10060289

Broeker, N. K., Roske, Y., Valleriani, A., Stephan, M. S., Andres, D., Koetz, J., et al. (2019). Time-resolved DNA release from an O-antigen-specific Salmonella bacteriophage with a contractile tail. *J. Biol. Chem.* 294, 11751–11761. doi: 10.1074/jbc.RA119.008133

Casjens, S. R., and Grose, J. H. (2016). Contributions of P2-and P22-like prophages to understanding the enormous diversity and abundance of tailed bacteriophages. *Virology* 496, 255–276. doi: 10.1016/j.virol.2016.05.022

Celluzzi, A., and Masotti, A. (2016). How our other genome controls our Epi-genome. *Trends Microbiol.* 24, 777–787. doi: 10.1016/j.tim.2016.05.005

Cenens, W., Makumi, A., Govers, S. K., Lavigne, R., and Aertsen, A. (2015). Viral transmission dynamics at single-cell resolution reveal transiently immune subpopulations caused by a carrier state association. *PLoS Genet.* 11:e1005770. doi: 10.1371/journal.pgen.1005770

Chiaruttini, N., de Frutos, M., Augarde, E., Boulanger, P., Letellier, L., and Viasnoff, V. (2010). Is the in vitro ejection of bacteriophage DNA quasistatic? A bulk to single virus study. *Biophys. J.* 99, 447–455. doi: 10.1016/j.bpj.2010.04.048

Crispim, J. S., Dias, R. S., Laguardia, C. N., Araujo, L. C., da Silva, J. D., Vidigal, P. M. P., et al. (2019). Desulfovibrio alaskensis prophages and their possible involvement in the horizontal transfer of genes by outer membrane vesicles. *Gene* 703, 50–57. doi: 10.1016/j.gene.2019.04.016

Deatherage, B. L., Lara, J. C., Bergsbaken, T., Barrett, S. L. R., Lara, S., and Cookson, B. T. (2009). Biogenesis of bacterial membrane vesicles. *Mol. Microbiol.* 72, 1395–1407. doi: 10.1111/j.1365-2958.2009.06731.x

Doron, S., Melamed, S., Ofir, G., Leavitt, A., Lopatina, A., Keren, M., et al. (2018). Systematic discovery of antiphage defense systems in the microbial pangenome. *Science* 359:eaar4120. doi: 10.1126/science.aar4120

Dramsi, S., Magnet, S., Davison, S., and Arthur, M. (2008). Covalent attachment of proteins to peptidoglycan. *FEMS Microbiol. Rev.* 32, 307–320. doi: 10.1111/j.1574-6976.2008.00102.x

Erez, Z., Steinberger-Levy, I., Shamir, M., Doron, S., Stokar-Avihail, A., Peleg, Y., et al. (2017). Communication between viruses guides lysis-lysogeny decisions. *Nature* 541, 488–493. doi: 10.1038/nature21049

Evilevitch, A. (2018). The mobility of packaged phage genome controls ejection dynamics. *elife* 7:e37345. doi: 10.7554/eLife.37345

Evilevitch, A., Gober, J. W., Phillips, M., Knobler, C. M., and Gelbart, W. M. (2005). Measurements of DNA lengths remaining in a viral capsid after osmotically suppressed partial ejection. *Biophys. J.* 88, 751–756. doi: 10.1529/biophysj.104.045088

Evilevitch, A., Lavelle, L., Knobler, C. M., Raspaud, E., and Gelbart, W. M. (2003). Osmotic pressure inhibition of DNA ejection from phage. *Proc. Natl. Acad. Sci. U. S. A.* 100, 9292–9295. doi: 10.1073/pnas.1233721100

Feiner, R., Argov, T., Rabinovich, L., Sigal, N., Borovok, I., and Herskovits, A. A. (2015). A new perspective on lysogeny: prophages as active regulatory switches of bacteria. *Nat. Rev. Microbiol.* 13, 641–650. doi: 10.1038/nrmicro3527

Gonzalez-Garcia, V. A., Pulido-Cid, M., Garcia-Doval, C., Bocanegra, R., van Raaij, M. J., Martin-Benito, J., et al. (2015). Conformational changes leading to T7 DNA delivery upon interaction with the bacterial receptor. *J. Biol. Chem.* 290, 10038–10044. doi: 10.1074/jbc.M114.614222

Grayson, P., Evilevitch, A., Inamdar, M. M., Purohit, P. K., Gelbart, W. M., Knobler, C. M., et al. (2006). The effect of genome length on ejection forces in bacteriophage lambda. *Virology* 348, 430–436. doi: 10.1016/j.virol.2006.01.003

Grin, I., Schwarz, H., and Linke, D. (2011). Electron microscopy techniques to study bacterial adhesion. *Adv. Exp. Med. Biol.* 715, 257–269. doi: 10.1007/978-94-007-0940-9_16

Guerrero-Mandujano, A., Hernandez-Cortez, C., Ibarra, J. A., and Castro-Escarpulli, G. (2017). The outer membrane vesicles: secretion system type zero. *Traffic* 18, 425–432. doi: 10.1111/tra.12488

Hsia, C. Y., Chen, L. X., Singh, R. R., DeLisa, M. P., and Daniel, S. (2016). A molecularly complete planar bacterial outer membrane platform. *Sci. Rep.* 6:32715. doi: 10.1038/srep32715

Huang, C. J., Quinn, D., Sadovsky, Y., Suresh, S., and Hsia, K. J. (2017). Formation and size distribution of self-assembled vesicles. *Proc. Natl. Acad. Sci. U. S. A.* 114, 2910–2915. doi: 10.1073/pnas.1702065114

Jin, Y., Sdao, S. M., Dover, J. A., Porcek, N. B., Knobler, C. M., Gelbart, W. M., et al. (2015). Bacteriophage P22 ejects all of its internal proteins before its genome. *Virology* 485, 128–134. doi: 10.1016/j.virol.2015.07.006

Keller, N., Berndsen, Z. T., Jardine, P. J., and Smith, D. E. (2017). Experimental comparison of forces resisting viral DNA packaging and driving DNA ejection. *Phys. Rev. E* 95:052408. doi: 10.1103/PhysRevE.95.052408

Kim, S. W., Park, S. B., Im, S. P., Lee, J. S., Jung, J. W., Gong, T. W., et al. (2018). Outer membrane vesicles from beta-lactam-resistant *Escherichia coli* enable the survival of beta-lactamsusceptible *E. coli* in the presence of beta-lactam antibiotics. *Sci. Rep.* 8:5402. doi: 10.1038/s41598-018-23656-0

Kintz, E., Davies, M. R., Hammarlof, D. L., Canals, R., Hinton, J. C. D., and van der Woude, M. W. (2015). A BTP1 prophage gene present in invasive non-typhoidal Salmonella determines composition and length of the O-antigen of the lipopolysaccharide. *Mol. Microbiol.* 96, 263–275. doi: 10.1111/mmi.12933

Kulp, A., and Kuehn, M. J. (2010). Biological functions and biogenesis of secreted bacterial outer membrane vesicles. *Annu. Rev. Biochem.* 64, 163–184. doi: 10.1146/annurev.micro.091208.073413

Latka, A., Maciejewska, B., Majkowska-Skrobek, G., Briers, Y., and Drulis-Kawa, Z. (2017). Bacteriophage-encoded virion-associated enzymes to overcome the carbohydrate barriers during the infection process. *Appl. Microbiol. Biotechnol.* 101, 3103–3119. doi: 10.1007/s00253-017-8224-6

Leavitt, J. C., Gogokhia, L., Gilcrease, E. B., Bhardwaj, A., Cingolani, G., and Casjens, S. R. (2013). The tip of the tail needle affects the rate of DNA delivery by bacteriophage P22. *PLoS One* 8:13. doi: 10.1371/journal.pone.0070936

Lee, C. H., and Tsai, C. M. (1999). Quantification of bacterial lipopolysaccharides by the purpald assay: measuring formaldehyde generated from 2-keto-3-deoxyoctonate and heptose at the inner core by periodate oxidation. *Anal. Biochem.* 267, 161–168. doi: 10.1006/abio.1998.2961

Leon, M., and Bastias, R. (2015). Virulence reduction in bacteriophage resistant bacteria. *Front. Microbiol.* 6:343. doi: 10.3389/fmicb.2015.00343

Loeb, M. R. (1974). Bacteriophage T4-mediated release of envelope components from *Escherichia-Coli*. *J. Virol.* 13, 631–641. doi: 10.1128/JVI.13.3.631-641.1974

Malge, A., Ghai, V., Reddy, P. J., Baxter, D., Kim, T. K., Moritz, R. L., et al. (2018). mRNA transcript distribution bias between Borrelia burgdorferi bacteria and their outer membrane vesicles. *FEMS Microbiol. Lett.* 365:fny135. doi: 10.1093/femsle/fny135

Mangenot, S., Hochrein, M., Radler, J., and Letellier, L. (2005). Real-time imaging of DNA ejection from single phage particles. *Curr. Biol.* 15, 430–435. doi: 10.1016/j.cub.2004.12.080

Manning, A. J., and Kuehn, M. J. (2011). Contribution of bacterial outer membrane vesicles to innate bacterial defense. *BMC Microbiol.* 11:258. doi: 10.1186/1471-2180-11-258

Mashburn, L. M., and Whiteley, M. (2005). Membrane vesicles traffic signals and facilitate group activities in a prokaryote. *Nature* 437, 422–425. doi: 10.1038/nature03925

Parent, K. N., Erb, M. L., Cardone, G., Nguyen, K., Gilcrease, E. B., Porcek, N. B., et al. (2014). OmpA and OmpC are critical host factors for bacteriophage Sf6 entry in Shigella. *Mol. Microbiol.* 92, 47–60. doi: 10.1111/mmi.12536

Park, M., Yoo, G., Bong, J. H., Jose, J., Kang, M. J., and Pyun, J. C. (2015). Isolation and characterization of the outer membrane of *Escherichia coli* with autodisplayed Z-domains. *BBA-Biomembranes* 1848, 842–847. doi: 10.1016/j.bbamem.2014.12.011

Parsegian, V. A., Rand, R. P., Fuller, N. L., and Rau, D. C. (1986). Osmotic stress for the direct measurement of intermolecular forces. *Methods Enzymol.* 127, 400–416. doi: 10.1016/0076-6879(86)27032-9

Pires, D. P., Oliveira, H., Melo, L. D. R., Sillankorva, S., and Azeredo, J. (2016). Bacteriophage-encoded depolymerases: their diversity and biotechnological applications. *Appl. Microbiol. Biotechnol.* 100, 2141–2151. doi: 10.1007/s00253-015-7247-0

Prevelige, P. (2006). "Bacteriophage P22" in *The bacteriophages*. ed. R. Calendar (Oxford: Oxford University Press), 457.

Prokhorov, N. S., Riccio, C., Zdorovenko, E. L., Shneider, M. M., Browning, C., Knirel, Y. A., et al. (2017). Function of bacteriophage G7C esterase tailspike in host cell adsorption. *Mol. Microbiol.* 105, 385–398. doi: 10.1111/mmi.13710

Reyes-Robles, T., Dillard, R. S., Cairns, L. S., Silva-Valenzuela, C. A., Housman, M., Ali, A., et al. (2018). Vibrio cholerae outer membrane vesicles inhibit bacteriophage infection. *J. Bacteriol.* 200:e00792–17. doi: 10.1128/jb.00792-17

Richter, W., Vogel, V., Howe, J., Steiniger, F., Brauser, A., Koch, M. H., et al. (2011). Morphology, size distribution, and aggregate structure of lipopolysaccharide and lipid a dispersions from enterobacterial origin. *Innate Immun.* 17, 427–438. doi: 10.1177/1753425910372434

Rostol, J. T., and Marraffini, L. (2019). (Ph)ighting phages: how bacteria resist their parasites. *Cell Host Microbe* 25, 184–194. doi: 10.1016/j.chom.2019.01.009

Rozycki, B., and Lipowsky, R. (2015). Spontaneous curvature of bilayer membranes from molecular simulations: asymmetric lipid densities and asymmetric adsorption. *J. Chem. Phys.* 142:054101. doi: 10.1063/1.4906149

Salmond, G. P. C., and Fineran, P. C. (2015). A century of the phage: past, present and future. *Nat. Rev. Microbiol.* 13, 777–786. doi: 10.1038/nrmicr03564

Schmidt, A., Rabsch, W., Broeker, N. K., and Barbirz, S. (2016). Bacteriophage tailspike protein based assay to monitor phase variable glucosylations in Salmonella O-antigens. *BMC Microbiol.* 16:207. doi: 10.1186/s12866-016-0826-0

Schwechheimer, C., and Kuehn, M. J. (2015). Outer-membrane vesicles from gram-negative bacteria: biogenesis and functions. *Nat. Rev. Microbiol.* 13, 605–619. doi: 10.1038/nrmicro3525

Schwechheimer, C., Sullivan, C. J., and Kuehn, M. J. (2013). Envelope control of outer membrane vesicle production in gram-negative bacteria. *Biochemistry* 52, 3031–3040. doi: 10.1021/bi400164t

Seed, K. D., Faruque, S. M., Mekalanos, J. J., Calderwood, S. B., Qadri, F., and Camilli, A. (2012). Phase variable O antigen biosynthetic genes control expression of the major protective antigen and bacteriophage receptor in Vibrio cholerae O1. *PLoS Pathog.* 8:e1002917. doi: 10.1371/journal.ppat.1002917

Silva, J. B., Storms, Z., and Sauvageau, D. (2016). Host receptors for bacteriophage adsorption. *FEMS Microbiol. Lett.* 363:fnw002. doi: 10.1093/femsle/fnw002

Smith, D., Tans, S., Smith, S., Grimes, S., Anderson, D., and Bustamante, C. (2001). The bacteriophage phi 29 portal motor can package DNA against a large internal force. *Nature* 413, 748–752. doi: 10.1038/35099581

Smith, P. K., Krohn, R. I., Hermanson, G. T., Mallia, A. K., Gartner, F. H., Provenzano, M. D., et al. (1985). Measurement of protein using bicinchoninic acid. *Anal. Biochem.* 150, 76–85. doi: 10.1016/0003-2697(85)90442-7

Susskind, M. M., Botstein, D., and Wright, A. (1974). Superinfection exclusion by P22 prophage in lysogens of *Salmonella-typhimurium*.III. Failure of superinfecting phage DNA to enter SieA+ lysogens. *Virology* 62, 350–366. doi: 10.1016/0042-6822(74)90398-5

Thein, M., Sauer, G., Paramasivam, N., Grin, I., and Linke, D. (2010). Efficient subfractionation of gram-negative bacteria for proteomics studies. *J. Proteome Res.* 9, 6135–6147. doi: 10.1021/pr1002438

Tindall, B. J., Grimont, P. A., Garrity, G. M., and Euzéby, J. P. (2005). Nomenclature and taxonomy of the genus *Salmonella*. *Int. J. Syst. Evol. Microbiol.* 55, 521–524. doi: 10.1099/ijs.0.63580-0

Toyofuku, M., Nomura, N., and Eberl, L. (2019). Types and origins of bacterial membrane vesicles. *Nat. Rev. Microbiol.* 17, 13–24. doi: 10.1038/s41579-018-0112-2

Vidakovic, L., Singh, P. K., Hartmann, R., Nadell, C. D., and Drescher, K. (2018). Dynamic biofilm architecture confers individual and collective mechanisms of viral protection. *Nat. Microbiol.* 3, 26–31. doi: 10.1038/s41564-017-0050-1

Volgers, C., Savelkoul, P. H. M., and Stassen, F. R. M. (2018). Gram-negative bacterial membrane vesicle release in response to the host-environment: different threats, same trick? *Crit. Rev. Microbiol.* 44, 258–273. doi: 10.1080/1040841x.2017.1353949

Wang, C. Y., Tu, J. G., Liu, J., and Molineux, I. J. (2019). Structural dynamics of bacteriophage P22 infection initiation revealed by cryo-electron tomography. *Nat. Microbiol.* 4, 1049–1056. doi: 10.1038/s41564-019-0403-z

Whitfield, C., and Trent, M. S. (2014). Biosynthesis and export of bacterial lipopolysaccharides. *Annu. Rev. Biochem.* 83, 99–128. doi: 10.1146/annurev-biochem-060713-035600

Wu, E. L., Fleming, P. J., Yeom, M. S., Widmalm, G., Klauda, J. B., Fleming, K. G., et al. (2014). *E. coli* outer membrane and interactions with OmpLA. *Biophys. J.* 106, 2493–2502. doi: 10.1016/j.bpj.2014.04.024

Conflict of Interest: The authors declare that the research was conducted in the absence of any commercial or financial relationships that could be construed as a potential conflict of interest.

Advantages of publishing in Frontiers

OPEN ACCESS
Articles are free to read for greatest visibility and readership

FAST PUBLICATION
Around 90 days from submission to decision

HIGH QUALITY PEER-REVIEW
Rigorous, collaborative, and constructive peer-review

TRANSPARENT PEER-REVIEW
Editors and reviewers acknowledged by name on published articles

Frontiers
Avenue du Tribunal-Fédéral 34
1005 Lausanne | Switzerland

Visit us: www.frontiersin.org
Contact us: frontiersin.org/about/contact

REPRODUCIBILITY OF RESEARCH
Support open data and methods to enhance research reproducibility

DIGITAL PUBLISHING
Articles designed for optimal readership across devices

FOLLOW US
@frontiersin

IMPACT METRICS
Advanced article metrics track visibility across digital media

EXTENSIVE PROMOTION
Marketing and promotion of impactful research

LOOP RESEARCH NETWORK
Our network increases your article's readership